University of Arkansas, Fayetteville

ScholarWorks@UARK

Graduate Theses and Dissertations

5-2015

Amount of Uncertainty in the Methods Utilized to Design Drilled Shaft Foundations

Morgan Race
University of Arkansas, Fayetteville

Follow this and additional works at: https://scholarworks.uark.edu/etd

 Part of the Civil Engineering Commons, and the Geotechnical Engineering Commons

Citation

Race, M. (2015). Amount of Uncertainty in the Methods Utilized to Design Drilled Shaft Foundations. *Graduate Theses and Dissertations* Retrieved from https://scholarworks.uark.edu/etd/1149

This Dissertation is brought to you for free and open access by ScholarWorks@UARK. It has been accepted for inclusion in Graduate Theses and Dissertations by an authorized administrator of ScholarWorks@UARK. For more information, please contact uarepos@uark.edu.

Amount of Uncertainty in the Methods Utilized to Design Drilled Shaft Foundations

Amount of Uncertainty in the Methods Utilized to Design Drilled Shaft Foundations

A dissertation submitted in partial fulfillment
of the requirements for the degree of
Doctor of Philosophy in Engineering

by

Morgan Race
University of Arkansas
Bachelor of Science in Civil Engineering, 2011

May 2015
University of Arkansas

This dissertation is approved for recommendation to the Graduate Council.

_____
Dr. Richard Coffman
Dissertation Director

_____
Dr. Michelle Bernhardt
Committee Member

_____
Dr. Norman Dennis
Committee Member

_____
Dr. Ed Pohl
Committee Member

ABSTRACT

In 2001, load and resistance factor design (LRFD) for deep foundations was required by the American Association of State Highway and Transportation Officials (AASHTO). Following implementation of LRFD, localized calibration of resistance factors using data from the states of Colorado, Florida, Kansas, Louisiana/Mississippi, Missouri allowed these states to utilize higher resistance factors during design. However, characterizing the uncertainty in the design of DSF, regarding the geotechnical investigation methods and the utilized software programs, higher values of resistance factors may be calibrated to more efficiently design DSF with the same level of reliability.

Three test sites within the state of Arkansas, identified as the Siloam Springs Arkansas Test Site (SSATS), the Turrell Arkansas Test Site (TATS), and the Monticello Arkansas Test Site (MATS), were utilized to perform full-scale load tests on DSF. At each site, three geotechnical investigation methods (Arkansas State Highway and Transportation Department [AHTD], Missouri Department of Transportation [MODOT], and the University of Arkansas [UofA]) were utilized to obtained geotechnical parameters. The design of three DSF, at each site, was then performed, and the amount of resistance was predicted, using commercially available software (FB-Deep and SHAFT). At each site, the results obtained from bi-directional load tests were compared with the predicted values and the construction methods and problems (i.e. rock embedment length at the SSATS, collapsed excavation at the TATS, and equipment failure/concrete placement at the MATS) are presented herein.

Two site-specific and a geologic-specific calibrations were performed by utilizing the results from the bi-directional load tests that were performed in Arkansas, the Bayesian updating, and the Monte Carlo simulation techniques. For each geotechnical investigation method and for

each software program that was utilized during the DSF design, posterior distribution parameters were calculated based on previous calibration databases (i.e. the national database or the Louisiana/Mississippi database). Resulting resistance factor values were calculated for the geologic-specific mixed soils within the state of Arkansas. The calculated resistance factors ranged from 0.57 to 0.80 for total resistance. Furthermore, the FB-Deep software program is recommended in conjunction with the MODOT or UofA geotechnical investigation methods to design of DSF in Arkansas.

ACKNOWLEDGEMENTS

I would like to thank many people for the help and support throughout my time as a University of Arkansas student. First, I would like to thank Dr. Richard Coffman for the opportunity to perform this research project and guidance throughout the long process. Similarly, I would like to thank my committee members, Dr. Norman Dennis, Dr. Ed Pohl, and Dr. Michelle Bernhardt, for their support and educational guidance. I would also like to thank all of the organizations who made this project possible. These organizations include, but are not limited to: the Arkansas Highway and Transportation Department, the International Association of Foundation Drilling, Loadtest, Inc., the Missouri Department of Transportation, McKinney Drilling Company, Aldridge Construction Company. Similarly, I would like to thank the editors and reviewers of the Deep Foundations Journal and the Geotechnical and Geological Engineering Journal for their constructive input about the submitted articles. Sarah Bey, a previous graduate student, was an integral part of this research project and I want to thank her for her help with the research and for her friendship during the long days/nights. I want to also thank other graduate students, including but not limited to: Matthew Nanak, Omar Conte, Cyrus Garner, Sean Salazar, Yi Zhao, and Elvis Ishimwe for the scholastic support and friendship throughout the years. Last, but not least, I would like to thank my parents and Kevin Tipton for their unwavering emotional support during the entire process.

TABLE OF CONTENTS

LIST OF FIGURES

LIST OF TABLES

CHAPTER 1: INTRODUCTION

1.1. Background

In the design of drilled shaft foundations (DSF), the amount of uncertainty must be considered while predicting how the foundation will behave when subjected to specified loading conditions. As opposed to the direct relationship between the amount of uncertainty and the risk of failure, an indirect relationship exists between the risk of failure and the cost for a given foundation (i.e. a lower risk of failure results in a more expensive foundation). A reduction in the amount of uncertainty is therefore required to reduce the cost for a given foundation while maintaining the same level of risk. Specifically, the total amount of uncertainty may be characterized as the amount of uncertainty in the: available soil data, soil probability distribution model, software programs utilized in the design of DSF, construction methods, and full-scale testing.

The amount of uncertainty associated with the soil data is dependent upon the geotechnical investigation methods that are utilized to determine values of soil properties, including but not limited to the: total unit weight (γ_t), undrained shear strength of cohesive soil (c_u), friction angle of cohesionless soil (ϕ'), and unconfined compressive strength of rock (q_u). There is inherent uncertainty in the probability distribution model for all of the soil parameters that is generally attributed to a lack of data (due to monetary restrictions and scheduling restrictions associated with the collection of data during the geotechnical investigation). Numerous design methods/software programs exist to determine the interaction of the soil and a DSF. The amount of uncertainty within the software programs that are utilized for the design of DSF is associated with the amount of variation within the initial soil data and the amount of variation of the DSF geometry after construction. The construction methods that are utilized to

construct the DSF are also an integral component in the total amount of uncertainty associated with the design of DSF. Although the amount of uncertainty within full-scale testing is related to the soil data, software programs, and construction methods, there is also uncertainty associated with the type of full-scale testing method that is employed. Characterization of the amount of uncertainty that is associated with each of the components of the design and associated with the construction of the DSF will allow for the construction of more dependable and more efficient (same risk of failure for reduced cost) DSF.

Numerous geotechnical investigation methods and software programs can be utilized to predict the interaction between the soil deposit and the DSF. As presented in Figure 1.1, the amount of reliability associated with a drilled shaft foundation is dependent upon the difference between the amount of resistance ($\bar{R}$) and loading ($\bar{Q}$), and also the amounts of uncertainty within each of these values (σ_R and σ_Q, respectively). Specifically, more uncertainty in the resistance values will result in larger values of probability of failure.

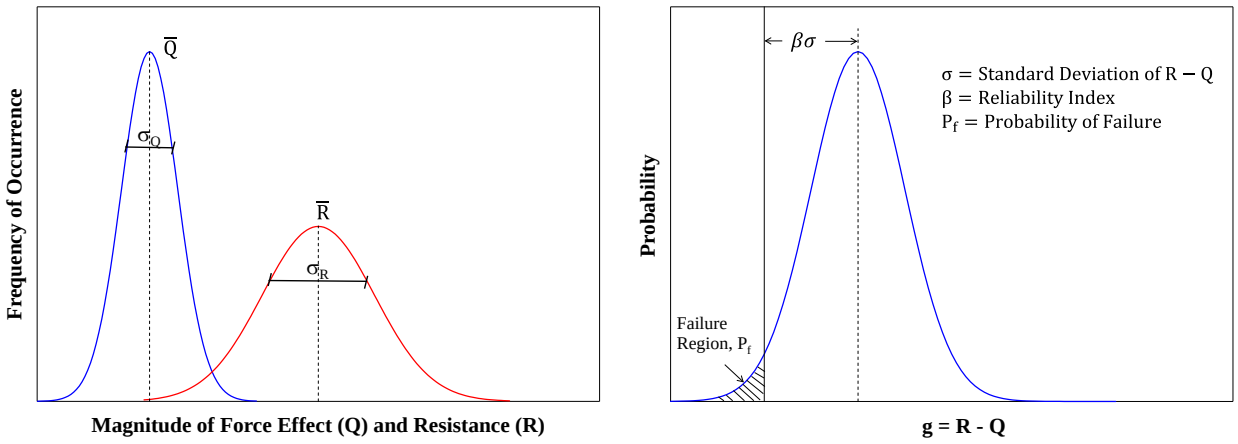

Figure 1.1. a) Force and resistance frequency distribution and b) probability distribution of the difference in the resistance and applied forces (modified from Brown et al. 2010).

1.2. Benefits to Geotechnical Engineering Community

The determination of the amount of uncertainty in the design of drilled shaft foundations, as attributed to the effects of the geotechnical investigation methods and the design methodologies/software program, will enable a more efficient design in terms of reliability and cost. In particular, a localized (site-specific or geological deposit-specific) calibration of the resistance factors will be advantageous for the state of Arkansas and to the geotechnical community at large. Specifically, the benefits from this research will include the following.

- Establishment of the amount of uncertainty associated with different geotechnical investigation methods in relation to the soil property values.
- Determination of the amount of uncertainty associated with the design methods/software programs to more accurately predict the soil-structure interaction.
- Verification of the effects of construction methods upon the soil-structure interaction, as determined from full-scale testing.
- New statistical procedures (Bayesian Updating) to develop site-specific and geological specific resistance factors from small datasets.
- Determination of site-specific and geology-specific resistance factors for the state of Arkansas.

The evaluation of the amount of uncertainty in the design of DSF, and with the calibration of the resistance factors for DSF constructed in Arkansas, will reduce the cost of constructing these foundations while maintaining the value of the probability of failure. Characterization of the amount of uncertainty in the field and laboratory geotechnical investigation methods will enable the implementation of a more efficient geotechnical investigation program. The implemented program will thereby optimize the precision (low

variability) and decrease the construction cost (equipment usage, manpower). By developing a new geotechnical investigation program, the difference between the predicted and measured resistance of the DSF will be reduced, and consequently the reliability will be increased. Similarly, by comparing the measured and predicted capacity values that were obtained by performing full-scale load tests in Arkansas, an appropriate (more accurate) design methodology will be developed.

1.3. Dissertation Overview

Three (3) project tests sites, located within the state of Arkansas, were investigated: Monticello, Siloam Springs, and Turrell (Figure 1.2). The Monticello Arkansas Test Site (MATS), located in Southeastern Arkansas, is comprised of deltaic deposits (mixed layers of clay and sandy soils). The MATS is located south of Monticello, Arkansas, within Drew County and is within the right-of-way of the future I-69 extension. The future bridge at this site will be utilized for vehicles traveling on I-69 to pass over the railroad tracks that are located to the South and West of Highway 35. The Siloam Springs Arkansas Test Site (SSATS) is located in Northwestern Arkansas and is comprised of hard limestone overlain by cherty clay. The proposed site, located to the East of Siloam Springs, Arkansas, is located adjacent to the current Highway 16 Bridge that spans across the Illinois River. The Turrell Arkansas Test Site (TATS), located in Northeastern Arkansas, is located within the New Madrid Seismic Zone and within the Mississippi Embayment. The alluvial deposits at TATS consist of a clay layer underlain by clean, saturated sand. The soil at the TATS is anticipated to liquefy when subjected to the predicted earthquake conditions (design mean earthquake magnitude of 7.5 and peak ground acceleration of 0.64g with a 7 percent probability of exceedance in 75 years). This site is located

within the interchange between southbound lanes of Highway 63 and eastbound lanes of Interstate 55.

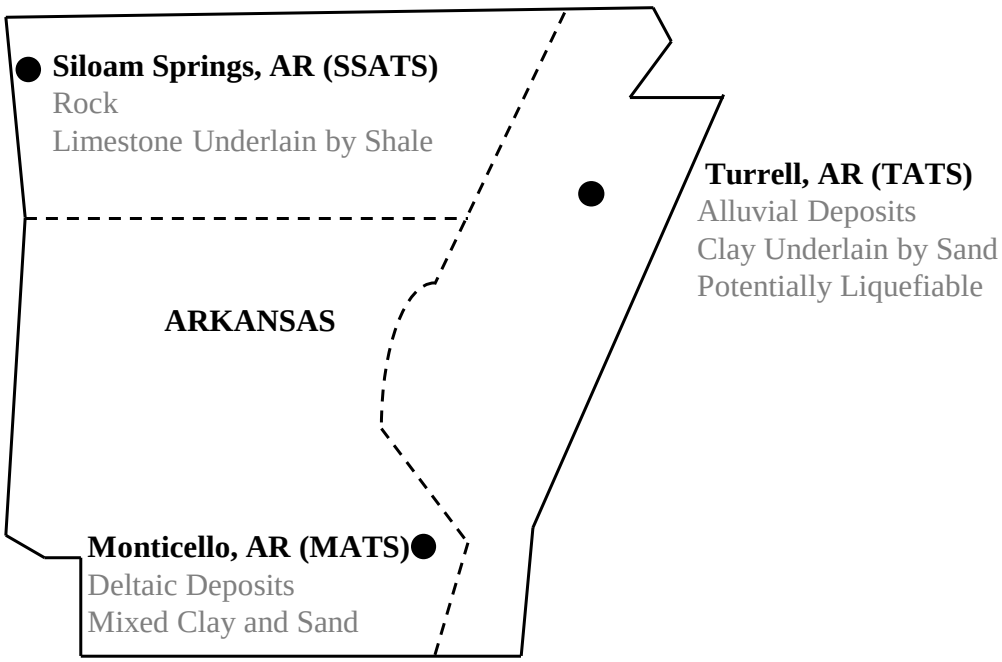

Figure 1.2. Locations of test sites within Arkansas.

For the required axial capacity of 11.6MN, the design lengths were 27.9m and 21.9m for the 1.2m and 1.8m diameter DSF at the MATS, respectively. The design lengths of the DSF at the SSATS, controlled by the minimum embedment length in rock of 3m, were 7.9m for both the 1.2m and 1.8m diameter DSF for the 9.9MN required axial capacity. At the TATS, the design lengths were 26.2m and 18.9m for the 1.2m and 1.8m diameter DSF, respectively, for the 8.8MN required axial capacity. The DSF were constructed at each of the test sites then tested using a bi-directional load cell.

Utilizing the results from the bi-directional load cell test, the effects of the construction techniques and problems were analyzed. Similarly, the as-built dimensions of the DSF were utilized to predict the axial resistance of the DSF using the geotechnical investigation methods and the software programs. Subsequently, the bias factor values (ratio of measured resistance to

predicted resistance) were determined for various movements (i.e. 5%D, 1%D, and 1.27cm) for all of the DSF at the three test sites. Because the amount of data was small (a maximum of six for the total resistance in soil deposits), the Bayesian updating method was employed along with the Monte Carlo simulation method to determine the resistance factor values for site-specific and soil deposit-specific calibration studies for the state of Arkansas.

1.4. Dissertation Organization

The hypothesis of this research is that a reduction of the amount of uncertainty, from better geotechnical investigation methods and better design methods will enable better prediction of the interaction between the soil deposit and the DSF. Specifically, the following tasks that were completed to determine the amount of uncertainty associated with the geotechnical investigation and DSF design methods will be discussed in detail within the dissertation.

- Field and laboratory geotechnical investigations were performed at three sites within the state of Arkansas (Monticello, Siloam Springs, and Turrell).
- Statistical analyses were performed on the obtained soil properties to determine the statistical difference and the amount of variation between the different geotechnical investigation methods.
- Different software programs were compared, such as FB-Deep and SHAFT, to determine the amount of uncertainty associated with the programs.
- Full-scale testing of DSF were performed, at the aforementioned three test sites, using Osterberg load cells.
- Resistance factors were developed and can be used to design DSF within the state of Arkansas.

Specifically, the research that was conducted for the Arkansas Highway and Transportation Department Transportation Research Committee Project 1204 (AHTD TRC-1204) project will be described in nine chapters within this dissertation. A summary of relevant literature review are included in Chapters 2 and 3 [Soil Testing Methods and DSF Analysis within Chapter 2 and DSF Testing and Reliability Analysis within Chapter 3]. The contents of Chapters 4 through 8 have been published or are in preparation to submit for publication. These chapters include differences in predicted resistance from the geotechnical investigation methods and the design methodologies (Chapter 4), discussion on DSF in moderately hard to hard limestone (Chapter 5), discussion on DSF with a collapsed excavation (Chapter 6), discussion on the effects of construction methods for DSF at the MATS (Chapter 7), and documentation about the determination of resistance factors using the Bayesian updating method (Chapter 8). A summary of the research findings that were discussed in this dissertation and recommendations are presented in Chapter 9.

Specifically, the statistical analysis of soil property that were determined from various geotechnical investigation methods and various DSF design methods are described in Chapter 4. Contributions to the publication was made by Sarah Bey and Dr. Richard Coffman, but Morgan Race (the author of this manuscript) was the lead author of the journal article that is contained in Chapter 4. The reference for the paper is: Race, M. L., Bey, S.M. and Coffman, R.A. (2015). "Statistical Analysis to Determine Appropriate Design Methodologies of Drilled Shaft Foundations." *GEGE Journal*, DOI: 10.1007/s10706-015-9854-z.

A technical paper about the design of DSF in hard limestone at the Siloam Springs Arkansas Test Site (SSATS) is contained within Chapter 5. The contributions made by Morgan Race and Richard Coffman included the unit side resistance in moderately hard to hard limestone

and recommended movement utilized for the design of DSF. The reference for the paper is: Race, M. L. and Coffman, R.A. (2015). “Load Tests on Drilled Shaft Foundations in Moderately Strong to Strong Limestone.” *DFI Journal*, DOI: 10.1179/1937525514Y.0000000004.

The assessment of the load test results of drilled shaft foundations (a collapsed and an uncollapsed) at the Turrell Arkansas Test Site is presented in Chapter 6. In particular, the effects of a collapsed excavation were determined by comparing the measured response from full-scale load test with the predicted responses that were obtained from software programs. The reference for the paper is: Race, M.L. and Coffman, R.A. (2015). “Response of a Drilled Shaft Foundation Constructed in a Redrilled Shaft Excavation Following Collapse.” *DFI Journal*, DOI: 10.1179/1937525515Y.0000000003.

A case study about the problems associated with the DSF construction at the Monticello Arkansas Test Site is presented in Chapter 7. Specifically, the effects of the construction problems at the MATS were discussed in relation to the load-movement response, the unit side resistance-movement response, and the unit base resistance-movement response from the full-scale load tests. The reference for the paper is: Race, M.L. and Coffman, R.A. (2015). “Case Study: Drilled Shaft Foundation Construction Problems.” *International Journal of Geotechnical Case Histories*, Submitted for Review, IJGCH-S86.

A technical paper discussing the calibration of resistance factors utilizing the Bayesian analysis method for DSF for different types of soil stratigraphy within Arkansas is presented in Chapter 8. Site-specific and geologic soil deposit-specific calibration studies were performed to determine resistance factor values for DSF within the state of Arkansas. The reference of the paper is: Race, M.L., Bernhardt, M.L., and Coffman, R.A. (2015). “Utilization of a Bayesian

Updating Method for Calibration of Resistance Factors." *Journal of Geotechnical and Geoenvironmental Engineering*, In Preparation.

A summary of the results and recommendations throughout this dissertation including, but not limited to, a suitable geotechnical investigation method, the effects of construction methods, and obtained resistance factor values is presented in Chapter 9. Recommendations include: limiting the design of DSF in moderately hard to hard limestone to 0.1%D or 0.2cm movement, predicting the resistance of a DSF with a collapsed excavation, and determining the resistance of a DSF with poor concrete placement. Resistance factor values are recommended based on the geotechnical investigation method and the software program that are utilized during the design of the DSF.

1.5. References

Brown, D., Turner, J., and Castelli, R. (2010). "Drilled Shafts: Construction Procedures and LRFD Methods." FHWA Publication No. NHI-10-016, Federal Highway Administration, Washington, D.C., 970 pgs.

Race, M. L., Bey, S.M. and Coffman, R.A. (2015). "Statistical Analysis to Determine Appropriate Design Methodologies of Drilled Shaft Foundations." GEGE Journal, DOI: 10.1007/s10706-015-9854-z.

Race, M. L. and Coffman, R.A. (2015). "Load Tests on Drilled Shaft Foundations in Moderately Strong to Strong Limestone." DFI Journal, DOI: 10.1179/1937525514Y.0000000004.

Race, M.L. and Coffman, R.A. (2015). "Response of a Drilled Shaft Foundation Constructed in a Redrilled Shaft Excavation Following Collapse." DFI Journal, DOI: 10.1179/1937525515Y.0000000003.

CHAPTER 2: LITERATURE REVIEW: Drilled Shaft Foundation Analysis

2.1. Chapter Overview

The procedure for the design of drilled shaft foundations (DSF) includes the determining the soil properties from geotechnical investigation data and the soil-shaft interaction with design equations/software programs. The geotechnical investigation methods discussed include, but are not limited to, the standard penetration test, the cone penetration test, and the unconsolidated undrained triaxial compression test. The design equations presented are recommended by the Federal Highway Administration for the design of DSF in cohesive soil, cohesionless soil, and rock. Similarly, two software programs, FB-Deep and SHAFT, are discussed herein.

2.2. Field and Laboratory Geotechnical Investigation Techniques

Geotechnical techniques include field and laboratory testing methods to determine soil and rock properties such as total unit weight, undrained shear strength of cohesive soils, and friction angle of cohesionless soils. In particular, from the specific geotechnical investigation methods performed, the soil properties are determined by using empirical correlation values, empirical equations, or direct measurements. The amount of uncertainty in the soil property values is dependent upon the employed geotechnical investigation method, the type of soil tested, and the inherent variability of the test site (i.e. horizontal or vertical variability of the soil).

2.2.1. Field Techniques

Geotechnical investigations entail performing field and laboratory tests on clay, sand, or rock samples. The standard penetration test (SPT), performed in accordance with ASTM D1586 (2011), is an in situ testing method that is commonly used to characterize geomaterials in Arkansas. The SPT consists of hammering a 30mm split spoon sampler (Figure 2.1a) into

geomaterials, with a 63.5kg hammer, for a penetration of 45.7cm while recording the number of blows required to drive the sampler for each 15.2cm increment. The blow count (N) is the sum of the number of blows that were required to drive the sampler through the last 30.5cm of penetration. Energy and overburden pressure corrected blow count ($N_{1,60}$) are calculated by taking the N value and the sampling depth into account (Equations 2.1 through 2.3). Another in situ testing method is the cone penetration test (CPT), as performed in accordance with ASTM D3441 (2011). This method consists of a cone with a surface area of $10cm^2$ (Figure 2.1b) being pushed in the ground while the tip resistance (q_t), side friction (f_s), pore pressure (u), and shear wave velocity (V_s) are recorded. Other tests that may be performed in the field, to characterize geomaterials, include the torvane (TV) and the pocket penetrometer (PP). By performing these tests, values for the total unit weight, the undrained shear strength, and the internal friction angle are estimated or measured.

$$N_{60} = \frac{N \cdot \eta_H \cdot \eta_B \cdot \eta_S \cdot \eta_R}{60} \qquad \text{(Das 2013)} \qquad \text{Equation 2.1}$$

$$N_{1,60} = C_N \cdot N_{60} \qquad \text{(Das 2013)} \qquad \text{Equation 2.2}$$

$$C_N = \sqrt{\frac{95.8[\text{kPa}]}{\sigma'_v}} \qquad \text{(Liao and Whitman 1986)} \qquad \text{Equation 2.3}$$

N_{60}, in Equation 2.1, is the energy corrected blow count, N is the blow count value, η_H is the hammer efficiency (%), η_B is the correction for borehole diameter, η_S is the sampler correction, and η_R is the correction for rod length. $N_{1,60}$, Equation 2.2, is the overburden corrected blow count and C_N is the overburden correction factor. σ_v', Equation 2.3, is the effective vertical overburden pressure (kPa).

Figure 2.1. Photographs of a) the California split spoon sampler used for the SPT (Coffman 2011a) and b) the cone used for the CPT (as used during the geotechnical investigation at the MATS, TATS, and SSATS) by Coffman (2011b).

The methods used to obtain the various soil properties from field testing techniques include empirical correlations and empirical equations. Specifically, empirical correlations with the SPT blow count data are used to estimate the: soil shear strength (c_u), total unit weight (γ_T), and internal friction angle (ϕ') for cohesive and cohesionless soils. Correlations, from Vanikar (1986), are presented in Tables 2.1 and 2.2. The use of empirical equations enables determination of soil property values from SPT, CPT, TV, and PP tests. Likewise, empirical equations can also be used to determine the estimated friction angle (ϕ') and undrained shear strength (c_u) from SPT blow count values (Terzaghi and Peck 1967, Peck et al. 1974, Schmertmann 1975), as presented in Equations 2.4 through 2.7. Common direct measurements from the CPT test include tip resistance (q_t), sleeve friction (f_s), and pore pressure (u) measurements. Empirical equations are also commonly used to calculate the soil property values from tip resistance, side resistance, and pore pressure measurements that are obtained from conducting CPT. Utilizing the data from the CPT, soil types can be determined from the ratio of tip resistance to friction ratio (Q_t-F_e) and from the ratio of tip resistance to the normalized pore pressure ratio (Q_t-B_q) as presented in Figure 2.2. The equations utilized to obtain soil type and property values from CPT

measurements are also presented in Equations 2.8 through 2.14 (Robertson and Cabal 2012). Equations 2.6 and 2.7 were modified from the original versions (Terzaghi and Peck 1967, Hara et al. 1974) to determine the undrained shear strength in metric units.

Table 2.1. Empirical values for friction angle (ϕ), relative density (D_r), and total unit weight (γ) of granular soils based on the corrected blow count (N') of a standard split spoon sampler [modified from Vanikar 1986].

Description	Very Loose	Loose	Medium	Dense	Very Dense	
Relative Density, D_r	0	0.15	0.35	0.65	0.85	1
Corrected Standard Penetration Number, N	0	4	10	30	50	
Approximate Angle of Internal Friction, ϕ' (^{o})	25-30	27-32	30-35	35-40	38-43	
Approximate Range of Moist Unit Weight, γ (kN/m^3)	11.0-15.7	14.1-18.1	17.3-20.4	17.3-22.0	20.4-23.6	

Table 2.2. Empirical values for unconfined compressive strength (q_u) based on the corrected blow count (N) of a standard split spoon sampler [modified from Vanikar 1986].

Consistency	Very Soft	Soft	Medium	Stiff	Very Stiff	Hard
Unconfined Compressive Strength, q_u (kPa)	0	23.9	47.9	95.7	191.5	383.0
Standard Penetration Resistance, N	0	2	4	8	16	32
Approximate Range in Saturated Unit Weight, γ_{sat} (kN/m^3)		15.7-18.9	17.3-20.4	18.9-22.0		

The undrained shear strength is taken as 1/2 of the unconfined compressive strength. Use correlation for estsimating purposes only.

$$\phi = 54 - 27.6 \exp(-0.014 N_{1,60}) \quad \text{(Peck et al. 1974)} \quad \text{Equation 2.4}$$

$$\phi = \tan^{-1}[N/(12.2 + 2.9\sigma'_v)]^{0.34} \quad \text{(modified from Schmertmann 1975)} \quad \text{Equation 2.5}$$

$$s_u[\text{kPa}] = 100 * 0.06\ N \quad \text{(modified from Terzaghi and Peck 1967)} \quad \text{Equation 2.6}$$

$$s_u[\text{kPa}] = 100 * 0.29\ N^{0.72} \quad \text{(modified from Hara et al. 1974)} \quad \text{Equation 2.7}$$

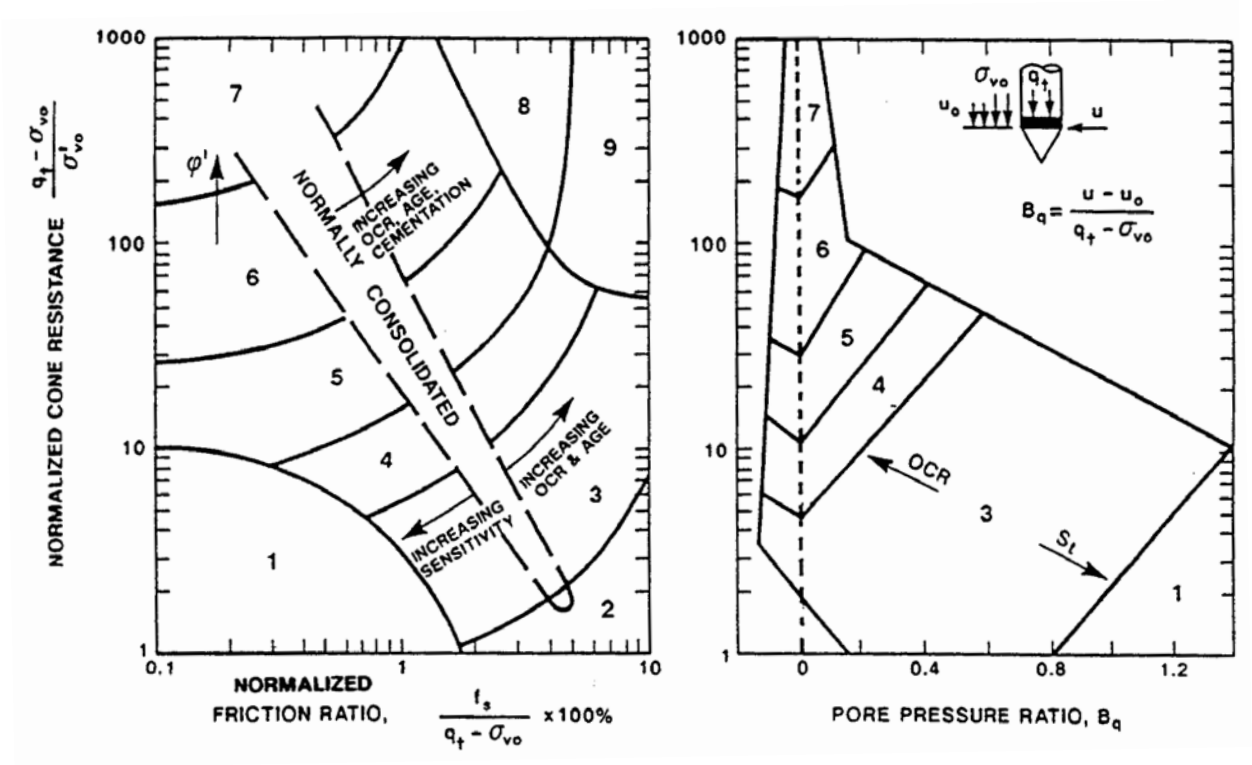

(a) **(b)**

Figure 2.2. Soil behavior type charts for determining the soil behavior normalized CPT data including a) Q_t and F_r and b) Q_t and B_q values [Robertson 1990].

$$Q_t = \frac{q_t - \sigma_{vo}}{\sigma'_{vo}}$$ (Robertson and Cabal 2012) Equation 2.8

$$F_r = \frac{f_s}{q_t - \sigma_{vo}}$$ (Robertson and Cabal 2012) Equation 2.9

$$B_q = \frac{u_2 - u_0}{q_t - \sigma_{vo}}$$ (Robertson and Cabal 2012) Equation 2.10

$$N_{60} = \frac{\left(\frac{q_t}{p_a}\right)}{8.5\left(1 - \frac{I_c}{4.6}\right)}$$ (Robertson and Cabal 2012) Equation 2.11

$$c_u(\text{kPa}) = 47.9 * \frac{q_t - \sigma_v}{N_{kt}}$$ (Robertson and Cabal 2012) Equation 2.12

$$\frac{\gamma_T}{\gamma_w} = 0.27\left[\log(R_f) + 0.36\log\left(\frac{q_t}{p_a}\right)\right] + 1.236$$ (Robertson and Cabal 2012) Equation 2.13

$$\phi'(\text{deg}) = 29.5 * B_q^{0.121}\left[0.256 + 0.336B_q + \log Q_t\right]$$ (Robertson and Cabal 2012) Equation 2.14

The variables used in Equations 2.8 through 2.14 include: the normalized cone tip resistance (Q_t), the corrected cone resistance (q_t), the in-situ vertical stress (σ_{vo}), the effective in-situ vertical stress (σ'_{vo}), the normalized friction ratio (F_r), the sleeve friction (f_s), the normalized pore pressure ratio (B_q), the pore pressure measured behind the cone (u_2), the in-situ equilibrium pore pressure (u_0), the corrected blow count value for 60 percent energy (N_{60}), the atmospheric pressure, 101.3kPa, (p_a), the soil type index (I_c), the undrained shear strength in units of kPa (c_u), a constant ranging from 10 to 18 (N_{kt}), the total unit weight of soil in pounds per cubic foot in units of kN/m^3 (γ_T), the unit weight of water in units of kN/m^3 (γ_w), the friction ratio (R_f), and the effective friction angle (ϕ').

2.2.2. Laboratory Testing Techniques

Index properties of geomaterials such as Atterberg limits, grain size, and specific gravity are typically obtained in the laboratory. The plastic limit (PL), the liquid limit (LL), and the plasticity index (PI) of cohesive soils as determined using ASTM D4318 (2010). The grain size of soil particles can be determined using a dry sieve, wet sieve, and/or hydrometers according to ASTM D421 (2010) and ASTM D422 (2010). The dry sieve analysis is utilized for cohesionless soils with low fines content. To determine the fines content of the soil, a wet sieve (#200 sieve) is commonly utilized. Hydrometers are utilized to determine the clay percentage for cohesionless and high fines content soils. The specific gravity of all soils can be determined using a water pycnometer as described in ASTM D854 (2010).

Laboratory tests used to characterize strength properties of geomaterials include the miniature vane (MV), as performed in accordance with ASTM D4648 (2011), the unconsolidated undrained triaxial compression test (UUTC), as performed in accordance with ASTM D2850 (2011), and the consolidated drained triaxial compression test (CDTC), as performed in accordance with ASTM D7181 (2011). The MV, UUTC, and CDTC devices are presented in Figure 2.3.

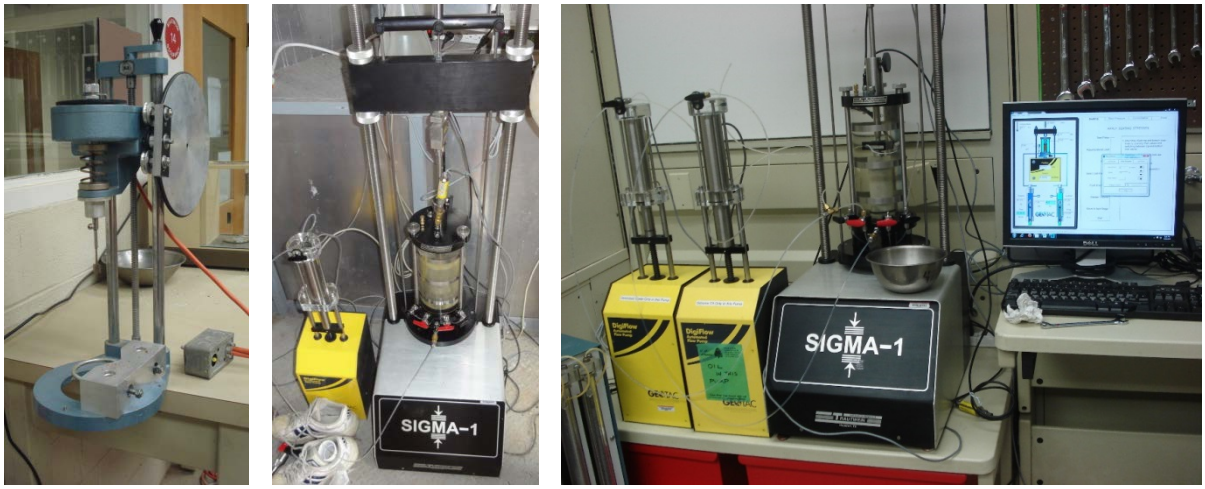

(a) (b) (c)

Figure 2.3. a) MV apparatus (Race 2013a), b) UUTC setup (Race 2012), and c) CDTC setup (Race 2013b).

2.2.3. Uncertainty Associated with Soil Properties

The amount of uncertainty within the soil properties is dependent upon the type of soil test that is utilized to test the soil, the type of soil, and the soil property of interest. The standard deviation for a given soil property is dependent upon the type of soil that is tested such as: highly plastic clay, medium plastic clay, low plastic clay, silt, sand, and gravel (Baecher and Christian 2003). The range of the coefficient of variation (COV) for the SPT can range between 14 and 100 percent while the range of the coefficient of variation for the CPT is 15 to 22 percent (Table 2.3). However, the mean (μ), standard deviation (σ), and COV values differ based upon the employed testing method and the type of soil. For example, according to Alshibli et al. (2009), the COV for the tip resistance, total unit weight, and overburden pressure from the CPT method (16 tests) were 19.6, 1.46, and 0.51 percent, respectively for "identical" soil deposits that were tested at the Louisiana Transportation Research Center Accelerated Load Facility Site. According to Wu (2013), the amount of uncertainty that is contributed by testing error is significantly smaller than the amount of uncertainty associated with the variability of the

material. In a similar fashion, interpolation regarding the lack of investigation into the depth of the groundwater elevation is commonly required because of the lack of water table depth sampling and temporal changes of the water table which also leads to larger amounts of uncertainty (Rogers and Chung 2013).

Table 2.3. Coefficient of variation for the SPT and the CPT [modified from Baecher and Christian 2003].

Test	Coefficient of Variation, COV (%)				
SPT	5-75	5-75	12-15	14-100	15-45
CPT	5	10-15	10-15	15-22	15-25

Along with the amount of uncertainty within the geotechnical investigation, the soil properties at a site vary depending upon the horizontal and/or vertical location within the site. The spatial variability of the soil has been previously determined using trend and autocovariance models (DeGroot 1996). According to DeGroot (1996), the estimates for the μ, the σ, and the COV values (Equations 2.15 to 2.17, respectively) are useful methods to characterize the amount of uncertainty of soil. A method which can be utilized to determine the soil variability (particularly the vertical spatial variability) is the trend method. The trend method, as presented in Figure 2.4, is utilized by implementing regression analysis (Equation 2.18) to the soil properties. Because the correlated relationship between soil property values is not considered in the trend method, the autocovariance method is recommended by DeGroot (1996). Specifically, the autocovariance function (Equation 2.19) is utilized to analyze the spatial variability of soil properties. The autocovariance functions have been previously estimated using the method of moments, the maximum likelihood method, or the best linear unbiased estimator method in geostatistics. In general, the autocovariance for in situ soil properties is greater in the horizontal direction than in the vertical direction (DeGroot 1996). Using the spatial variability of a site and

the available soil properties, the soil properties of the unsampled locations can be estimated using the trend or autocovariance methods.

$$\mu(x) = \frac{\sum_i^n x_i}{n} \quad \text{(DeGroot 1996)} \quad \text{Equation 2.15}$$

$$\sigma(x) = \left(\frac{\sum_i^n (x_i - \mu(x))^2}{n-1}\right)^{0.5} \quad \text{(DeGroot 1996)} \quad \text{Equation 2.16}$$

$$\mathrm{COV}(x) = \frac{\sigma(x)}{\mu(x)} \quad \text{(DeGroot 1996)} \quad \text{Equation 2.17}$$

$$x_i = t_i + \epsilon_i \quad \text{(DeGroot 1996)} \quad \text{Equation 2.18}$$

$$C_x(r) = \frac{\sum_i^n (x_i - \mu[x])(x_{i+r} - \mu[x])}{n-1} \quad \text{(DeGroot 1996)} \quad \text{Equation 2.19}$$

From Equation 2.15, $\mu(x)$ is the estimated mean of the soil property as a function of x, x_i is the soil property, and n is the number of samples. The variables utilized in Equations 2.18 and 2.19 include the soil property at depth i (x_i), the values of the trend function at depth i (t_i), the residual at depth i (ε_i), the autocovariance function (C_x), and the separation distance (r).

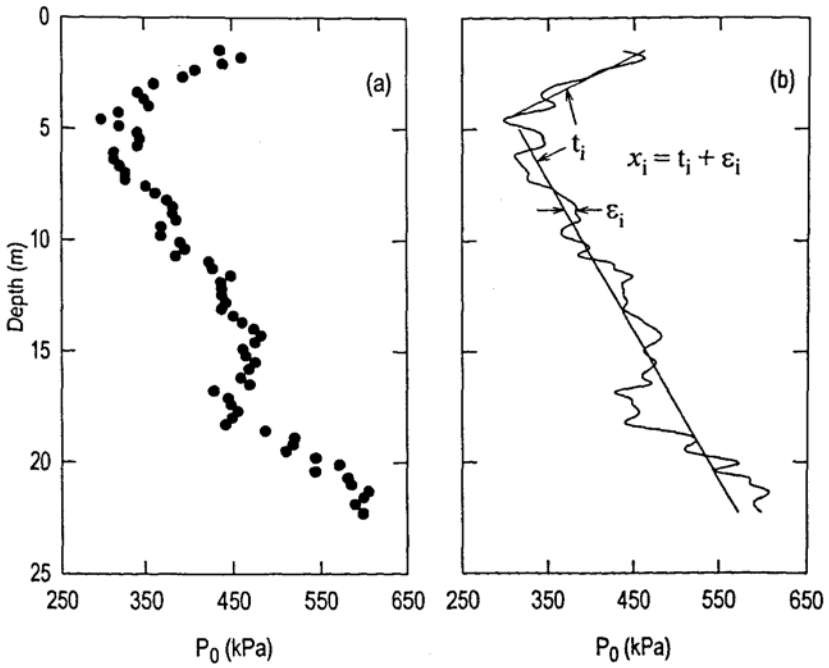

Figure 2.4. Trend method utilizing dilatometer readings at the University of Massachusetts Amherst National Geotechnical Experimental Testing Site (DeGroot 1996).

In Phoon et al. (2003), the modified Bartlett statistic was utilized to determine the stationarity of the soil. This method was recommended by Phoon et al. (2003), instead of the trend and autocovariance methods, because it enables the use of established hypothesis testing and rejection criteria. Following the determination of theoretical autocorrelation (as estimated using Equation 2.20), the critical modified Bartlett test statistic (for five percent significance level) was calculated using the equations that are in Table 2.4. The simplest and most widely used autocorrelation model for soil properties is the single exponential model (Phoon et al. 2003). To implement the modified Bartlett test for the stationarity of soil at a test site, three parameters (k, I_1, and I_2 in Equations 2.21 to 2.23, respectively) must be determined.

$$R(\tau = j\Delta z) = \frac{\sum_{i=1}^{n-j}\left[x(z_i)x(z_{i+j})\right]}{s^2(n-j-1)}$$ (Phoon et al. 2003) Equation 2.20

The variables in Equation 2.20 include the autocorrelation function (R), the absolute value of the depth coordinates (τ), a counter number (j), the sampling interval (Δz), the number of data points (n), the depth at point I (z_i), the depth at point i+j (z_{i+j}), and the sample variance (s^2).

Table 2.4. Critical modified Bartlett test statistic (five percent significance level) for autocorrelation model [modified from Phoon et al. 2003].

Autocorrelation Model	Rejection Criteria
Single Exponential	$(0.23k + 0.71)\ln(I_1) + 0.91k + 0.23$
Binary Noise	$(0.30k + 0.29)\ln(I_1) + 1.15k - 0.52$
Cosine Exponential	$(0.28k + 0.43)\ln(I_1) + 1.29k - 0.40$
Second-Order Markov	$(0.42k + 0.07)\ln(I_1) + 2.04k - 3.32$
Squared Exponential	$(0.73k + 0.98)\ln(I_1) + 2.35k - 2.45$

$$k = \frac{\delta}{\Delta z}$$ (Phoon et al. 2003) Equation 2.21

$$I_1 = \frac{n}{k}$$ (Phoon et al. 2003) Equation 2.22

$$I_2 = \frac{m}{k}$$ (Phoon et al. 2003) Equation 2.23

The variables utilized in Equation 2.21 include the number of points in one scale of fluctuation (k), the scale of fluctuation (δ), and the spacing between sample points (Δz). While, the variables in Equations 2.22 and 2.23 include the normalized sampling length (I_1), the total number of sample points in a soil record (n), the normalized segment length (I_2), and the number of sample points in one segment that corresponds to half of the sampling record (m).

2.3. Drilled Shaft Design

The predicted axial capacity of DSF in cohesive soil, cohesionless soil, and rock consists of the summation of the side resistance along the length of the DSF and the end bearing resistance at the base of the DSF. Multiple equations/software programs exist to determine the soil-shaft interaction, including FB-Deep and SHAFT software programs. There are full-scale load tests (bi-directional load cell [BLC] test, statnamic test, top-down test) that can be performed to confirm or exceed the predicted axial resistance of DSF. Case histories that describe results from BLC tests performed on DSF constructed in rock or constructed in soils are discussed herein.

2.3.1. Design Techniques

The axial capacity and the load-movement behavior of drilled shaft foundations (DSF) have been shown to be dependent upon the type of the geological formation (bedrock, cohesionless soil, cohesive soil, mixed soil layers). Therefore, the axial capacity of drilled shafts is the summation of the side resistance along the DSF and the end bearing resistance at the base of the DSF (Equation 2.24). As shown in Figure 2.5, the side resistance along a portion of the length of the DSF (R_{SN}) is calculated by using Equation 2.25 (the surface area of DSF times the unit side friction between the soil and the DSF). Likewise, the end bearing resistance of a DSF is calculated using the area of the base of the DSF times the unit end bearing resistance (Equation 2.26). Although the equations that have been previously used to calculate the side resistance and end bearing resistance were the same for all stratigraphy (rock, cohesive soil, and cohesionless soil), the methods that have been employed to calculate the unit side resistance and the unit end bearing resistance vary depending on the stratigraphy and exploratory methods that were

performed/utilized (as previously mentioned in Section 2.2). A general depiction of the resistance upon a DSF is presented in Figure 2.5.

$$R_{TN} = \sum_{i=1}^{n} R_{SN,i} + R_{BN} \qquad \text{(O'Neill and Reese 1999)} \qquad \text{Equation 2.24}$$

$$R_{SN} = \pi D f_s L \qquad \text{(Brown et al. 2010)} \qquad \text{Equation 2.25}$$

$$R_{BN} = \frac{\pi D^2}{4} q_b \qquad \text{(Brown et al. 2010)} \qquad \text{Equation 2.26}$$

The variables utilized in Equation 2.24 include: the total axial capacity (R_{TN}), the side resistance from layer I ($R_{SN,i}$), the layer number (n), and the end bearing resistance (R_{BN}). In Equations 2.25 and 2.26, the R_{SN} and R_{BN} terms are calculated using the following information: the diameter of the DSF (D), the unit side resistance of the soil (f_s), the length of the section (L), and the unit base resistance of the soil (q_b).

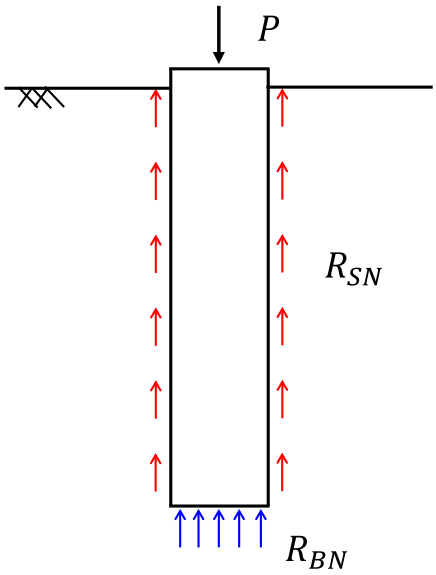

Figure 2.5. Free-body diagram of the soil/rock resistances of a DSF.

2.3.1.1. Cohesive Soils

As recommended by O'Neill and Reese (1970), the unit side resistance of a DSF in contact with cohesive soil is calculated using the Alpha method (Equation 2.27). In Equation 2.27, the shear strength reduction factor (α) has been employed because the peak stress in soil, due to movement of the pile, is less than the undrained shear strength of the soil. The value of α has been shown to be a function of the following variables: the type of soil, the strength of soil, the type of concrete, the depth of soil level, the method of construction, the time between casting and loading, and the time of loading (fast or slow). In particular, as presented in Table 2.5, the α coefficient varies based on the depth within the soil deposit and the undrained shear strength (s_u) as presented in Table 2.5. Like with the side resistance, O'Neill and Reese (1999) also showed that the end bearing resistance of a DSF in cohesive soil is also a function of the undrained shear strength of the soil (Equation 2.28).

$$f_s = \alpha \cdot c_{u,avg}$$ (Tomlinson 1957; O'Neill and Reese 1999) Equation 2.27

$$q_p = N_c^* \cdot s_u$$ (O'Neill and Reese 1999) Equation 2.28

Equations 2.27 and 2.28 are used to determine the resistance values in Equations 2.24 and 2.25. Specifically, the previously unpresented variables used in Equations 2.27 and 2.28include: the average undrained shear strength of the layer ($c_{u,avg}$), the bearing capacity constant (N_c^*), and the undrained shear strength from the base of the DSF to two times the diameter below the base of the DSF (s_u). Depending upon the Young's modulus of the soil (E_u), a factor approximately equal to the ratio of E_u to three times s_u (I_r), and the undrained shear strength of the soil (s_u), the end bearing capacity constant (N_c^*) ranges from 6.5 to 9.0, as presented in Table 2.6 (Brown et al. 2010).

Table 2.5. Evaluation of α (modified from Brown et al. 2010).

Value of α	Constraints
0	Ground surface to a depth of 5 feet or to the depth of seasonal moisture change
0.55	$\frac{s_u}{p_a} \leq 1.5$
$0.55 - 0.1\left(\frac{s_u}{p_a} - 1.5\right)$	$1.5 \leq \frac{s_u}{p_a} \leq 2.5$

Table 2.6. Values of end bearing capacity, N_c^* (modified from Brown et al. 2010).

Undrained Shear Strength, s_u (kPa)	$I_r \approx \frac{E_u}{3s_u}$	N_c^*
23.9	50	6.5
47.9	150	8.0
95.7	250-300	9.0

2.3.1.2. Cohesionless Soils

Furthermore, O'Neill and Reese (1999) suggested that the sections of the DSF that are in contact with cohesionless soil should be evaluated for unit side resistance and unit end bearing resistance using the Beta method (Equations 2.29 and 2.30). Another method of determining the unit end bearing resistance is presented in Equation 2.31.

$$f_s(\text{MPa}) = \sigma'_v \cdot k \cdot \tan\delta \quad \text{(Meyerhof 1976; O'Neill and Reese 1999)} \quad \text{Equation 2.29}$$

$$q_p(\text{MPa}) = \frac{0.0384 \cdot N \cdot L_b}{D} \cdot 0.384N \quad \text{(modified from Meyerhof 1976)} \quad \text{Equation 2.30}$$

$$q_p(\text{MPa}) = 0.0574 * N_{60} \leq 2.9\text{MPa} \quad \text{(modified from O'Neill and Reese 1999)} \quad \text{Equation 2.31}$$

The results from Equations 2.29 to 2.31 are commonly used to determine the resistance values by using the previously resented Equations 2.25 and 2.26. Variables that have not been previously presented that are utilized in Equations 2.29 to 2.31 include: the vertical effective stress in units of MPa (σ'_v), the coefficient of horizontal earth pressure (k), the side friction

between the soil and the DSF (δ), the length of the DSF within soil (L_b), and the diameter of the pile (D).

2.3.1.3. Rock

The axial capacity for DSF that are constructed in rock has been shown to also be predicted using the summation of the side resistances and the end bearing resistance. Numerous methods exist to calculate the unit side resistance values or end bearing values in rock. The calculation methods utilized for rock have been shown to be dependent upon the characteristics of the rock (strength, fracture, etc.) and the characteristics of the rock socket (smooth or rough) in which the capacity was measured or tested. As presented in Table 2.7, the methods that are used to calculate the side friction of rock include (but are not limited to) O'Neill and Reese (1999), Horvath and Kenney (1979), Carter and Kulhawy (1988), Rowe and Armitage (1987), and McVay et al. (1992). Likewise, the methods used to calculate the end bearing capacity of intact rock are found in: Rowe and Armitage (1987), AASHTO (1989), Kulhawy and Goodman (1980), Bishnoi (1968), Canadian Geotechnical Society (1985), and Zhang and Einstein (1998).

Table 2.7. Equations to calculate side friction and end bearing resistance for drilled shaft foundations constructed in rock.

Shaft Property	Equation	Source (modified from)
Side Friction (Unit)	$f_{max,i} = 0.65 p_a \left[q_{u,i}/p_a\right]^{0.5}$ $f_{max,i} = 0.8 \left[\frac{\Delta r}{r}\frac{L'}{L}\right]^{0.45} q_{u,i}$	O'Neill and Reese (1999)
	$f_s = 64.1\sqrt{q_u}$	Horvath and Kenney (1979)
	$f_s = 60.3\sqrt{q_u}$	Carter and Kulhawy (1988)
	$f_s = 138.8\sqrt{q_u}$	Rowe and Armitage (1987)
	$f_s = 185.7\sqrt{q_u}$	
	$f_s = 47.9\sqrt{q_u}\sqrt{q_t}$	McVay et al. (1992)
End Bearing (Unit)	$q_{max} = 2.7 q_u$	Rowe and Armitage (1987)
	$q_{max} = N_{ms} q_u$	AASHTO (1989)
	$q_{max} = 95.8 J c N_{cr}$	Kulhawy and Goodman (1980); Bishnoi (1968)
	$q_{max} = 3 q_u K_{sp} L$	Canadian Geotechnical Society (1985)
	$q_{max} = 462.7 {q_u}^{0.51}$	Zhang and Einstein (1998)

The variables that are presented in Table 2.7 and are utilized to determine the unit side resistance of the DSF in the rock include: the unit side resistance in units of kPa (f_s), the unconfined compressive strength of the intact rock in units of psi (q_u), and the tensile strength of the intact rock (q_t). The variables that are presented in Table 2.7 and are utilized to determine the end bearing resistance of rock include: the maximum unit end bearing resistance (q_{max}), a function of rock mass quality and rock type (N_{ms}), the correction factor depending on normalized spacing of horizontal joints (J), the cohesion of the rock mass (c), an empirical factor based on discontinuity spacing, socket width (K_{sp}), and discontinuity aperture, and the length of the DSF within soil (L).

As presented in Table 2.8, the current design methods that are used to predict the axial capacity and load-movement relationship for drilled shaft foundations in soils are outlined in Brown et al. (2010). As shown in Brown et al. (2010), the side resistance is calculated as the

surface area in contact with the soil multiplied by the unit side resistance for each type of soil (i.e. cohesive and cohesionless soil) and for rock. Similarly, as shown in Brown et al. (2010) the end bearing resistance is the determined by multiplying the surface area of the base of the drilled shaft foundation by the unit end bearing resistance. Although Brown et al. (2010) is currently used, the past design methods that have commonly been utilized to design DSF include O'Neill and Reese (1999) and Reese and O'Neill (1988). Based on results from Gunaratne (2006), as shown in Figure 2.6, for a 0.9m diameter DSF constructed in sandy soil, the cumulative side resistance ranges from approximately 890kN to 5338kN at a depth of 27.4 meters. As shown in Table 2.9, each of the components that are used to estimate the axial capacity of a DSF, such as side resistance of rock sockets.

Table 2.8. Design equations for side friction and end bearing resistance of DSF [modified from Brown et al. 2010].

DSF Resistance	Type of Geomaterial	Equation	Constraints
Side Resistance	Cohesive	$R_{SN} = \pi \cdot B \cdot \Delta z_i \cdot (\alpha \cdot s_u)_i$	α from Table 2.5
	Cohesionless	$R_{SN} = \pi \cdot B \cdot \Delta z_i \cdot (\sigma'_v \cdot k \cdot \tan\delta)$	
	Rock	$R_{SN} = \pi \cdot B \cdot \Delta z_i \cdot (0.65 \cdot \alpha_e \cdot \sqrt{q_u \cdot p_a})$	
End Bearing Resistance	Cohesive	$R_{BN} = \frac{\pi \cdot B^2}{4}(N_c^* \cdot s_u)$	$N_c^* \leq 9.0$
	Cohesionless	$R_{BN} = \frac{\pi \cdot B^2}{4}(57.4 \cdot N_{60})$	$q_{BN} = 57.4N_{60}$ or $q_{BN} \leq 2.9MPa$
	Rock	$R_{BN} = \frac{\pi \cdot B^2}{4}(N_{cr}^* \cdot q_u)$	$N_{cr}^* = 2.5$

Table 2.9. DSF side shear design methods for rock sockets [modified from Gunaratne 2006].

Source	Side Shear Resistance, f_s (MPa)	
Carter and Kulhawy (1988)	$f_s = 0.0144 \cdot q_u$	for $q_u \leq 1.9$MPa
Horvath and Kenney (1979)	$f_s = 0.0642 \cdot {q_u}^{0.5}$	for $q_u \leq 1.9$MPa
McVay et al. (1992)	$f_s = 0.0479 \cdot {q_u}^{0.5} \cdot {q_t}^{0.5}$	

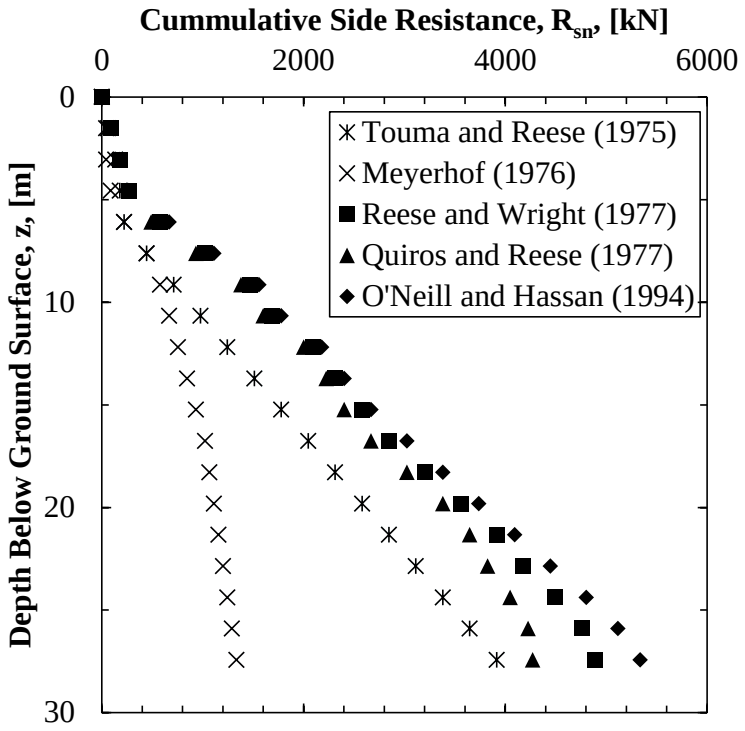

Figure 2.6. Comparison of estimated side shear capacities in sandy soil for a 0.9m diameter DSF [modified from Gunaratne 2006].

2.3.2. Static Estimation Software Programs

Two commonly utilized software programs that can predict the axial capacity of DSF are FB-Deep, version 2.04 (2012), (Townsend 2003a, Townsend 2003b) and SHAFT, version 2012, (Reese et al. 2012a, Reese et al. 2012b). The FB-Deep software program was developed by the Bridge Software Institute at the University of Florida. The SHAFT software program was commercially released in 1987 by Dr. Lymon C. Reese; since then seven versions of SHAFT have been released by ENSOFT, Inc.

The axial capacity and load-movement values, as obtained by using FB-Deep or SHAFT, are predicted by utilizing methods obtained from the Federal Highway Administration (FHWA) report FHWA-NHI-10-016 (Brown et al. 2010) and the American Association of State Highway and Transportation Officials (AASHTO) Load and Resistance Factor Design (LRFD) Bridge Design Specifications (AASHTO 2007). Using the FB-Deep software program, SPT values are utilized with empirical relationships (to CPT data) as developed for typical Floridian soils (Schmertmann 1967; Bloomquist et al. 1992). Specifically, measured soil properties (direct CPT or SPT-CPT relationships) are utilized to predict axial capacity by using the relationships developed by Schmertmann (1978), Bustamante and Gianeselli (1982), and Bloomquist et al. (1992). The axial capacity, as obtained using the SHAFT software program, is predicted based on the analysis methods developed by: O'Neill and Reese (1999), Skempton (1951), and Sheikh and O'Neill (1986) for cohesive soil; by O'Neill and Reese (1999), Meyerhof (1976), and Quiros and Reese (1977) for non-cohesive soil; and by Hovarth and Kenney (1979), Canadian Geotechnical Society (1978), and Bieniawski (1984) for rock. Moreover, the developed load-movement curves are predicted based on the normalized displacement curves obtained from Reese and O'Neill (1988).

2.3.3. Other Design Considerations

According to Brown et al. (2010), improper construction methods employed by contractors may compromise the quality of DSF. Specifically, the placement of concrete (i.e. workability of concrete and compatibility of the rebar and concrete), the stability of the excavation, and the contamination of the soil (i.e. the bond between concrete and soil) are construction factors that have been shown to affect the axial capacity of DSF (Brown 2004). Furthermore, an unbalanced fluid pressure (drilling fluid pressure and the hydrostatic

groundwater pressure) within a drilled excavation (stress relief) may cause soil softening and lead to the formation of large cavities around temporary casing (Brown 2004). According to Brown (2004), in areas with potential caving ground conditions, full length segmental casing has proven to be effective at improving stability of the excavation prior to and during placement of the concrete.

According to Brown et al. (2010), other considerations in the design of DSF in cohesive soils include the resistance at the top portion of the DSF and the use of temporary or permanent casing. Specifically, common practice is to ignore the resistance of the top 1.5m of the DSF due to wetting and drying cycles. Similarly, the resistance at the bottom one diameter length of the DSF has previously been ignored (O'Neill and Reese 1999 and AASHTO 2007) due to a "zone of tension"; however, this has not be confirmed by full-scale load testing (Brown et al. 2010). Finally, when permanent casing is used, the side resistances along the DSF are reduced. Recommended reduction factors for DSF with permanent steel casing range from 0.5 to 0.75 (Brown et al. 2010).

2.3.4. Uncertainty in Design of Drilled Shaft Foundations

In addition to the uncertainty associated with the geotechnical investigation, uncertainty exists within the design and implementation of DSF. Although related to piles and not DSF, Olson and Iskander (2009) stated that the use of 1993 API RP-2A resulted in an underprediction of axial capacity for shorter piles (pile lengths less than 20 meters) and an overestimation for piles greater than 20 meters in length. Moreover, Petek et al. (2002) indicated that the geometry of a DSF, in particular location and extent of any defects occurring during the construction process, can adversely (or beneficially) affect the axial capacity and load-movement curves. As stated in Kort and Kostaschuk (2007), the irregularity of the shape of the DSF was evaluated

using case studies and numerical modeling software program (FLAC). Specifically, a load test that was performed on a DSF in Molokai, Hawaii, that had a portion in a 1.2m diameter DSF with a length of 25m that had a cave of approximately 4.3m in diameter. The assumption that the collapsed DSF would be stronger than a DSF with a uniform diameter was evaluated by performing numerical modeling. It was determined that the upward movement (for a bi-directional load test) for a DSF with a bulge was half of what the upward movement would be for a DSF without a bulge (for the same applied load).

Depending on the method/software program utilized in the design of a DSF, the predicted capacity value has been shown to include numerous types of uncertainty. Specifically, according to Zhang et al. (2004), sources of uncertainty have been found in the: inherent soil variability, loading effects, time effects, errors in soil boring, sampling method employed, in situ and laboratory testing, characterization of shear strength, and stiffness of soils. This uncertainty is accounted for by using load and resistance factors in a LRFD methodology.

2.4. Full-Scale Field Testing of Drilled Shaft Foundations

According to Brown et al. (2010), three primary field tests are commonly used to measure the axial or lateral capacity of DSF. These methods include: top-down load testing, bi-directional (Osterberg) load testing, and Statnamic load testing. Full-scale load tests are performed to 1) determine the load transfer characteristics for the side and base resistance or 2) verify the capacity of a test/production DSF (Brown et al. 2010). Based on Brown et al. (2010), the primary benefits and limitations of full-scale load testing are summarized in Table 2.10.

Table 2.10. Summary of the benefits and limitations of field load tests [modified from Brown et al. 2010].

Benefits	Limitations
1. Test can provide a direct measure of resistance of the geologic formation and performance of the construction methods 2. The design methodology (i.e. software program/design equations) can be refined to accurately represent the geologic conditions. 3. The overall reliability of the foundation is improved. 4. Higher resistance factors can be used in the design of DSF. 5. A more efficient design of the DSF can be utilized by reducing DSF length (reducing cost and time).	1. The measurement of field load tests may be limited in highly variable geology. 2. Monetary resources and time are required for field load tests. 3. Likely there is no economic benefit for small projects (small number of DSF). 4. In cases where the design of the DSF is controlled by some other consideration such as scour, field load testing may not be beneficial.

2.4.1. Conventional (Top-Down) Load Testing

According to Brown et al. (2010), the conventional top-down load testing is the most reliable method to measure the static characteristic of the DSF. Kyfor et al. (1992) stated that static top-down testing can be performed using three methods: 1) load applied directly onto a platform on the pile head, 2) load applied by using a jack against a loaded platform, or 3) load applied by using a jack against a beam anchored to piles/shafts/anchors. Static top-down load tests are typically performed on smaller diameter DSF in soil because high capacity DSF (in rock and large diameter) require large loads to be used for the reaction system. A photograph of the conventional full-scale load test is presented in Figure 2.7. In regards to the reaction system, the system is designed for horizontal adjustment to avoid twisting and eccentric loading. Furthermore, in accordance with ASTM D1143 (2013), five percent of the “anticipated failure load” is maintained for four to 15 minutes for at least five loading increments.

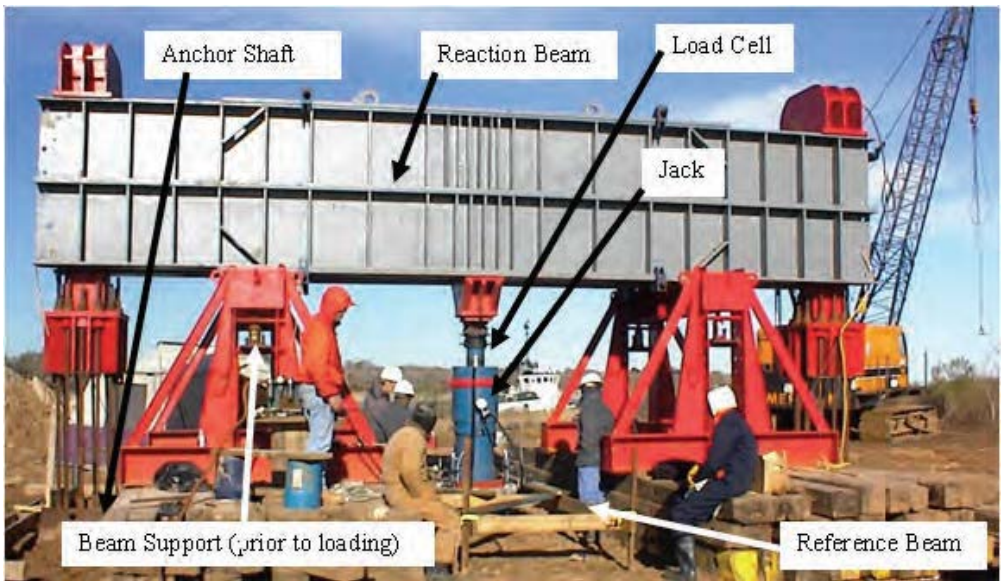

Figure 2.7. Conventional static full-scale load test on DSF [photograph from Bill Isenhower in Brown et al. 2010].

2.4.2. Bi-Directional Load Testing

According to Osterberg (1984), an equivalent top-down (conventional) load-movement curve may be determined from data obtained from a bi-directional full-scale load test which typically utilizes a bi-directional load cell (BLC) or an Osterberg Cell (O-Cell). Furthermore, the shaft movement attributed to 1) the side resistance and to 2) the end bearing resistance may be determined, using a BLC, during the full-scale load test. The method described in Osterberg (1984) is commonly utilized to develop the equivalent top-down load-movement curve from the full-scale load test using an O-Cell.

An equal upward and downward force is exerted from the BLC. At various times, the values of the water pressure within the BLC are measured, recorded, and also converted into values of force (utilizing a calibration curve). Likewise, at various times, the movements of telltale indicators, located within steel pipes that are welded to the top and bottom steel plates of the BLC, are measured and recorded using displacement gages and a data logger, respectively. These force and movement readings are recorded until: 1) the maximum capacity of either the

side resistance or end bearing is achieved, 2) too much movement has occurred, or 3) the maximum capacity of the BLC device has been reached. The upward and downward movements of the BLC are then used to determine the equivalent full-scale top-down load-movement curves as presented in Figure 2.8.

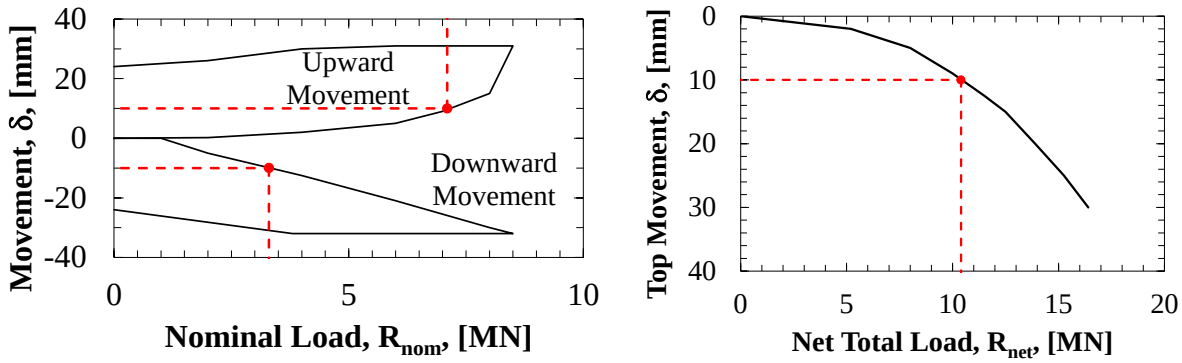

Figure 2.8. Typical data from a full-scale load test using an O-Cell a) upward and downward movement curves and b) equivalent top-down load-movement curve [modified from Osterberg 1984].

The BLC can be used in a single level, multi-level, or in conjunction with conventional top-down loading to acquire measurement of the DSF resistance. Furthermore, bi-directional load tests can be performed on production DSF as long as the void is grouted and the upward movement is limited to 1.3cm (recommended by Brown et al. 2010). There is very small comparative test data for BLC tests and conventional top-down load tests; however, the difference in loading conditions between the BLC test and the top-down tests were described in McVay et al. (1994) and in O'Neill et al. (1996) and include the lower amount of compression in the concrete and the load transfer increases with depth for the BLC test (instead of decreases with depth in a conventional top-down test). According to Brown et al. (2010), analytical models (from Shi 2003) have been used to suggest that the equivalent top-down load movement curve from BLC testing may underpredict side resistance.

For example, equivalent top-down load-movement curve for BLC testing were derived from tests described in Kishida et al. (1992) and Ogura et al. (1995). The conversion method to go from BLC to top-down was developed from a total of four drilled shaft/driven pile foundations (three in compression and one in tension). From a comparison between DSF with BLC and adjacent bored piles in Singapore, it was determined that there was a four percent difference in ultimate capacity between the shaft with a BLC and the shaft without a BLC (Molnit and Lee 1998). Similarly, by using finite element method, Fellenius et al. (1999) concluded that the load-movement curve from top load testing (conventional load test) can be predicted by using the equivalent load-movement curve from BLC testing,.

2.4.3. Rapid Load Testing

Rapid load testing is utilized to apply loading such that the inertial and damping effects of the DSF in soil/rock are important. The load pulse to the DSF, as applied during a Statnamic load test, involves a mass of approximately five to ten percent of the predicted axial capacity be applied onto the test DSF in accordance with ASTM D7383 (2010). As mentioned in Brown et al. (2010), two types of rapid load tests have been utilized. These tests have included dropping a heavy mass onto a soft cushion that was located on top of the test DSF or using combustion gas pressure to accelerate a heavy mass on top of the test DSF. The Statnamic loading device is a type of rapid loading test which can apply top loads up to 5000 tons. The loading and subsequent displacements and strains of the DSF (Figure 2.9) can be utilized to determine the static axial resistance of the DSF by using the procedures described in Brown et al. (2010). Although the rapid load test is quick and large can be applied, the rate effects must be considered and the maximum test load is still limited.

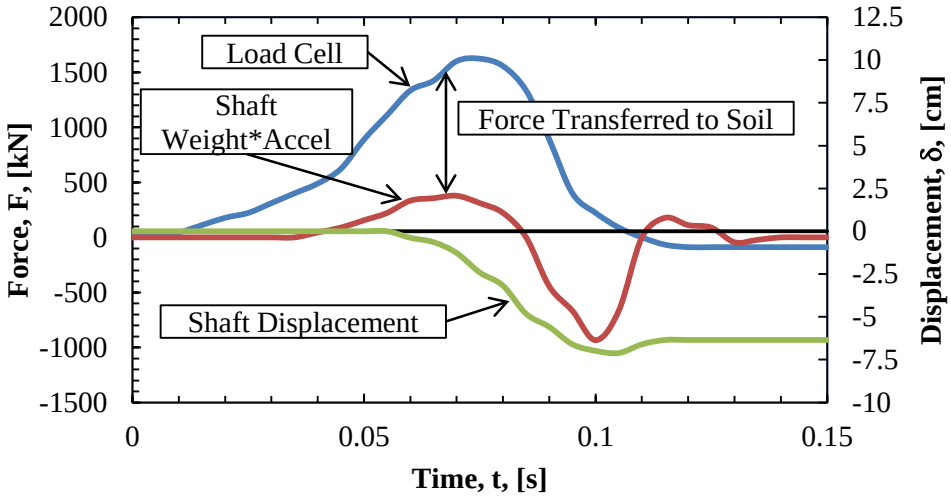

Figure 2.9. Force and displacement measurements of a rapid load test (Statnamic) on a DSF [modified from Brown et al. 2010].

2.4.4. Case Histories Utilizing Bi-Directional Load Tests

2.4.4.1. Case Histories in Rock

BLC tests are commonly utilized to compare the predicted and measured values of unit side resistance and the values of end bearing resistance. This type of load testing has been utilized to test DSFs constructed in very weak rock (approximately q_u = 0.69MPa), as reported in McIntosh and Knott [2000], to moderately strong rock (approximately unconfined compressive strength [f'_r] equal to 68.9MPa), as reported in Gunnink and Keihne (2002). According to Gunnink and Kiehne (2002), three DSFs were embedded in Pennsylvanian aged limestone and shale with rock socket lengths of 1.4m, 1.5m, and 1.6m for Shaft 1, Shaft 2, and Shaft 3, respectively. For Shafts 1, 2, and 3, failure (identified as the inability of DSF to hold the applied load) occurred at loads of 3,500kN, 1,500kN, and 3,800kN, respectively, with unit side resistance values of 2.3MPa, 0.9MPa, and 2.3MPa and end bearing resistance values of 21.4MPa, 9.1MPa, and 22.9MPa, respectively. As reported in Castelli and Fan (2002), in Jacksonville, Florida, four test shafts with diameters of 91.5cm, 122.0cm, 183.0cm, and 183.0cm

were tested using BLCs. One of the DSF (91.5cm diameter) was founded in cemented limestone with a design side resistance resistance of 1,440kPa. Based on this test, the predicted unit side resistance values (1,440kPa), as obtained from the McVay et al. (1992) method, was consistent with the measured value (1,240kPa) in the limestone.

Brown (2009) discussed two DSFs that were constructed in Nashville, Tennessee. From the observed unit side resistance values, it was determined that mobilization of the unit side resistance occurred at a displacement of 0.5cm. The movements of the two DSF were only one percent (approximately 1.3cm and 0.8cm downward movement of the BLCs) of the base diameter (effective base diameters of 1.0m and 0.7m, respectively) when the base resistance values were determined. From the full-scale load tests, it was determined that design values (side resistance values of 0.96MPa) could be utilized that were higher than the values that had been previously used at similar sites.

In Axtell and Brown (2011), four 3.5m diameter DSFs were utilized in the design and construction of the New Mississippi River Bridge located north of St. Louis, Missouri. The test shaft for these foundations was socketed 7.1m into moderately strong limestone ($f'_r > 69$MPa with an average f'_r value of approximately 166MPa). However, for Piers 11 and 12, there was a layer of lower strength rock that was approximately 1.5m thick with f'_r value equal to 35MPa at a depth of 6.1m (near the bottom of the designed DSF length). Four BLCs (total capacity of 213.5MN) were used at one level to confirm the side and base resistance values and the quality of the construction methods. The average unit end bearing and unit side resistance in the rock socket were 22MPa and 2.1MPa, respectively (Axtell and Brown 2011). These values were not the ultimate strength values because very small movements were measured (displacement values less than 0.4cm in either direction corresponding to 0.1 percent of the diameter of the DSF).

Values of end bearing resistance are sometimes not utilized or not accounted, in the state of Florida, for in the design of DSF constructed in limestone due to the brittle and karstic nature of the limestone (Castelli and Fan 2002). However, the end bearing resistance for a 915mm diameter by 12.53m long DSFF that was founded on or in limestone was significant (8.33MPa at a displacement value of 6mm). In the Newberry area in Florida, due to difficult subsurface conditions that include very soft limestone with poor consistency and karstic conditions, a BLC was installed to estimate the shear strength of the Ocala limestone (McIntosh and Knott, 2000). For a drilled shaft foundation with a design capacity of 8100kN, the measured capacity that was obtained by personnel from Loadtest, Inc. was 9780kN, when accounting for the contribution of end bearing of the drilled shaft foundation. According to Castelli and Fan (2002), the end bearing resistance may be relied upon in the design of DSF in the state of Florida if a BLC is used to verify the capacity of the DSF.

Three BLC tests were performed in North Central Texas to determine the relationship between the values of soil and rock properties obtained from Texas cone penetration tests (TCPT) and the axial capacity of drilled shaft foundations (Nam and Vipulanandan 2010). Two drilled shafts were constructed in weak clay shale (q_u < 5MPa) and one drilled shaft was constructed in moderately weak limestone (q_u < 20MPa). Based on the results presented in Nam and Vipulanandan (2010), it was determined the TCPT may be used to predict the axial capacity of drilled shaft foundations in cases where the rock joints prevent the collection of intact rock cores, which therefore prevents the determination of the in-situ value for the uniaxial unconfined compressive strength of the rock.

2.4.4.2. Case Histories in Soils

To characterize the side resistance and end bearing resistance in soils, full-scale load tests have also been performed. A load test on DSF near the Phoenix Sky Harbor International Airport was performed in alluvial sand, gravel, and cobbles (Rabab'ah et al. 2011). The axial capacity of the DSF was two to three times the value of the axial capacity that was predicted by using the AASHTO (2002) method. The measures value of the side resistance was up to five times higher than the predicted value of the side resistance using equations from O'Neill and Reese (1999), Meyerhof (1976), and Kulhawy (1991). In Hammond (2004), the axial capacity of eight DSF in alluvial deposits (clays underlain by very dense sand with some silt and gravel) was tested using BLC tests. From the measured side resistance values, the Alpha and Beta values were determined for the cohesive and cohesionless soils, respectively. The average Alpha value for the silty clay was determined to be 0.57 with a coefficient of variation (COV) of 0.35. The scatter of the Alpha values was likely due to the range in the soil type (stiff clay to loose silt) and inaccurate cohesion estimates. The average Beta values for the cohesionless soils were 0.24, 0.20, and 0.25 for silty sand, sand, and sand with gravel, respectively. The Beta values did not decrease with depth as suggested by the Beta method that was presented in O'Neill and Hassan (1994). Overall, the total measured side resistance values for only two of the eight DSF were less than predicted values (by 12 and 25 percent). The recommended tip resistance was 2.88MPa based on the tip resistance values from the eight DSF.

2.4.4.3. Effects of Construction Techniques

Previous studies have been conducted to investigate the effects of construction practices. These studies (Brown 2002, Mullins and Ashmawy 2005) were performed at the Auburn University National Geotechnical Experimentation Site. The examined construction techniques

included the use of: bentonite slurry, polymer slurry (dry pellet form and liquid form), temporary casing, free-fall placement of concrete within dry excavations, varied rebar spacing, different aggregate size within the concrete, and different values of concrete slump. Problems associated with construction techniques (i.e. soil inclusions) were also introduced into two of the DSF (Brown 2002). It was concluded that the axial capacity for the shafts constructed using bentonite slurry was lower than the capacity obtained from the other construction methods (except for soils that had low hydraulic conductivity). The soil inclusions had no short term effect on the axial capacity of the DSF; however, structural failure was not an issue with the low stresses that were applied to the foundation during testing (Brown 2002). Instead, the concrete properties and slurry properties have been identified by Mullins and Ashmawy (2005) to be the primary causes of problems in DSF.

Eight case histories with poor construction techniques (i.e. inadequate bottom cleanout, failure to use drilling fluids, poor concrete placement, and improper drilling tools) were evaluated in Schmertmann et al. (1998). Specifically, BLC were utilized to detect the effects of poor construction techniques on the axial capacity of DSF. As described in Schmertmann et al. (1998), larger values of downward displacement were observed as a result of poor cleanout procedures within DSF. Similarly, low side shear values at large values of displacement (>100mm of displacement at 0.4MN of load compared to 6mm of displacement at 6.1MN of load) were attributed to hydrostatic imbalance. The cases presented in Schmertmann et al. (1998) were dramatic examples of poor construction techniques; however, the effects of the construction techniques on the load-movement behavior of the DSF were confirmed using full-scale BLC testing.

Similarly, base grouting is cost effective in cohesionless soils and this method also provides increased reliability due to the resulting uplift testing provided by the base grouting process, even while neglecting the beneficial effects on the end bearing capacity (Dapp et al. 2006). For the Audubon Bridge project, located on the Mississippi River, full-scale BLC tests were performed on a single ungrouted shaft and nine base grouted shafts (Dapp and Brown 2010). The results obtained from one of the DSF, a DSF that was redrilled in the same location following excavation collapse, are of particular interest. Specifically, as reported in Dapp et al. (2006), the upward displacement resulting from base grouting being performed on this DSF resulted in approximately 1.9cm of movement (far in excess of the average 0.25cm of movement that were observed for the other 75 DSF (Figure 2.10).

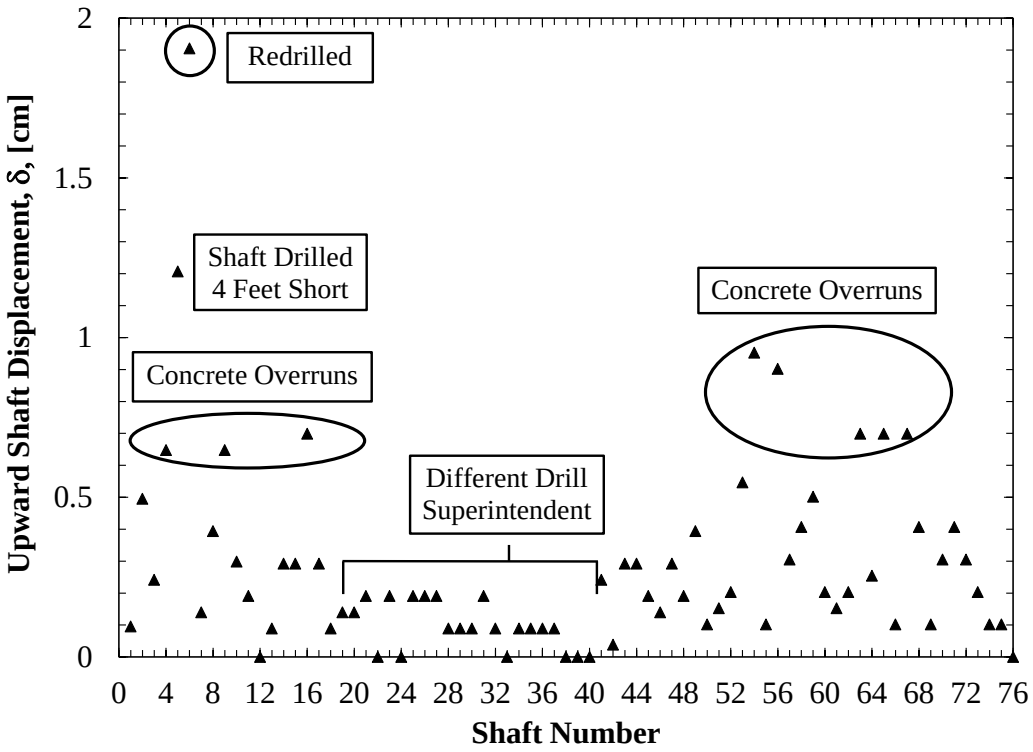

Figure 2.10. Upward displacement of various DSF as a result of post-grouting [modified from Dapp et al. 2006].

The methods utilized to construct a DSF affect the strength properties of a DSF, as verified by a full-scale load test. The use of drilling fluid (dry, polymer slurry, bentonite slurry) in certain types of stratigraphy (i.e. shale, limestone, clay, or sand) can decrease the side resistance of the DSF. As reported in Brown (2002), the axial capacity values of DSF when bentonite slurry, polymer slurry in dry pellet form, and polymer slurry in liquid form were used to construct the DSF resulted in smaller values of axial capacity for the DSF constructed using the bentonite slurry. Furhermore, the DSF constructed using the bentonite slurry did not exhibit a strain softening response like the DSF constructed using the polymer slurry. A greater increase in resistance was also observed, during the load test, for the DSF that was constructed using the bentonite slurry than for the DSF constructed using the polymer slurry.

2.5. Summary

The two primary steps in the design of DSF are 1) the collection of geotechnical investigation data and 2) the utilization of design equations/software programs to determine the size (diameter and length) of the DSF. In each of these two steps, there are multiple methods to obtain the soil property values and to decide the soil-shaft interaction model. The amount of uncertainty relating to the design of DSF is dependent upon the soil type, the geotechnical investigation method, and the design equations/software programs utilized. Finally, as discussed in the case histories, uncertainty can also be introduced during the construction of the DSF because there are multiple construction methods (i.e. excavation constructed in the dry, with polymer slurry, or bentonite slurry).

2.6. References

Alshibli, K.A., Okeil, A.M., Alramahi, B., and Zhang, Z. (2009). “Statistical Assessment of Repeatability of CPT Measurements.” GeoFlorida 2009: Contemporary Topics in In Situ Testing, Analysis and Reliability of Foundations, Orlando, Fl, March 15-19, 2009, pp. 87-94.

American Association of State Highway and Transportation Officials (1989). Standard Specifications for Highway Bridges 14th Ed., AASTHO, Washington, D.C.

American Association of State Highway and Transportation Officials (2001). LRFD Bridge Design Specifications, AASTHO, Washington, D.C.

American Association of State Highway and Transportation Officials (2007). LRFD Bridge Design Specifications, Fourth Ed., AASTHO, Washington, D.C., 1938 pgs.

American Society for Testing and Materials (2011). "Standard Test Method for Particle-Size Analysis of Soils." Annual Book of ASTM Standards, Designation D422, Vol. 4.08, ASTM, West Conshohocken, PA.

American Society for Testing and Materials (2011). "Standard Test Methods for Specific Gravity of Soil Solids by Water Pycnometer." Annual Book of ASTM Standards, Designation D854, Vol. 4.08, ASTM, West Conshohocken, PA.

American Society for Testing and Materials (2013). "Standard Test Methods for Deep Foundations Under Static Axial Compressive Load." Annual Book of ASTM Standards, Designation D1143, Vol. 4.08, ASTM, West Conshohocken, PA.

American Society for Testing and Materials (2012). "Standard Test Method for Standard Penetration Test (SPT) and Split-Barrel Sampling of Soils." Annual Book of ASTM Standards, Designation D1586, Vol. 4.08, ASTM, West Conshohocken, PA.

American Society for Testing and Materials (2012). "Standard Test Method for Unconsolidated-Undrained Triaxial Compression Test on Cohesive Soils." Annual Book of ASTM Standards, Designation D2850, Vol. 4.08, ASTM, West Conshohocken, PA.

American Society for Testing and Materials (2012). "Standard Test Method for Mechanical Cone Penetration Tests of Soil." Annual Book of ASTM Standards, Designation D3441, Vol. 4.08, ASTM, West Conshohocken, PA.

American Society for Testing and Materials (2011). "Standard Test Methods for Liquid Limit, Plastic Limit, and Plasticity Index of Soils." Annual Book of ASTM Standards, Designation D4318, Vol. 4.08, ASTM, West Conshohocken, PA.

American Society for Testing and Materials (2012). "Standard Test Method for Laboratory Miniature Vane Shear Test for Saturated Fine-Grained Clayey Soil." Annual Book of ASTM Standards, Designation D4648, Vol. 4.08, ASTM, West Conshohocken, PA.

American Society for Testing and Materials (2012). "Method for Consolidated Drained Triaxial Compression Test for Soils." Annual Book of ASTM Standards, Designation D7181, Vol. 4.08, ASTM, West Conshohocken, PA.

American Society for Testing and Materials (2010). "Standard Test Methods for Axial Compressive Force Pulse (Rapid) Testing of Deep Foundations." Annual Book of ASTM Standards, Designation D7383, Vol. 4.09, ASTM, West Conshohocken, PA.

Axtell, P.J. and Brown, D.A. (2011). "Case History – Foundations for the New Mississippi River Bridge – St. Louis." Deep Foundations Institute, DFI Journal, Vol. 5, No. 2, pp. 3-15.

Baecher, G. and Christian, J. (2003). Reliability and Statistics in Geotechnical Engineering. Wiley, pp. 618.Bieniawski (1984)

Bishnoi, B. (1968). *Bearing Capacity of a Closely Jointed Rock*. PhD thesis, Georgia Institute of Technology, Atlanta, Ga.

Bloomquist, D., McVay, M., and Hu, Z. (1992). "Updating Florida Department of Transportation's (FDOT) Pile/Shaft Design Procedures Based on CPT and DTP Data." Florida Department of Transportation, BD-545, RPWO No. 43, MF Project 00005780, 199 pgs.

Brown, D.A. (2002). "Effect of Construction on Axial Capacity of Drilled Foundations in Piedmont Soils." Journal of Geotechnical and Geoenvironmental Engineering, Vol. 128, No. 12, pp. 967-973.

Brown, D.A. (2004). "Zen and the Art of Drilled Shaft Construction: The Pursuit of Quality." Geo-Institute International Conference on Drilled Foundations, ASCE Geotechnical Special Publication No. 124, pp. 19-33.

Brown, D.A. (2009). "Load Testing of Drilled Shaft Foundations in Limestone." Report for ADSC Southeast Chapter, Nashville, TN, Feb. 2009, 103 pgs.

Brown, D., Turner, J., and Castelli, R. (2010). "Drilled Shafts: Construction Procedures and LRFD Methods." FHWA Publication No. NHI-10-016, Federal Highway Administration, Washington, D.C., 970 pgs.

Bustamante, M. and Gianeselli, L. (1982). "Pile Bearing Capacity Prediction by Means of Static Penetrometer CPT." Proceedings of the 2nd European Symposium on Penetration Testing Vol. 2, pp. 493-500.

Canadian Geotechnical Society (1978). Canadian Foundation Engineering Manual. BiTech Publishers Ltd., Vancouver, B.C.

Canadian Geotechnical Society (1985). Canadian Foundation Engineering Manual. Second Ed., BiTech Publishers Ltd., Vancouver, B.C.

Carter, J. P. and Kulhawy, F. H. (1988). "Analysis and Design of Drilled Shaft Foundations Socketed into Rock." Report EL-5918, Electric Power Research Institute, Palo Alto, Calif.

Castelli, R. and Fan, K. (2002). "Lateral Load Test Results on Drilled Shafts in Marl at Jacksonville, Florida." Deep Foundations 2002, Orlando, FL, Feb. 14-16, pp. 824-835.

Coffman, R.A. (2011a). *California Split-Spoon Sampler at the TATS.* Photograph taken October 2011.

Coffman, R.A. (2011b). *Cone Penetration Test at the TATS.* Photograph taken October 2011.

Dapp, S.D. and Brown, D.A. (2010). "Evaluation of Base Grouted Drilled Shafts at the Audubon Bridge." GeoFlorida 2010: Advanced in Analysis, Modeling, and Design, GSP 199, pp. 1553-1562.

Dapp, S.D., Muchard, M., and Brown, D.A. (2006). "Experiences with Base Grouted Drilled Shafts in the Southeastern United States." Proceedings of 10th International Conference on Deep Foundations, Amsterdam, Netherlands, 10 pgs.

Das, B. (2013). Fundamentals of Geotechnical Engineering, 4th Ed. Cengage Learning, Stamford, CT.

DeGroot, D. (1996). “Analyzing Spatial Variability of In Situ Soil Properties.” ASCE, Geotechnical Special Publication 58, Vol. 1, pp. 210-238.

FB-Deep (2012). Bridge Software Institute, Gainesville, Florida, Version 2.04.

Fellenius, B., Atlae, A., Kulesza, R., and Hayes, J. (1999). “O-Cell Testing and FE Analysis of a 28m Deep Barrette in Manila, Philippines.” Journal of Geotechnical and Environmental Engineering, Vol. 125, No. 7, pp. 566-575.

Gunaratne, M. (2006). *The Foundation Engineering Handbook*. CRC Press, Florida, pp. 613.

Gunnink, B. and Kiehne, C. (2002). Capacity of Drilled Shafts in Burlington Limestone. Journal of Geotechnical and Geoenvironmental Engineering, Vol. 128, No. 7, pp. 539-545.

Hammond, D. (2004). “Drilled Shaft Load Test Program for Approach Spans of U.S. Hwy. 82 over the Mississippi River.” GeoTrans 2004: Geotechnical Engineering for Transportation Projects, Los Angeles, CA, July 27-31, pp. 1270-1279.

Hara, A., Ohta, T., Niwa, M., Tanaka, S., and Banno, T. (1974). “Shear Modulus and Shear Strength of Cohesive Soils.” Soils and Foundation, Vol. 14, No. 3 pp. 1-12.

Horvath, R. and Kenney, T. (1979). “Shaft Resistance of Rock-socketed Drilled Piers.” Proceedings of Symposium on Deep Foundations, American Society of Civil Engineers, Atlanta, Georgia, pp. 182-214.

Kishida, H., Tsubakihara, Y., and Ogura, H. (1992). “Pile Loading Tests at Osaka Amenity Park Project.” Deep Foundation Practice 1992, Singapore, Nov. 4-6, pp. 131-137.

Kort, D. and Kostaschuk, R. (2007). “Sonar Calipering of Slurry Constructed Bored Piles and the Impact of Pile Shape on Measured Capacity.” 8th Canadian Geotechnical Conference, Ottawa, Canada, Oct. 21-24, pp. 1622-1630.

Kulhawy, F. (1991). “Drilled Shaft Foundations.” Foundation Engineering Handbook, 2nd Ed.H.Y. Fang, ed., Van Nostrand-Reinhold, New York.

Kulhawy, F. and Goodman, R. (1980). “Design of Foundations on Discontinuous Rock.” Proc. Int. Conf. on Struct. Found. On Rock, A.A. Balkema, Rotterdam, Netherlands, pp. 209-220.

Kyfor, Z., Schnore, A., Carlo, T., and Baily, P. (1992). “Static Testing of Deep Foundations.” Federal Highway Administration, FHWA-SA-91-042, 174 pgs.Liao and Whitman 1986

McIntosh, K. and Knott, R. (2000). “Geotechnical Challenges in Weak Rock and Karst Conditions.” GeoDenver 2000: New Technological and Design Developments in Deep Foundations, Denver, CO, Aug. 5-8, pp. 80-95.

McVay, M., Huang, S., and Casper, R. (1994). *Numerical Simulation of Drilled Shafts for Osterberg Pullout, and Axial Compression Loading in Florida Limestone*. Final Report, Department of Civil Engineering, University of Florida, Gainesville, FL.

McVay, M. C., Townsend, F. C., and Williams, R. C. (1992). "Design of Socketed Drilled Shafts in Limestone." Journal of Geotechnical. Engineering, ASCE, Vol. 118, No. 10, pp. 1626-1637.

Meyerhof, G. (1976). “Bearing Capacity and Settlement of Pile Foundations.” Journal of Geotechnical Engineering, Vol. 102, No. 6T3, pp. 195-228.

Monlit, T. and Lee, J.S. (1998). “Comparison Report, Osterberg Cell Test Method (PTP14) Versus Kentledge Test Method (PTP15).” MRT C701, Singapore, prepared for Hyundai, 18 pgs.

Mullins, G. and Ashmawy, A.K. (2005). “Factors Affecting Anomaly Formation in Drilled Shafts – Final Report.” Florida Department of Transportation BC-353-19, 276 pgs.

Nam, M.S. and Vipulanandan, C. (2010). “Relationship Between Texas Cone Penetration Tests and Axial Resistance of Drilled Shafts Socketed in Clay Shale and Limestone.” Journal of Geotechnical and Geoenvironmental Engineering, Vol. 136, No. 8, pp. 1161-1165.

Ogura, H., Sumi, M., Kishida, H., and Yoshifuka, T., translated by Mandan B. Karkee (1995). “Application of Pile Toe Load Test to Cast-in-place Concrete Pile and Precast Pile.” Geotop Corporation with permission from the Japanese Geotechnical Society, Tokyo, Japan, Foundation Drilling Magazine, ADSC, Vol. 23, No. 6, pp. 23-28.

Olson, R. and Iskander, M. (2009). “Axial Load Capacity of Un-tapered Piles in Cohesionless Soils.” International Foundation Congress and Equipment Expo, pp. 231-238.

O’Neill, M. and Hassan, K. (1994). “Drilled Shafts: Effects of Construction on Performance and Design Criteria.” Proceedings of the International Conference on Design and Construction of Deep Foundations, Vol. 1, pp. 137-187.

O’Neill, M. and Reese, L. (1970). “Behavior of Axially Loaded Drilled Shafts in Beaumont Clay.” TDOT Report 89-8.

O’Neill, M. and Reese, L. (1999). “Drilled shafts: Construction Procedures and Design Methods.” FHWA Publication No. IF-99-025, Federal Highway Administration, Washington, D.C., 537 pgs.

O’Neill, M., Townsend, F., Hassan, K., Buller, A., and Chan, P. (1996). “Load transfer for drilled shafts in intermediate geomaterials.” *FHWA Publication No. RD-95-172*, Federal Highway Administration, Washington, D.C., 196 pgs.

Osterberg, J. O., (1984). “A New Simplified Method for Load Testing Drilled Shafts.” Foundation Drilling, Vol. XXIII, No. 6 (July/August, 1984), International Association of Foundation Drilling (ADSC), 9 pgs.

Peck, R., Hanson, W., and Thornburn, T. (1974). Foundation Engineering. Second Ed., John Wiley and Sons Inc., 544 pgs.

Petek, K., Felice, C., and Holtz, R. (2002). “Capacity Analysis of Drilled Shafts with Defects.” Feep Foundations, pp. 1120-1135.

Phoon, K.K., Quek, S., and An, P. (2003). “Identification of Statistically Homogeneous Soil Layers Using Modified Barlett Statistics.” Journal of Geotechnical and Geoenvironmental Engineering, Vol. 129, No. 7, pp. 649-659.

Quiros, G. and Reese, L. (1977). “Design Procedures for Axially Loaded Drilled Shafts” FHWA Publication No. TX78-1765F, Federal Highway Administration Final Report, Washington, D.C., 176 pgs.

Race, M.L. (2012). *Unconsolidated Undrained Triaxial Compression Test.* Photograph taken Feb. 2012.

Race, M.L. (2013a). *Miniature Vane Laboratory Test.* Photograph taken March 2013.

Race, M.L. (2013b). *Consolidated Drained Triaxial Compression Test on Sand.* Photograph taken Nov. 2013.

Rabab'ah, S., Niedzielski, J., Elsayed, A., Bodour, W., Durkee, D. (2011). "Comparison of Drilled shaft Design Methods for Drilled Shafts in Sand, Coarse Gravel, and Cobble Soils." Geo-Frontiers 2011, Dallas, TX, March 13-16, pp. 212-221.

Reese, L. C. and O'Neill, M. W. (1988). ''Drilled Shafts; Construction Procedures and Design Methods.'' Rep. No. FHWA-HI-88-42, U.S. Dept. of Transp., Federal Highway Administration, Washington, D.C.

Reese, L., Wang, S., Arrellaga, J., and Vasquez, L. (2012a). "SHAFT v2012- User's Manual: A Program for the Study of Drilled Shafts Under Axial Loads." ENSOFT, INC. Austin, Texas, 186 pgs.

Reese, L., Wang, S., Arrellaga, J., and Vasquez, L. (2012b). "SHAFT v2012- Technical Manual: A Program for the Study of Drilled Shafts Under Axial Loads." ENSOFT, INC. Austin, Texas, 76 pgs.

Reese, L. C. and Wright, S. J. (1977). "Drilled Shaft Design and Construction Guidelines Manual." Implementation Package 77-21, U.S. Department of Transportation., Washington, D.C.

Robertson, P.K. (1990). "Soil Classification Using the Cone Penetration Test." Canadian Geotechnical Journal, Vol. 27, pp. 151-158.

Robertson, P.K. and Cabal, K.L. (2012). "Guide to Cone Penetration Testing for Geotechnical Engineering." Gregg Drilling and Testing, Inc, 145 pgs.

Rogers, J. and Chung, J. (2013). "Distinguishing Between Data Uncertainty and Natural Variability in Virtual Geotechnical Databases." GSP 229, Foundation Engineering in the Face of Uncertainty, pp. 444-455.

Rowe, R.K. and Armitage, H.H. (1987). "A Design Method for Drilled Piers in Soft Rock." Canadian Geotechnical Journal, Vol. 24, pp. 114–125.

Schmertmann, J. H. (1967). "Guidelines for Use in the Soils Investigation and Design of Foundations for Bridge Structures in the State of Florida." Research Bulletin 121 (RB-121), Report Prepared for the FDOT by the University of Florida, Gainesville, Florida.

Schmertmann, J.H. (1975). "Measurement of in-situ shear strength." Proceedings of the ASCE Conference on In-Situ Measurements of Soil Properties, Raleigh, North Carolina, June 1-4.

Schmertmann, J.H. (1978). "Guidelines for Cone Test, Performance, and Design." FHWA Publication No. TS-78209, Federal Highway Administration, Washington, D.C., 145 pgs.

Schmertmann, J.H., Hayes, J.A., Molnit, T., and Osterberg, J.O. (1998). "O-Cell Testing Case Histories Demonstrate the Importance of Bored Pile (Drilled Shaft) Construction Technique." Proceedings of Fourth International Conference on Case Histories in Geotechnical Engineering, St. Louis, Missouri, pp. 1103-1115.

SHAFT (2012). ENSOFT, INC. Austin, Texas, Version 2012.

Sheikh, S. and O'Neill, M. (1986). “Long-term Behavior of Expansive Concrete Drilled Shafts.” Canadian Journal of Civil Engineering, Vol. 13, No. 2, pp. 213-217.

Shi, L. (2003). *The Effect of Load Direction on Axial Capacity of Deep Foundations.* PhD dissertation, Auburn University, Auburn, AL, 680 pgs.

Skempton, A. (1951). “The Bearing Capacity of Clays.” Proceedings from Building Research Congress, London, Vol. 1, pp. 180-189.

Terzaghi, K. and Peck, R. (1967). *Soil Mechanics in Engineering Practice.* Second Ed., Wiley, 752 pgs.

Tomlinson, M. (1957). “The Adhesion of Piles Driven in Clay Soils.” Proc. Of the 4th Int. Conf. on Soil Mech. And Found. Eng., Vol. 2, pp. 66-71.

Touma, F. and Reese, L. (1974). “Behavior of Bored Piles in Sand.” Journal of Geotechnical Engineering Division, ASCE, Vol. 100, No. GT7, pp. 749-761.

Townsend, F. (2003a). “SHAFT-SPT Validation Problems.” Bridge Software Institute. Gainesville, Florida, 91 pgs.

Townsend, F. (2003b). “User’s Guide for SHAFT-SPT.” Bridge Software Institute. Gainesville, Florida, 16 pgs.

Vanikar, S. (1985). Manual on Design and Construction of Driven Pile Foundations. U.S. Department of Transportation Federal Highway Administration, FHWA-DP-66-1 (Revision 1), 57 pgs.

Wu, T. (2013). “Geotechnical Uncertainties and Reliability-Based Design.” Foundation Engineering in the Face of Uncertainty, pp. 271-282.

Zhang, L. and Einstein, H. (1998). “End Bearing Capacity of Drilled Shafts in Rock.” Journal of Geotechnical and Geoenvironmental Engineering, Vol. 124, No. 7, pp. 574-584.

Zhang, L., Tang, W., Zhang, L., and Zheng, J. (2004). “Reducing Uncertainty of Prediction from Empirical Correlations.” Journal of Geotechnical and Geoenvironmental Engineering, Vol. 130, No. 5, pp. 526-534.

CHAPTER 3: LITERATURE REVIEW: Statistical Analyses

3.1. Chapter Overview

The literature discussed in Chapter 3 includes, but is not limited to, statistical methods to compare datasets and to perform reliability analyses. The Bayesian updating technique is similarly discussed along with previous engineering application of statistical analyses performed within civil engineering. In particular, the localized calibration of resistance factors for DSF in the states of Colorado, Florida, Kansas, Louisiana, and Missouri are discussed.

3.2. Statistical Analysis

Statistical analyses may be performed to determine the statistical difference in the mean value, in the variance values of a dataset, or between empirical distribution types. In particular, these statistical methods include the T-test, the Wilcoxon test, the F-test, the Shapiro-Wilks test, and the Kolmogorov-Smirnov test. Similarly, multivariate statistical analyses, such as the Hotelling's T^2 test, may be performed to determine the statistical difference between two multivariate datasets (a multivariate dataset contains multiple, correlated variables). Bayesian analysis is introduced with regards to the Bayesian updating method that may be utilized to update/predict property characterization within civil engineering. Finally, reliability methods, such as the first-order second-moment method, the Monte Carlo simulation method, and the first-order reliability method, are introduced herein.

3.2.1. Introduction to Statistical Testing Methods

As presented in Table 3.1 and according to Geher et al. (2014), two types of errors are commonly associated with statistical testing: type I error (α) and type II error (β) as presented in. The two hypotheses that are commonly utilized for statistical testing of mean values include: the

initial or null hypothesis (H_o) that the values of the mean of the two samples are equal and the alternative hypothesis (H_a) that the mean values of the two samples are different. The null hypothesis is typically represented as H_0: $\mu_1 = \mu_2$ and the alternative hypotheses are represented as H_a: $\mu_1 < \mu_2$, $\mu_1 > \mu_2$, or $\mu_1 \neq \mu_2$ (Geher et al. 2014). The probability that the null hypothesis is rejected even though the null hypothesis is true (type I error) is limited to five percent (5%). Because the significance level (type I error, α) is five percent, the corresponding confidence that the alternative hypothesis is true when the null hypothesis is rejected is 95 percent.

Table 3.1. Error types for statistical testing (modified from Geher et al. 2014).

	Null Hypothesis (H_0) is True	**Null Hypothesis (H_0) is False**
Reject Null Hypothesis	Type I Error (α)	Correct
Fail to Reject Null Hypothesis	Correct	Type II Error (β)

For univariate statistical testing, important descriptive characteristics include the value of the sample mean and the value of the variance for a given variable (Equations 3.1 and 3.2, respectively). According to Rencher (2002), the sample mean and variance ($\bar{y}$ and s^2, respectively) are unbiased estimators for the population mean and variance (μ and σ, respectively), meaning, for example, that the expected value of the sample variance will be equivalent to the population variance (Equation 3.3). The variables in Equation 3.1 include: the mean of the variable ($\bar{y}$), the number of samples within the dataset (n), and the individual observations within the dataset (y_i). The new variables utilized in Equations 3.2 and 3.3 include: the sample variance (s^2), the expected value of a sample (E), and the population variance (σ^2).

$$\bar{y} = \frac{1}{n}\sum_{i=1}^{n} y_i \qquad \text{(Rencher 2002)} \qquad \text{Equation 3.1}$$

$$s^2 = \frac{\sum_{i=1}^{n}(y_i - \bar{y})^2}{n-1} \qquad \text{(Rencher 2002)} \qquad \text{Equation 3.2}$$

$$E(s^2) = \sigma^2 \qquad \text{(Rencher 2002)} \qquad \text{Equation 3.3}$$

Rencher (2002) also states that for bivariate datasets, the covariance of the variables is a measurement of the relationship between the two variables (i.e. if variable x is increased then variable y will also increase). The sample covariance between two variables with the same number of samples (n) is defined in Equation 3.4 with x_i and $\bar{x}$ being the observation and the mean values of sample x and y_i and $\bar{y}$ being the observation and the mean values of sample y. Therefore, according to Rencher (2002), the sample correlation or the standardized covariance is then defined as the covariance between dataset x and dataset y divided by the product of the sample standard deviation of x and the sample standard deviation of y (Equation 3.5).

$$s_{xy} = \frac{\sum_{i=1}^{n}(x_i - \bar{x})(y_i - \bar{y})}{n-1} \qquad \text{(Rencher 2002)} \qquad \text{Equation 3.4}$$

$$r_{xy} = \frac{s_{xy}}{s_x s_y} = \frac{\sum_{i=1}^{n}(x_i - \bar{x})(y_i - \bar{y})}{\sqrt{\sum_{i=1}^{n}(x_i - \bar{x})^2 \sum_{i=1}^{n}(y_i - \bar{y})^2}} \qquad \text{(Rencher 2002)} \qquad \text{Equation 3.5}$$

In Equation 3.4, s_{xy} is the sample covariance between dataset x and dataset y. The sample correlation between dataset x and dataset y, the sample standard deviation of dataset x, and the sample standard deviation of dataset y are represented by r_{xy}, s_x, and s_y, respectively in Equation 3.5.

According to Casella and Berger (2002), multivariate datasets consist of multiple univariate variables which are measured/observed from the same dataset and which have strong covariance or correlation between the variables. The descriptive statistics (i.e. mean, covariance, and correlation) are commonly described using matrices as presented in Equation 3.6 (an example of a covariance matrix with p variables). The diagonal elements of a covariance matrix (in this case s_{11}, s_{22}, and s_{pp}) are the sample variances of the individual p variables whereas the other elements are the covariance between different combinations of the variables. Single numerical representations of multivariate variance such as generalized sample variance and generalized sample correlation are typically determined by calculating the determinate of the respective sample covariance and correlation matrices. Similarly, the total sample variance is commonly the summation of the sample variance of each variable.

$$\boldsymbol{S} = (s_{jk}) = \begin{pmatrix} s_{11} & s_{12} & \dots & s_{1p} \\ s_{21} & s_{22} & \dots & s_{2p} \\ \vdots & \vdots & & \vdots \\ s_{p1} & s_{p2} & \dots & s_{pp} \end{pmatrix} \qquad \text{(Rencher 2002)} \qquad \text{Equation 3.6}$$

3.2.1.1. Univariate Two Sample Statistical Testing

Two-sample statistical tests that can be utilized to determine the statistical difference between two datasets include the: T-test, Wilcoxon test, and Kolomorov-Smirnov test. Snedecor and Cochran (1989) state that the T-test is a parametric test of the mean values of two samples and includes the assumption that the data from the two samples is normally distributed. As explained by Snedecor and Cochran (1989), the t statistic is calculated using the mean and variance values from the two samples (Equation 3.7) after which, the probability that the null hypothesis is true is determined using the student t-distribution. As further described in Section

3.2.1.1, the student t-distribution converges onto the normal distribution as the degree of freedom increases to infinity (Smith 1986). The probability that the null hypothesis is true, also known as the p-value, is determined by considering the tail of the distribution (Figure 3.1). Note that the data is being presented to illustrate the reason behind the utilization of the t-test

$$t = \frac{\overline{X_1} - \overline{X_2}}{\sqrt{\frac{S_1^2}{n_1} + \frac{S_2^2}{n_2}}}$$ (Snedecor and Cochran 1989) Equation 3.7

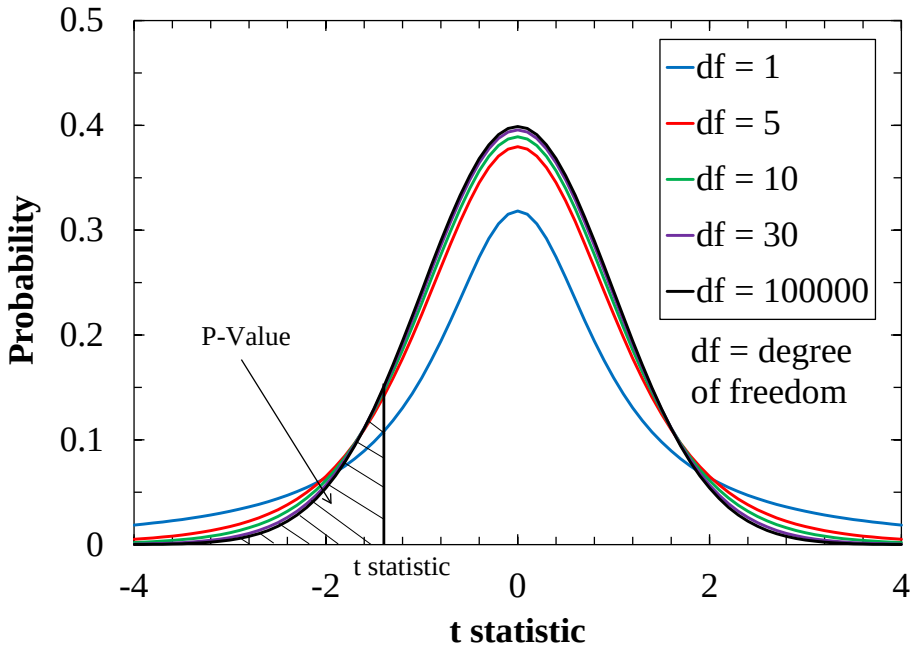

Figure 3.1. Determination of the p-value from the student t-distribution for a null hypothesis of $\mu_1 < \mu_2$ when utilizing Equation 3.7 (modified from Snedecor and Cochran 1989).

Correspondingly, the two sample Wilcoxon test, also known as the Mann-Whitney test, is a nonparametric statistical test of the mean values as determined using Equation 3.8. Based on the information reported in Gibbons and Chakraborti (2003), the Wilcoxon test is a free distribution test based on signed ranking values, but the magnitudes of the differences are

ignored. Specifically, the p-value from the two sample Wilcoxon test is determined by using the signed rank distribution (Kloke and McKean 2014). An example of the signed rank distribution utilized for two samples with six and four observations, respectively, is presented in Figure 3.2 to illustrate the utilization of the Wilcoxon test.

$$U = \sum_{i=1}^{n_1} \sum_{j=1}^{n_2} D_{ij}$$ (Gibbons and Chakraborti 2003) Equation 3.8

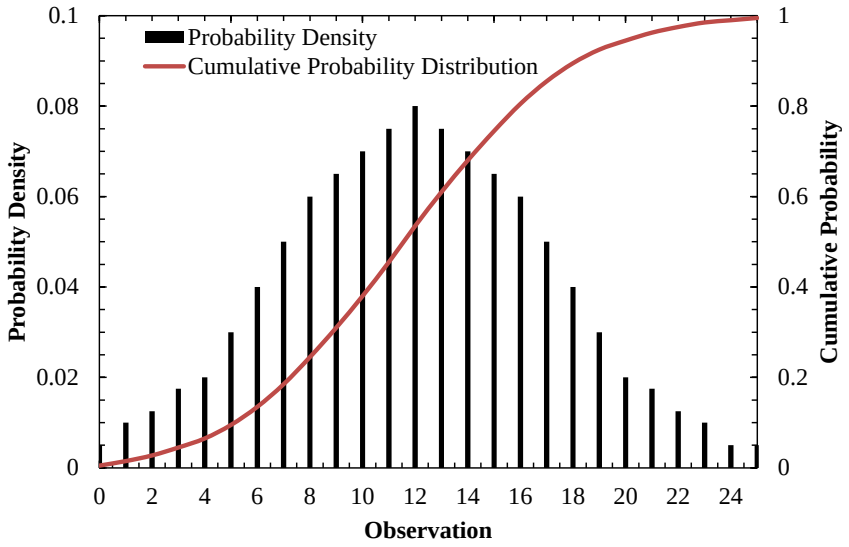

Figure 3.2. Probability density and cumulative probability function of the Wilcoxon statistic for two samples with six and four observations, respectively (modified from Kloke and McKean 2014).

The Kolmogorov-Smirnov (KS) test is a nonparametric testing method based upon the absolute difference between the observations in two sample sets (Equations 3.9 and 3.10) as described in Chakravart et al. (1967). The two-sample KS test is used to determine the difference of the two samples based on empirical distributions (Figure 3.3). These statistical testing methods can be utilized to determine whether there is strong evidence that there is a

statistical difference between two different samples of data (i.e. the p-value is less than 0.05 for a 95 percent confidence that there is a statistical difference between the two datasets).

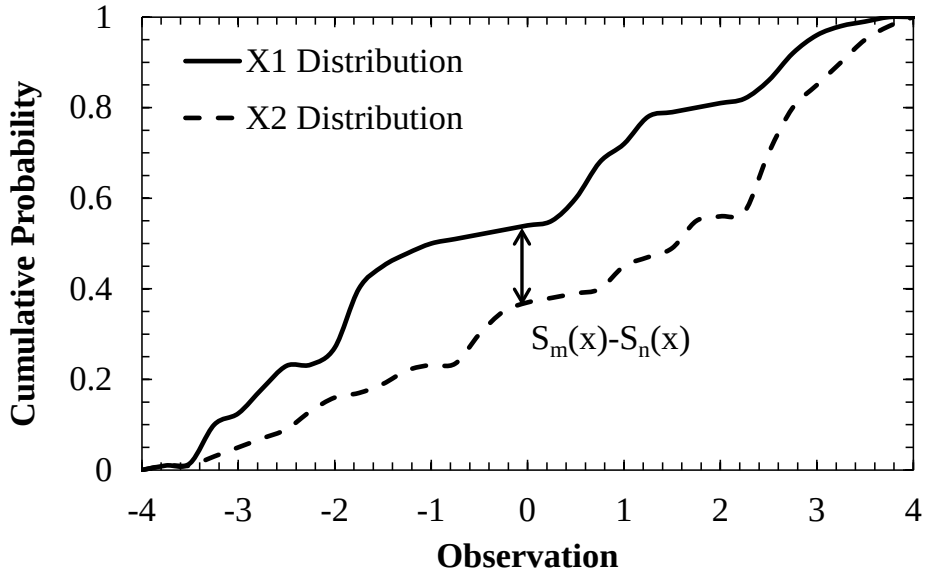

Figure 3.3. Empirical cumulative probability density distribution utilized for the KS test (modified from Chakravart et al. 1967).

$$D_{m,n} = \max_{x} |S_m(x) - S_n(x)| \quad \text{(Gibbons and Chakraborti 2003)} \qquad \text{Equation 3.9}$$

$$S(x) = \frac{1}{n}\sum_{i=1}^{n} I(x_i \leq x) \quad \text{(Gibbons and Chakraborti 2003)} \qquad \text{Equation 3.10}$$

The variables used in Equations 3.7 to 3.10 include: the mean of Sample 1 ($\overline{X_1}$), the mean of Sample 2 ($\overline{X_2}$), the standard deviation of Sample 1 (S_1), the standard deviation of Sample 2 (S_2), the number of samples in Sample 1 (n_1), the number of samples in Sample 2 (n_2), the indicator function which is one (1) if observations from Sample 1 are greater than those from Sample 2 and zero (0) otherwise (D_{ij}), the number of times an observation in Sample 2 precedes an

observation in Sample 1 in a paired arrangement for the sample sets (U), the distance statistic ($D_{m,n}$)and with the indicator value with value of one (1) when $x_i \leq x$ and zero (0) otherwise (I).

According to (Snedecor and Cochran 1989), statistical testing for the difference in the value of the variance (and consequently the standard deviation) of two samples is determined using the F-test. As presented in Figure 3.4, the F-test is a parametric test of variance based upon the F distribution (also known as the chi-squared distribution). The test statistic for the F-test is provided in Equation 3.11 where s_1^2 is the variance of Sample 1, s_2^2 is the variance of Sample 2 and the F statistic is distributed as an F distribution with degrees of freedom $n_1 - 1$ and $n_2 - 1$.

$$F = \frac{s_1^2}{s_2^2} \sim F_{(n_1-1, n_2-1)} \qquad \text{(Snedecor and Cochran 1989)} \qquad \text{Equation 3.11}$$

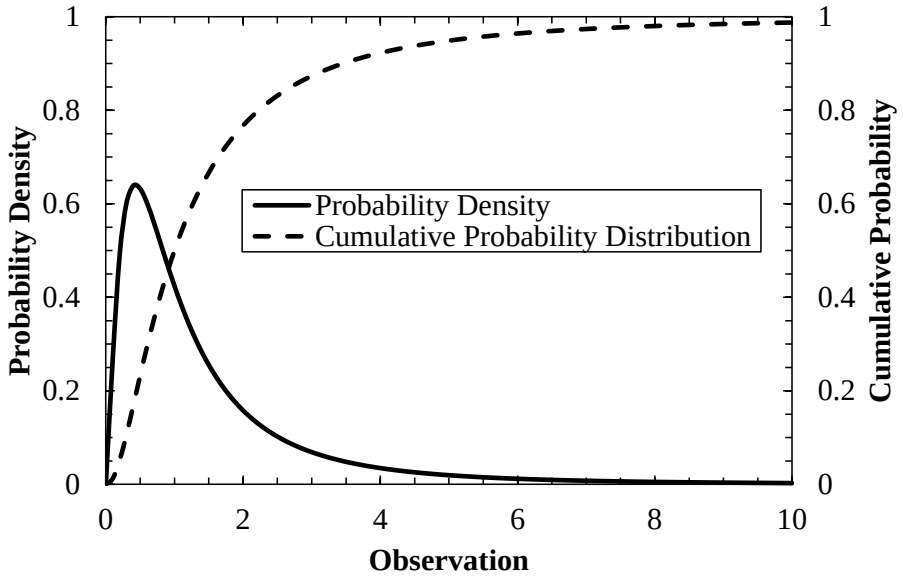

Figure 3.4. F distribution utilized for the F-test (modified from NIST/SEMATECH 2012).

3.2.1.2. Distribution Tests

As stated in multiple sources (Lumb 1970, Baecher and Christian 2003), distribution types that are commonly utilized for soil properties included the normal distribution, the lognormal distribution, the beta distribution, and the Weibull distribution. Baecher and Christian (2003) also mention that other distributions such as the binomial, the Poisson, and the exponential distributions are sometimes utilized to model random variables such as the number of dam failures, the number of rock fractures, or other stochastic processes. Examples of distribution types in geotechnical engineering include the normal distribution of uncorrected SPT blow count data from Baecher (1987a) and the beta distribution of friction angle of sand from Harr (1987).

The univariate normal distribution, presented in Rencher (2002) and defined by the mean and variance of random variable y in Equation 3.12, is the most common univariate distribution. Similar to the univariate normal distribution, the student t distribution is symmetrically distributed about the mean but the standard deviation increases as the degree of freedom is decreased. As presented previously, as the degree of freedom approaches infinity, the student t distribution approaches the normal distribution (Figure 3.1). The multivariate normal distribution is represented by Equation 3.13, as a function of the mean vector ($\boldsymbol{\mu}$) and the covariance matrix ($\boldsymbol{\Sigma}$). According to Lumb (1970), the beta distribution has been previously used in geotechnical engineering because the distribution can be modified to fit many datasets (Figure 3.5). Specifically, the beta distribution can be represented as a function of a shape parameter (α) and a scale parameter (β) as presented in Equations 3.14 and 3.15 (gamma function). As discussed in Evans et al. (2000) and Johnson et al. (1994), the Weibull function, represented by Equation

3.16, is similarly a function of a shape and scale parameter that has been previously used and/or modified to fit soil datasets; the Weibull function is presented in Figure 3.6.

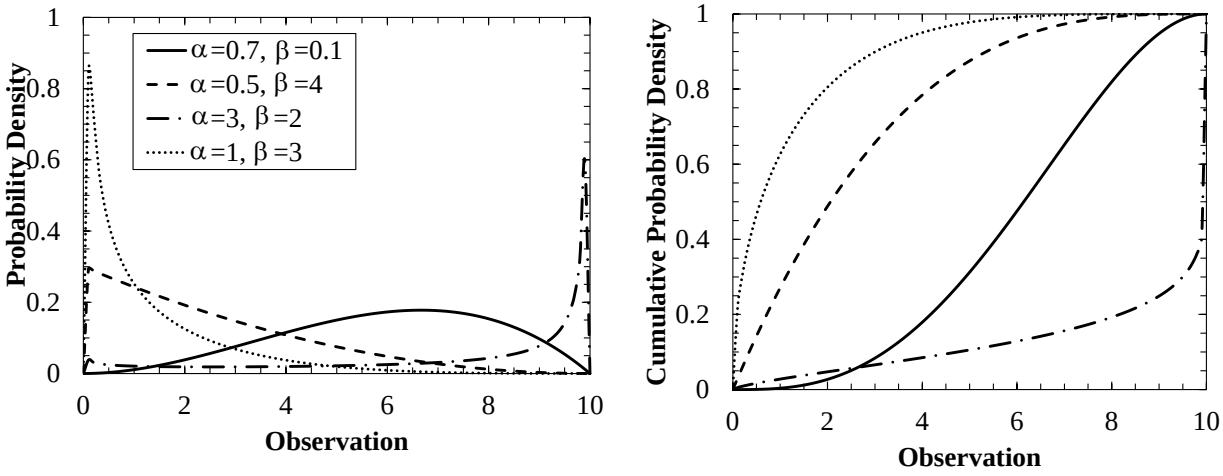

Figure 3.5. Four beta distributions with varying shape and scale parameters a) probability density and b) cumulative probability density distribution (modified from NIST/SEMATECH 2012).

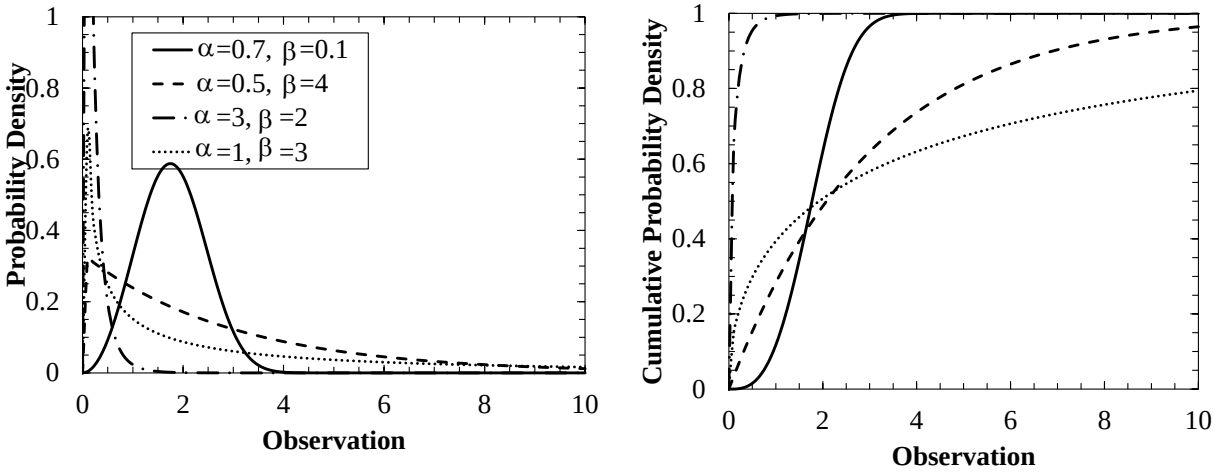

Figure 3.6. The Weibull distribution with varying shape and scale parameters a) probability density and b) cumulative probability density distribution (modified from Johnson et al. 1994).

$$f(y) = \frac{1}{\sqrt{2\pi}\sqrt{\sigma^2}} e^{\frac{-(y-\mu)}{2\sigma^2}}$$ (Rencher 2002) Equation 3.12

$$g(\boldsymbol{y}) = \frac{1}{p\sqrt{2\pi}\boldsymbol{\Sigma}^{1/2}} e^{-(\boldsymbol{y}-\boldsymbol{\mu})'\boldsymbol{\Sigma}^{-1}(\boldsymbol{y}-\boldsymbol{\mu})/2}$$ (Rencher 2002) Equation 3.13

$$f(x) = \frac{\Gamma(\alpha+\beta)}{\Gamma(\alpha)\Gamma(\beta)} x^{\alpha-1}(1-x)^{\beta-1}$$ (Evans et al. 2000) Equation 3.14

$$\Gamma(\alpha+1) = \alpha\Gamma(\alpha)$$ (Evans et al. 2000) Equation 3.15

$$f(x) = \frac{\alpha}{\beta}\left(\frac{x}{\beta}\right)^{\alpha} e^{-(x/\beta)^{\alpha}}$$ (modified from Cassady and Nachlas 2008) Equation 3.16

According to Shapiro and Wilk (1965), the normality of a dataset can be evaluated using the Shapiro-Wilks test for the univariate case. The Shapiro-Wilks test is a parametric testing method used to determine if a sample is normally distributed within a 95 percent confidence interval. Similarly, as stated in NIST/SEMATECH (2012), the chi-square goodness-of-fit test can also be utilized to determine the degree to which the data can be modeled by using a normal distribution. The nonparametric method to determine the "best" distribution of a particular univariate dataset is the Kolomorov-Smirnov (KS) test. As mentioned in Chakravart et al. (1967), the one sample KS test is used to determine the probability that the distribution of the sample corresponds to the tested distribution. As shown in Figure 3.7, in the one sample KS test, the sample is compared to the expected value of a distribution type, particularly the normal distribution or the lognormal distributions. The probability density function is provided in

Equation 3.17. The new variables in Equation 3.17 include: the kernel function (K), the observation number (x), the sample number (n), and the bandwidth (h>0).

$$f_h(x) = \frac{1}{nh}\sum_{i=1}^{n} K\left(\frac{x - x_i}{h}\right) \quad \text{(Silverman 1986)} \qquad \text{Equation 3.17}$$

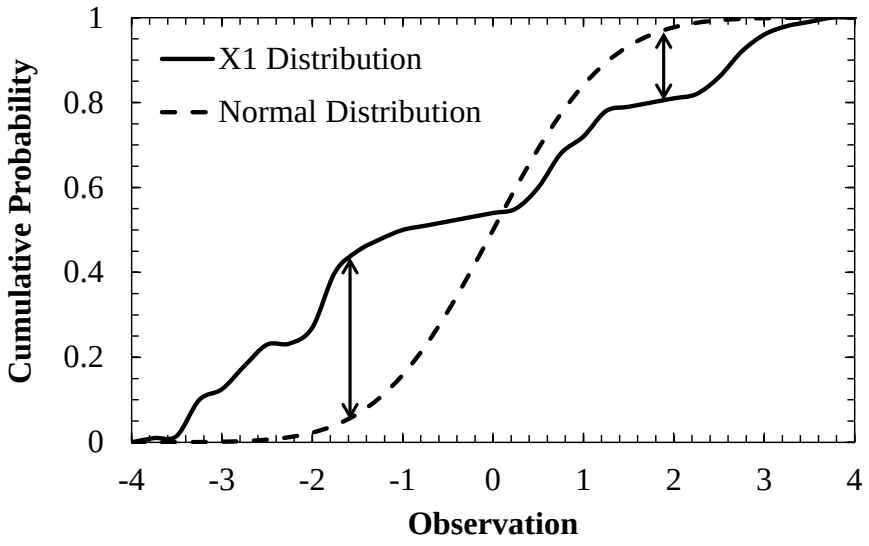

Figure 3.7. KS test compared to a normal distribution graphical representation (modified from NIST/SEMATECH 2012).

3.2.1.3. Multivariate Statistical Analysis

As stated in Rencher (2002), multivariate statistical analyses are typically utilized when there is a correlation between multiple variables within the dataset. An example of a multivariate dataset is measurements of people including height, weight, and resting heart rate (Rencher 2002). For the case in which data are interdependent, univariate statistical analysis is not sufficient to characterize/compare the data since the relationship between the variables is not accounted for. Multivariate multiple regression is utilized to determine the viability of using

multivariate statistical testing, then statistical tests such as the Two-Sample T^2 test are utilized to determine the statistical difference between two multivariate datasets. As presented in Rencher (2002), the T^2 statistic is determined using Equations 3.18 through 3.21, by using the sample mean vectors with the assumption that the two sample covariance vectors are equivalent (in order for the T^2 statistic to have a T^2 distribution). The variables utilized in Equation 3.18 through Equation 3.21 include: the matrix of sum of squares and cross products i ($\boldsymbol{W_i}$), the number of samples in dataset i (n_i), the covariance matrix for dataset i ($\mathbf{S_i}$), the population covariance matrix ($\mathbf{S_{pl}}$), the calculated statistic for the probability of p and a degree of freedom of n_1+n_2-2 ($\mathbf{T^2_{p,n_1+n_2-2}}$), and is the matrix of the mean values of dataset i ($\bar{\mathbf{y}}_i$).

$$\mathbf{W_1} = (n_1 - 1)\mathbf{S_1} \qquad \text{(Rencher 2002)} \qquad \text{Equation 3.18}$$

$$\mathbf{W_2} = (n_2 - 1)\mathbf{S_2} \qquad \text{(Rencher 2002)} \qquad \text{Equation 3.19}$$

$$\mathbf{S_{pl}} = \frac{1}{n_1 + n_2 - 2}(\mathbf{W_1} + \mathbf{W_2}) \qquad \text{(Rencher 2002)} \qquad \text{Equation 3.20}$$

$$\mathbf{T^2_{p,n_1+n_2-2}} = \frac{n_1 n_2}{n_1 + n_2}(\bar{\mathbf{y}}_1 - \bar{\mathbf{y}}_2)'\mathbf{S_{pl}^{-1}}(\bar{\mathbf{y}}_1 - \bar{\mathbf{y}}_2) \qquad \text{(Rencher 2002)} \qquad \text{Equation 3.21}$$

3.2.2. Bayesian Analysis

As discussed in Hoff (2009) and Lee (2012), Bayesian analysis is derived from Bayes theorem (Equation 3.22) which states that the probability of event θ given event y is equivalent to the product of the probability of event θ and the probability of event y given event θ divided by the probability of event y. By transforming Equation 3.22, the resulting probability of θ given

y is a function of the known probability of θ and the likelihood probability of y given θ, as presented in Equation 3.23.

$$p(\theta|y) = \frac{p(\theta)p(y|\theta)}{p(y)} \qquad \text{(Hoff 2009 and Lee 2012)} \qquad \text{Equation 3.22}$$

$$p(\theta|y) = \frac{p(y|\theta)p(\theta)}{\int p(y|\theta)p(\theta)d\theta} \qquad \text{(Hoff 2009 and Lee 2012)} \qquad \text{Equation 3.23}$$

Bayesian inference can be utilized to determine the posterior mean and variance of a sample set in relation to prior and sampled distributions. The prior distribution is from either a population distribution with a known mean and variance or a larger sampled distribution. For a normally distributed prior population and a normally distributed sampled dataset, the posterior distribution is also a normal distribution with a mean value and variance value that are calculated using Equations 3.24 through 3.28.

$$\lambda_n = \frac{\tilde{\tau}_p^2}{\tilde{\tau}_p^2 + n_s\tilde{\sigma}_s^2}\lambda_p + \frac{n_s\tilde{\sigma}_s^2}{\tilde{\tau}_p^2 + n_s\tilde{\sigma}_s^2}\lambda_s \qquad \text{(Hoff 2009)} \qquad \text{Equation 3.24}$$

$$\tilde{\tau}_p^2 = \frac{1}{\tau_p^2} = \frac{\kappa_p}{\zeta_p^2} \qquad \text{(Hoff 2009)} \qquad \text{Equation 3.25}$$

$$\tilde{\sigma}_s^2 = \frac{1}{\zeta_s^2} \qquad \text{(Hoff 2009)} \qquad \text{Equation 3.26}$$

$$\tau_n^2 = \frac{1}{\tilde{\tau}_p^2 + \frac{n_s}{\zeta_s^2}} \qquad \text{(Hoff 2009)} \qquad \text{Equation 3.27}$$

$$\tau_n^2 = \frac{n_n}{\zeta_n^2} \qquad \text{(Hoff 2009)} \qquad \text{Equation 3.28}$$

The parameters utilized in Equation 3.24 include: the posterior mean (λ_n), the prior precision ($\tilde{\tau}_p^2$ as calculated using Equation 3.25), the number of sampled data (n_s), the sample variance ($\tilde{\sigma}_s^2$), the mean of the prior distribution (λ_p), and the mean of the sampled data (λ_s). The new variable included in Equation 3.25 is the influence factor of the prior distribution (κ_p), which ranges from zero to the number of data in the prior distribution. Furthermore, new variables in Equation 3.26 through Equation 3.28 include: the precision of the sampled data (ζ_s^2), the variance of the posterior distribution (τ_n^2), the number representing the total number of posterior data points ($n_n = \kappa_p + n_s$), and the precision of the posterior distribution (ζ_n^2).

Bayesian analyses have been utilized in civil engineering particularly for model updating or predicting property characterization, by using Bayesian analyses techniques. In particular, Goh et al. (2005) utilized Bayesian analysis as a neural network to determine the undrained side resistance along DSF as a relationship to the undrained shear strength, the effective overburden stress, and the alpha factor. The Bayesian updating method has also been utilized to predict the load-settlement behavior of footings, as presented in Najjar et al. (2011), the deterioration of concrete bridges, as presented in Enright and Frangopol (1999), the deterioration of bridge infrastructures regarding health monitoring, as presented in Taflanidis and Gidaris (2013), and slope failure probability, as presented in Cheung and Tang (2000). Similarly, the Bayesian updating method has been utilized to determine the resistance factors for driven piles as presented in Park et al. (2012) and Jabo (2014).

3.2.3. Statistical Analyses in Civil Engineering

In geotechnical engineering, the distribution type for soil parameters has been speculated to be normal, lognormal, or beta distributed (Lumb 1970, Harrop-Williams 1986). Undrained shear strength is sometimes modeled as a normal or beta distribution according to Chi-squared tests; however, the lognormal distribution, which has been most suggested for use, is not an accurate distribution for undrained shear strength according to Lumb (1970). Furthermore, according to Brejda et al. (2000) from observations based on tests performed on a regional scale, most soil properties are not normally distributed according.

Statistical principles have also been used in determining the probability of failure for geotechnical structures (Luo et al. 2013) and for analyzing CPT and falling weight deflectometer (FWD) tests (Niazi et al. 2011, Lopez-Caballero et al. 2011, respectively). Yang et al. (2008) and Yu et al. (2012) have also utilized statistical bias to compare methods for determining the nominal capacity of DSF when using BLC. Two sample and one sample statistical testing techniques such as the T-test, Wilcoxon test, and F-test have been utilized to verify the variance in sample homogeneity and data consistency for normally distributed asphalt compaction testing data (Bo et al. 2013). Likewise, Unanwa and Mahan (2012) utilized the T-test to analyze normalized 28-day compressive strengths of concrete cylinders for highway bridges in California.

Variability and uncertainty in the soil properties were characterized by Bilgin and Mansour (2013), in relation to the under-prediction or over-prediction of settlement, by using empirical equations to calculate the compression index. Natural variability as compared with the uncertainty in the determination of soil properties is discussed in Rogers and Chung (2013) in

relation to virtual geotechnical databases, and in Uzielli and Mayne (2013), in relation to the strength (friction angle and stiffness) of sands. The spatial variability of soil properties is necessary in the design of DSF, as discussed in Phoon et al. (2003) and Cao et al. (2013). In particular, as discussed in Phoon et al. (2003), the modified Bartlett statistic is utilized to determine the homogeneity of soil layers. The amount of uncertainty in reliability-based design and load resistance factor design (as will be discussion in Section 3.3), with respect to geotechnical engineering properties (i.e. soil types, soil properties, etc.), have been previously investigated in Wu (2013) and Fan and Liang (2013). The recent publication dates of many of the aforementioned articles are indicative of the newfound importance of utilizing statistical methods to better assess design approaches.

3.2.4. Simulation Methods

3.2.4.1. Monte Carlo Simulation Method

According to Haldar and Mahadevan (2000), the Monte Carlo simulation method is comprised of six major principles including: 1) expressing the problem with respect to the random variables of interest, 2) randomly generating variable values, 3) determining the parameters of the probability density function (PDF) and probability mass function (PMF) for all the random variables, 4) through numerical experimentation, evaluate the problem for each set of the random variables, 5) determine probabilistic data for multiple sets of data, and 6) determine the accuracy and efficiency of the simulated model. As discussed in Misra et al. (2007), the Monte Carlo simulation method consists of a series of trials where a random number is generated from the assumed/obtained probability distribution function for each random variable. The number of trials is dependent upon the chosen level of reliability. According to Baecher and

Christian (2003), more than 200,000 trials are required to achieve 95% confidence that the error was 0.005. The Monte Carlo simulation method used in the calibration of resistance factors for deep foundations is a probabilistic application (as opposed to a stochastic application process) to determine properties such as site characterization properties and soil-shaft interaction properties through random, but constrained, number generation. One example of using the Monte Carlo simulation method, as presented in Misra and Roberts (2006), was to model the shear modulus (K) parameter for a certain type of soil as a lognormal distribution (Figure 3.8). Specifically, the Monte Carlo simulation method has been used (rather than the first order second moment method) because soil properties and soil-shaft interaction behavior are nonlinear. Although the Monte Carlo simulation method is a good simulation method, particularly for soil properties, some deficiencies are present when utilizing the Monte Carlo method. According to Niederreiter (1992), these deficiencies include generating “true” random samples and only obtaining probabilistic error bounds when the Monte Carlo method is used to perform numerical integration.

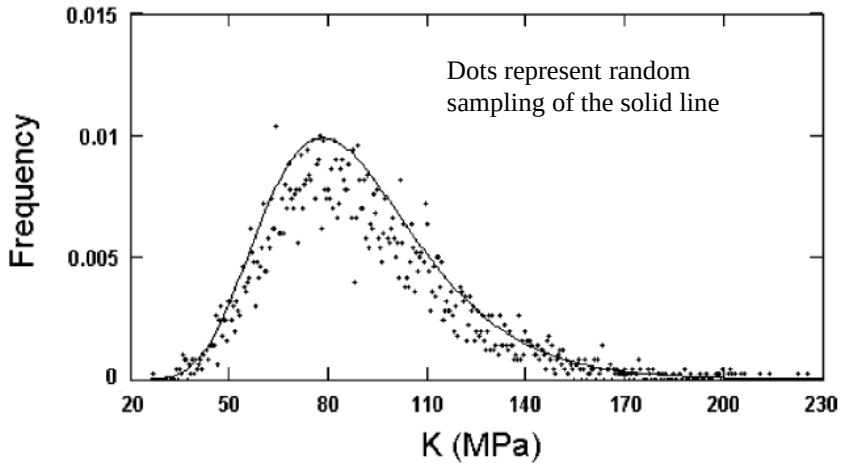

Figure 3.8. Random values of the shear modulus of shaft-soil interface from using a log-normal distribution (Misra and Roberts 2006).

3.2.4.2. First Order Second Moment

As discussed in Baecher and Christian (2003), first order second moment (FOSM), also known as mean value first order second moment, is based on the first order Taylor series for the mean, variance, and standard deviation values. In general, if there are N variables, then N partial derivatives are evaluated and 2N+1 points are used for numerical approximation for FOSM. A performance function is commonly utilized in along with the FOSM to evaluate properties such as probability of failure (as presented in Equations 3.29 and 3.30) when the random variables are normally distributed. According to Haldar and Mahadevan (2000), deficiencies associated with the FOSM include disregarding the variable distribution information, neglecting the higher order (second, third, etc.) terms which could introduce significant error, and the failure of the safety index to remain constant under some performance functions (mechanically equivalent). The new variables in Equations 3.29 and 3.30 include: the reliability index (β), the mean value of the random variable R (μ_R), the mean value of the random variable S (μ_S), the variance value of the

random variable R (σ_R^2), the variance value of the random variable S (σ_S^2), and the probability of failure (p_f).

$$\beta = \frac{\mu_R - \mu_S}{\sqrt{\sigma_R^2 + \sigma_S^2}} \quad \text{(Haldar and Mahadevan 2000)} \quad \text{Equation 3.29}$$

$$p_f = 1 - \Phi(\beta) \quad \text{(Haldar and Mahadevan 2000)} \quad \text{Equation 3.30}$$

3.2.4.3. First Order Reliability Method

According to Zhao and Ono (1999), in structural reliability, the first order reliability moment (FORM) has been considered to be one of the most reliable computational methods. The first order reliability method (FORM) is based upon the Hasofer and Lind (1974) approach that is described using Equation 3.31. Specifically, the FORM is an approximation of the integral of the probability of failure since the higher order terms are removed. The range of values for which the FORM can be implemented (instead of the second order reliability moment) is given in Equation 3.32 and the empirical range of the FORM is presented in Figure 3.9. The FORM is typically only accurate for small number of random variables and when the performance function is linear (Zhao and Ono 1999). The general approach to the FORM, as suggested by Zhao and Ono (1999), is as follows: 1) determine the point fitting limit state surface, 2) compute the total principal curvature, and 3) compute the probability of failure.

The variables in Equation 3.31 include: a random variable (x_i), the mean of the random variable x (μ_{x_1}), function of the random variable x (g[x]), the function of the mean of the random variable x ($g[\mu_x]$), and the partial integral of the function with respect to the random variable x

($\frac{\partial g}{\partial x_i}$). Variables in Equation 3.32 are the standard normal probability function (Φ) and the reliability index (β).

$$g(x_1, \ldots, x_n) \approx g(\mu_{x_1}, \ldots, \mu_{x_n}) + \sum_{i=1}^{n} (x_i - \mu_{x_1}) \frac{\partial g}{\partial x_i}$$ (Hasofer and Lind 1974) Equation 3.31

$$|\Phi(-\beta_s) - \Phi(-\beta_F)| \leq 0.05\Phi(-\beta_s)$$ (Zhao and Ono 1999) Equation 3.32

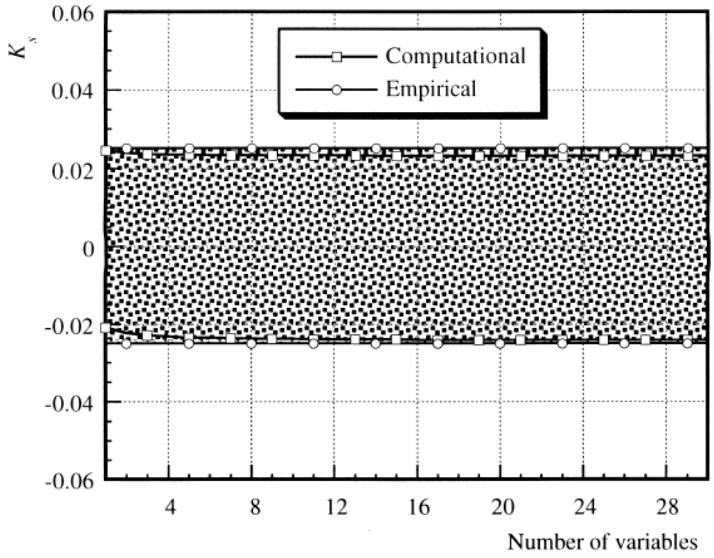

Figure 3.9. Computational and empirical range of FORM with respect to the number of variables (Zhao and Ono 1999).

3.3. Calibration of Resistance Factors for Deep Foundations

According to a survey performed by Paikowsky (2004), 90 percent of personnel (43 state highway officials and 2 FHWA personnel) utilized allowable stress design (ASD), 35 percent also used AASHTO load factor design, and 28 percent also used AASHTO LRFD. Similarly, for design of DSF, the static axial capacity was evaluated by: 36 using the α-method (Reese and O'Neill 1988), 41 using the β-method (Reese and O'Neill 1988), nine using Reese and Wright

(1977) method for side friction in cohesionless soils, 39 using the FHWA (O'Neill et al. 1996) method for intermediate geomaterials, 11 using the Carter and Kulhawy (1988) method for intermediate geomaterials, and 11 used other methods. The amount of people still utilizing ASD instead of LRFD, as of 2004, prompted the national calibration of resistance factors (Paikowsky 2004) and other localized calibrations of load and resistance factors for deep foundations.

3.3.1. Load and Resistance Factor Design for Drilled Shaft Foundations

According to Paikowsky (2004), until 2001, the ASD method was used to design deep foundations within the United States. Under this methodology, a global factor of safety (FS) was utilized (Equation 3.33) instead of load and resistance factors. While the value of FS varied depending on the level of reliability required when considering economics, factors such as bias and conservatism of the methods were not accounted for by utilizing this method (Paikowsky 2004). A resistance factor (ϕ, which is not the same as the aforementioned friction angle that utilized the same variable) is calculated using Equation 3.34 based on first order second moment (FOSM) analysis by assuming lognormal distributions for the variables associated with the resistance. According to Nowak (1999), to correspond with the current structural code, first order reliability method (FORM) was used to determine resistance factor calibration for deep foundations. The relationship between the resistance factors calculated using FOSM and FORM (for a target reliability index of 2.33) is presented in Figure 3.10. The suggested resistance factors (and the related FS), as obtained from Paikowsky (2004) are presented in Table 3.2. Using this methodology, the resistance factor is dependent upon the analysis method (design equations/software program), the soil type, the variability within the soil, and the number of load tests. The resistance factors are significantly increased by performing at least one full-scale load

test, particularly in soil with low variability (Table 3.3). These resistance factors are based on a national database of static load tests that were collected from across the United States. As discussed in more detail in Sections 3.3.3 through 3.3.7, localized calibrations of resistance factors have been performed for DSF since 2004.

$$Q \leq Q_{all} = \frac{R_n}{FS} = \frac{Q_{ult}}{FS}$$ (Paikowsky 2004) Equation 3.33

$$\phi = \frac{\lambda_R \cdot (\sum \gamma_i \cdot Q_i) \cdot \sqrt{\frac{1 + COV_Q^2}{1 + COV_R^2}}}{\overline{Q} \cdot \exp\left\{\beta_T \sqrt{\ln\left[(1 + COV_R^2)(1 + COV_Q^2)\right]}\right\}}$$ (Barker et al. 1991; Paikowsky 2004) Equation 3.34

The variables utilized in Equation 3.33 include: the design load (Q), the allowable design load (Q_{all}), the resistance of the structure (R_n), the factor of safety (FS), and, the ultimate resistance (Q_{ult}). New variables utilized in Equation 3.34 include: the resistance factor (ϕ), the bias factor of resistance (λ_R), the i^{th} load factor (γ_i), the i^{th} load (Q_i), the coefficient of variation of the load (COV_Q), the coefficient of variation of the resistance (COV_R), the mean load ($\overline{Q}$), and the target reliability index (β_T).

Table 3.2. Resistance factors and associated factors of safety with efficiency measures for analysis methods of drilled shaft foundations (modified from Paikowsky 2004).

Pile Type or Construction	Soil Type	Method of Analysis	β = 2.33 β = 3.00 **Resistance Factor, ϕ**	γ_L = 1.75 **Efficiency, ϕ/λ**	γ_D = 1.2 **Factor of Safety, FS**	DL/LL = 2 **Actual Mean FS, FS x λ**
Mixed	All	R&W Skin[1]	0.45	0.42	3.18	3.41
			0.33	0.31	4.34	4.64
Mixed	Rock	C&K Total[2]	0.60	0.48	2.38	2.93
			0.45	0.37	3.13	3.86
Mixed	Sand & Clay	FHWA Skin[3]	0.78	0.63	1.81	2.26
			0.63	0.50	2.25	2.81

[1]Reese and Wright (1977) Method
[2]Carter and Kulhawy (1988) Method
[3]FHWA AASHTO (2001) Method

Table 3.3. Resistance factor values as a function of the number of load tests, site variability, and target reliability (modified from Paikowsky 2004).

Site Variation	Number of Load Tests, N	Soil Coefficient of Variation, COV	Target Reliability, β		
			2.00	**2.33**	**3.00**
Low	1	0.18	0.86	0.80	0.67
	2	0.13	0.96	0.89	0.78
Medium	1	0.27	0.73	0.65	0.53
	2	0.19	0.85	0.78	0.66
High	1	0.36	0.61	0.54	0.42
	2	0.25	0.75	0.68	0.55

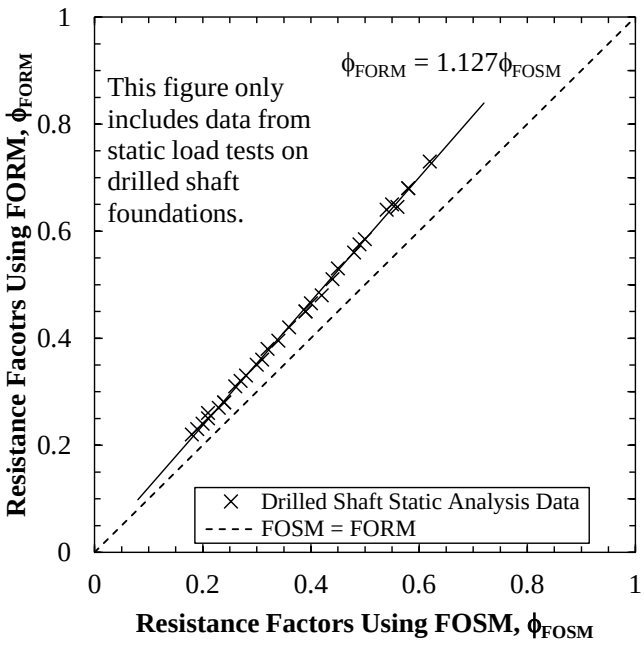

Figure 3.10. Comparison of resistance factors calculated using FOSM and FORM for a target reliability of $\beta = 2.33$ (modified from Paikowsky 2004).

3.3.2. Site Specific Resistance Factor Calibration

As described in Basu and Salgado [2012] and presented in Table 3.4, resistance factors were determined for different: DSF dimensions, live load to dead load ratios, probability of failure, and soil profiles. Moreover, resistance factors for side and base resistance values for DSF in normally consolidated sand have been determined in Basu and Salgado (2012) as presented in Table 3.5. Salgado and Woo (2011) recommended that resistance factors for base and side resistance in cohesive soils are 0.70 and 0.75, respectively, for a probability of 10^{-3} and 0.65 and 0.70, respectively, for a probability of failure of 10^{-4}. Similarly Fan and Liang (2013) determined that the probability of failure for DSF varied based on the soil variability model (i.e. distribution type, standard deviation of soil properties). Moreover, according to Klammler et al. (2013), the types of soil testing and DSF testing (i.e. site specific load testing, boring within the DSF

footprint, and off-site boring data) affected the uncertainty of the design of a DSF therefore affected the resistance factors and the design unit side resistance depending upon the type of site investigation that was performed. For multiple geological site investigation types (load testing [LT], center boring in the shaft footprint [CB], and off site data [OS]), certain resistance factors and design unit side resistance were determined, as presented in Table 3.6. In Liang and Li (2013), resistance factors for a database of 65 top-down load tests for DSF in cohesive soils, cohesionless soils, or mixed soils were determined using the Monte Carlo simulation method (Table 3.7). The bias that was used to calculated the resistance factors, by Liang and Li (2013), was defined as the measured nominal resistance from a given load test divided by the predicted resistance that was obtained from the SHAFT program (Reese et al. 2001), a program that employed the O'Neill and Reese (1999) method.

Table 3.4. Mean and standard deviation of resistance factors for drilled shaft foundations in six soil types using load factors of 1.25 and 1.75 for dead loads and live loads, respectively (modified from Basu and Salgado 2012).

Soil Profile	Probability of Failure, p_f	Mean		Standard Deviation	
		$(RF)^{code}_{side}$	$(RF)^{code}_{base}$	$(RF)^{code}_{side}$	$(RF)^{code}_{base}$
1	10^{-3}	0.805	0.916	0.027	0.062
	10^{-4}	0.704	0.809	0.029	0.077
2	10^{-3}	0.801	0.970	0.023	0.050
	10^{-4}	0.715	0.831	0.052	0.103
3	10^{-3}	0.823	0.959	0.024	0.069
	10^{-4}	0.723	0.851	0.053	0.101
4	10^{-3}	0.821	0.955	0.022	0.069
	10^{-4}	0.721	0.848	0.051	0.101
5	10^{-3}	0.815	0.956	0.026	0.069
	10^{-4}	0.713	0.847	0.048	0.098
6	10^{-3}	0.835	0.920	0.031	0.031
	10^{-4}	0.740	0.813	0.076	0.079

Table 3.5. Recommended resistance factors for side and base resistance for DSF constructed in normally consolidated sand from Basu and Salgado [2012].

Probability of Failure, p_f	Side Resistance Factors	Base Resistance Factors
0.001	0.70	0.75
0.0001	0.65	0.70

Table 3.6. Resistance factor (ϕ) and design unit side resistance (f_{des}) for multiple geological site investigations and a shaft length of 10m (modified from Klammler et al. 2013).

f_n (MN/m^2)	LT		LT+CB		OS		LT+OS		LT+CB+OS	
	ϕ	f_{des} (MN/m^2)	ϕ	f_{des} (MN/m^2)	ϕ	f_{des} (MN/m^2)	ϕ	f_{des} (MN/m^2)	ϕ	f_{des} (MN/m^2)
0.65			0.64	0.35					0.72	0.46
0.86			0.75	0.53					0.78	0.58
1.14	0.46	0.34	0.74	0.7	0.51	0.47	0.63	0.51	0.77	0.72
U[1]			0.69	0.48					0.74	0.55

U[1] – expected values of ϕ and f_{design} for unknown f_n

Table 3.7. Calibrated total resistance factors for drilled shaft foundations (modified from Liang and Li 2013).

β_T = 3.0	ϕ calibrated by fit to all data	ϕ calibrated by fit to tail
Current Study	0.45 (0.45) in clay (15 cases) 0.51 (0.50) in sand (18 cases) 0.35 in mixed soils (65 cases)	0.56 (0.55) in clay (8 cases) 0.52 (0.50) in sand (10 cases) 0.52 in mixed soils (35 cases)
Paikowsky (2004) and AASHTO (2007)	0.45 in cohesive soils 0.55 in cohesionless soils 0.60 in IGM/weak rock	

Load tests on DSF in weak rock (generally shale, siltstone/sandstone, and limestone) were performed using a BLC and are reported in Yang et al. (2008). The resistance factors based on these 19 load tests (parameters obtained for a Monte Carlo simulation that based on the total side resistance, as presented in Table 3.8) were determined to be 0.55 and 0.69 for a β of three by using for the total side resistance and the unit side resistance, respectively. Based on this data, the determined resistance factors were close to those recommended for determination of side resistance by AASHTO (2007).

Table 3.8. Parameters for the Monte Carlo Simulation based on the Lognormal Distribution (Yang et al. 2008).

Parameter	Total Side Resistance	Unit Side Resistance
μ_R	4.3	4.3
σ_R	3.4	3.0
COV_R	0.79	0.70

3.3.3. Colorado

In the state of Colorado, DSF are commonly used as the foundation system for bridges, earth embankments, high-rise buildings, and residential buildings. In weak rock deposits, a prevalent geologic feature in Colorado, the SPT-based "Denver method," as described in Vessley and Liu (2006), is typically used to determine the allowable end bearing and side resistance

(Equations 3.35 and 3.36). The "Denver method" along with a required minimum embedment length of 10 to 15 feet, depending upon the weathering of the rock, were analyzed by Abu-Hejleh et al. (2003). Abu-Hejleh et al. (2003) determined that the weathered rock in Colorado should be treated as stiff clay instead of rock (based on the findings of the full-scale load tests). The use of LRFD, as required in AASHTO (2006), was considered impractical as a design practices in Colorado because the typical foundation capacity, in the geology of Colorado, is typically lower than the value that is obtained by using standard practice (Vessely and Liu 2006). However to utilize the "Denver method," resistance factors should be determined based on design of DSF using the "Denver method" as prescribed in Vessely and Liu (2006).

$$q_{allowable}(ksf) = \frac{N}{2} \qquad \text{(Vessely and Liu 2006)} \qquad \text{Equation 3.35}$$

$$f_{allowable}(ksf) = \frac{N}{20} \qquad \text{(Vessely and Liu 2006)} \qquad \text{Equation 3.36}$$

3.3.4. Florida

As described in McVay et al. (2002), in the state of Florida, localized resistance factors were calibrated for DSF constructed in limestone. As previously mentioned, DSF are a common foundation type for structures constructed in Florida limestone. Six bridge sites where BLC and Statnamic tests were performed were used to determine the cost benefits obtained by LRFD. A total of 23 BLC tests and 12 Statnamic tests were used to determine the cost benefits of using resistance factors (McVay et al. 2002). Because the amount of resistance contributed by the end bearing component of the total capacity is typically disregarded for the design of DSF in the state of Florida, only the results for the measured and the predicted unit skin friction were compared. For all but one site, the measured unit skin friction values were greater than the predicted skin

friction values and the measured standard deviation values were also less than the predicted standard deviation values. The obtained resistance factors (ϕ) were calculated to range from 0.36 to 0.81 for failure probabilities ranging from 2×10^{-6} to 0.08. In summary, for DSF constructed in Florida limestone, economical savings were achieved by including full-scale load testing (BLC or Statnamic) in combination with the associated increase in the resistance factor (ϕ).

3.3.5. Kansas

According to the Kansas Department of Transportation (KDOT 2013), DSF in Kansas are considered as a viable foundation system when the conditions include that: 1) the bedrock being located less than 10 feet below ground surface, 2) the water table is relatively high and a deep cofferdam would be required, 3) a spread footing foundation would be uneconomical, and 4) concerns exist about vibrations, noise, or overhead clearance. Misra et al. (2007) utilized the "t-z" method to model the soil resistance along the length of the drilled shaft foundation, for non-linear load-displacement behavior, by using the Monte Carlo simulation method. Through this approach, the probabilistic reliability index was calculated using Equations 3.37 and 3.38. As mentioned in Misra et al. (2007), the reliability index was based on a cumulative distribution frequency for DSF axial capacity for an allowable displacement of 10mm. Unlike the probabilistic methods in Misra et al. (2007), Equation 3.39 can be utilized to quickly and easily determine resistance factors for the design of DSF. Procedures to determine the service limit state resistance factors for DSF under compressive loading was also discussed in Misra and Roberts (2009). Specifically, the subsequent load capacity relationships for allowable top displacements of 10mm and 20mm were utilized to determine the resistance factors for the service limit state. The resistance factors, with respect to the soil-shaft interface coefficient of

variation (COV) for a 1520mm DSF, are presented in Figure 3.11. In Roberts et al. (2011), documentation is presented on a 1.07m diameter DSF that was installed in shale bedrock for a length of 4.2m. Based on a performance-based design, the resistance factors for service and strength limits states were 0.52 and 0.65, respectively (Roberts et al. 2011).

$$\beta = -\phi^{-1}(p_f) \qquad \text{(Misra et al. 2007)} \qquad \text{Equation 3.37}$$

$$p_f = \phi\left(\frac{\ln(1) - \mu_{lnFS}}{\sigma_{lnFS}}\right) \qquad \text{(Misra et al. 2007)} \qquad \text{Equation 3.38}$$

$$\phi_R = \frac{l_R\left(\frac{\gamma_D E(Q_D)}{E(Q_L)} + \gamma_L\right)\sqrt{\frac{1+\Omega_{QD}^2+\Omega_{QL}^2}{1+\Omega_R^2}}}{\left(\lambda_{QD}\frac{E(Q_D)}{E(Q_L)} + \lambda_{QL}\right)e^{\beta\sqrt{ln\left[(1+\Omega_R^2)\left(1+\Omega_{QD}^2+\Omega_{QL}^2\right)\right]}}} \qquad \text{(Roberts et al. 2011)} \qquad \text{Equation 3.39}$$

The variables used in Equations 3.37 through 3.39 include: the reliability index (β), the cumulative standard normal distribution function (ϕ), probability of failure at the service limit state (p_f), the log mean of the factor of safety (μ_{lnFS}), the log standard deviation of the factor of safety (σ_{lnFS}), the resistance factor (ϕ_R), bias of the dead load (λ_{QD}), bias of the live load (λ_{QL}), bias of resistance (λ_R), dead load factor (γ_D), live load factor (γ_L), COV for dead load (Ω_{QD}), COV for live load (Ω_{QL}), COV for resistance (Ω_R), and the dead load to live load ratio ($E(Q_D)/E(Q_L)$).

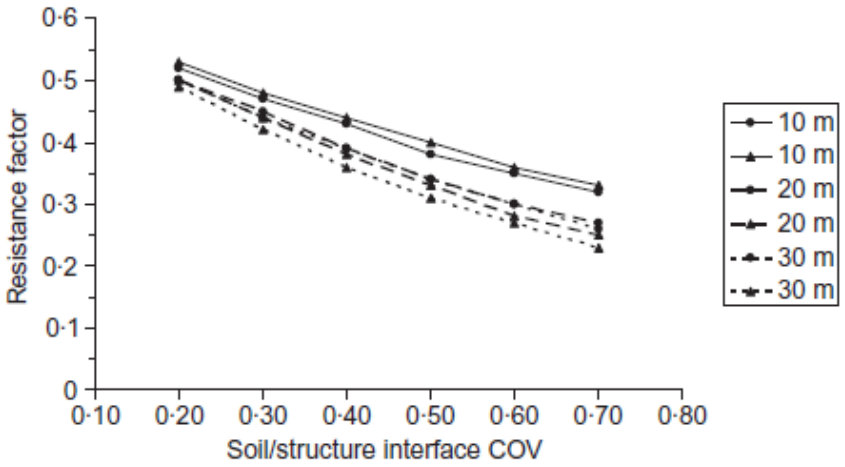

Figure 3.11. Resistance factors for service limit state with respect to COV of the soil-shaft interface parameters for top displacements of 10mm (•) and 20mm (▲), from Misra and Roberts (2009).

3.3.6. Louisiana

As described in Abu-Farsakh et al. (2010), to calibrate localized resistance factors in Louisiana, a database of 26 drilled shafts were obtained from the states of Louisiana and Mississippi. The load-movement behavior of the drilled shaft foundations was predicted using the SHAFT software program. The measured load-movement behavior of these drilled shafts meet the FHWA five percent diameter movement failure criterion (5%D) and the axial nominal resistance was determined using BLC tests (22) or conventional top-down static load tests (4). A Monte Carlo simulation was performed to determine the resistance factors for the Strength I limit state that is described in AASHTO (2007). The target reliability index (β) was calculated using the closed-form solution provided in Equation 3.40, that was proposed by Withiam et al. (1998) and Nowak (1999). Based on the results of the research performed in Louisiana, Yu et al. (2012), the proposed resistance factor was 0.60 (0.590 or 0.598) which is significantly greater than the

recommended resistance factors of 0.45 for cohesive soils as obtained by Paikowsky (2004) and 0.55 in cohesionless soils as obtained by AASHTO (2007). Finally, using the SHAFT software program, the predicted resistance from the DSF was less than the measured drilled shaft resistance by an average of 17 percent (Figure 3.12). The new variables used in Equation 3.40 include: the reliability index (β), and the mean of the resistance loads ($\bar{R}$).

$$\beta = \frac{ln\left[\bar{R}/\bar{Q}\sqrt{\left(1+COV_Q^2\right)/\left(1+COV_R^2\right)}\right]}{\sqrt{ln\left[\left(1+COV_Q^2\right)\left(1+COV_R^2\right)\right]}} \qquad \text{(Yu et al. 2012)} \qquad \text{Equation 3.40}$$

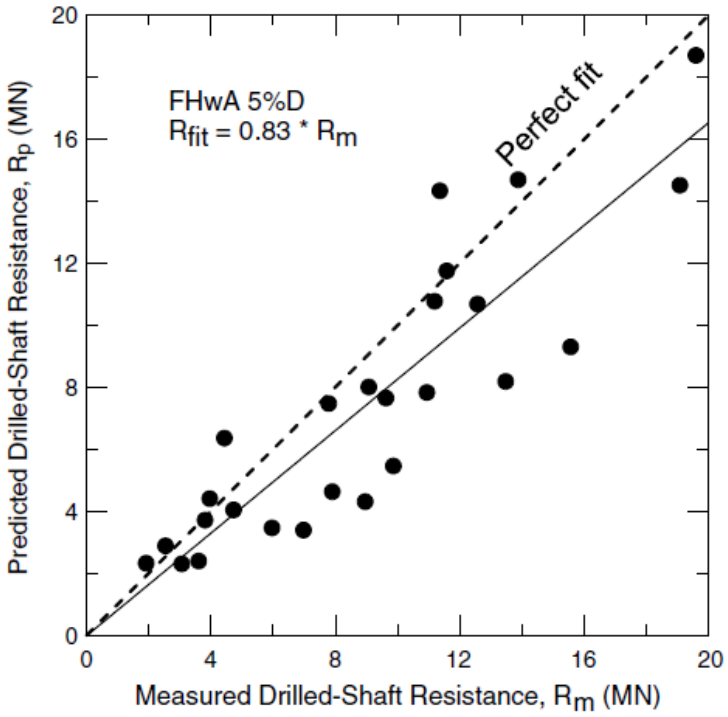

Figure 3.12. Measured resistances as a function of predicted resistances from 26 drilled shaft foundations in Louisiana and Mississippi (from Yu et al. 2012).

3.3.7. Missouri

As reported in Loehr et al. (2013), the localized calibration of resistance factors in the state of Missouri focused upon the geotechnical investigation methods at the site and the type of geologic features (i.e. clay or rock). According to Loehr et al. (2013), the coefficient of variation (COV) was determined to be dependent upon the soil type and upon the geotechnical investigation method. Based on the findings, while not necessarily true in all cases, more advanced or extensive the site characterizations, resulted in less variability and net cost savings from reduced construction costs (Loehr et al. 2013). To calibrate the resistance factors based on the amount of variability and uncertainty resulting from the site characterization, a performance function (g) was utilized (Equation 3.41). The resulting calibration of the resistance factor was based on the COV values for undrained shear strength of cohesive soil or the uniaxial compressive strength of rock, as presented in Figure 3.13. The variables used in Equation 3.41 include: a deterministic design relation for geotechnical resistance (R), probabilistic "model uncertainty" parameter to represent bias (M), the probabilistic live load effect (LL), and the probabilistic dead load effect (DL).

$$g = R(x)M(\bar{x}) - LL - DL \geq 0 \qquad \text{(Loehr et al. 2013)} \qquad \text{Equation 3.41}$$

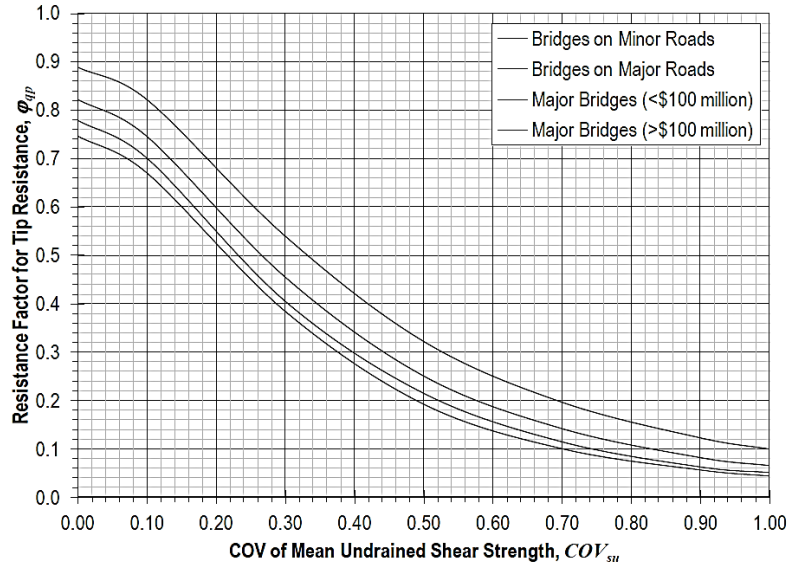

(a)

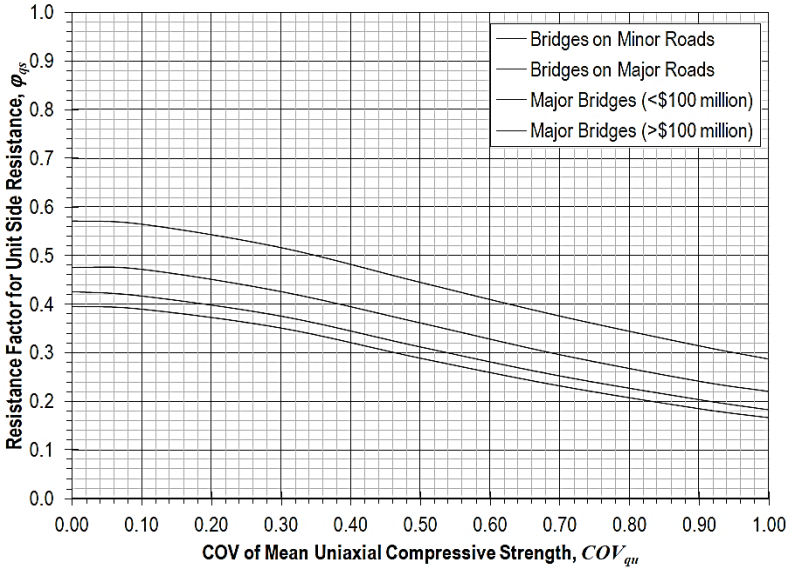

(b)

Figure 3.13. Resistance factors for a) tip resistance of DSF in clay and b) side resistance of DSF in rock (from Loehr et al. 2013).

In Vu (2013), the service limit resistance factors were calibrated for DSF in Missouri. From BLC tests on DSF, empirical normalized load transfer functions (unit side and unit end bearing resistance) were determined as presented in Figure 3.14, for the normalized unit end bearing resistance. From sensitivity analyses performed by Vu (2013) on the determined

resistance factors, it was determined that the uniaxial compressive strength of the rock, the unit side resistance prediction method, the side load transfer, and the applied load were the most sensitive variables (Figure 3.15). From the research performed by Vu (2013), resistance factors for drilled shaft foundations in Missouri can be determined using Equation 3.42. New variables in Equation 3.42 include: the resistance factor (φ), the coefficient of variation (COV), coefficient for different probability of failure (c_{pf}), and coefficient for different ratios of drilled shaft lengths to diameters ($c_{L/D}$).

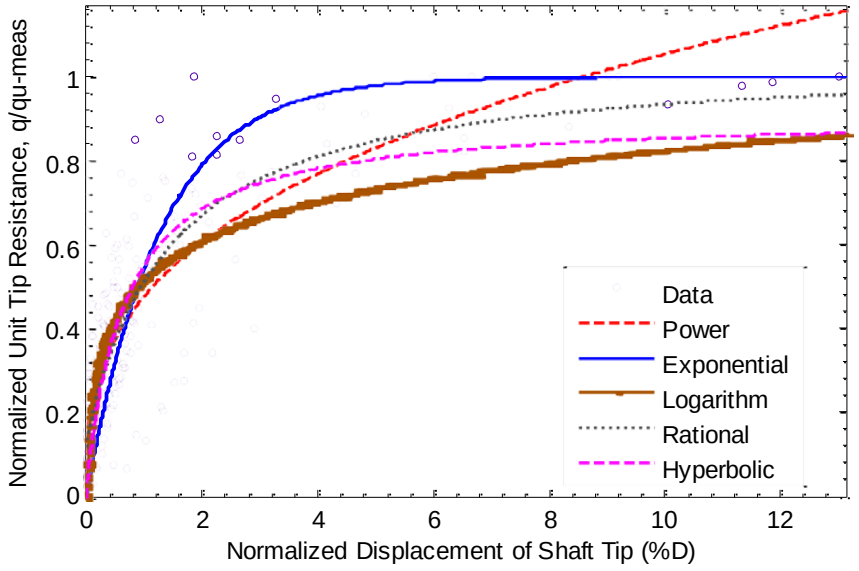

Figure 3.14. Five empirical regression functions of normalized load-displacement curves based on ordinary least squares regression (from Vu 2013).

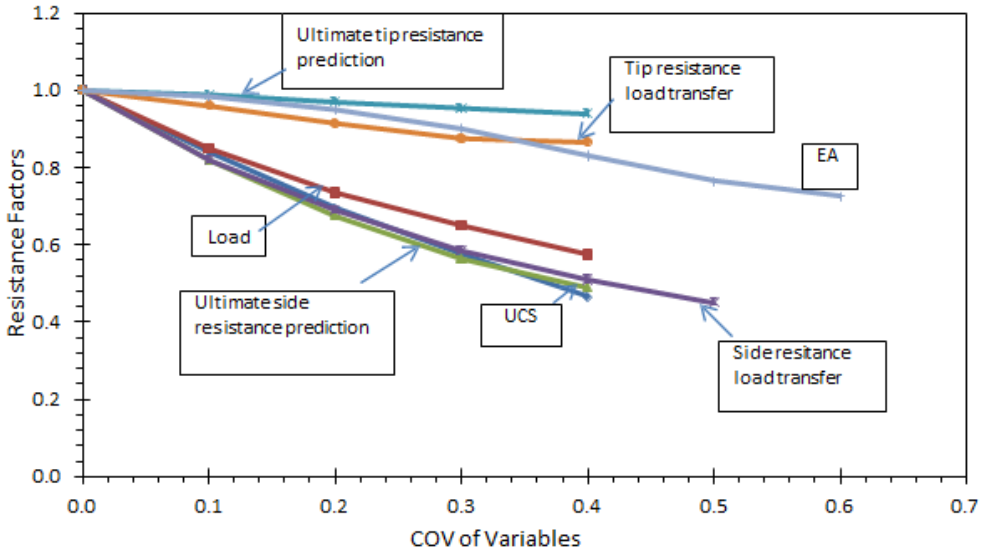

Figure 3.15. Sensitivity analysis of resistance factors as a function of the coefficient of variation of design variables (from Vu 2013).

$$\phi = \left[\frac{(5 - \mathrm{COV}) * \theta - \mathrm{COV}}{10} + c_{pf}\right] * c_{L/D} \qquad \text{(Vu 2013)} \qquad \text{Equation 3.42}$$

3.4. Chapter Summary

The statistical analyses discussed in this chapter included hypothesis testing, reliability analysis techniques that could be utilized to calibrate resistance factor values. Applications of statistical testing in civil engineering ranged from determining: the average concrete compressive strength with a confidence level of 95 percent, variability in soil properties, and the amount of uncertainty in reliability design. In particular, the first-order second-moment method, first-order reliability method, and the Monte Carlo simulation method were discussed in relation to calibration studies across the United States. Results from the resistance factor calibration studies included higher resistance factor values, less uncertainty in the design process, and cost savings.

3.5. References

Abu-Farsakh, Y.M., Yu, X., Yoon, S., and Tsai, C. (2010). "Calibration of Resistance Factors Needed in the LRFD of Drilled Shafts." Rep. No. 470, Louisiana Transportation Research Center, Baton Rouge, LA.

Abu-Hejleh, N., O'Neill, M., Hannemann, D., and Atwooll, W. (2003). "Improvement of the Geotechnical Axial Design Methodology for Colorado's Drilled Shafts Socketed in Weak Rocks." Report No. CDOT-DTD-R-2003-6, Colorado Department of Transportation Research, 192 pgs.

American Association of State Highway and Transportation Officials (2001). LRFD Bridge Design Specifications, AASTHO, Washington, D.C.

American Association of State Highway and Transportation Officials (2006). AASHTO LRFD Bridge Design Interim Specifications, Third Ed., AASTHO, Washington, D.C.

American Association of State Highway and Transportation Officials (2007). LRFD Bridge Design Specifications, Fourth Ed., AASTHO, Washington, D.C., 1938 pgs.

Baecher, G. (1987a). "Statistical Analysis of Geotechnical Data." Vicksburg, US Army Corps of Engineers, Waterways Experiment Station.

Baecher, G. and Christian, J. (2003). Reliability and Statistics in Geotechnical Engineering. Wiley, pp. 618.

Barker, R M, Duncan, J. M., Rojiani, K. B., Ooi, P. S. K., Tan, C. K. and Kim, S. G. (1991). Manuals for Design of Bridge Foundations, NCHRP Report 343, Transportation Research Board, Washington D.C.

Basu, D. and Salgado, R. (2012). "Load and Resistance Factor Design of Drilled Shafts in Sand." Journal of Geotechnical and Geoenvironmental Engineering, Vol. 138, No. 12, pp. 1455-1469.

Bilgin, O. and Mansour, E. (2013). "Variability of Soil Properties and Reliability of Empirical Equations on Soil Settlement Predictions." GeoCongress 2013: Foundation Engineering in the Face of Uncertainty, San Diego, CA, March 3-7, pp. 298-307.

Bo, S., Da-in, G., and Li, M. (2013). "Study on a Test Data Validation Method for Asphalt Pavements." Journal of Highway and Transportation Research and Development, Vol. 7, No. 1, pp. 9-16.

Brejda, J.J., Moorman, T.B., Smith, J.L., Karlen, D.L., Allan, D.L., and Dao, T.H. (2000). Distribution and Variability of Surface Soil Properties at a Regional Scale." Soil Science Society of America Journal, Vol. 64, No. 3, pp. 974-982.

Cao, Z., Wang, J., and Wang, Y. (2013). “Effects of Spatial Variability on Reliability on Reliability-Based Design of Drilled Shafts.” GeoCongress 2013: Foundation Engineering in the Face of Uncertainty, San Diego, CA, March 3-7, pp. 602-616.

Carter, J. P. and Kulhawy, F. H. (1988). "Analysis and Design of Drilled Shaft Foundations Socketed into Rock." Report EL-5918, Electric Power Research Institute, Palo Alto, Calif.

Casella, G. and Berger, R. (2002). *Statistical Inference.* Cengage Learning, 660pgs.

Cassady, C. and Nachlas, J. (2008). Probability Models in Operations Research. CRC Press, Boca Raton, FL, 208 pgs.

Chakravarti, I., Laha, R., Roy, J. (1967). *Handbook of Methods of Applied Statistics, Volume I.* John Wiley and Sons, 160 pgs.

Cheung, R. and Tang, W. (2000). “Bayesian Calibration of Slope Failure Probability.” Geo-Denver 2000, Denver, Colorado, August, pp. 72-85.

Enright, M.P. and Frangopol, D.M. (1999). “Condition Prediction of Deteriorating Concrete Bridges Using Bayesian Updating.” Journal of Structural Engineering, Vol. 125, No. 10, pp. 1118-1125.

Evans, M., Peacock, B., and Hastings, N. (2000). *Statistical Distributions*, 3rd ed. John Wiley and Sons, New York.

Fan, H. and Liang, R. (2013). “Reliability-Based Design of Laterally Loaded Piles Considering Soil Spatial Variability.” GeoCongress 2013: Foundation Engineering in the Face of Uncertainty, San Diego, CA, March 3-7, pp. 475-486.

Geher, G. and Hall, S. (2014). *Straightforward Statistical: Understanding the Tools of Research.* Oxford University Press, New York, 481 pgs.

Gibbons, J.D. and Chakraborti, S. (2003). *Nonparametric Statistical Inference.* Marcel Dekker, Inc. New York.

Goh, A., Kulhawy, F., and Chua, C. (2005). “Bayesian Neural Network Analysis of Undrained Side Resistance of Drilled Shafts.” Journal of Geotechnical and Geoenvironmental Engineering, Vol. 131, No. 1, pp. 84-93.

Haldar, A. and Mahadevan, S. (2000). *Probability, Reliability, and Statistical Methods in Engineering Design*. Wiley, New York.

Harr, M. (1987). *Reliability-Based Design in Civil Engineering*. McGraw-Hill, New York.

Harrop-Williams, K. (1986). “Probability Distribution of Strength Parameters in Uniform Soils.” Journal of Engineering Mechanics, Vol. 112, No. 3, pp. 345-350.

Hasofer, A. and Lind, N. (1974). “Exact and Invariant Second-Moment Code Format.” Journal of Engineering Mechanics Division, Vol. 100, No. 1, pp. 111-121.

Hoff, P.D. (2009). *A First Course in Bayesian Statistical Methods.* Springer, New York, pp. 270.

Jabo, J. (2014). *Reliability-Based Design and Acceptance Protocol for Driven Piles*. Ph.D. dissertation, University of Arkansas. Ann Arbor: ProQuest/UMI, 268 pgs. (Publication No. 3667200).

Johnson, N., Kotz, S., Balakrishnan, N. (1994). *Continuous Univariate Distributions Vol. 1, 2nd Ed.* John Wiley & Sons, New York, 756 pgs.

Kansas Department of Transportation. (2013). LRFD Bridge Design Manual. Chapter 3 Section 10, 54 pgs.

Klammer, H., McVay, M., Faraone, M., and Horhota, D. (2013). “An Approach to Assess LRFD-f from Load Test and Borehole Data In and Outside the Footprint of a Drilled Shaft.” GeoCongress 2013: Foundation Engineering in the Face of Uncertainty, San Diego, CA, March 3-7, pp. 617-632.

Kloke, J. and McKean, J. (2014). *Nonparametric Statistical Methods Using R.* Chapman & Hall/CRC Press, 283 pgs.

Lee, P. (2012). *Bayesian Statistics: An Introduction (4th Edition).* John Wiley & Sons, 488 pgs.

Liang, R. and Li, J. (2009). “Resistance Factors Calibrated from FHWA Drilled Shafts Static Top-Down Test Data Base.” GeoFlorida 2009: Contemporary Topics in In Situ Testing, Analysis, and Reliability of Foundations, Orlando, FL, March 15-19, pp. 387-395.

Loehr, J.E., Bowders, J.J., Rosenblad, B.L.,, Luna, R., Maerz, N., Stephenson, R.W., Likos, W.J., and Ge, L. (2013). “Implementation of LRFD Methods to Quantify Value of Site Characterization Activities.” Proc. Of the 18th Int. Conf. on Soil Mech. And Geotech. Eng., Paris, pp. 1831-1834.

Lopez-Caballero, F., Gaspar, A.P.T, and Gomes-Correia, A. (2011). “Uncertainty and Sensitivity Analysis of FWD Test.” GeoHunan 2011: Emerging Technologies for Design, Construction, Rehabilitation, and Inspection of Transportation Infrastructure, China, June, pp. 49-56.

Lumb, P. (1970). “Safety Factors and the Probability Distribution of Soil Strength.” Canadian Geotechnical Journal, Vol. 7, No. 3, pp. 225-242.

Luo, Z., Atamturktur, S., and Juang, H. (2013). “Bootstrapping for Characterizing the Effect of Uncertainty in Sample Statistics for Braced Excavations.” Journal of Geotechnical and Geoenvironmental Engineering, Vol. 139, No. 1, pp. 13-23.

McVay, M.C., Ellis, R.D., Birgisson, B., Consolazio, G., Putcha, S., and Lee, S.M. (2002). "Use of LRFD, Cost and Risk to Design a Drilled Shaft Load Test Program in Florida Limestone." Transportation Research Record 1808, Transportation Research Board, Washington, DC, 19 pgs.

Misra, A. and Roberts, L. (2006). "Axial Service Limit State Analysis of Drilled Shafts Using Probabilistic Approach." Geotechnical and Geological Engineering, Vol. 24, No. 6, pp. 1561-1580.

Misra, A. and Roberts, L. (2009). "Service Limit State Resistance Factors for Drilled Shafts." Geotechnique, Vol. 59, No. 1, pp. 53-61.

Misra, A., Roberts, L., and Levorson, S. (2007). "Reliability Analysis of Drilled Shaft Behavior Using Finite Difference Method and Monte Carlo Simulation." Geotechnical Geology Engineering, Vol. 25, pp. 65-77.

Najjar, S.S. and Saad, M. (2011). "Bayesian Updating of Load Settlement Curves for Footings on Cohesionless Soil." Geo-Risk 2011: Risk Assessment and Management, Atlanta, Georgia, June, pp. 263-270.

Niazi, F., Mayne, P., and Wang, Y. (2011). "Statistical Analysis of Cone Penetration Tests and Soil Engineering Parameters at the National Geotechnical Experimentation Clay Site, Texas A&M University." ASCE Geotechnical Special Publication No. 211, Proc. GeoFrontiers 2011: Advances in Geotechnical Engineering, Dallas, Texas, March, pp. 2998-3007.

Niederreiter, H. (1992). Random Number Generation and Quasi-Monte Carlo Methods. Society for Industrial and Applied Mathematics, Philadelphia, PA, 243 pgs.

NIST/SEMATECH (2012). *NIST/SEMATECH e-Handbook of Statistical Methods.* <http:// <http://www.itl.nist.gov/div898/handbook>, Jan 2014.

Nowak, A.S. (1999). "Calibration of LRFD Bridge Design Code." NCHRP Report 368, National Cooperative Highway Research Program, Transportation Research Board, Washington, D.C.

O'Neill, M. and Reese, L. (1999). "Drilled shafts: Construction Procedures and Design Methods." FHWA Publication No. IF-99-025, Federal Highway Administration, Washington, D.C., 537 pgs.

O'Neill, M., Townsend, F., Hassan, K., Buller, A., and Chan, P. (1996). "Load transfer for drilled shafts in intermediate geomaterials." *FHWA Publication No. RD-95-172*, Federal Highway Administration, Washington, D.C., 196 pgs.

Paikowsky, S.G. (2004). "Load and Resistance Factor Design (LRFD) for Deep Foundations." NCHRP Report 507, National Cooperative Highway Research Program, Transportation Research Board of the National Academies, Washington, D.C. 126 pgs.

Park, J.H., Kim, D., and Chung, C.K. (2012). “Implementation of Bayesian Theory on LRFD of Axially Loaded Driven Piles.” Computers and Geotechnics, Vol. 42, pp. 73-80.

Phoon, K.K., Quek, S., and An, P. (2003). “Identification of Statistically Homogeneous Soil Layers Using Modified Barlett Statistics.” Journal of Geotechnical and Geoenvironmental Engineering, Vol. 129, No. 7, pp. 649-659.

Reese, L. C. and O’Neill, M. W. (1988). ‘‘Drilled Shafts; Construction Procedures and Design Methods.’’ Rep. No. FHWA-HI-88-42, U.S. Dept. of Transp., Federal Highway Administration, Washington, D.C.

Reese, L.C., Wang, S.T., and Arrellaga, J.A. (2001). “SHAFT Version 5.0 for Windows, A Program for the Study of Drilled Shafts Under Axial Loads.” ENSOFT, INC., Austin, Texas.

Reese, L. C. and Wright, S. J. (1977). “Drilled Shaft Design and Construction Guidelines Manual." Implementation Package 77-21, U.S. Department of Transportation., Washington, D.C.

Rencher, A. (2002). *Methods of Multivariate Analysis*, 2nd ed. John Wiley & Sons, Inc., 715 pgs.

Roberts, L., Fick, D., and Misra, A. (2011). “Performance-Based Design of Drilled Shaft Bridge Foundations.” Journal of Bridge Engineering, Vol. 16, No. 6, pp. 745-758.

Rogers, J. and Chung, J. (2013). “Distinguishing Between Data Uncertainty and Natural Variability in Virtual Geotechnical Databases.” GSP 229, Foundation Engineering in the Face of Uncertainty, pp. 444-455.

Salgado, R. and Woo, S. (2011). “Load and Resistance Factor Design for Axially Loaded Drilled Shafts.” 2011 Pan-Am CGS Geotechnical Conference, Toronto, Canada, Oct. 2-6.

Shapiro, S. and Wilk, M. (1965). “An analysis of variance test for normality (complete samples).” Biometrika, Vol. 52, No. ¾, pp. 591-611.

Silverman, B.W. (1986). “Density Estimation for Statistics and Data Analysis.” Monographs on Statistics and Applied Probability, London, Chapman and Hill, 22 pgs.

Smith, G.N. (1986). *Probability and Statistics in Civil Engineering*. Nichols Publishing Company, 241 pgs.

Snedecor, G.W. and Cochran, W.G. (1989). *Statistical Methods*. Iowa State University Press, 503 pgs.

Taflanidis, A.A. and Gidaris, I. (2013). “Health Monitoring and Bayesian Updating of Deteriorating Bridge Infrastructures.” Structures Congress 2013, Pittsburgh, Pennsylvania, May, pp. 398-409.

Unanwa, C. and Mahan, M. (2014). “Statistical Analysis of Concrete Compressive Strengths for California Highway Bridges.” Journal of Performance of Constructed Facilities 28, Special Section: Performance of Bridges under Critical Natural Hazards, pp. 157-167.

Uzielli, M. and Mayne, P. (2013). “Bayesian Characterization of Transformation Uncertainty for Stregnth and Stiffness of Sands.” Geo-Congress 2013: Foundation Engineering in the Face of Uncertainty, San Diego, CA, March 3-7, pp. 368-384.

Vessely, M., Liu, H. (2006). “LRFD and Drilled Shaft Design in Colorado.” GEO-Volution, pp. 132-148.

Vu, T. (2013). *Load and Resistance Factor Design of Drilled Shafts at the Service Limit State*. PhD Dissertation, University of Missouri-Columbia. Ann Arbor: ProQuest/UMI, 405 pgs. (Publication No. 3577978).

Withiam, J.L., Voytko, E.P., Barker, R.M., Duncan, J.M., Kelly, B.C., Musser, S.C., and Elias, V. (1998). Load and Resistance Factor Design (LRFD) for Highway Bridge Substructures. Report FHWA HI-98-032. Federal Highway Administration, Washington, D.C.

Wu, T. (2013). “Geotechnical Uncertainties and Reliability-Based Design.” Foundation Engineering in the Face of Uncertainty, pp. 271-282.

Yang, X., Han, J., Henthorne, R., and Parsons, R. (2008). “Statistical Analysis of O-Cell Test Data for Nominal Load Capacities of Drilled Shafts.” ASCE Geotechnical Special Publication No. 178, Proc. GeoCongress 2008: Geosustainability and Geohazard Mitigation, New Orleans, Louisiana, March, pp. 90-97.

Yu, X., Abu-Farsakh, M., Yoon, S., Tsai, C., and Zhang, Z. (2012). “Implementation of LRFD of Drilled Shafs in Louisiana.” Journal of Infrastructure Systems, Vol. 18, No. 2, pp. 103-112.

Zhao, Y. and Ono, T. (1999). “A General Procedure for First/Second-Order Reliability Method (FORM/SORM).” Structural Safety, Vol. 21, No. 2, pp. 95-112.

CHAPTER 4: Statistical Analysis to Determine Appropriate Design Methodologies for DSF

4.1. Chapter Overview

Three types of geotechnical investigation methods were performed at three test sites in Arkansas. The three different geotechnical investigation methods were identified as the Arkansas Highway and Transportation Department (AHTD) method, the Missouri Department of Transportation (MODOT) method, and the University of Arkansas (UofA) method. The respective methods will be discussed in detail in this chapter. Statistical testing methods including the T-test, Wilcoxon test, and F-test were performed to determine if there was a statistical difference between the soil properties that were determined by using the difference geotechnical investigation methods. The axial capacity values were also statistically analyzed, as a function of depth, in regard to the software program and the geotechnical investigation data that were utilized for design. Finally, it was determined that there was a relationship between the axial capacity values and the number of statistically different soil properties. It was recommended to perform the MODOT geotechnical investigation method for cohesive soils and loose to medium dense cohesionless soils due to the rapid testing times and due to the low coefficient of variability values. In general, in the design of drilled shaft foundations, it was determined that the 1) geotechnical investigation method and 2) software program that is utilized in the design must be considered.

The paper enclosed in this chapter has been accepted for publication within the Geotechnical and Geological Engineering Journal. The full reference is: Race, M.L, Bey, S.M., and Coffman, R.A. (2015). “Statistical Analysis to Determine Appropriate Design Methodologies of Drilled Shaft Foundations.” GEGE Journal, DOI: 10.1007/s10706-015-9854-z.

4.2.Additional Results

The spatial variability across the tests sites was considered during the design of the DSF at the three sites in Arkansas. The coefficient of variation (COV) was calculated for each soil property value that was obtained from each of the geotechnical investigation methods at each test site as a function of depth and by the corresponding soil layer. The tables with the respective COV values are presented within Appendix A in Tables A.1 through A.17 for the Siloam Springs Arkansas Test Site (SSATS), within Tables A.18 through A.30 for the Turrell Arkansas Test Site (TATS), and within Tables A.31 through A.41 for the Monticello Arkansas Test Site (MATS). The COV values were calculated based on 1.5m sampling intervals, based on the corresponding soil layers (cohesive or cohesionless soil), and based on the site (to a depth of 30.5m). For low, medium, and high variability at a given site, the COV values as recommended by Paikowsky et al. (2004), are less than 0.25, between 0.25 and 0.4, and greater than 0.4. Based on these definitions, the site variability of each site for each soil property is presented in Table 4.1. The COV values varied by as much as 20 percent even though the variability definition based on the geotechnical investigation method were similar in most cases.

Table 4.1. Site variability for the three test sites, based on the soil property and stratigraphy type.

Test Site	Soil Property	Stratigraphy Type	Site Variability		
			AHTD	MODOT	UofA
SSATS	Blow Count (N)	Cherty Clay	High	High	High
	Total Unit Weight (γ_T)	Cherty Clay	Low	Low	Low
		Limestone	N/A	N/A	Low
		Shale	N/A	N/A	Low
	Rock Quality Designation (RQD)	Limestone	Medium	N/A	Medium
	Compressive Strength (f'_r)	Limestone	N/A	N/A	Medium
TATS	Blow Count (N)	Clay	High	Medium	N/A
		Sand	High	High	High
	Total Unit Weight (γ_T)	Clay	Low	Low	Low
		Sand	Low	Low	Low
	Undrained Shear Strength (c_u)	Clay	High	High	High
	Friction Angle (ϕ)	Sand	Low	Low	Low
MATS	Blow Count (N)	Clay	High	High	N/A
		Sand	Medium	Medium	Medium
	Total Unit Weight (γ_T)	Clay	Low	Low	Low
		Sand	Low	Low	Low
	Undrained Shear Strength (c_u)	Clay	High	High	High
	Friction Angle (ϕ)	Sand	Low	Low	Low

In addition to the statistical testing performed to determine the statistical difference within the soil properties due to the geotechnical investigation method, statistical analyses were also performed to determine the distribution of the of the soil properties. The Shapiro-Wilks test and the Kolmogorov-Smirnov test were utilized to determine the probability that the soil property values were normally or log-normally distributed. The probability of the distribution types for the soil properties collected at the TATS and the MATS are presented within Table 4.2 and within Table 4.3, respectively. For soil properties, such as the total unit weight of sand (only one p-value is greater than 0.05), it was 95 percent probable that neither the normal nor the log-normal distribution “fit” the data for either test site. Much of the data for the soil property values did not “fit” well with the normal or log-normal distributions because the soil that was tested was not uniform with depth (even within the clay or sand layers). It is possible that the distributions

are bi-normal with two peaks which denote the two different soil layers within the dataset. The soil properties were not tested for each individual soil layer because there was not enough data to establish a “best fit” distribution for a given soil layer.

Table 4.2. Probability values of the distribution type for soil properties at the MATS.

Soil Property	Measurement Method	p-Value Shapiro-Wilks Normal	p-Value Kolmogorov-Smirnov Normal	p-Value Kolmogorov-Smirnov Log-normal
Corrected Blow Count (Sand)	AHTD	0.175	0.000	0.002
	MODOT	0.377	0.000	0.056
	UofA	0.976	0.043	0.004
Undrained Shear Strength (Clay)	AHTD	0.000	0.000	0.000
	MODOT	0.003	0.980	0.547
	UofA	0.000	0.000	0.060
Total Unit Weight (Clay)	AHTD	0.000	0.000	0.000
	MODOT	0.556	0.000	0.000
	UofA	0.018	0.000	0.000
Total Unit Weight (Sand)	AHTD	0.000	0.000	0.000
	MODOT	0.083	0.002	0.000
	UofA	0.038	0.000	0.000

Note: If the p-value is less than 0.05 then the distribution is not the identified distribution.

Table 4.3. Probability values of the distribution type for the soil properties at the TATS.

Soil Property	Measurement Method	P-Value Shapiro-Wilks Normal	P-Value Kolmogorov-Smirnov Normal	P-Value Kolmogorov-Smirnov Log-normal
Corrected Blow Count (Sand)	AHTD	0.000	0.000	0.123
	MODOT	0.027	0.000	0.378
	UofA	0.000	0.000	0.036
Undrained Shear Strength (Clay)	AHTD	0.014	0.192	0.098
	MODOT	0.000	0.004	0.017
	UofA	0.000	0.002	0.109
Total Unit Weight (Clay)	AHTD	0.000	0.000	0.000
	MODOT	0.002	0.087	0.000
	UofA	0.316	0.001	0.000
Total Unit Weight (Sand)	AHTD	0.000	0.000	0.000
	MODOT	0.000	0.000	0.000
	UofA	0.007	0.000	0.000

Note: If the p-value is less than 0.05 then the distribution is not the identified distribution.

Statistical Analysis to Determine Appropriate Design Methodologies of Drilled Shaft Foundations

Morgan L. Race, SM.ASCE, EIT[1], Sarah M. Bey, SM.ASCE, EIT[2], and
Richard A. Coffman, M.ASCE., PhD, PE, PLS[3]

4.3.Abstract

Detailed geotechnical investigations were performed at two sites within the state of Arkansas (Monticello and Turrell). The soil parameters, predicted axial capacity, and predicted load-movement response values varied depending on 1) which geotechnical investigation methods and/or 2) which predictive software programs (FB-Deep, SHAFT) were utilized. The uncertainty associated with the different soil properties and the discrepancies between the different software programs are discussed. Parametric and nonparametric statistical testing methods, including the: T-test, F-Test, and Wilcoxon test were utilized to evaluate the soil parameters (corrected blow count, total unit weight, and undrained shear strength) and the predicted axial capacity data. No statistical differences (95 percent confidence interval) were observed for the respective undrained shear strength, total unit weight (clay), and correlated corrected blow count parameters as determined from University of Arkansas (UofA) method and from Missouri Department of Transportation (MODOT) method. However, differences were observed for the predicted axial capacity and load-movement values that were predicted using the aforementioned soil parameters (percent differences ranging from 0.5 to 29.2 percent for load-movement values). Because an inverse relationship was observed between the percent difference in the load-movement values and the number of statistically similar soil properties, it was determined that the predicted axial capacity and predicted load-movement response were dependent upon the soil sampling and testing methods and the utilized software program.
Keywords: Statistics; Subsurface Investigations; Soil Sampling; Drilled Shaft Foundation Design

4.4. Introduction

Current geotechnical investigation methods employed by the Arkansas State Highway and Transportation Department (AHTD) and other transportation departments fail to quantify the amount of uncertainty associated with drilling and sampling processes. By effectively quantifying the amount of uncertainty through advanced site characterization techniques and axial capacity prediction techniques, cost savings may be obtained without sacrificing public safety. Soil properties such as the: corrected blow count of sand (N_{60}), total unit weight of sand and clay (γ_T), and undrained shear strength of clay (c_u) are commonly used in the design of deep foundations. Specifically, the values of these soil parameters are utilized in design equations (and predictive software programs) regardless of the accuracy and bias of the geotechnical testing method that was used to collect the data. The variation within the values of predicted axial capacity and load-movement response for drilled shaft foundations (DSF) is attributed to the uncertainty in 1) the soil properties and 2) the design methodologies utilized within the predictive software programs (e.g. FB-Deepv2.04 or SHAFTv2012).

To investigate the amount of bias and uncertainty related to the soil sampling and testing methods, various methods for obtaining the aforementioned soil properties were performed by the Arkansas Highway and Transportation Department (AHTD), the Missouri Department of Transportation (MODOT), and the University of Arkansas (UofA) at two sites in the state of Arkansas. These methods included, but were not limited to, the utilization of standard penetration testing (SPT), cone penetration testing (CPT), and unconsolidated undrained triaxial compression testing (UU), respectively. This uncertainty within the soil sampling and testing methods was evaluated using parametric and nonparametric statistical testing methods to determine the mean and variance values (T-test, F-test, and Wilcoxon test). The site

characterization methods (AHTD, MODOT, UofA) were statistically evaluated by comparing the respective soil parameter values that were obtained from each testing technique. Similarly, the predicted axial capacity and load-movement values were evaluated based on the values of the input soil parameters and the predictive software programs.

4.5. Background

4.5.1. Static Estimation Programs

FB-Deep and SHAFT are two commercially available programs to predict the axial capacity and the load-movement response of DSF in various geomaterials. Values for the axial capacity and the load-movement response are predicted utilizing methods obtained from the American Association of State Highway and Transportation Officials (AASHTO) Load and Resistance Factor Design (LRFD) Bridge Design Specifications (AASHTO 2007) and from the Federal Highway Administration (FHWA) report FHWA-NHI-10-016 (Brown et al. 2010). The primary difference between the two programs is the method (correlations or equations) that are utilized to determine the soil properties from the input parameters (soil type, blow count [N], γ_T, and c_u). For completeness, the design steps and methodology that were utilized to perform the aforementioned analyses for the Arkansas sites by using FB-Deep and SHAFT are further described in detail by Bey (2014).

4.5.1.1. Bridge Software Institute FB-Deep

FB-Deep (Townsend 2003a; Townsend 2003b; FB-Deep 2012) is a program utilized to determine the static capacity of DSF. The software was developed by the Bridge Software Institute at the University of Florida. Site specific soil parameters such as soil type, N, γ_T, and c_u, as obtained or correlated from SPT or CPT data, may be utilized in the FB-Deep program to predict the static axial capacity. Empirical relationships between the SPT and CPT data, as

developed for typical Floridian soils (Schmertmann 1967; Bloomquist et al. 1992), are employed for SPT input data. Site soil properties (direct CPT or SPT-CPT relationships) are then utilized to predict axial capacity using relationships developed by Schmertmann (1978), Bustamante and Gianeselli (1982), and Bloomquist et al. (1992).

4.5.1.2. Ensoft, Inc. SHAFT

SHAFT (Reese et al. 2012a; Reese et al. 2012b; SHAFT 2012) is an estimation program used to determine the static response of DSF. The program was commercially released in 1987 under the direction of Dr. Lymon C. Reese. Since 1978, seven versions of SHAFT have been distributed by ENSOFT, Inc. Soil properties utilized in SHAFT include soil type, N, γ_T, and c_u. The amount of axial movement, quantity of load, and the distribution of load along the DSF are predicted using SHAFT. Additionally, LRFD reduction factors for side friction and tip resistance in each soil layer may be specified for each geostrata layer. The axial capacity is predicted based on the analysis methods developed by: Skempton (1951), Sheikh and O'Neill (1986), and O'Neill and Reese (1999) for cohesive soil; Meyerhof (1976), Quiros and Reese (1977), and O'Neill and Reese (1999) for non-cohesive soil. Load-movement responses are predicted based on normalized displacement curves obtained from Reese and O'Neill (1988).

4.5.2. Statistical Evaluation Methods

Statistical evaluation methods can be utilized to determine the statistical difference (to 95 percent confidence) between two samples. In particular, parametric and nonparametric two-sample statistical testing methods are commonly used to determine the statistical difference between corresponding mean and variance values. The conditions for applying parametric or nonparametric statistical evaluation methods are presented in Table 4.4. For statistical testing of mean values (parametric and nonparametric), the following hypotheses are evaluated: 1) the

initial hypothesis (H_o): the mean values of two independent samples are equivalent, and 2) the alternative hypothesis (H_a): the mean values of the two independent samples are not equivalent. The probability that the null hypothesis is rejected when the null hypothesis is true (type I error [α]) is limited to five percent (5%). Because the type I error is five percent, the corresponding confidence level that the alternative hypothesis is true when the null hypothesis is rejected is 95 percent (95%).

Table 4.4. Conditions for the use of parametric and nonparametric statistical methods.

Valid for:	Parametric Methods	Nonparametric Methods
Distribution Type	Normal (Lognormal)	All*
Sample Size	> 30	All*
Mean	T-test	Wilcoxon Test
Variance	F-test	-

* All distribution types include, but are not limited to: Beta, Exponential, Uniform.

Statistical evaluation methods have been used sparingly within civil engineering. In geotechnical engineering, statistics has been used to: determine the probability of failure for geotechnical structures, as described in Luo et al. (2013), determine the homogeneity of soil layers, as described in Phoon et al. (2003), and analyze CPT and falling weight deflectometer (FWD) tests, as described in Niazi et al. (2011) and Lopez-Caballero et al. (2011), respectively. Yang et al. (2008) and Yu et al. (2013) have also utilized statistical bias to compare methods for determination of the nominal capacity of DSF using the bi-directional load cell test (BLC). The T-test, F-test, and Wilcoxon test were also used to verify that the predictive axial capacity values varied depending on the exploration and sampling methods employed during geotechnical investigations (Race et al. 2013). Similarly, as described in Bo et al. (2013), the F-test and T-test were used to verify the amount of variance in sample homogeneity and the amount of data consistency, respectively, for normally distributed data from asphalt compaction testing. Furthermore, Unanwa and Mahan (2012) utilized the T-test to analyze the normalized 28-day

compressive strengths of concrete cylinders for highway bridges in California. The recent publication dates of many of the aforementioned articles indicate the newfound importance of considering statistical methods to better assess civil engineering design approaches.

4.6. Methods and Materials

4.6.1. Drilling, Sampling, and Testing

Within the state of Arkansas, detailed geotechnical investigations were performed at two sites (Monticello and Turrell). The Monticello Arkansas Test Site (MATS), is located in the southeastern portion of Arkansas and is comprised of fluvial, deltaic deposits. The Turrell Arkansas Test Site (TATS) is located within the Mississippi Embayment in the northeastern portion of Arkansas within the New Madrid Seismic Zone and is comprised of fluvial deposits. The site investigations that were performed at those sites included traditional boreholes (10 total at the MATS and 12 total at the TATS) and five attempted CPT soundings within a 929m^2 testing area at the MATS and the TATS, as presented in Figure 4.1 (Coffman 2011). The AHTD drilling and sampling methods included the use of SPT (ASTM D1586 2012), that utilized a standard split-spoon sampler (30mm diameter), in all soils. The UofA drilling and sampling methods included the use of 1) the SPT that utilized a California sampler (62mm diameter), in cohesionless soils, 2) the Osterberg hydraulic fixed-piston Shelby tube sampler in soft to firm clay, and 3) the Pitcher barrel Shelby tube sampling in stiff to hard clay. The MODOT sampling method included the use of a 100-kN capacity five-channel (tip resistance, sleeve friction, pore pressure, seismic, tilt) cone following ASTM D3441 (2012) testing procedures, in all soils.

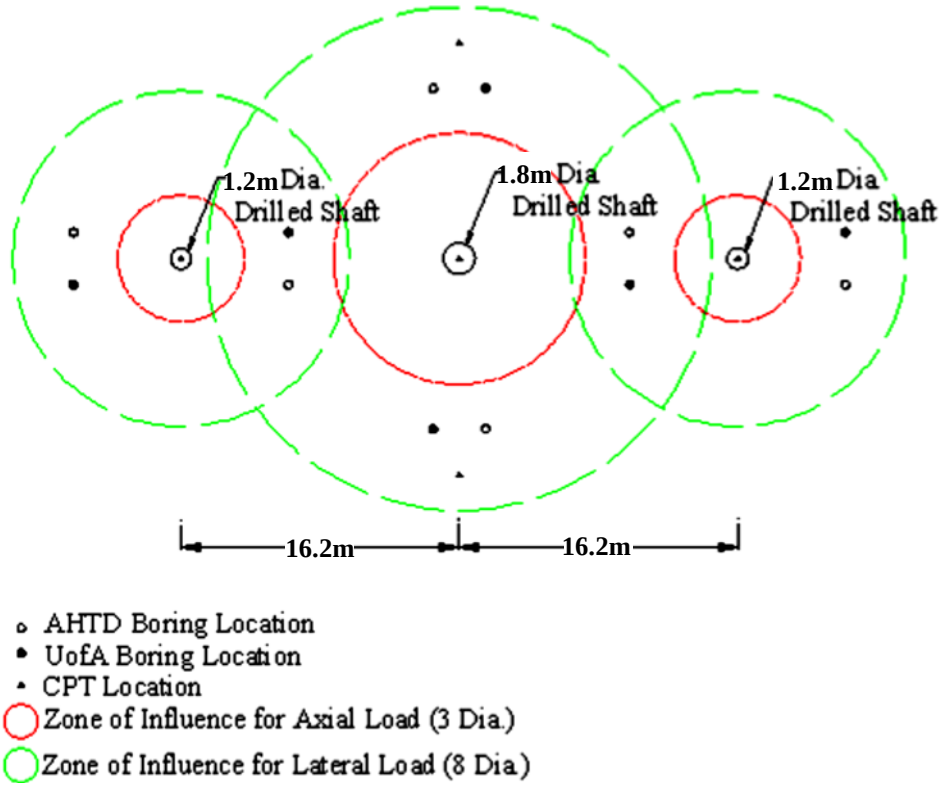

Figure 4.1. Typical borehole and drilled shaft layout for all test sites [modified from Coffman (2011c)].

The soil properties that were compared using statistical testing methods included: corrected blow count, total unit weight, and undrained shear strength. The methods for determining the soil properties, based on the soil sampling and testing methods, are presented in Table 4.5. For example, the blow count values were obtained by following the procedures outlined in ASTM D1586 (2012) for the AHTD and UofA methods, or were calculated from the CPT measurements (MODOT method) using Equation 4.1. The total unit weight and undrained shear strength values for cohesive soils and the total unit weight and friction angle values for non-cohesive soils were correlated from Vanikar (1986) [AHTD method]. The undrained shear strength and total unit weight values, as obtained from CPT measurements (for the MODOT method), were calculated using Equations 4.2 and 4.3, respectively. The undrained shear strength

values (UofA method) were directly obtained from unconsolidated undrained (UU) triaxial compression tests, as performed following the procedures outlined in ASTM D2850 (2012). The total unit weight values for the Uof A method were calculated from mass and volume measurements collected for trimmed sample of extruded soil sections that were obtained from Shelby tubes (clay) or from mass and volume measurements obtained from 15.24cm long soil sections that were recovered from the California split spoon sampler (sand). The mean values (and uncertainty) of the corrected blow count (N_{60}), total unit weight (γ), and undrained shear strength (c_u) that were obtained from the sites and different sampling methods (AHTD, MODOT, and UofA) are presented in Figure 4.2.

Table 4.5. Soil property determination method for various soil sampling and testing methods.

Soil Property	Soil Sampling Method		
	AHTD	**MODOT**	**UofA**
Corrected Blow Count	Calculated[1]	Calculated[2]	Calculated[3]
Undrained Shear Strength	Correlated[4]	Calculated[5]	Measured[6]
Total Unit Weight	Correlated[4]	Calculated[7]	Measured[8]

[1]Corrected for hammer efficiency
[2]Equation 1 (originally in Robertson and Cabal [2012])
[3]Empirical equation from Race and Coffman (2013)
[4]Correlation from Vanikar (1986)
[5]Equation 2 (originally in Robertson and Cabal [2012])
[6]Measured from UU tests on soil samples
[7]Equation 3 (originally in Robertson and Cabal [2012])
[8]Calculated from the diameter, length, and weight measurements of soil samples

$$N_{60} = \frac{\left(\frac{q_t}{p_a}\right)}{8.5\left(1 - \frac{I_c}{4.6}\right)} \quad \text{(Robertson and Cabal 2012)} \quad \text{Equation 4.1}$$

$$c_u(ksf) = \frac{q_t - \sigma_v}{N_{kt}} \quad \text{(Robertson and Cabal 2012)} \quad \text{Equation 4.2}$$

$$\frac{\gamma_t}{\gamma_w} = 0.27\left[log(R_t) + 0.36log\left(\frac{q_t}{p_a}\right)\right] + 1.236 \quad \text{(Robertson and Cabal 2012)} \quad \text{Equation 4.3}$$

Within Equations 4.1 through 4.3, N_{60} is the energy corrected blow count, q_t is the tip resistance, p_a is the atmospheric pressure, I_c is the soil behavior type index, c_u is the undrained shear strength, σ_v is the vertical overburden pressure, N_{kt} is a cone factor value (14 for this study), γ is the total unit weight, γ_w is the unit weight of water, and R_t is the friction ratio.

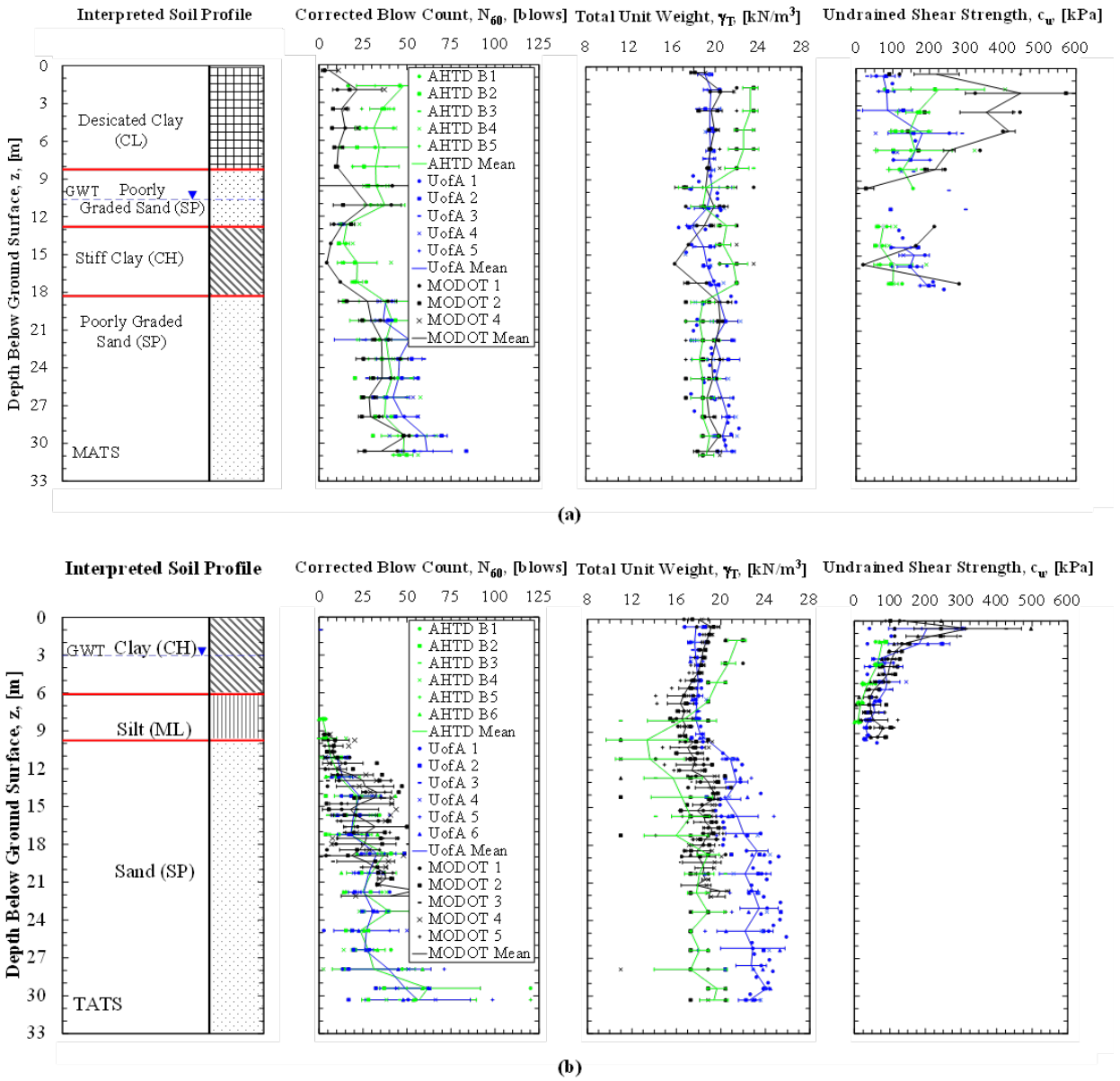

Figure 4.2. Soil properties determined using AHTD, MODOT, and UofA geotechnical investigation methods at a) MATS and b) TATS [modified from Race et al. (2013), Race and Coffman (2013), and Race and Coffman (2015)].

4.6.2. Design Prediction Procedures

The effect of the amount of uncertainty, in the values of the given soil properties and on the values of the predicted axial capacity and the predicted load-movement response, as obtained from FB-Deep and SHAFT, were evaluated. For each site, required values of given soil properties (total unit weight, corrected blow count, undrained shear strength, and friction angle) were input into FB-Deep and SHAFT. Specifically, to determine the static axial capacity and load-movement response for clay layers encountered at all sites, tip resistance (q_t) from MODOT CPT, c_u values from UofA UU testing, or correlated c_u values obtained from AHTD SPT N_{60} values were ingested into FB-Deep and SHAFT. For sand layers, the N_{60} values obtained from AHTD or UofA SPT methods or the correlated to N_{60} values obtained from MODOT CPT parameters were input into FB-Deep. The N_{60} values from SPT and CPT methods and correlated friction angle (ϕ) values were also input into SHAFT for sand layers. The mean soil properties (N_{60}, γ_T, c_u, and ϕ) for soil layers at the MATS and the TATS are presented in Table 4.6. Specifically, the predicted axial capacities and load-movement response were generated based on various DSF diameters (1.2m or 1.8m), various lengths (Table 4.7), and various soil properties at each site (previously presented in Figure 4.2). For completeness, the results from the full-scale load tests performed on DSF at the TATS is presented in Race and Coffman (2015).

Table 4.6. Mean soil properties determined using the AHTD, MODOT, and UofA geotechnical investigation methods for the MATS and the TATS.

Site	Soil Type	Layer Depth [m]	AHTD				MODOT				UofA			
			N_{60}	γ_T	c_u	ϕ	N_{60}	γ_T	c_u	ϕ	N_{60}	γ_T	c_u	ϕ
MATS	Clay	0.0-9.1	36	22.7	165	-	13	19.6	318	-	-	19.5	115	-
	Sand	9.1-12.2	35	19	-	34.4	23	19.5	-	28.8	13	19.5	-	30
	Clay (Stiff)	12.2-18.3	22	20.9	85	-	9	17.8	169	-	-	19	157	-
	Sand	18.3-30.5	42	18.9	-	36	34	19.8	-	33.5	47	20.6	-	36.7
TATS	Clay	0.0-6.1	13	20.6	61	-	-	18	136	-	-	17.8	115	-
	Silt	6.1-9.1	4	16.2	14	-	-	16.6	53	-	-	17.9	46	-
	Sand	9.1-30.5	30	17.2	-	32.6	24	18.2	-	31.1	29	22.3	-	32.5

Note: N_{60} in blows, γ_T in kN/m^3, c_u in kPa, and ϕ in degrees

Table 4.7. Drilled shaft foundation and soil sampling properties for the test sites (MATS and TATS).

Site	Required Capacity [MN]	DSF Design Length [m]		Number of Boreholes			Depth of Boreholes [m]		
		1.2m DSF	1.8m DSF	AHTD	MODOT	UofA	AHTD	MODOT	UofA
MATS	11.6	27.9	21.9	5	3	5	30.5	21.31	30.5
TATS	8.8	26.4	18.7	6	5	6	30.5	22.9	30.5

[1]Only one sounding to 21.3m, the other soundings hit refusal at 9.1m

4.6.3. Statistical Testing

For each soil property (N_{60}, c_u, γ_t), the values obtained from the AHTD, MODOT, and UofA methods were statistically evaluated by soil type (clay or sand) for the data collected at the MATS and the TATS. The soil property values were paired (by location and depth within boreholes) with the corresponding property values obtained from different sampling and testing methods within the adjacent boreholes (Table 4.8). For example, the data in the UofA corrected blow count values in cohesionless soil was statistically compared with the data in the AHTD corrected blow count values in cohesionless soil and the MODOT corrected blow count values in cohesionless soil using the aforementioned parametric and nonparametric tests. The quantity of independent values in each dataset ranged from 20 to 70; therefore, the previously described parametric and nonparametric statistical testing methods were utilized to analyze the differences in the multiple sampling and testing methods. Specifically, the numbers of independent values that were utilized for the statistical testing of the soil sampling and testing methods are presented in Table 4.9.

Table 4.8. Adjacent boreholes used for statistical testing at the a) MATS and b) TATS.

(a)

UofA	AHTD	MODOT
UofA 1	AHTD 3	MODOT 4
UofA 2	AHTD 4	-
UofA 3	AHTD 2	MODOT 1
UofA 4	AHTD 1	MODOT 2
UofA 5	AHTD 5	-

(b)

UofA	AHTD	MODOT
UofA 1	AHTD 1	MODOT 1
UofA 2	AHTD 2	MODOT 2
UofA 3	AHTD 3	-
UofA 4	AHTD 4	MODOT 3
UofA 5	AHTD 5	MODOT 5
UofA 6	AHTD 6	MODOT 4

Table 4.9. Quantity of independent values utilized in the statistical analysis of the soil properties.

Site	Compared Methods		Number of Samples (Clay)			Number of Samples (Sand)	
			Blow Count, N	Total Unit Weight, γ_T	Undrained Shear Strength, c_u	Blow Count, N	Total Unit Weight, γ_T
MATS	AHTD	MODOT	15*	22*	18*	22*	18*
	AHTD	UofA	-	47	31	53	45
	MODOT	UofA	-	23*	20*	23*	23*
TATS	AHTD	MODOT	28*	28*	25*	35	36
	AHTD	UofA	-	34	26*	70	70
	MODOT	UofA	-	32	35	35	36

*If less than 30 samples, nonparametric analyses were utilized to ensure that results from parametric analyses could be utilized.

The predicted axial capacity values (as calculated from the mean soil property values determined using the different geotechnical investigation methods) that were generated from the SHAFT and FB-Deep programs were also compared at 1.5m increments throughout the soil profile. Additional statistical analysis testing was performed on mean values and total values (mean, mean plus one standard deviation [Mean+1SD], and mean minus one standard deviation [Mean-1SD]) of predicted axial capacity for each soil testing method and each estimation program at each site (MATS and TATS). The mean values of the predicted axial capacity were evaluated using the T-Test and the Wilcoxon Test. The variances of the predicted axial capacities

and predicted load-movement response were evaluated using the F-Test. The predicted axial capacity values were paired based on the size (diameter and length) of each designed DSF.

For the statistical testing, the rejection criteria was a decimal probability value (p-value) of 0.05 (95 percent confidence level). Therefore, the probability that the null hypothesis (i.e. the mean or variance values of the two datasets are the same) was limited to five percent. Furthermore, the coefficient of variation (COV) was calculated to assess the precision of the soil parameters from the respective geotechnical investigation methods (AHTD, MODOT, or UofA). The purpose of the aforementioned statistical testing of the methods that were utilized to determine the soil property values and the predicted axial capacity values was to:

- determine the difference in the mean values of soil properties,
- determine the difference in the variance values of the soil properties,
- determine the difference in the mean values of the predicted axial capacity values,
- compare the precision of the soil sampling and testing methods, and
- evaluate whether the predicted axial capacity was dependent upon the soil sampling and testing method (particularly, if significantly lower values of axial capacity were predicted utilizing lower values of soil properties).

4.7. Results and Recommendations

4.7.1. Soil Sampling and Testing Methods

Utilizing the T-test, the F-test, and the Wilcoxon test, the difference in the mean and variance values for the N_{60}, c_u, and γ_T values were evaluated. As presented in Table 4.10 and Table 4.11, if the p-value (for the mean) was greater than 0.05 then the respective datasets were considered not statistically different. Conversely, if the p-value was less than 0.05, then the respective datasets are considered statistically different with 95 percent confidence. Based on the

results from the statistical analyses, the methods used to obtain the corrected blow count values were statistically the same for both of the sites analyzed. The CPT equations and the SPT empirical transfer function as described in Race and Coffman (2013) [to convert from the California sampler to the standard split spoon sampler] are also sufficiently calibrated to estimate N_{60} for sand using a standard split spoon sampler (within the 95 percent confidence interval).

Table 4.10. Statistical testing results of soil property data collected at MATS.

Soil Property	Compared Methods		P-Value			Methods with Greater Values
			T-Test[1]	Wilcoxon Test[2]	F-Test[3]	
Corrected Blow Count (Sand)	AHTD	MODOT	0.245*	0.212*	0.625*	-
	AHTD	UofA	0.072*	0.007	0.198*	UofA
	MODOT	UofA	0.309*	0.227*	0.819*	-
Undrained Shear Strength (Clay)	AHTD	MODOT	0.001	0.000	0.000	MODOT
	AHTD	UofA	0.769*	0.318*	0.111*	-
	MODOT	UofA	0.025	0.003	0.000	MODOT
Total Unit Weight (Clay)	AHTD	MODOT	0.000	0.000	0.269*	AHTD
	AHTD	UofA	0.000	0.000	0.001	AHTD
	MODOT	UofA	0.657*	0.665*	0.310*	-
Total Unit Weight (Sand)	AHTD	MODOT	0.001	0.001	0.266*	MODOT
	AHTD	UofA	0.000	0.000	0.024	UofA
	MODOT	UofA	0.003	0.007	0.310*	UofA

[1]Parametric test of the mean
[2]Nonparametric test of the mean
[3]Parametric test of the variance
*Statistically similar values

Table 4.11. Statistical testing results of soil property data collected at TATS.

Soil Property	Compared Methods		T-Test[1]	P-Value Wilcoxon Test[2]	F-Test[3]	Methods with Greater Values
Corrected Blow Count (Sand)	AHTD	MODOT	0.312*	0.399*	0.317*	-
	AHTD	UofA	0.617*	0.594*	0.056*	-
	MODOT	UofA	0.240*	0.306*	0.022	-
Undrained Shear Strength (Clay)	AHTD	MODOT	0.000	0.000	0.000	MODOT
	AHTD	UofA	0.000	0.000	0.000	UofA
	MODOT	UofA	0.707*	0.152*	0.417*	-
Total Unit Weight (Clay)	AHTD	MODOT	0.002	0.001	0.000	AHTD
	AHTD	UofA	0.511*	0.094*	0.000	-
	MODOT	UofA	0.188*	0.155*	0.000	-
Total Unit Weight (Sand)	AHTD	MODOT	0.002	0.001	0.000	MODOT
	AHTD	UofA	0.000	0.000	0.075*	UofA
	MODOT	UofA	0.000	0.000	0.129*	UofA

[1]Parametric test of the mean
[2]Nonparametric test of the mean
[3]Parametric test of the variance
*Statistically similar values

At the MATS, the undrained shear strength values that were determined using the AHTD and UofA methods were statistically similar, but the undrained shear strength determined using the MODOT method was statistically different than both the AHTD and UofA methods (Table 4.10). Alternatively, the undrained shear strength determined that were by the MODOT and UofA methods were statistically similar for the cohesive soil at the TATS, but the undrained shear strength determined using the AHTD method was statistically different (Table 4.11). Because there was no observed pattern for the undrained shear strength sampling methods at the various sites, it was determined that the values obtained for undrained shear strength were dependent on more than the sampling method. The type of clay (e.g. plasticity, strength, amount of saturation, amount of desiccation, etc.) may also have an influence upon the measured/correlated undrained shear strength values; however, there was not enough data on the

cohesive soil at the two test sites to statistically evaluate the soil properties in relation to the type of clay.

The total unit weight values for clay, as determined using the MODOT and UofA methods for both sites, were statistically similar for both sites. Other than these two methods producing similar total unit weight values, none of the methods for determining total unit weight in clay or sand were statistically similar. For the MATS, the total unit weight values, except those determined in the clay using the MODOT and UofA methods, were statistically different (Table 4.10). For the TATS, the total unit weight within the sand as determined using the AHTD, MODOT, and UofA were not statistically similar to each other. Within the clay at the TATS, the AHTD and UofA methods and the MODOT and UofA methods were statistically similar (Table 4.11). Because the majority of the total unit weight values were not statistically similar, the total unit weight may be dependent upon the characteristics of the clay and sand as well as the soil sampling method. Therefore, the sampling method and the previously mentioned soil characteristics should be considered when designing DSF.

4.7.2. Predicted Axial Capacity and Load-Movement

The results from the statistical evaluation, that was performed using the predicted values of axial capacity (that were obtained from ingestion of the geotechnical investigation data, as acquired from the different soil sampling methods, into the FB-Deep and SHAFT programs) are presented in Table 4.12 and Table 4.13. The predicted axial capacities, as a function of depth for a 1.2m diameter DSF and as obtained from the FB-Deep and SHAFT programs for the AHTD, UofA, and MODOT methods, are presented in Figure 4.3. In regard to axial capacity, the use of AHTD sampling data provided the lowest results at the design length [10.0MN at MATS and 7.1MN at TATS] in the FB-Deep program while the use of UofA sampling data in the SHAFT

program provides the highest results at the design length [10.9MN at MATS and 11.1MN at TATS].

Table 4.12. Statistical comparison of predicted static axial capacity of a DSF based on the geotechnical investigation method.

Site	Program	Compared Methods		P-Value T-Test[1]	P-Value Wilcoxon Test[2]	P-Value F-Test[3]	Methods with Greater Values
MATS	FB-Deep	AHTD	MODOT	0.000	0.000	0.081*	MODOT
		AHTD	UofA	0.000	0.000	0.767*	AHTD
		UofA	MODOT	0.000	0.000	0.147*	MODOT
	SHAFT	AHTD	MODOT	0.000	0.000	0.015	MODOT
		AHTD	UofA	0.630*	0.665*	0.448*	-
		UofA	MODOT	0.000	0.000	0.091*	MODOT
TATS	FB-Deep	AHTD	MODOT	0.000	0.000	0.048	MODOT
		AHTD	UofA	0.000	0.000	0.000	UofA
		UofA	MODOT	0.000	0.000	0.000	UofA
	SHAFT	AHTD	MODOT	0.134*	0.565*	0.030	-
		AHTD	UofA	0.000	0.000	0.001	UofA
		UofA	MODOT	0.000	0.000	0.244*	UofA

[1]Parametric test of the mean
[2]Nonparametric test of the mean
[3]Paramteric test of the variance
*Statistically similar values

Table 4.13. Statistical comparison of predicted static axial capacity of a DSF based on the commercial program utilized.

Site	Values Tested	Geotechnical Investigation Method	Average Percent Difference from values from SHAFT (%)		P-Value			Program Resulting in Greater Output Values
			1.2m	1.8m	T-Test[1]	Wilcoxon Test[2]	F-Test[3]	
MATS	Total[4]	AHTD	-		0.084*	0.057*	0.827*	-
		MODOT			0.000	0.000	0.955*	SHAFT
		UofA			0.000	0.000	0.959*	SHAFT
	Mean	AHTD	3.1	0.3	0.800*	0.747*	0.840*	-
		MODOT	1.1	-0.5	0.731*	0.350*	0.656*	-
		UofA	11.2	9.8	0.001	0.002	0.706*	SHAFT
TATS	Total[4]	AHTD	-		0.000	0.000	0.039	SHAFT
		MODOT			0.000	0.000	0.270*	SHAFT
		UofA			0.569*	0.243*	0.216*	-
	Mean	AHTD	9.1	4.9	0.000	0.000	0.640*	SHAFT
		MODOT	38.0	40.7	0.000	0.000	0.482*	SHAFT
		UofA	15.2	11.6	0.000	0.000	0.039	SHAFT

[1]Parametric test of the mean
[2]Nonparametric test of the mean
[3]Paramteric test of the variance
[4]Mean, Mean plus one standard deviation, and mean minus one standard deviation values
*Statistically similar

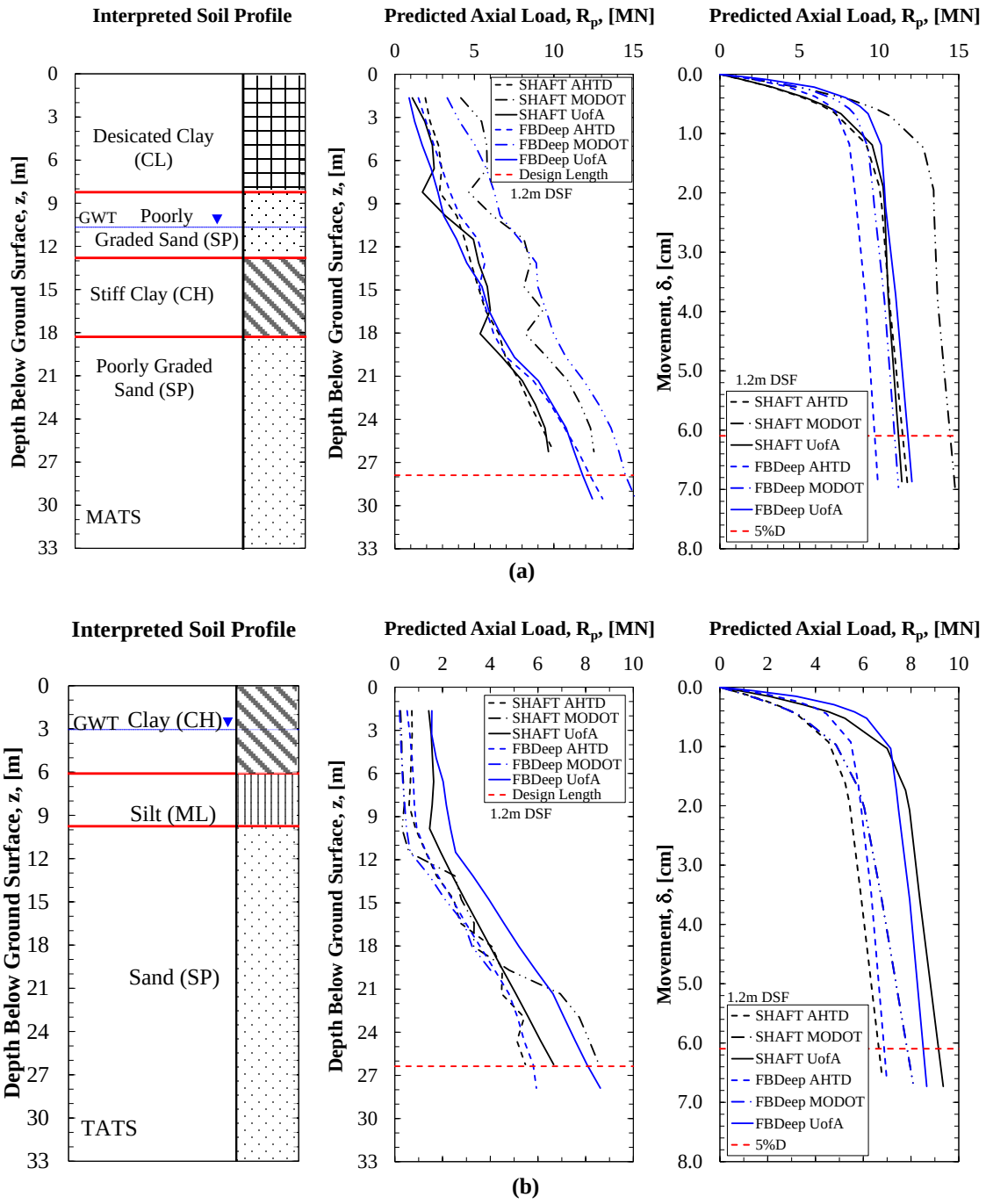

Figure 4.3. Predicted axial capacity and load-movement characteristics of DSF at a) MATS and b) TATS [modified from Race et al. (2013)].

As presented in Table 4.12, the predicted axial capacity values were compared in relation to the soil sampling and testing method utilized within the predictive software programs. At the MATS, the axial capacity determined from the mean AHTD and UofA methods, using SHAFT,

are statistically similar but the other axial capacity datasets were not statistically similar. At the TATS, the axial capacity obtained from the AHTD and MODOT methods, using SHAFT, were statistically similar. The variances of the predicted axial capacities at the MATS were statistically similar except for when comparing the AHTD and MODOT methods using SHAFT. Conversely, the variances of the predicted axial capacities at the TATS are statistically different except when using soil properties from the MODOT and UofA methods and the SHAFT program. At the MATS, the axial capacity values were not statistically similar, the axial capacity predicted using the MODOT method was generally greater than the axial capacity generated using the AHTD and UofA methods. Conversely, at the TATS, the axial capacity predicted from utilizing the UofA method was typically greater than the axial capacity that was predicted using the AHTD and MODOT methods.

In Table 4.13, the axial capacity values were compared based on the program utilized. At the MATS, the total values (Mean, +1SD, and -1SD) using the AHTD method and the mean values using the AHTD and MODOT methods are statistically similar. For the other compared datasets at the MATS, the axial capacity values, predicted using SHAFT, were statistically greater than the values predicted using FB-Deep. The average percent difference (percent difference of the axial capacity values averaged with depth) confirms that there is a significant difference in the axial capacity values as determined using the T-test and Wilcoxon test. The variance of the axial capacity datasets was statistically similar for all datasets except for the total values using the AHTD method and the mean values using the UofA method at the TATS. Because the majority of the variances are statistically the same when comparing the prediction programs, the difference in variance in the predicted axial capacities was primarily attributed to the soil sampling and testing methods and not attributed to the program that was utilized.

The predicted values of load-movement response (that were obtained from the ingestion of the values obtained from different soil sampling methods into the FB-Deep and SHAFT programs, as presented in Figure 4.3) were evaluated 1) at movement values of five percent of the diameter and 2) at the onset of plunging failure. By comparing the sampling methods through the relationship to the load-movement response, greater values of load were predicted when the MODOT method was used then when the values obtained from the AHTD method were used (percent differences ranging from 11.4 to 20.6 percent difference at movement values corresponding to five percent of the diameter and from 11.4 to 20.2 percent difference at plunging failure). Likewise, the load values produced by using the data obtained from the UofA method were greater than the load values produced by using the data obtained from the MODOT method by percent differences ranging from 0.5 to 14.4 percent difference at movement values corresponding to five percent of diameter and from 0.1 to 13.3 percent difference at plunging failure (except for the load values from the MODOT data at MATS when SHAFT was utilized that were 28.9 and 29.2 percent difference greater, respectively). The lowest average difference in load-movement response obtained from the SHAFT and FB-Deep programs was obtained when comparing the predicted values for the DSF designed at the TATS. The lowest difference in load-movement response was likely due to the primarily homogeneity of the soil at the TATS. As shown in Figure 4.4 and as previously mentioned in Section 4.6.1, the percent differences between the predicted capacity values at five percent of the diameter were a function of the number of statistically similar soil properties. Even though the percent differences between the soil properties was not considered, there was an inverse trend between the percent difference and the number of statistically similar soil properties. Therefore, the soil sampling and testing method should be considered when designing DSF.

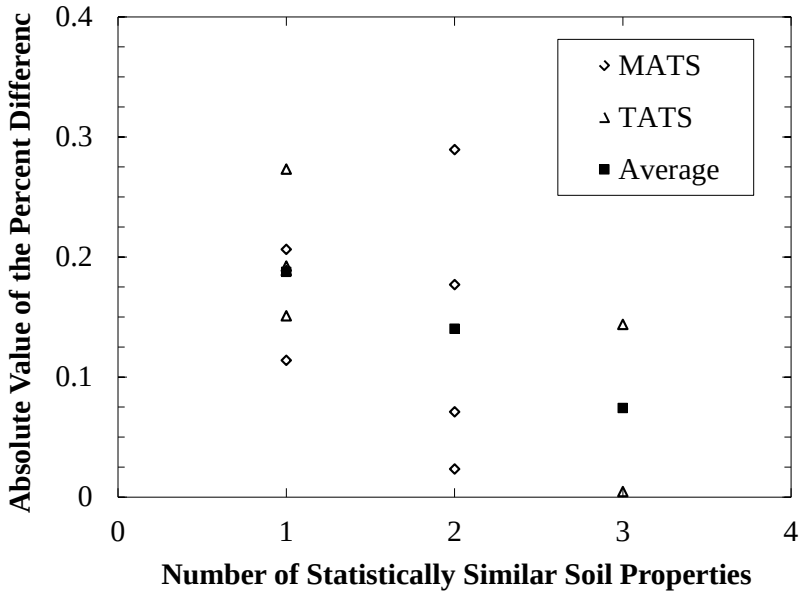

Figure 4.4. Absolute values of the percent difference of the load values at movements of five percent of the diameter as a function of the number of statistically similar soil properties.

4.7.3. Recommended Methods

At the TATS, the coefficient of variation (COV) of c_u for the AHTD, MODOT, and UofA sampling methods are 0.33, 0.39, and 0.45, respectively. At the TATS, the average COV for γ_T for the AHTD, MODOT, and UofA sampling methods are 0.12, 0.02, and 0.05, respectively. The average COV for c_u and γ_T at MATS vary slightly (by five percent or less) between the three (3) sampling methods. Based on the COV data, it is recommended that the MODOT and UofA methods be used to characterize the soil. In particular, the MODOT method is recommended for geotechnical investigations conducted in soft/weak soils because it was more precise (lowest COV for γ_T) and because it was faster than the other methods. Even though the COV values obtained using the MODOT method were slightly larger for the c_u than the COV value obtained when using the AHTD method, the MODOT method is still recommended because the mean c_u values for the MODOT and UofA are statistically similar (these values are

not statistically similar to AHTD values). The MODOT method is not recommended for geotechnical investigations in gravelly and hard soils because the CPT cone may be damaged (as presented previously by the lower penetration depths). In combination with the MODOT method, at least one borehole is also recommended to initially characterize the soil (soil type and hard/soft consistently) and to provide index properties for the soil deposit. The UofA method is recommended for use in gravelly and hard soils because this method is more precise than the AHTD method is capable of being performed in all soils. It was determined that the predicted axial capacity and load-movement response varies depending upon the soil sampling and testing method and the design method. Therefore when designing DSF, it is further recommended that individual resistance factors be developed for different types of soil sampling and testing methods (e.g. AHTD, MODOT, or UofA) as well as different design methods (e.g. SHAFT or FB-Deep).

4.8. Conclusions

The results obtained from the statistical analyses of the soil property, axial capacity, and load-movement data were used to evaluate 1) the effects of soil sampling and testing techniques and 2) the different in algorithms used in software programs that were utilized to obtain predicted values of static axial capacity and load-movement response. Based on the statistical evaluation methods (T-test, Wilcoxon test, and F-test), it was determined that the soil property values were dependent upon the soil sampling and testing method as well as soil characteristics such as soil type, stiffness/hardness, and degree of desiccation. The axial capacity and load values from load-movement response obtained by using the MODOT and UofA methods were typically greater (and more precise based on the full-scale load tests in Race and Coffman [2015]) than the values obtained by using AHTD methods. Similarly, the predicted axial capacity

and load-movement response values that were determined using SHAFT were generally greater than the values determined when using FB-Deep. To evaluate the impact of the soil sampling and testing methods on the predicted axial capacity and load-movement response, it was determined that there was an inverse relationship between the percent difference in the predicted capacity at five percent of the diameter and the number of statistically significant soil properties.

Based on the statistical comparison of the soil sampling procedures and the calculated COV values, it is recommended that the MODOT method be used in soft/weak to medium hard soils and the UofA method be used in gravelly or hard soils. In combination with MODOT testing, soil samples should also be collected from at least one borehole to assess the index properties of the soil. Successively, the 1) soil sampling and testing method and 2) design method should be considered with designing DSF due to the effects of the parameters on the predicted axial capacity and load-movement values.

4.9. Acknowledgments

The authors thank the editor and reviewers of this manuscript for their constructive comments that improved the quality of the manuscript. The authors also thank the Arkansas State Highway and Transportation Department and the Missouri Department of Transportation for assisting with the geotechnical site investigations that were performed at the sites listed in this paper.

4.10. References

American Association of State Highway and Transportation Officials (2007) LRFD Bridge Design Specifications, Fourth Ed., AASTHO, Washington, D.C., pp. 1938.

American Society for Testing and Materials (2012) “Standard Test Method for Standard Penetration Test (SPT) and Split-Barrel Sampling of Soils.” Annual Book of ASTM Standards, Designation D1586, Vol. 4.08, ASTM, West Conshohocken, PA.

American Society for Testing and Materials (2012) “Standard Test Method for Mechanical Cone Penetration Tests of Soil.” Annual Book of ASTM Standards, Designation D3441, Vol. 4.08, ASTM, West Conshohocken, PA.

American Society for Testing and Materials (2012) “Standard Test Method for Unconsolidated-Undrained Triaxial Compression Test on Cohesive Soils.” Annual Book of ASTM Standards, Designation D2850, Vol. 4.08, ASTM, West Conshohocken, PA.

Bey S (2014) “Cost-benefit Analysis for Load Resistance Factor Design (LRFD) of Drilled Shafts in Arkansas.” M.S. Thesis, University of Arkansas, Fayetteville, Arkansas, pp. 410.

Bloomquist D, McVay M, Hu Z (1992) “Updating Florida Department of Transportation’s (FDOT) Pile/Shaft Design Procedures Based on CPT and DTP Data.” Florida Department of Transportation, BD-545, RPWO No. 43, MF Project 00005780, pp. 199.

Bo S, Da-in G, Li M (2013) “Study on a Test Data Validation Method for Asphalt Pavements.” Journal of Highway and Transportation Research and Development (English Edition), Vol. 7, No. 1, pp. 9-16.

Brown D, Turner J, Castelli R (2010) “Drilled Shafts: Construction Procedures and LRFD Methods.” FHWA Publication No. NHI-10-016, Federal Highway Administration, Washington, D.C., pp. 970.

Bustamante M , Gianeselli L (1982) “Pile Bearing Capacity Prediction by Means of Static Penetrometer CPT.” Proceedings of the 2nd European Symposium on Penetration Testing Vol. 2, pp. 493-500.

Coffman R (2011c) “Load and Resistance Factor Design (LRFD) Site Specific Variability in Laboratory and Field Measurements and Correlations.” TRC-1204 Project Proposal to Arkansas State Highway and Transportation Department, pp. 58.

FB-Deep (2012) Bridge Software Institute, Gainesville, Florida, Version 2.04.

Lopez-Caballero F, Gaspar A, Gomes-Correia A (2011) “Uncertainty and Sensitivity Analysis of FWD Test.” GeoHunan 2011: Emerging Technologies for Design, Construction, Rehabilitation, and Inspection of Transportation Infrastructure, China, June, pp. 49-56.

Luo Z, Atamturktur S, Juang H (2013) “Bootstrapping for Characterizing the Effect of Uncertainty in Sample Statistics for Braced Excavations.” Journal of Geotechnical and Geoenvironmental Engineering, Vol. 139, No. 1, pp. 13-23.

Meyerhof G (1976) “Bearing Capacity and Settlement of Pile Foundations.” Journal of Geotechnical Engineering, Vol. 102, No. 6T3, pp. 195-228.

Niazi F, Mayne P, Wang Y (2011) “Statistical Analysis of Cone Penetration Tests and Soil Engineering Parameters at the National Geotechnical Experimentation Clay Site, Texas A&M University.” ASCE Geotechnical Special Publication No. 211, Proc. GeoFrontiers 2011: Advances in Geotechnical Engineering, Dallas, Texas, March, pp. 2998-3007.

O'Neill M, Reese L (1999) "Drilled Shafts: Construction Procedures and Design Methods." FHWA Publication No. IF-99-025, Federal Highway Administration, Washington D.C., pp. 537.

Phoon K, Quek S, An P (2003) "Identification of Statistically Homogeneous Soil Layers Using Modified Barlett Statistics." Journal of Geotechnical and Geoenvironmental Engineering, Vol. 129, No. 7, pp. 649-659.

Quiros G, Reese L (1977) "Design Procedures for Axially Loaded Drilled Shafts" FHWA Publication No. TX78-1765F, Federal Highway Administration Final Report, Washington, D.C., pp. 176.

Race M, Bey S, Coffman R (2013) "Discussion of 'Implementation of LRFD of Drilled Shafts in Louisiana' by Xinbao Yu, Murad Y. Abu-Farsakh, Sungmin Yoon, Ching Tsai, and Zhongjie Zhang." Journal of Infrastructure Systems 19(3): 351-355.

Race M, Coffman R (2013) "Effect of Uncertainty in Site Characterization on the Prediction of Liquefaction Potential for Bridge Embankments in the Mississippi Embayment." ASCE Geotechnical Special Publication No. 231, Proc. GeoCongress 2013: Stability and Performance of Slopes and Embankments III, San Diego, California, March, pp. 888-897.

Race M, Coffman, R (2015) "Response of a Drilled Shaft Foundation Constructed in a Redrilled Shaft Excavation Following Collapse." Deep Foundations Institute Journal, Accepted.

Reese L, O'Neill M (1988) ''Drilled Shafts; Construction Procedures and Design Methods.'' Rep. No. FHWA-HI-88-42, U.S. Dept. of Transp., Federal Highway Administration, Washington, D.C.

Reese L, Wang S, Arrellaga J, Vasquez L (2012a) "SHAFT v2012- User's Manual: A Program for the Study of Drilled Shafts Under Axial Loads." ENSOFT, INC. Austin, Texas, pp. 186.

Reese L, Wang S, Arrellaga J, Vasquez L (2012b) "SHAFT v2012- Technical Manual: A Program for the Study of Drilled Shafts Under Axial Loads." ENSOFT, INC. Austin, Texas, pp. 76.

Robertson P, Cabal K (2012) "Guide to Cone Penetration Testing for Geotechnical Engineering." Gregg Drilling and Testing, Inc, pp. 145.

Schmertmann J (1967) "Guidelines for Use in the Soils Investigation and Design of Foundations for Bridge Structures in the State of Florida." Research Bulletin 121 (RB-121), Report Prepared for the FDOT by the University of Florida, Gainesville, Florida.

Schmertmann J (1978) "Guidelines for Cone Test, Performance, and Design." FHWA Publication No. TS-78209, Federal Highway Administration, Washington, D.C., pp. 145.

SHAFT (2012) ENSOFT, INC. Austin, Texas, Version 2012.

Sheikh S, O'Neill M (1986) “Long-term Behavior of Expansive Concrete Drilled Shafts.” Canadian Journal of Civil Engineering, Vol. 13, No. 2, pp. 213-217.

Skempton A (1951) “The Bearing Capacity of Clays.” Proceedings from Building Research Congress, London, Vol. 1, pp. 180-189.

Townsend F (2003a) “SHAFT-SPT Validation Problems.” Bridge Software Institute. Gainesville, Florida, pp. 91.

Townsend F (2003b) “User’s Guide for SHAFT-SPT.” Bridge Software Institute. Gainesville, Florida, pp. 16.

Unanwa C, Mahan M (2014) “Statistical Analysis of Concrete Compressive Strengths for California Highway Bridges.” Journal of Performance of Constructed Facilities 28, SPECIAL SECTION: Performance of Bridges under Critical Natural Hazards, pp. 157-167.

Vanikar S (1986) Manual on Design and Construction of Driven Pile Foundations. U.S. Department of Transportation Federal Highway Administation, FHWA-DP-66-1 (Revision 1), pp. 57.

Yang X, Han J, Henthorne R, Parsons R (2008) “Statistical Analysis of O-Cell Test Data for Nominal Load Capacities of Drilled Shafts.” ASCE Geotechnical Special Publication No. 178, Proc. GeoCongress 2008: Geosustainability and Geohazard Mitigation, New Orleans, Louisiana, March, pp. 90-97.

Yu X, Abu-Farsakh M, Yoon S, Tsai C, Zhang Z (2012) “Implementation of LRFD of Drilled Shafs in Louisiana.” Journal of Infrastructure Systems, Vol. 18, No. 2, pp. 103-112.

CHAPTER 5: DSF at the SSATS

5.1. Chapter Overview

At the Siloam Springs Arkansas Test Site (SSATS), three drilled shaft foundations were constructed in moderately strong to strong limestone ($f'_r \sim 100MPa$). The design depth was 7.9m for 1.2m and 1.8m DSF, but the constructed depths of the West 1.2m, Center 1.8m, and East 1.2m DSF were 7.9m, 6.4m, and 7.0m, respectively. A bi-directional load cell (BLC) test was performed on each of the DSF at the SSATS and the results are presented herein. The constructed depths of the DSF at the SSATS were altered during construction due to lack of time and cost of equipment, but this field-change was problematic for the BLC testing. Specifically, because of the field-change there was not enough upward resistance in the Center 1.8m and East 1.2m DSF to sufficiently resist the base resistance of the DSF. Other problems regarding the BLC tests on the DSF at the SSATS include: time lag between the excavation construction and the concrete pouring, pour concrete below the BLC for the West 1.2m diameter DSF, and misplaced telltales on the BLC for the Center 1.8m and East 1.2m diameter DSF.

The design of DSF in moderately hard to hard limestone can be significantly reduced (from the required 3.0m rock socket) regarding axial capacity. From the equivalent top-down load-movement curves, the movement did not exceed 0.1 percent of the diameter size for any of the DSF. Due to the low movement for these tests and other BLC tests conducted in hard limestone, it is recommended that the design of DSF in moderately hard to hard limestone be limited to the service limit (0.2cm or 0.1%D). Based on the results obtained from the SSATS, the measured unit side resistance of the weathered rock was predicted by utilizing procedures in McVay and Niraula (2004). However, the unit side resistance of the competent rock was not accurately predicted because the ultimate capacity of the DSF was not measured due to the small

upward movement of the West 1.2m DSF during the BLC test. Furthermore, the ultimate capacity for the unit base resistance was not measured because of the bad concrete below the BLC for the West 1.2m diameter DSF and because there was not enough resistance in the upward direction to resist the base resistance for the Center 1.8m and East 1.2m diameter DSF.

The paper enclosed in this chapter has been accepted for publication within the Deep Foundations Institute Journal. The full reference is: Race, M. L. and Coffman, R.A. (2015). "Load Tests on Drilled Shaft Foundations in Moderately Strong to Strong Limestone." DFI Journal, Vol. 9, No. 1, pp. 1-10, DOI: 10.1179/1937525514Y.0000000004.

5.2. Additional Results

For completeness, additional results from the DSF at the SSATS are presented below and were also presented in Bey (2014). Specifically, the amount of upward and downward creep of the DSF at the SSATS is presented in Figure 5.1. There was no creep limit for the BLC tests on the DSF at the SSATS; therefore, there does not need to be any reduction of the axial capacity (at least for the measured axial load).

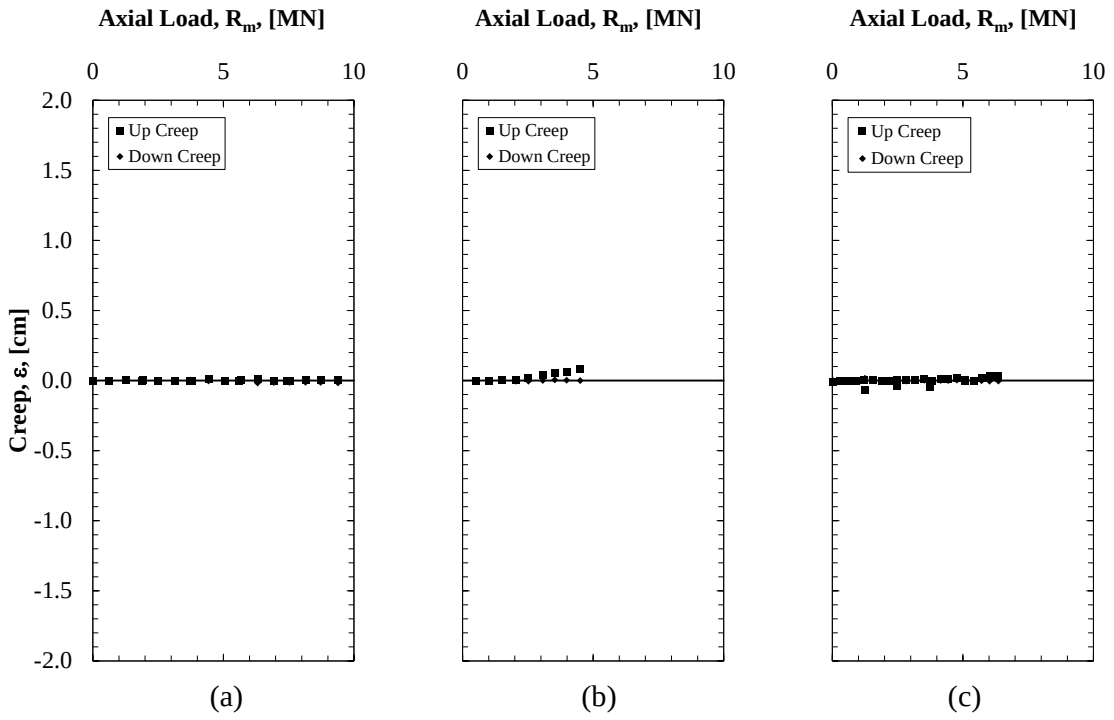

Figure 5.1. Upward and downward creep of the top and bottom of the bi-directional load cell from the full-scale load tests for the a) West 1.2m, b) Center 1.8m, and c) East 1.2m DSF at the SSATS.

Besides the statistical analysis method presented in this chapter, regression analysis was utilized to determine a numerical difference between the predicted and measured equivalent top-down load-movement curves. The slope (β_0) and intercept (β_1) linear regression parameters were determined for each of the predicted and measured load-movement curves at small movements (Table 5.1). Only the linear portion of the load-movement curve was utilized to evaluate the load-movement characteristics of the DSF. Specifically, the nonlinear portion of the load-movement curves (axial load values larger than 10 MN [2248 kip]) was not utilized for this comparison method. The β_0 parameter for all drilled shaft foundations at SSATS was significantly less (70.4 to 3300 percent less) when predicted using SHAFT and FB-Deep than when utilizing the Coyle and Reese (1966) method (excluding UofA geotechnical investigation method). The closest predictive slope parameter (β_0) that was obtained from the commercial

software programs was obtained from the FB-Deep program in combination with the UofA data. The β_0 parameter was underpredicted based on the Coyle and Reese (1966) method utilizing the t-z and Q-z curves. The predicted intercept parameters (β_1) ranged from -3.1 to 0.0 while the measured β_1 values ranging from -0.0073 to -0.0033. The nearest slope values (i.e. lowest percent difference) to the measured values were determined using SHAFT and Coyle and Reese (1966) methods with the UofA data.

Table 5.1. Linear regression parameters β_0 (slope) and β_1 (intercept) for the load-movement curves obtained for the drilled shaft foundations at the SSATS.

Type	Method		West 1.2m		Center 1.8m		East 1.2m	
			β_0	β_1	β_0	β_1	β_0	β_1
Measured	Osterberg Load Test		0.010	-0.007	0.007	-0.005	0.008	-0.003
Predicted	SHAFT (2012)	AHTD	0.080	-0.006	0.111	-0.015	0.139	-0.011
		UofA	0.024	0.000	**0.014**	**-0.004**	**0.022**	**-0.002**
	FB-Deep (2012)	AHTD	0.084	-1.841	0.254	-3.113	0.084	-1.494
		UofA	0.011	-0.405	0.008	-0.385	0.012	-0.350
	Coyle and Reese (1966)	Rock	0.002	-0.001	0.001	-0.001	0.002	-0.001
		Rock and Soil	**0.005**	**-0.008**	0.002	-0.003	0.005	-0.007
		Rock (limits)	0.003	-0.002	0.002	-0.001	0.003	-0.001
		Rock and Soil (limits)	0.006	-0.010	**0.003**	**-0.004**	0.006	-0.009

Note: Bolded numbers correspond to the best prediction method

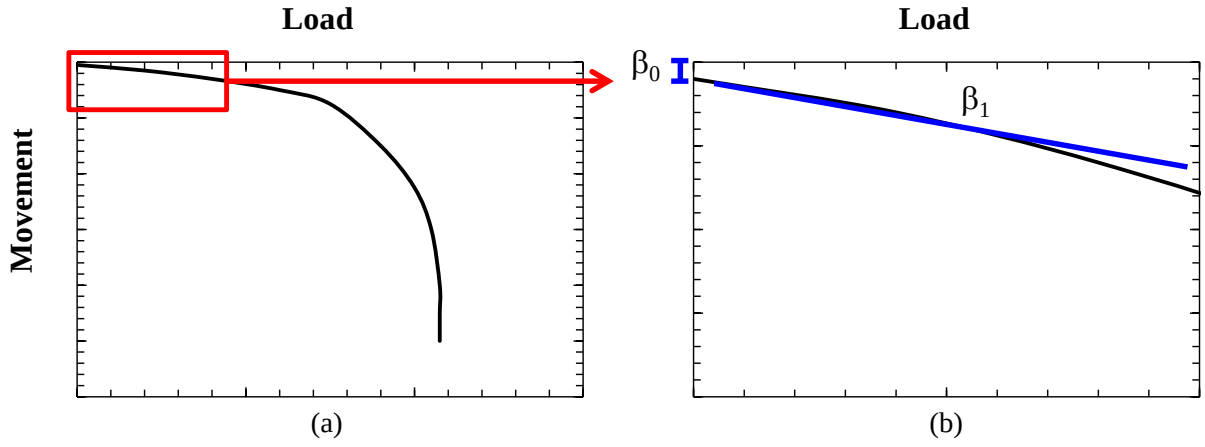

Figure 5.2. a) A typical top-down load-movement curve and b) linear regression variables utilized for the analysis in Table 5.1.

Lateral load predictions were obtained from the LPILE (2012) software program. Based on the as-built dimensions of the DSF at the SSATS, the predicted movement for lateral load was 0.037cm, 0.019cm, and 0.037cm for the West 1.2m, Center 1.8m, and East 1.2m DSF, respectively for the UofA geotechnical investigation method (presented in Figure 5.3). Based on the required design load for the DSF constructed at the SSATS (Table 5.2), the p-y curves for all three of the soil sampling and testing methods are presented in Appendix C in Figure C.8.

Table 5.2. Lateral loading design requirements for DSF at the SSATS.

Loading Type	Amount of Load		
	Axial	Longitudinal	Transverse
Force (MN)	2.260	0.062	0.062
Moment (MN*m)	N/A	0.459	0.117

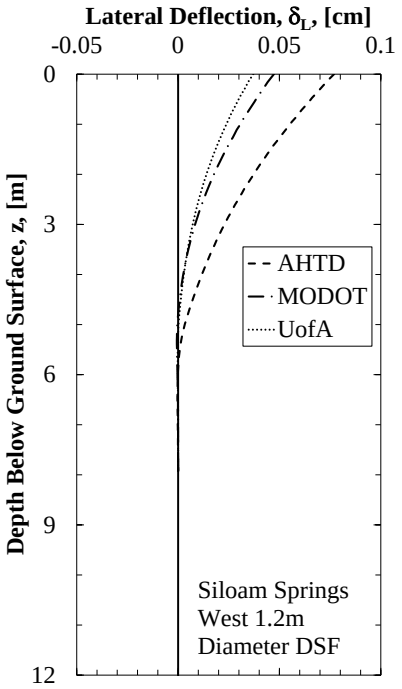

Figure 5.3. Lateral deflection of the West 1.2m diameter DSF at the SSATS as predicted utilizing LPILE (2012) and the obtained geotechnical investigation data.

Load Tests on Drilled Shaft Foundations in Moderately Strong to Strong Limestone

Morgan L. Race[1] and Richard A. Coffman[2]

5.3. Abstract

Three drilled shaft foundations (DSFs) were constructed in moderately strong to strong limestone at the Siloam Springs Arkansas Test Site (SSATS). The embedment lengths within the limestone were 3.0, 1.5, and 2.1 meters for the DSF with diameters of 1.2, 1.8, and 1.2 meters, respectively. The DSFs were instrumented to facilitate cross-hole sonic logging testing and full-scale load testing using bi-directional load cells (BLCs). Lessons learned from construction included the: 1) proper concrete pouring techniques, 2) ability to retrofit improperly installed telltale instrumentation, and 3) influence of rock socket length in moderately strong to strong limestone. Recommended design, construction, and testing techniques in moderately strong to strong limestone are presented. Based on the full-scale testing, t-z model recommendations for weathered limestone and moderately strong to strong limestone are presented and discussed. Comparison of unit side resistance with design recommendations is considered.

5.4. Introduction

The ultimate axial capacity values for DSFs depends upon the site conditions, design parameters and methods, construction methods, and testing methods. Therefore, prior to construction the site conditions at the SSATS were characterized and the axial capacity estimates were obtained using commercially available programs (FB-Deep and SHAFT) and hand calculations. The various rock socket lengths for the DSFs at the SSATS were attributed to the combination of time constraints and the strength of the limestone deposits. As expected, the measured upward and downward movements and the corresponding end bearing and side shear values varied based upon the construction methods (i.e. rebar placement, concrete pouring,

duration between drilling and concrete pouring) and the geometry of the DSFs. The problems encountered and the subsequent lessons learned, particularly the lessons associated with the construction and full-scale testing, are discussed herein along with recommendations developed from the full-scale load testing.

5.5. Previous Case Histories

Bi-directional load tests are commonly utilized to compare the predicted and measured values of unit side resistance and end bearing resistance. This type of load testing has been utilized to test DSFs constructed in moderately strong rock (approximately unconfined compressive strength [f'_r] equal to 68.9MPa), as reported in Gunnink and Keihne (2002). According to Gunnink and Kiehne (2002), three DSFs were embedded in Pennsylvanian aged limestone and shale with rock socket lengths of 1.4m, 1.5m, and 1.6m for Shaft 1, Shaft 2, and Shaft 3, respectively. For Shafts 1, 2, and 3, failure (the inability of DSF to hold the applied load) occurred at loads of 3,500kN, 1,500kN, and 3,800kN, respectively, with unit side resistance values of 2.3MPa, 0.9MPa, and 2.3MPa and end bearing resistance values of 21.4MPa, 9.1MPa, and 22.9MPa, respectively.

Brown (2009) discussed two DSFs that were constructed in Nashville, Tennessee. From the observed unit side resistance values, it was determined that mobilization of the unit side resistance occurred around 0.5cm. For the end bearing resistance of the two DSFs, the movements were only one percent (approximately 1.3cm and 0.8cm downward movement of the BLCs) of the base diameter (effective base diameters of 1.0m and 0.7m, respectively). From the full-scale load tests, it was determined that design values (side resistance values of 0.96MPa) could be utilized that were higher than the values that had been historically used at similar sites.

The C value from Equation 5.1 [Brown et al. 2010] was calculated to be 0.4 using the measured unit side resistance and unconfined compressive strength of the rock (Brown 2009).

In Axtell and Brown (2011), four 3.5m diameter DSFs were utilized in the design and construction of the New Mississippi River Bridge located north of St. Louis, Missouri. The test shaft for these foundations was socketed 7.1m into moderately strong limestone (f'_r > 69MPa with an average f'_r approximately 166MPa). However, for Piers 11 and 12, there was a layer of lower strength rock that was approximately 1.5m thick with f'_r equal to 35MPa at a depth of 6.1m. Four BLCs, each with a total capacity of 213.5MN, were used to confirm the side and end bearing resistance values and the quality of the construction methods. The average unit end bearing and unit side resistance in the rock socket were 22MPa and 2.1MPa, respectively (Axtell and Brown 2011). These values were not the ultimate strength values because very small movements were measured (displacement values less than 0.4cm in either direction corresponding to 0.1% of the diameter of the shafts). Using the measured side resistance values, it was determined that the FHWA method that is utilized to estimate unit side resistance in hard rock is viable for the limestone at this site with a C value equal to 0.5.

$$f_s = C * p_a * \left(\frac{q_u}{p_a} \right)^{0.5}$$ Brown et al. (2010) Equation 5.1

The variables from Equation 5.1 are defined as: f_s, the unit side resistance (MPa), C, an empirical constant, p_a, the atmospheric pressure (0.1013 MPa), and q_u, the unconfined compressive strength of the rock (MPa).

5.6. Methods and Materials

The SSATS is located next to the bridge on Highway 16 that spans the Illinois River (Figure 5.4). The geotechnical site characterization of the soil and rock was performed with the help of the personnel from the Arkansas State Highway and Transportation Department (AHTD),

the Missouri of Transportation Department (MODOT), and the University of Arkansas (UofA). The drilled shaft foundations were constructed by personnel from Aldridge Construction and tested by personnel from Loadtest Inc., GEI Consultants, and the UofA.

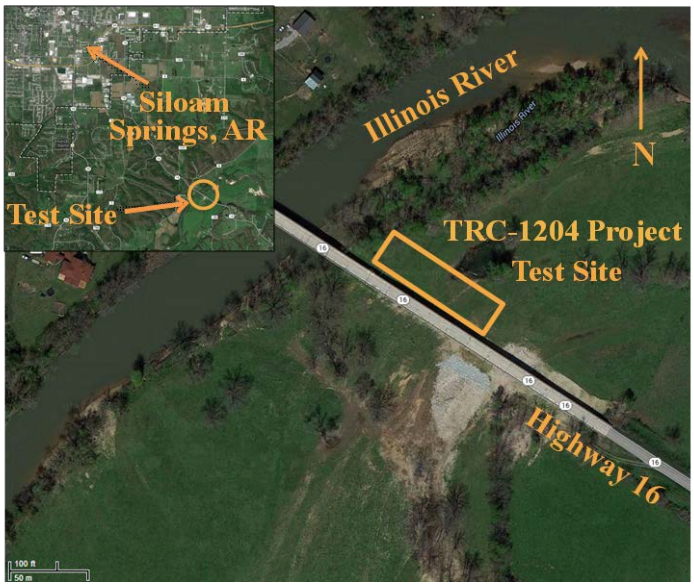

Figure 5.4. Location of the SSATS [Google Earth 2012; Bey 2014].

5.6.1. Soil and Rock Characterization

The methods utilized to classify the soil and rock properties at the SSATS included standard penetration test (SPT), cone penetration test (CPT), and uniaxial unconfined compression test (UC). The stratigraphy at the SSATS consists of 4.9m of cherty clay underlain by 18.3m of strong limestone. The UofA drilling and sampling method consisted of drilling six boreholes and sampling with the SPT using a California split spoon sampler (60mm inner diameter) in soil and a diamond encrusted rock corer in the rock. Utilizing this method, rock quality designation (RQD) values were measured and recorded for all of the extracted rock cores. UC and confined triaxial compression tests were also performed to determine the unconfined compressive strength (f'_r) and modulus of elasticity (E) of the rock, respectively. The total unit weight of soil and rock (γ_T), the undrained shear strength of soil (c_u), and the friction angle of

soil (ϕ) were determined from these tests. The AHTD method consisted of collecting blow count values utilizing the SPT as conducted with a standard split spoon sampler (30mm inner diameter), in the soil and of coring the rock to obtain RQD values for the limestone. The MODOT method consisted of collecting data utilizing the CPT within the soil; no rock data was collected using the MODOT method. The soil and rock properties are presented in Figure 5.5. Based on the average RQD (70%) and f'_r (100MPa) values obtained from the UofA method, the rock at the SSATS classified as a high quality, moderately strong to strong limestone.

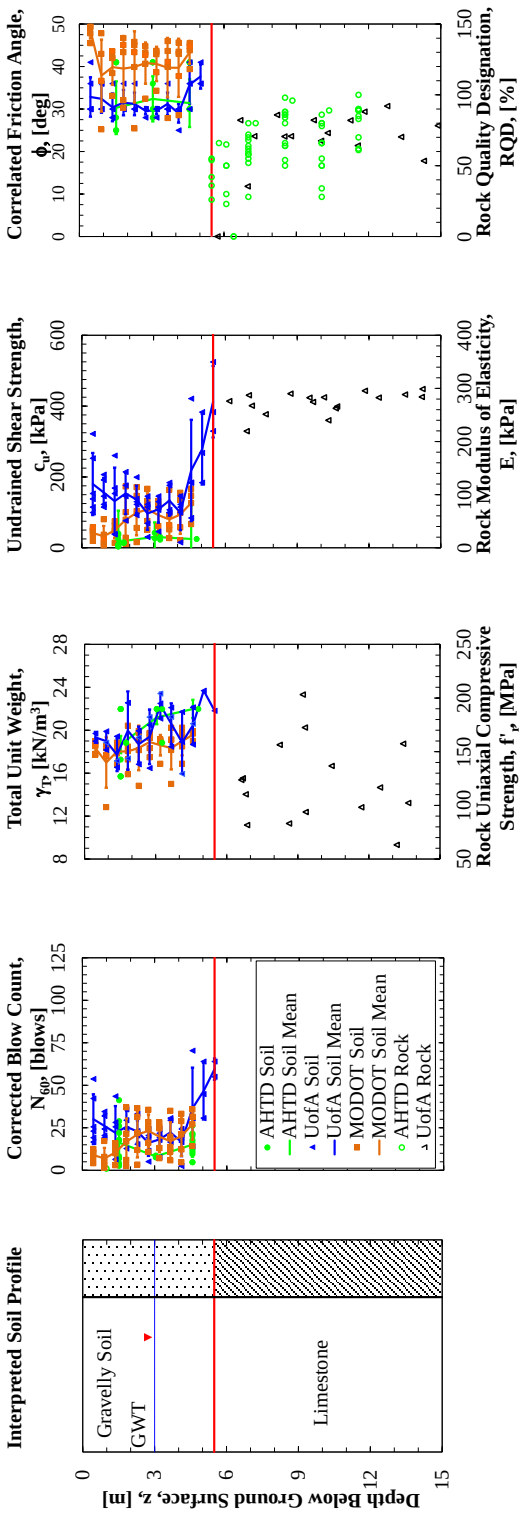

Figure 5.5. Soil and rock properties at the SSATS [modified from Race et al. 2014].

5.6.2. Design Methods and Considerations

As stipulated by the AHTD, the required axial capacity and rock socket length for each drilled shaft foundation at the SSATS were 9.9MN and 3.0m, respectively (Schubel 2013). The methods utilized to predict the axial capacity for the drilled shaft foundations included: FB-Deep [2012], SHAFT [2012], and hand calculations using the Brown et al. [2010] and Coyle and Reese [1966] methods. Using the t-z analysis method described in Coyle and Reese (1966), the load-movement curves were predicted for four different soil/rock models: rock only, rock and soil, rock only with strength limits (q_{max} = 2.9MPa), and rock and soil with strength limits. The maximum unit side resistance and maximum end bearing resistance, as predicted using FB-Deep and SHAFT (at movements of five percent times the diameter [5%D]), are presented in Table 5.3 for all of the DSFs at the SSATS.

Table 5.3. Predicted unit side shear resistance and end bearing resistance using the FB-Deep and the SHAFT programs upward and downward movements corresponding to 5%D movement for the respective DSF.

			FB-Deep		SHAFT	
Shaft Designation	**DSF Len. (m)**	**DSF Dia. (m)**	**Unit Side Resistance of Rock (MPa)**	**End Bearing Resistance (MPa)**	**Unit Side Resistance of Rock (MPa)**	**End Bearing Resistance (MPa)**
West 1.2m	7.9	1.2	2.3	76.5	0.01	23.2
Center 1.8m	6.4	1.8	2.4	9.2	0.18	0.8
East 1.2m	7.0	1.2	2.3	11.7	0.13	1.1

5.6.3. Construction of Drilled Shaft Foundations

Three DSFs, designated as the West 1.2m diameter, the Center 1.8m diameter, and the East 1.2m diameter, were installed at the SSATS. For the West 1.2m, Center 1.8m, and East 1.2m diameter DSFs, the lengths to the bottom of the DSFs, from the ground surface, were 7.9m, 6.4m, and 7.0m, respectively. Although the designed rock socket length for each DSF was 3.0m, the as-built rock socket lengths were 3.0m, 1.5m, and 2.1m for the West 1.2m, Center 1.8m, and

East 1.2m diameter DSFs, respectively. The depths of the DSFs were modified because there was a time constraint for the project and because the limestone was stronger than expected. For example, significantly more time was required and drill bit teeth were used to drill to the required depth for the West 1.2m diameter DSF than was expected, due to the strength of the limestone.

Each DSF was instrumented with four vibrating wire strain gages (Geokon Model 4200 series vibrating wire strain gages), five telltale pipes (1.3cm inner diameter black iron pipe), four cross-hole sonic logging (CSL) tubes (5.1cm inner diameter black iron pipe), and a BLC. The diameters of the BLC, installed in the drilled shaft foundations, were 40.6cm, 50.8cm, and 40.6cm for the West 1.2m, Center 1.8m, and East 1.2m diameter DSFs, respectively. The as-built schematics of all of the DSFs are presented in Figure 5.6. The socket characteristics (socket length and socket surface area) of the DSFs at the SSATS are summarized in Table 5.4.

Table 5.4. Geometry of the DSF at the SSATS.

Shaft Designation	Dia. (m)		Depth Below Ground Surface (m)		Rock Socket Length (m)	Rock Socket Surface Area (m^2)
	Within Soil	Within Rock	Bi-Directional Load Cell	Bottom		
West 1.2m	1.5	1.2	7.3	7.9	3.0	22.6
Center 1.8m	2.0	1.8	5.8	6.4	1.5	17.0
East 1.2m	1.5	1.2	6.4	7.0	2.1	15.8

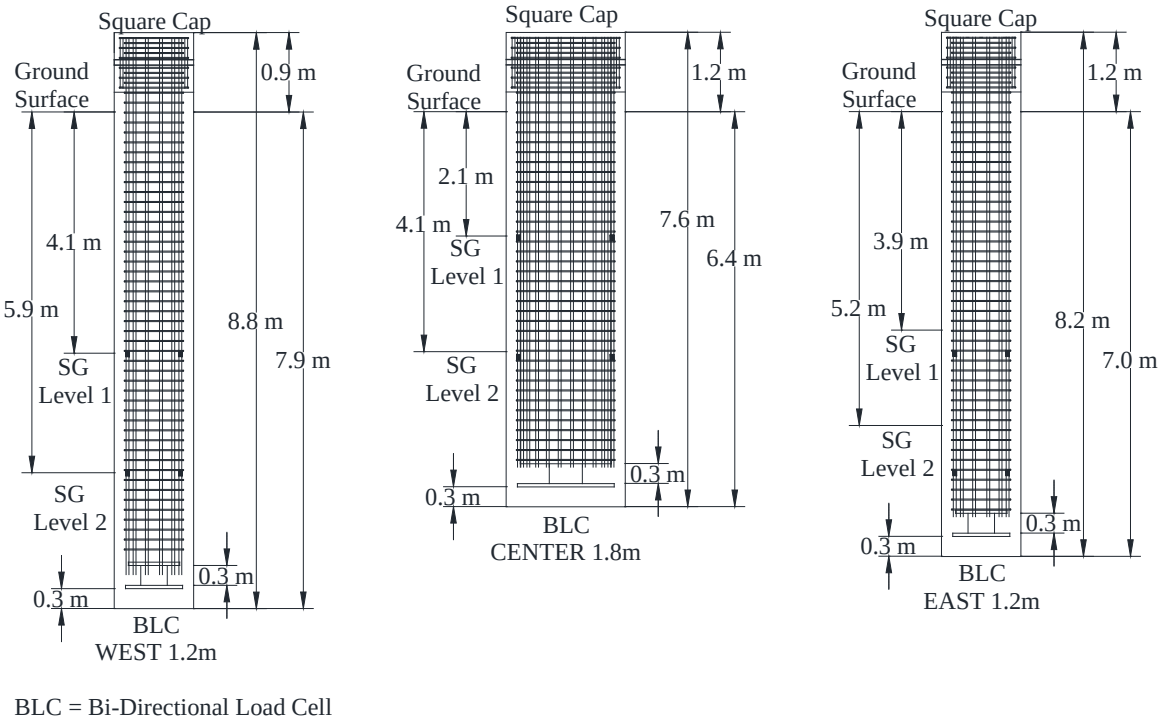

Figure 5.6. As-built schematics for a) West 1.2m, b) Center 1.8m, and c) East 1.2m DSF at the SSATS.

5.6.4. Full-Scale Load Testing

CSL testing was performed to determine the quality of concrete within the DSFs, particularly relating to the concrete placement technique. It was determined that the concrete placed within all three DSFs was of good quality (GEI Consultants 2014). Based on the results obtained from the full-scale load testing (utilizing a BLC), the movements of the top and bottom of the BLCs were calculated (Figure 5.7) for all of the DSFs. Furthermore, the strain gage and mobilized load transfer characteristics for the drilled shafts at SSATS are presented in Figure 5.8 and Figure 5.9, respectively. The measured unit side resistance and end bearing resistance, as functions of movement (upward for unit side resistance; downward for end bearing resistance), are presented in Figure 5.10 and Figure 5.11, respectively.

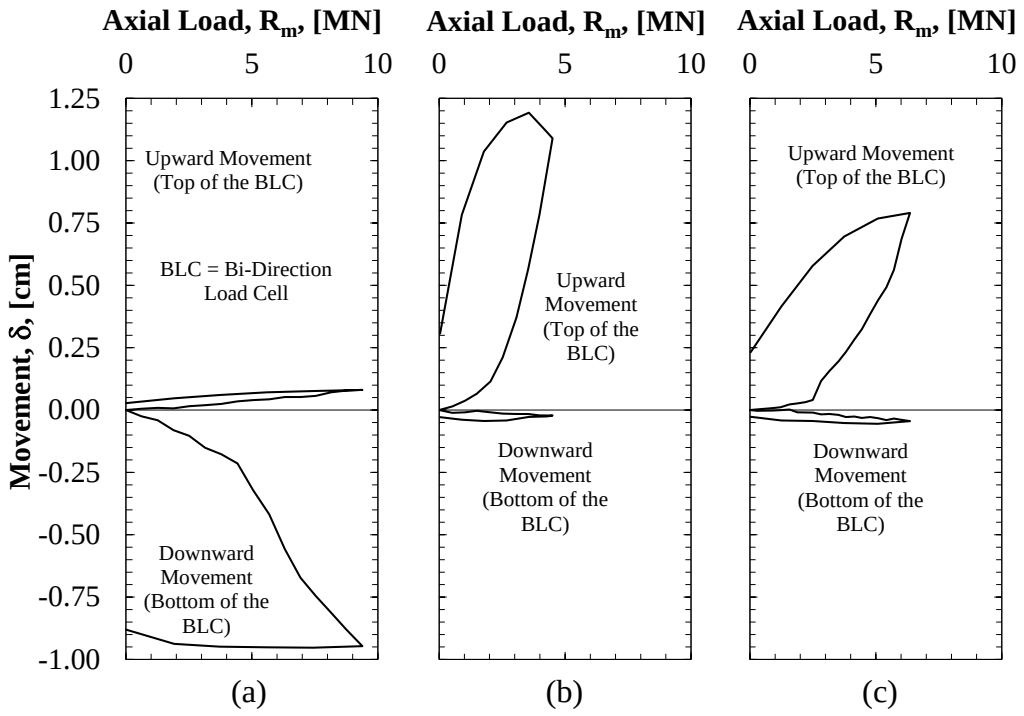

Figure 5.7. Upward and downward movement of the top and bottom of the bi-directional load cell from the full-scale load tests for the a) West 1.2m, b) Center 1.8m, and c) East 1.2m DSF at the SSATS.

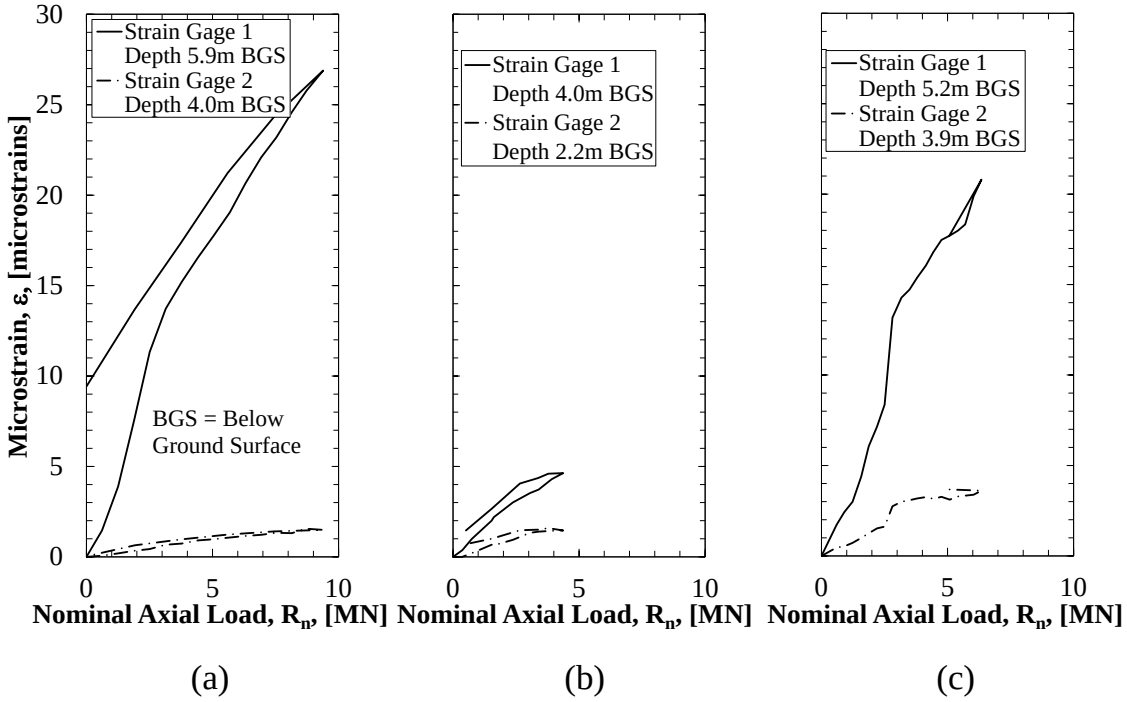

Figure 5.8. Strain gage readings during full-scale load testing for the a) West 1.2m, b) Center 1.8m, and c) East 1.2m DSF at the SSATS.

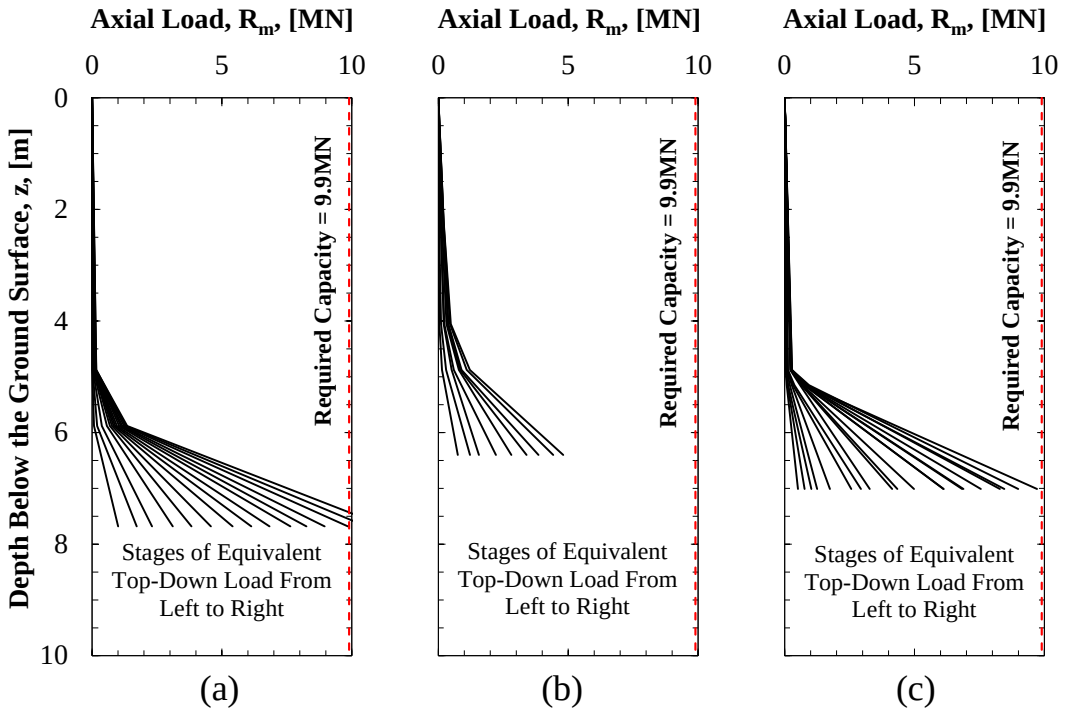

Figure 5.9. Measured load transfer behavior along the DSF as the equivalent top load was increased during the full-scale load tests for the a) West 1.2m, b) Center 1.8m, and c) East 1.2m DSF at the SSATS.

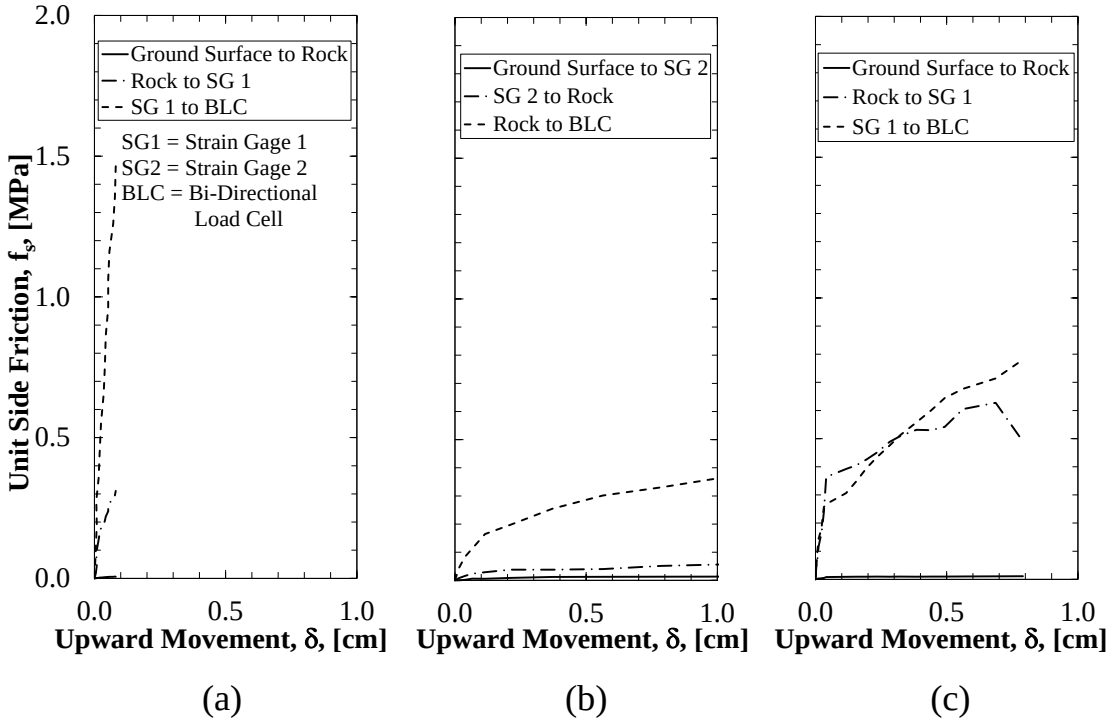

Figure 5.10. Measured unit side resistance for a) West 1.2m, b) Center 1.8m, and c) East 1.2m DSF at the SSATS.

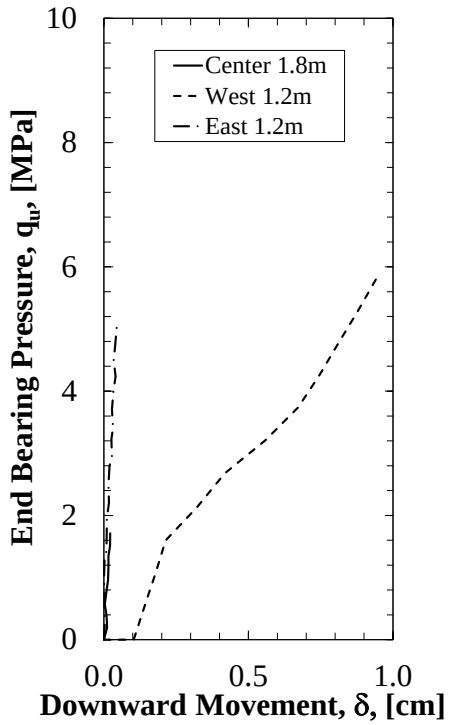

Figure 5.11. Measured end bearing resistance for a) West 1.2m, b) Center 1.8m, and c) East 1.2m DSF at the SSATS.

5.7. Results and Recommendations

5.7.1. Construction Methods

Possible reasons that exist for the difference in the measured downward movements include: 1) poor concrete placement below the load cell for the West 1.2m diameter DSF (possible entrapment of debris below the bottom of the base plate), 2) bad telltale contact between the retrofit telltale rod and bottom steel plate within the Center 1.8m and East 1.2m diameter DSFs, and/or 3) shorter than designed rock socket lengths for the Center 1.8m and East 1.2m diameter DSFs. As presented in Figure 5.7 for the West 1.2m diameter DSF, the downward movement is significantly larger than the downward movements obtained during the full-scale load testing conducted on the Center 1.8m and East 1.2m diameter DSFs. The concrete for the 1.8m diameter DSF was poured 2.5 days after the excavation was completed while the concrete for the 1.2m diameter DSFs was poured shortly after completion of the excavation. Similarly, the

shorter rock socket length for the Center 1.8m diameter DSF resulted in lower values of side resistance (hence larger upward movements) even though the rock socket surface area for the Center 1.8m diameter DSF was larger than the rock socket surface area for the East 1.2m diameter DSF. Consequently, consideration of construction methods, including the time dependent nature of the rock texture and the amount of time required to excavate, are important parameters of interest when determining the axial capacity and load-movement response for drilled shaft foundations.

The lessons learned from the installation of the drilled shaft foundations at the SSATS included: 1) verify that each piece of instrumentation is installed correctly, 2) excavate the rock socket to a depth that is deep enough to balance the side shear resistance and the BLC capacity (for bi-directional load testing purposes only), 3) utilize a large enough BLC to a) mobilize at least 2.5 times the unconfined compressive strength of the limestone or b) mobilize at least 0.1%D or 0.2%D of movement in both directions, 4) place the concrete into the excavation within a day of completing the rock socket excavation, and 5) ensure proper concrete placement (particularly below the BLC when conducting bi-directional load testing). With proper construction methods that encourage these five lessons, higher quality data will be obtained for full-scale load testing of DSFs in moderately strong to strong limestone. These lessons primarily deal with the acquisition of data from full-scale load tests, but the time to placement and the methods for concrete placement are important for any DSF installation.

5.7.2. Small Movements

Like with the other aforementioned case histories, the three DSFs at SSATS did not reach the FHWA (Brown et al. 2010) failure criteria of a movement of five percent of the diameter (5%D) in the downward direction. In moderately strong to strong limestone, the movements will

be dependent upon the side resistance above the BLC and the size of the BLC. As presented in Table 5.5, the values obtained from the FB-Deep software program, using the AHTD soil/rock sampling methods are the most similar to the values of the measured load-movement response at the final values of measured equivalent movement (0.11cm, 0.03cm, and 0.07cm for the West 1.2m, Center 1.8m, and East 1.2m diameter DSFs, respectively). The comparison of the measured and predicted equivalent top-down load-movement response is presented in Figure 5.12. The three closest predictive methods include FB-Deep using AHTD sampling method, Coyle and Reese (1966) rock only method, and the FHWA/Brown et al. (2010) method. To accurately design DSFs in moderately strong to strong limestone, design methodologies should be modified to predicted capacity at low movements (0.1%D or 0.2%D). The downward movement of the DSFs at the SSATS during full-scale load testing was less than 0.1% of the diameter. Except within weathered limestone, the minimal upward and downward movements were less than the movement required to develop the ultimate unit side resistance or end bearing resistance, respectively. Therefore, it is recommended that the design methodologies incorporate the behavior of DSFs at small movements for DSFs constructed in moderately strong to strong rock formations. Full-scale load testing can be problematic using top-down load tests or bi-directional load tests in moderately strong to strong limestone due to the large required loads and the balance of loads resulting in rock socket lengths that are much larger than will be required for production DSFs. If the stratigraphy changes (weathered versus competent rock) the observed behavior for the test DSF may not represent that of the production DSFs.

Table 5.5. Load values corresponding to final top-down equivalent movement for the DSF at the SSATS.

Type	Method		Top-Down Equivalent Resistance (MN) West 1.2m	Center 1.8m	East 1.2m
Final Top-Down Equivalent Movement (cm)			0.11	0.03	0.07
Percent of Diameter Movement (%)			0.09	0.02	0.06
Measured	Bi-Directional Load Test		11.0	4.3	9.4
Predicted	SHAFT (2012)	AHTD	1.4	0.3	0.5
		UofA	4.7	2.4	3.1
	FB-Deep (2012)	AHTD	15.6	3.2	5.5
		UofA	59.5	45.1	47.9
	Coyle and Reese (1966)	Rock	16.6	9.9	11.5
		Rock and Soil	6.0	4.9	4.0
		Rock (Limits)	9.2	5.7	6.0
		Rock and Soil (Limits)	4.9	3.8	5.7
	Brown et al. (2010)		22.0	13.3	17.7

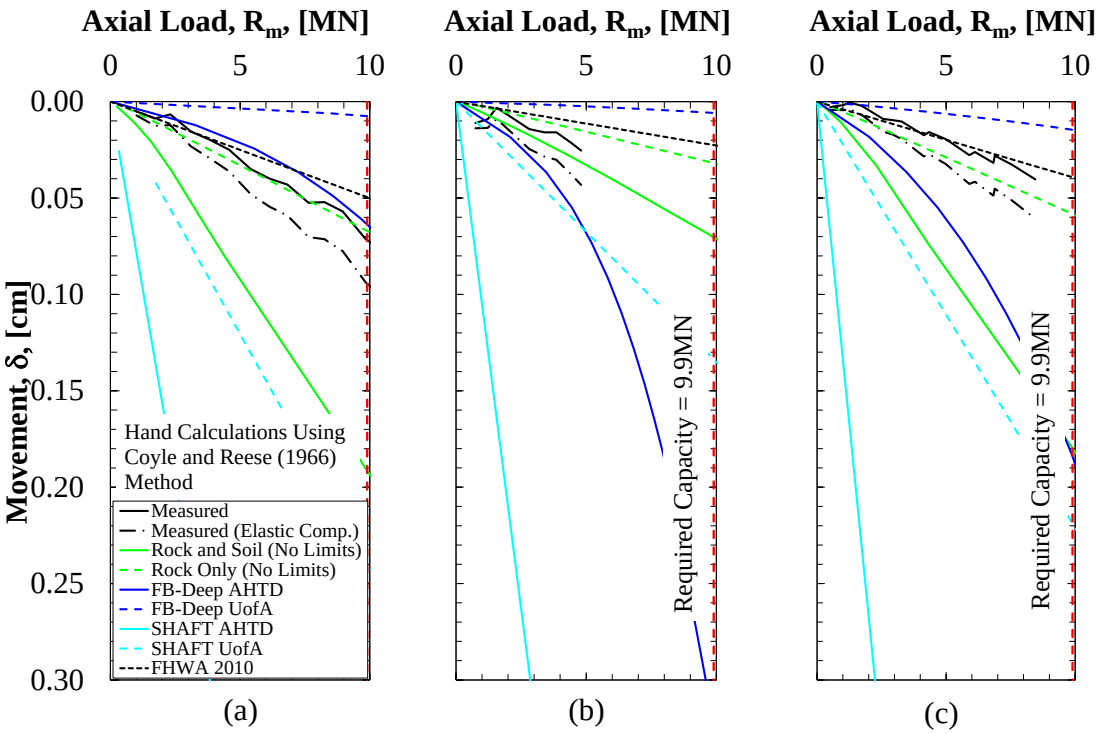

Figure 5.12. Top-down equivalent load-movement curves for the a) South 1.2m, b) Center 1.8m, and c) North 1.2m DSF at the SSATS.

The C value, as determined using Equation 5., the measured unit side resistance values, and the unconfined compressive strength of the rock, was 0.43 in competent, moderately strong to strong limestone. This C value is consistent with the C value determined for moderately strong to strong limestone in Brown (2009) and Axtell and Brown (2011). In weathered moderately strong to strong limestone, the C value ranged from 0.11 to 0.17. The C value for the weathered moderately strong to strong limestone is likely underestimated because the intact rock sample utilized for the unconfined compressive strength is not a representative sample for the in-situ rock strength. The visual differences in the competent and weathered moderately strong to strong limestone are presented in Figure 5.13.

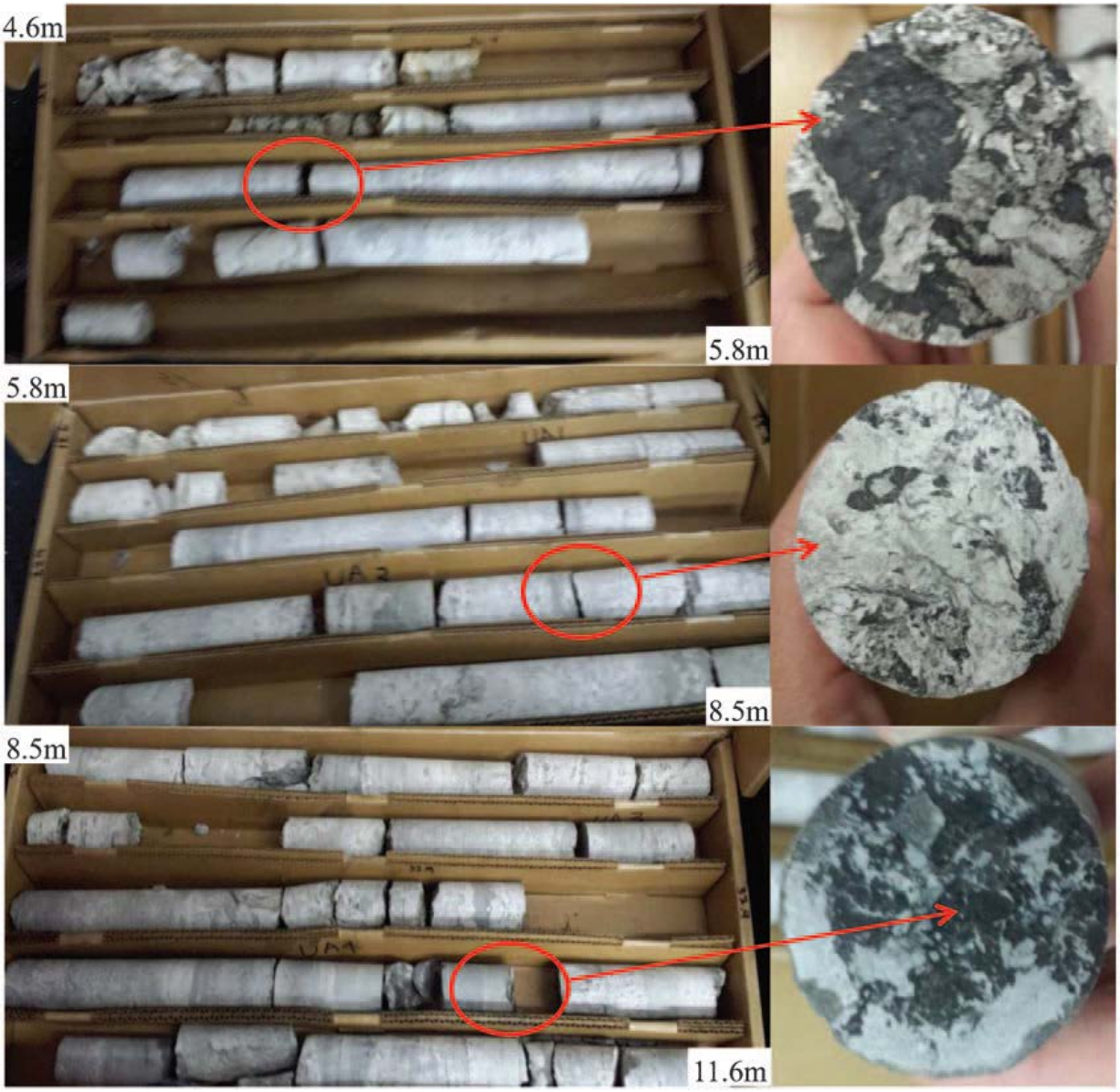

Figure 5.13. Photographs of rock cores obtained from SSATS [modified from Bey (2014)].

5.7.3. Side Resistance

The mobilized unit side resistance (within the rock), as determined for each drilled shaft foundation, varied from 0.4MPa to 1.5MPa. The unit side resistance curves for the Center 1.8m and East 1.2m diameter DSFs were comparable. Although weathering was only slightly indicated by the RQD results that were obtained during the geotechnical investigation (as previously presented in Figure 5.5), a 1.5m thick layer of weathered limestone was present at the SSATS.

This determination stemmed from the measured unit side resistance values for the Center 1.8m and East 1.2m diameter DSFs (short rock socket lengths) being significantly less than the measured resistance for the West 1.2m diameter DSF (long rock socket length). Furthermore, the unit side resistance value for the West 1.2m diameter DSF was a combined value for the weathered limestone and the competent, moderately strong to strong limestone. The normalized unit side resistance values for the rock socket (unit side resistance/rock socket length) were 0.5MPa/m, 0.2MPa/m, and 0.4MPa/m for the West 1.2m, Center 1.8m, and East 1.2m diameter DSFs, respectively. Based on these values, the strength of the weathered rock dominated the side resistance capacity of the Center 1.8m diameter DSF. The measured unit side resistance of 1.5MPa in the rock for the West 1.2m diameter DSF (at 0.1%D) exceeded the predicted unit side resistance value of 1.0Mpa (at 5%D) that was obtained using SHAFT.

T-z responses were developed for the weathered limestone and for the moderately strong to strong limestone. In general, the t-z response within the weathered limestone may be modeled using the procedures presented in McVay and Niraula (2004), as shown in Figure 5.14a. The t-z response within the moderately strong to strong limestone (Figure 5.14b) may also be modeled using McVay and Niraula (2004); however, there was not enough measured movement to characterize the full t-z response within moderately strong to strong limestone at the SSATS. The initial response is linear, but the movement required to exceed this linear response is unknown (predicted between 0.1cm < δ < 0.2cm for this case). In many cases, the movement of the DSF in moderately strong to strong limestone will not exceed 1%D (1.2cm for 1.2m diameter DSFs or 1.8cm for 1.8m diameter DSFs); therefore, a t-z response model for small movements is sufficient within the moderately strong to strong limestone. A ratio of 0.3 for the unit side resistance (f_s) to maximum unit side resistance (f_{smax}), as determined using the prediction

methods presented in Brown et al. (2010), is recommended for movements up to 0.1%D or for movements less than 0.2cm. A recommended q-z response is not presented herein because of the small downward movements (< 0.1cm) that were observed or the entrapped debris beneath the BLC.

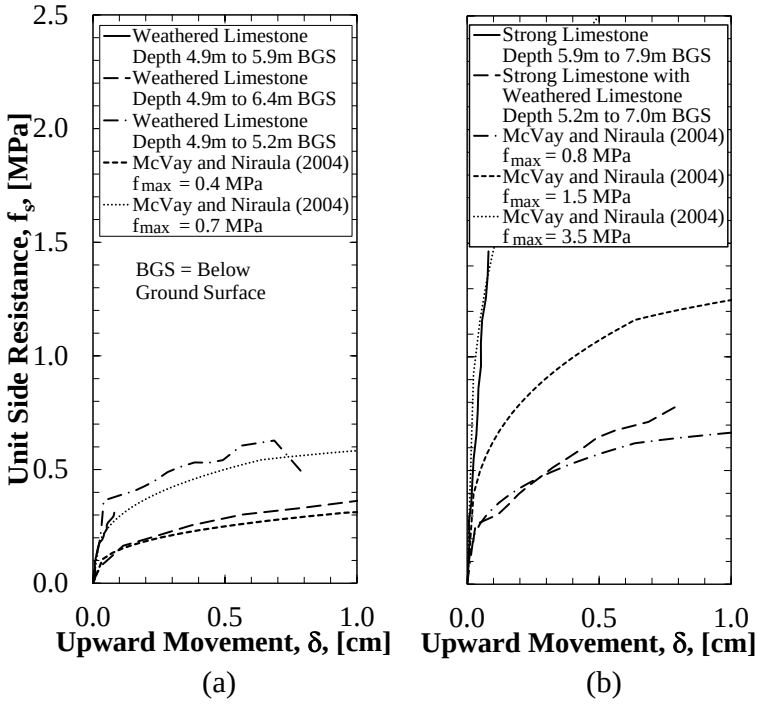

Figure 5.14. Determined t-z curves for a) weathered limestone and b) moderately strong to strong limestone at the SSATS.

5.7.4. End Bearing Resistance

The ultimate end bearing resistance for the limestone at the SSATS was not determined because 1) the capacity of the BLC was maximized or 2) there was insufficient side shear resistance to balance the end bearing resistance. Measured end bearing resistance values of 5.9, 5.0, and 1.7MPa were determined for all three of the DSFs based on the bi-directional load testing. At same downward displacement values, the end bearing resistance values measured for the West 1.2m diameter DSF were less than the end bearing resistance values measured for the Center 1.8m and East 1.2m diameter DSFs. However, the other DSFs at the SSATS (Center 1.8m

and East 1.2m diameter DSFs), there was not enough downward movement (due to the imbalance in upward and downward resistance forces) to determine accurate values of end bearing resistance. For the same amount of small movements, the end bearing resistance for the Center 1.8m diameter DSF was smaller than the end bearing resistance for the East 1.2m diameter DSF. The difference in the end bearing resistance further supports the finding of the influence of the weathered limestone layer. Because there was not enough side resistance to offset the end bearing resistance, it is recommended that the DSF, that will be tested using BLC(s), be embedded to a depth at which the side resistance is equal to the gross capacity of the BLC (to ensure that the balanced forces will maximize the BLC).

5.8. Conclusions

Three DSFs, with varying rock socket lengths, were constructed and tested at the SSATS within moderately strong to strong limestone. The field-change of shortening the length of two of the rock sockets was problematic because there was not enough side resistance to balance the end bearing resistance (causing larger upward movements than downward movements). When performing a full-scale load test utilizing BLC, an embedment length within rock of 3.0m or 2.5 times the diameter is recommended to balance the upward and downward loads to overcome the low values of side resistance for DSFs with short rock socket lengths.

The mobilized unit side resistance values, within the rock, were less for short rock socket lengths than for long rock socket lengths due to the presence of weathered limestone layer (1.5m thick), located at the soil/rock interface at the SSATS. The mobilized end bearing resistance was significantly less than the predicted end bearing resistance; however, the ultimate end bearing pressure was not measured due to the small amounts of movements for the end of the respective DSFs. The lag in time between the completion of the excavation and the beginning of concrete

placement may diminish axial capacity, as observed at the SSATS, because small particles may settle to the bottom of the hole and/or lubricate the side wall of the limestone excavation.

The t-z response for weathered limestone can be modeled using the procedures in McVay and Niraula (2004). However, the full t-z responses, for moderately strong to strong limestone, were not modeled for the SSATS because of the small amounts of measured movements; a ratio of 0.3 for the unit side resistance to the maximum unit side resistance for movements less than 0.2 cm or 0.1%D is suggested. Finally, for DSF in moderately strong to strong limestone, it is recommended to modify the design methodologies to include only behavior at small movements (0.1%D). This is recommended to more effectively design DSFs in moderately strong to strong limestone because the load generated from full-scale load tests will not be enough to reach 4%D-5%D movement (unless the strong rock beneath the DSF fails).

5.9. Acknowledgements

The authors thank the Arkansas State Highway and Transportation Department, the Missouri Department of Transportation, ADSC – the International Association of Foundation Drilling, GCC Midcontinent Concrete Company, Aldridge Construction, GEI Consultants, Inc., Foundation Technologies, Inc., and Loadtest, Inc., for financial and/or in kind contributions. The authors also thank the reviewers of the article at the DFI Journal for providing constructive comments that improved the quality of the manuscript.

5.10. References

Axtell, P.J. and Brown, D.A. (2011). “Case History – Foundations for the New Mississippi River Bridge – St. Louis.” Deep Foundations Institute, DFI Journal, Vol. 5, No. 2, pp. 3-15.

Bey, S.M. (2014). “Cost-benefit Analyses for Load Resistance Factor Design (LRFD) of Drilled Shafts in Arkansas.” MS thesis, University of Arkansas, Fayetteville, AR, USA, 410 pgs.

Brown, D.A. (2009). “Load Testing of Drilled Shaft Foundations in Limestone.” Nashville, TN. Report for ADSC Southeast Chapter, Feb. 2009, 103pgs.

Brown, D., Turner, J., and Castelli, R. (2010). “Drilled Shafts: Construction Procedures and LRFD Methods.” FHWA Publication No. NHI-10-016, Federal Highway Administration, Washington, DC, 970 pgs.

Coyle, H.M. and Reese, L.C. (1966). “Load Transfer for Axially Loaded Piles in Clay.” Journal of Soil Mechanics and Foundation Division, Vol. 93, No. 8, pp. 261-278.

FB-Deep (2012). Bridge Software Institute, Gainesville, Florida, Version 2.04.

GEI Consultants (2014). “Integrity Testing of Drilled Foundation Shafts Siloam Springs, Arkansas.” Report for TRC-1204, March 2014, 21 pgs.

Google Earth (2012). Version 6.1.0.

Gunnink, B. and Kiehne, C. (2002). “Capacity of Drilled Shafts in Burlington Limestone.” Journal of Geotechnical and Geoenvironmental Engineering, Vol. 128, No. 7, pp. 539-545.

McVay, M.C. and Niraula, L. (2004). “Development of P-Y Curves for Large Diameter Piles/Drilled Shafts in Limestone for FBPIER.” Florida Department of Transportation Report No. 4910-4504-878-12, 158 pgs.

Schubel, A. (2013). Personal Communication, November 14, 2013.

SHAFT (2012). ENSOFT, INC. Austin, Texas, Version 2012.

CHAPTER 6: DSF at the TATS

6.1. Chapter Overview

Three DSF were constructed at the Turrell Arkansas Test Site (TATS) designated as the North 1.2m, Center 1.8m, and South 1.2m DSF. The site stratigraphy consisted of 6.1m of clay, 3.0m of liquefiable silty sand underlain by at least 21.3m of liquefiable medium dense to dense sand. The slurry level within the North 1.2m DSF dropped overnight, during the night of December 18, 2015, causing a collapse within the silty sand layer which is described in the subsequent pages. The BLC test results from the Center 1.8m DSF are presented in Section 6.2. The difference in the measured unit side resistance of the collapsed DSF (North 1.2m), particularly in relation to the uncollapsed DSF (South 1.2m), and to the predicted value of resistance is discussed herein. The measured unit end bearing resistance of the collapsed DSF was remediated by drilling an additional 0.3m below the bottom of the DSF. The collapse within the excavation of the DSF, in this case, was modelled in FB-Deep and SHAFT by 1) a total unit weight reduction in the silty sand layer and 2) an increased length of the silty sand layer by 1.5m below the original depth. Additionally, the BLC test results from the Center 1.8m DSF are discussed in relation to the measured results from the South 1.2m DSF. The measured unit side resistance and unit end bearing resistance are compared to determine the scaling effects for a 1.2m to a 1.8m DSF.

This paper enclosed within this chapter has been accepted for publication within the Deep Foundations Institute Journal. The full reference for the paper is: Race, M.L. and Coffman, R.A. (2015). “Response of a Drilled Shaft Foundation Constructed in a Redrilled Shaft Excavation Following Collapse.” DFI Journal, DOI: 10.1179/1937525515Y.0000000003.

6.2. Additional Results

The construction of the Center 1.8m DSF was completed during December 2013. The primary construction problem for the Center 1.8m DSF was the welds connecting bottom of the BLC to the bottom rebar cage broke when the cage was being lifted to be placed into the excavation. Further information on the construction and testing procedures occurring on the DSF at the TATS was presented in Bey (2014). The measured upward and downward movement, load transfer, creep, top-down equivalent load-movement curve, unit side resistance, and unit end bearing resistance for the Center 1.8m DSF from the BLC test are presented in Figure 6.1.

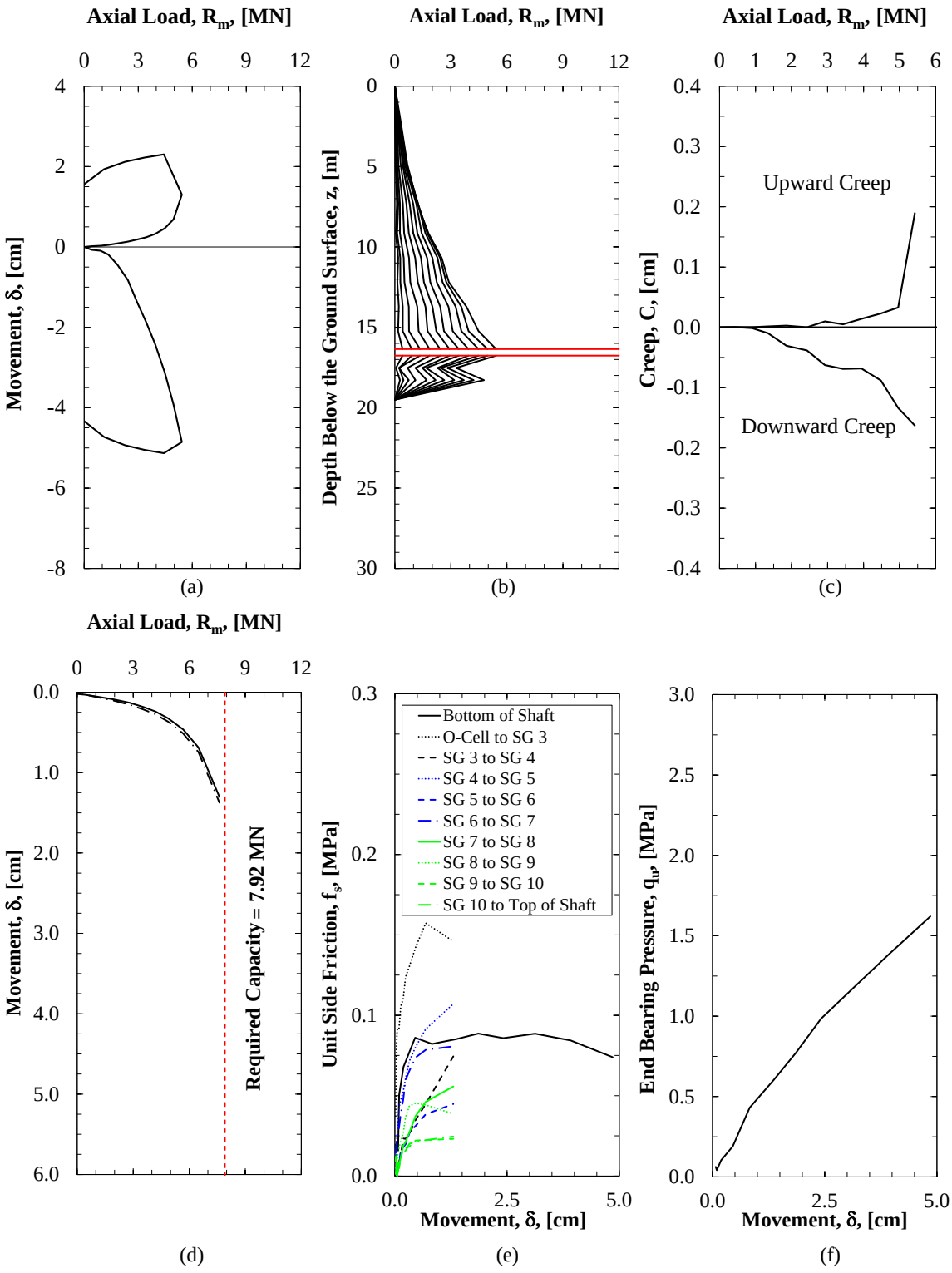

Figure 6.1. Measured BLC test results of a) upward and downward movement, b) load transfer, c) upward and downward creep, d) equivalent top-down load-movement curve, e) unit side resistance curves, and f) unit end bearing curve for the Center 1.8m DSF.

The scaling effects of DSF have typically only been considered in rock to predict the unit end bearing resistance from a measured unit end bearing resistance of a smaller DSF. The scaling factor for a 1.2m DSF to a 1.8m DSF, based on Figure 17-7 presented in Brown et al. (2010), is 0.8 for the unit side resistance in rock. While the ultimate unit end bearing resistance was not measured, the ratio of the measured unit end bearing resistance for the Center 1.8m DSF to the South 1.2m DSF was 1.68 (Figure 6.2) at the maximum amount of movement for the South 1.2m diameter DSF. Similarly, a comparison of the measured unit side resistance in clayey, silty, and sandy soil is presented in Figure 6.3. Moreover, the numerical unit side resistance and the scaling factor ratio for the Center 1.8m and the South 1.2m DSF is presented in Table 6.1. The average scaling factor ratio for the unit side resistance is 1.0 compared to the value of 0.8 that is recommended for rock.

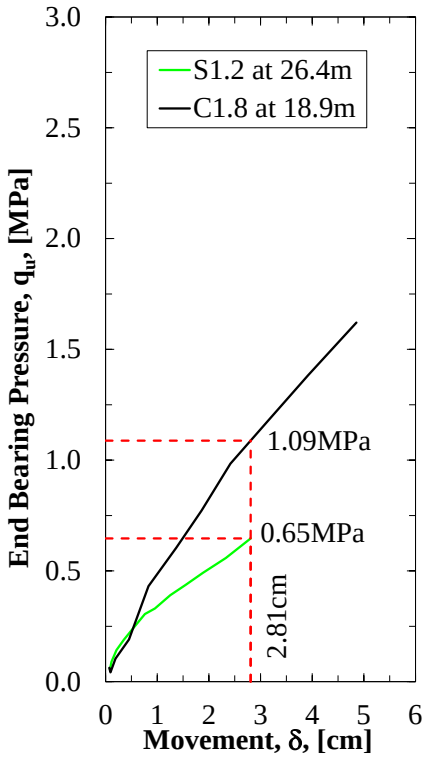

Figure 6.2. Comparison of the measured unit end bearing resistance for the South 1.2m and Center 1.8m DSF at the TATS.

Table 6.1. Measured unit side resistance comparison and the scaling factor for the South 1.2m and Center 1.8m DSF at the TATS.

Depth [m]	Soil Type	Unit Side Resistance, f_s, [MPa]		Scaling Ratio
		South 1.2m DSF	Center 1.8m DSF	
0.0 to 2.4	Clay	0.016	0.023	1.44
2.4 to 4.9	Clay	0.032	0.023	0.72
4.9 to 7.3	Clay	0.049	0.041	0.84
7.3 to 9.1	Silt	0.046	0.053	1.15
10.7 to 12.2	Sand	0.072	0.043	0.60
12.2 to 13.7	Sand	0.104	0.102	0.98
15.2 to 16.5	Sand	0.173	0.150	0.87
16.8 to 18.3	Sand	0.056	0.084	1.50

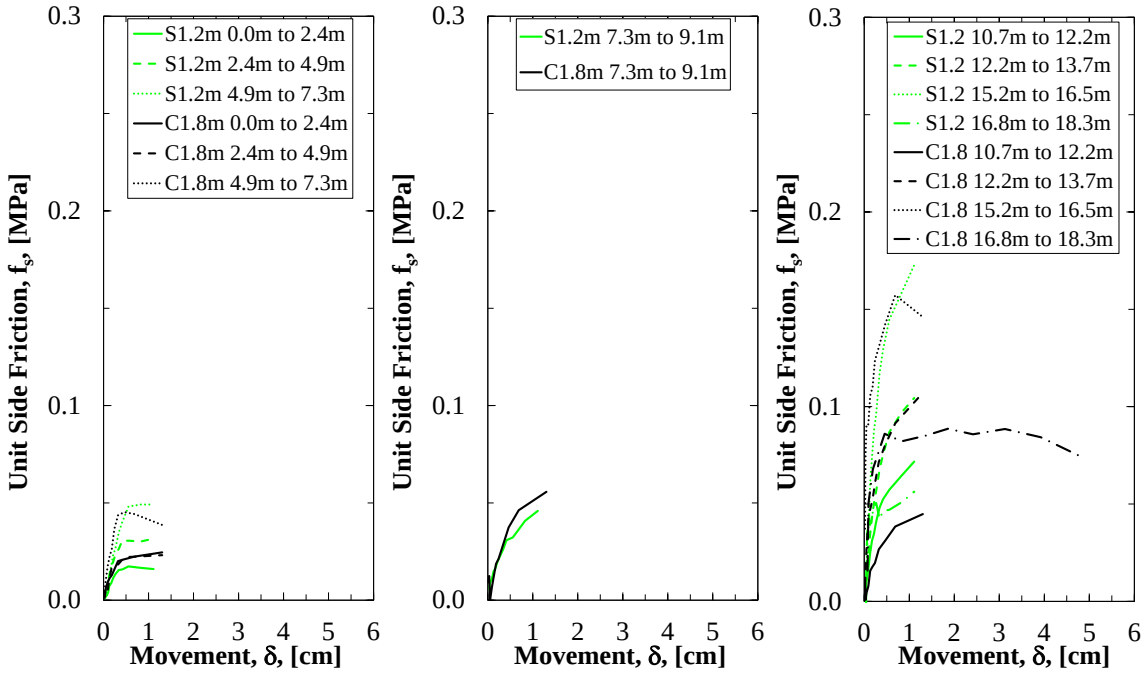

(a) (b) (c)

Figure 6.3. Comparison of the measured unit side resistance values for the South 1.2m and Center 1.8m DSF at the TATS in a) clayey soil, b) silty soil, and c) sandy soil.

Lateral load predictions were obtained from the LPILE (2012) software program. Based on the as-built dimensions of the DSF at the TATS, the predicted top movement for the lateral load was 0.411cm, 0.094cm, and 0.410cm for the North 1.2m, Center 1.8m, and South 1.2m DSF, respectively (as presented in Figure 6.4). Based on the required design load for the DSF constructed at the TATS (Table 6.2), the p-y curves for all three of the soil sampling and testing

methods are presented in Appendix C in Figure C.9 based on the required design load for the DSF at the TATS.

Table 6.2. Lateral loading requirements for the DSF at the TATS as provided by AHTD.

Loading Type	Amount of Load		
	Axial	**Longitudinal**	**Transverse**
Force (MN)	2.202	0.211	0.070
Moment (MN*m)	N/A	1.974	0.335

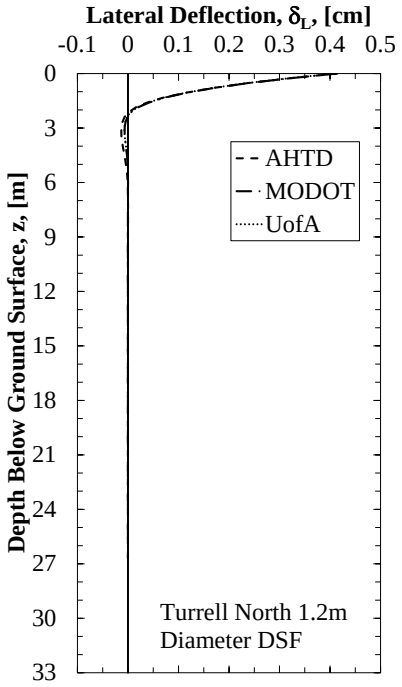

Figure 6.4. Lateral deflection of the North 1.2m diameter DSF at the TATS as predicted utilizing LPILE (2012) and the obtained geotechnical investigation data.

Response of a Drilled Shaft Foundation Constructed in a Redrilled Shaft Excavation Following Collapse

Morgan L. Race, SM.ASCE, EIT[1]
Richard A. Coffman, M.ASCE., PhD, PE, PLS[2]

6.3. Abstract

Two drilled shaft foundations (DSF) of equal size (1.2m diameter) were installed at the Turrell Arkansas Test Site (TATS). The soil stratigraphy at the TATS consisted of 6.1m of clay underlain by 3.0m of silt underlain by sand. After drilling the excavation for the North 1.2m DSF, the silty soil collapsed from the sidewall of the excavation into the bottom of the excavation. Following the collapse, the excavation was redrilled and the construction of the DSF was completed.

The measured capacity, unit side resistance, and end bearing resistance of the South 1.2m diameter DSF were predicted by using software programs and mean values of soils data. The measured response of the North 1.2m diameter DSF was backward modeled to determine the appropriate strength and stress reduction. Based on the measured data for this site, a 10 percent reduction in unit weight within the silt layer and a modification of the soil properties within the top 3.0m of the sand layer produced predicted responses that matched the measured responses.

6.4. Introduction

The process of constructing drilled shaft foundations (DSF) involves: assembling the rebar cage, drilling the DSF excavation, inserting the rebar cage into the excavation, pouring the concrete, and curing the concrete. During each of these stages, multiple complications associated with drilling methods, cleanout procedures, and concrete pouring techniques may occur causing discrepancies between the predicted and measured behavior of the respective DSF. Moreover, complications resulting from a collapse of the excavation may comprise the DSF and lead to

actual values of unit side resistance or unit end bearing resistance being lower than the predicted values. Specifically, lower amounts of side resistance or end bearing resistance may be attributed to a decrease in the horizontal effective stress values or a decrease in the friction angle values that resulted from the collapse. The effects of problems encountered during construction may be mitigated by utilizing knowledge obtained from case histories where testing was conducted on full-scale DSF that were redrilled prior to construction due to excavation collapse. This knowledge is presented herein through the use of a literature review and a thorough discussion of a case history regarding two full-scale DSF constructed and tested at the TATS.

6.5. Literature Review

6.5.1. Construction Methods

Improper construction methods employed by contractors may compromise the quality of DSF. The stability of the excavation, the placement of concrete (i.e. workability of concrete and compatibility of the rebar and concrete), and the contamination of the soil (i.e. the bond between concrete and soil) are factors that may affect the axial capacity of DSF (Brown 2004). Furthermore, unbalanced fluid pressure (difference in pressure between the drilling fluid pressure and the hydrostatic groundwater pressure) within a DSF excavation may cause soil softening (stress relief), sidewall sloughing, reduced lateral stress, and may lead to the formation of large cavities around the temporary casing (Brown 2004). According to Brown (2004), in areas with potential caving ground conditions, full length segmental casing is effective at improving stability of the DSF excavation until and during concrete placement.

6.5.2. Case Studies

Previous studies that investigated the effects of construction practices, on the capacity of DSF, were performed (Brown 2002, Mullins and Ashmawy 2005) at the Auburn University

National Geotechnical Experimentation Site. The construction techniques that were examined included: the use of bentonite slurry, the use of polymer slurry (dry pellet form and liquid form), the use of temporary casing, free-fall placement of concrete within dry excavations, varied rebar spacing, different aggregate size within the concrete, and different values of concrete slump. Problems associated with construction techniques (i.e. soil inclusions) were also introduced into two of the DSF (Brown 2002). It was concluded that the measured capacity that was obtained by using the shafts constructed using bentonite slurry was lower than the measured capacity that was obtained from the other construction methods (except for soils with low hydraulic conductivity). The soil inclusions had no short term effect on the capacity of the DSF; however, structural failure was not an issue with the low stresses that were applied to the foundation during testing (Brown 2002). Instead, problems associated with concrete properties and slurry properties were identified (Mullins and Ashmawy 2005) as the primary causes for problems in DSF.

Eight case histories with poor construction techniques (i.e. inadequate bottom cleanout, failure to use drilling fluids, poor concrete placement, and improper drilling tools) were evaluated in Schmertmann et al. (1998). Specifically, bi-directional load cell (BLC) devices were utilized to detect the effects of poor construction techniques on the axial capacity of each DSF. As described in Schmertmann et al. (1998), larger values of downward displacement were observed, using BLC, as a result of poor cleanout procedures within DSF. Additionally, low unit side resistance values at large displacements (0.4MN of load at greater than 100mm of displacement as compared to 6.1MN of load at 6mm of displacement) were attributed to hydrostatic imbalance. The cases presented in Schmertmann et al. (1998) were dramatic

examples of poor construction techniques; however, the effects of the construction techniques on the movement-resistance behavior of the DSF were confirmed using full-scale BLC testing.

Base grouting of DSF is a common construction practice to increase the end bearing capacity for the DSF. Specifically, base grouting is cost effective in cohesionless soils and this method also provides increased reliability due to the resulting uplift testing provided by the base grouting process, even while neglecting the beneficial effects on the end bearing capacity (Dapp et al. 2006). As reported in Dapp et al. (2006), the upward displacement that resulted from base grouting being performed on a DSF, that was constructed in an excavation that was redrilled, was approximately 1.9cm of movement (far in excess of the average 0.25cm of movement observed for the other 75 DSF, and almost twice the amount of movement of the DSF with the next closest amount of movement [Figure 6.5]).

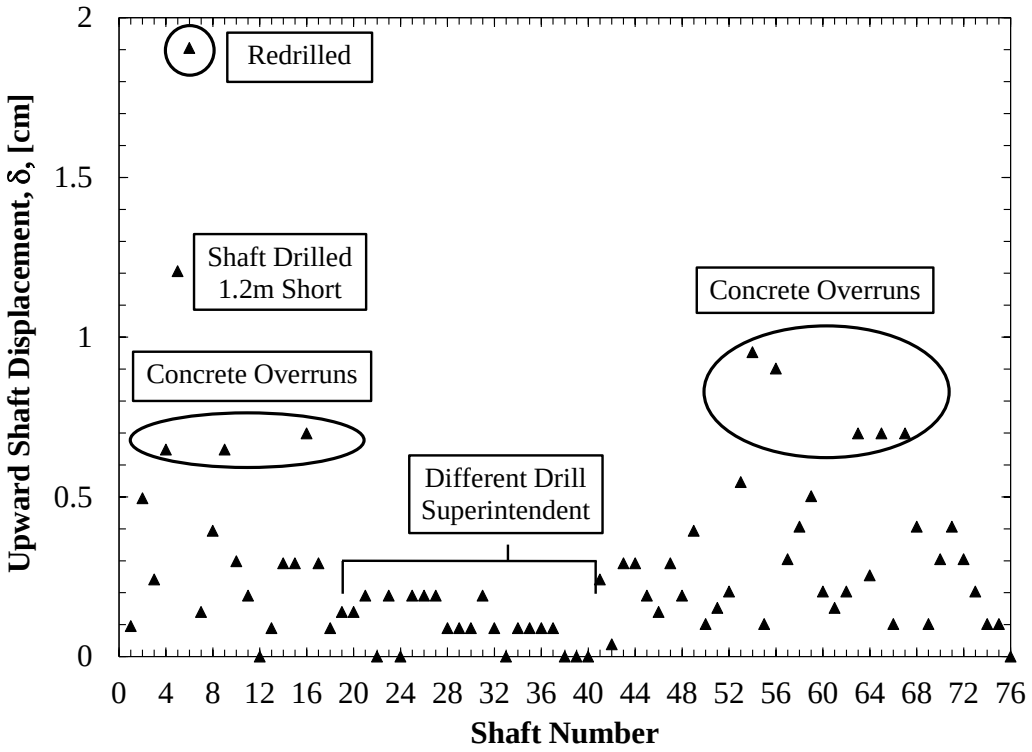

Figure 6.5. Upward displacement of DSF as a results of post-grouting (modified from Dapp et al. 2006).

6.6. Methods and Materials

6.6.1. Initial Axial Capacity-Depth and Movement-Resistance Predictions

Two software programs (FB-Deep [2012] and SHAFT [2012]) were utilized to predict 1) the axial capacity (axial resistance) as a function of depth and 2) the axial resistance as a function of movement, for a given foundation length. Specifically, the response of the DSF were predicted, using the computer programs, by utilizing the methods described in the Federal Highway Administration (FHWA) report FHWA-NHI-10-016 (Brown et al. 2010) and the American Association of State Highway and Transportation Officials (AASHTO) Load and Resistance Factor Design (LRFD) Bridge Design Specifications (AASHTO 2007). The different empirical methods that were utilized to predict the unit side resistance and end bearing resistance included, but were not limited to: Schmertmann (1967) and Bustamante and Gianeselli (1982) in FB-Deep and Meyerhof (1976), Quiros and Reese (1977), and O'Neill and Reese (1999) in SHAFT. The predicted movement-resistance curves were developed by using the normalized settlement curves that were presented in Reese and O'Neill (1988).

The soil parameters that were used to determine the axial capacity and movement-resistance were determined from three different geotechnical investigation techniques. These techniques included: 1) the Arkansas State Highway and Transportation Department (AHTD) technique of conducting standard penetration tests using a standard (30mm diameter) split spoon sampler in all soil deposits, 2) the Missouri Department of Transportation MODOT) technique of conducting cone penetration tests using a $10cm^2$ cone in all soil deposits, and 3) the University of Arkansas (UofA) technique of conducting unconsolidated undrained triaxial compression tests in cohesive soil deposits and standard penetration tests using a California split spoon sampler

(60mm diameter) in cohesionless soil deposits. The obtained soil parameters were previously presented in Race and Coffman (2013) and Race et al. (2013), and are presented in Figure 6.6.

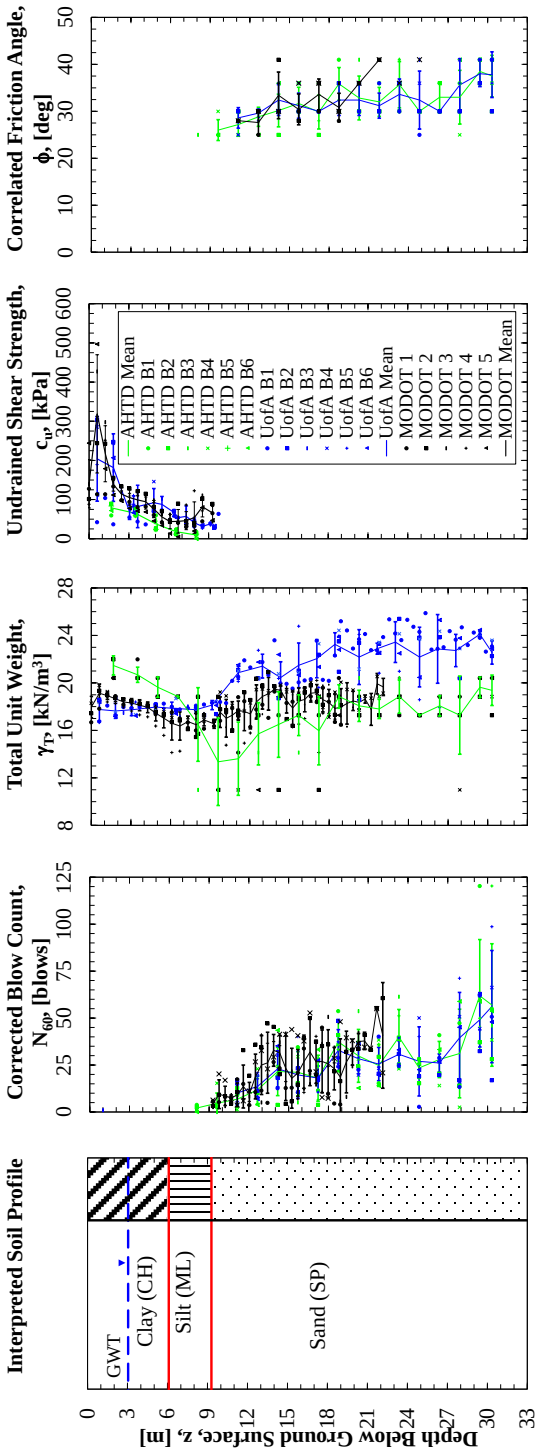

Figure 6.6. Soil properties, as determined by soil sampling and testing methods, at the TATS (modified from Race and Coffman 2013).

The average values of the aforementioned soil parameters were input into the software programs and the required depth below the ground surface (26.2m), as required to resist the design load (8.8MN), was obtained by using the UofA obtained soil parameters within the FB-Deep program. As presented in Table 6.3, the correlated or measured values of blow count or friction angle and the correlated or measured values of unit weight were input into the software programs to determine the axial capacity and the movement-resistance response. In SHAFT, "clay" was used to model the silty layer because an option for "silt" was unavailable (the soil options were limited to clay and sand), whereas the "silt" option was utilized in FB-Deep for the silt layer. The software programs were then utilized to compute: 1) the required length of the DSF to resist the required axial load, at a prescribed amount of movement (6.0cm as equal to five percent of the diameter of the DSF [5%D]), 2) the amount of resistance of the DSF as a function of increased movement, for the prescribed required length (26.2m), 3) the amount of unit side resistance of the DSF, within the given soil types and for the prescribed required length (26.2m), and 4) the amount of end bearing resistance for the prescribed required length (26.2m).

Table 6.3. Input parameters for the different software programs.

FB-Deep

	Clay/Slit		Sand	
AHTD	Correlated c_u[1]	Correlated γ_T[1]	Measured N[5]	Correlated γ_T[1]
MODOT	Correlated c_u[2]	Correlated γ_T[2]	Correlated N[2]	Correlated γ_T[2]
UofA	Measured c_u[3]	Measured γ_T[4]	Measured N[5]	Measured γ_T[4]

SHAFT

	Clay/Silt		Sand	
AHTD	Correlated c_u[1]	Correlated γ_T[1]	Measured N[5] or Correlated ϕ[1]	Correlated γ_T[1]
MODOT	Correlated c_u[2]	Correlated γ_T[2]	Correlated N[2] or Correlated ϕ[2,1]	Correlated γ_T[2]
UofA	Measured c_u[3]	Measured γ_T[4]	Measured N[5] or Correlated ϕ[1]	Measured γ_T[4]

[1] Correlated from blow count values using Vanikar (1986).
[2] Correlated from cone tip resistance, friction ratio, and soil index type using Robertson and Cabal (2012).
[3] Measured by unconsolidated undrained triaxial tests.
[4] Measured weight of the soil sample divided by measured volume of the soil sample.
[5] Measured during standard penetration tests.

Although the data obtained from the three geotechnical investigation methodologies were compared using both software programs for the resistance-depth and resistance-movement responses, the data obtained from the three geotechnical investigation methodologies were only compared using the FB-Deep software program for determination of the movement-unit side resistance and movement-end bearing resistance responses. The reason for only utilizing the FB-Deep software program was because it was the only program that enabled determination of unit side resistance and end bearing resistance at various levels of movement; the SHAFT program only enabled determination of the maximum values of unit side resistance and end bearing resistance.

6.6.2. Drilled Shaft Foundation Construction

Two 1.2m diameter DSF were installed at the TATS during the winter of 2013 (November and December). Each of the DSF was instrumented with ten sets of strain gauges (Geokon Model 4200), a 33cm diameter BLC, four CSL pipes (5.08cm inside diameter black iron pipe), and five telltale pipes (1.27cm inside diameter black iron pipe). Two sets of strain gauges were located within the clay layer, one set of strain gauges was located within the silt layer, and seven sets of strain gauges were located within the sand layer.

The excavation for the South 1.2m diameter DSF was initially drilled on November 18, 2013. On November 22, 2013, the pin used to connect the drilling bucket to the drilling rig sheared, while lowering the bucket into the excavation, causing the bucket to drop to a depth of 24.4m below the ground surface. The bucket was retrieved the following day; however, during the following week the drilling rig overturned due to difficult conditions (ice on the drill mats). Therefore, the hole for the South 1.2m diameter DSF was not extended to a final depth of 26.2m until December 2, 2013. The concrete for the South 1.2m diameter DSF was poured on December 3, 2013 after the excavation had been maintained open (to a depth of 24.4m, utilizing polymer slurry) for 15 days and subjected to the temperature conditions that are presented in Figure 6.7.

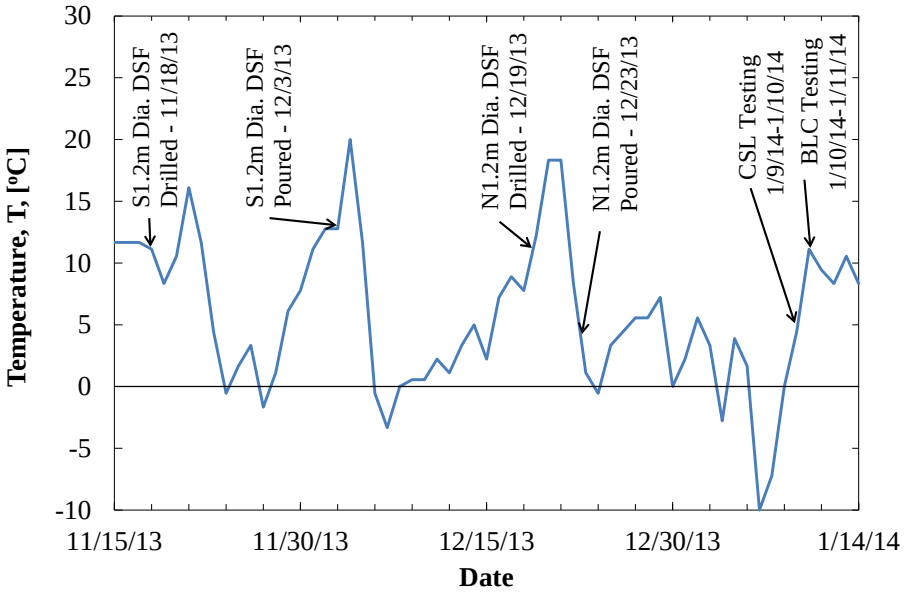

Figure 6.7. Average daily temperature at the TATS during construction and testing of the DSF.

The excavation for the North 1.2m diameter DSF was completed to a depth of 24.4m on December 17, 2013 and extended to the required final depth of 26.2m on December 18, 2013. While extending the hole from 24.4m to 26.2m, water began to be lost from the excavation. Although the water level within the excavation was maintained at the bottom of the temporary casing (7.0m below the ground surface), the amount of water/slurry that was pumped into the excavation to maintain that water level elevation was greater than the available capacity of slurry/water within the two storage tanks. To calibrate and utilize the sonic borehole diameter measurement tool, the water level within the excavation was required to be above the bottom of the temporary casing; therefore, water was added to the excavation from a nearby surface water pond without adding polymer to the water. This addition of supplementary surface water further exacerbated the rate of loss out of the excavation because it led to 1) an increase in the total head within the excavation and 2) a decrease in the viscosity of the slurry within the excavation.

After completion of the sonic borehole diameter testing, no water was added to the excavation and the bottom of the 27.4m long rebar cage was lowered approximately 15.2m into

the excavation to remain in that position overnight. On the morning of December 19, 2013, it was observed that the 3.0m thick silt layer that was located directly below the bottom of the temporary casing, and located between the stiff desiccated clay layer (above) and dense to very dense sand (below), had collapsed during the night, resulting in confinement of the bottom portion (bottom 9.1m) of the rebar cage (Figure 6.8). After removal of the rebar cage, and during the initiation of the redrilling process, the top of the 7.0m long temporary casing sunk approximately 2.0m into the excavation Therefore, to complete the North 1.2m diameter DSF by overdrilling to a depth of 26.5m, the 7.0m long temporary casing was removed from the excavation and a 12.2m long temporary casing was placed into the excavation to stabilize the collapsed silty soil. The geometries of the South and North 1.2m diameter DSF are presented in Table 6.4. The idealized volume of collapse (19.9m^3 that was identified as the volume of the excavation that filled in with soil) and the approximated volume of the collapse (3.8m^3 that was estimated using the amount of excess volume of concrete placed into the excavation, as compared to the South 1.2m diameter DSF) are presented in Table 6.4. The discrepancy between the idealized volume of collapse and the approximated volume of collapse was believed to be associated with 1) soil arching around the rebar cage, 2) the rebar cage taking up some of the displaced volume, 3) the temporary casing retaining the collapsing silty soil while the concrete was being poured and 4) a high total head (approximately 10m) within the concrete as the casing was removed from the soil profile. The concrete for the North 1.2m diameter DSF was poured, without further incident, on December 23, 2013.

Table 6.4. Geometry of the 1.2m diameter DSF at the TATS.

Shaft Designation	Dia. [m]	Depth [m]	Surface Area [m^2]		Neat Volume of Concrete Required [m^3]	Approximate Volume of Concrete Used [m^3]
			Clay/Silt	Sand		
South 1.2m	1.2	26.21	35.02	65.38	33.4	48.2
North 1.2m	1.2	26.52	36.16	66.54	33.8	53.9

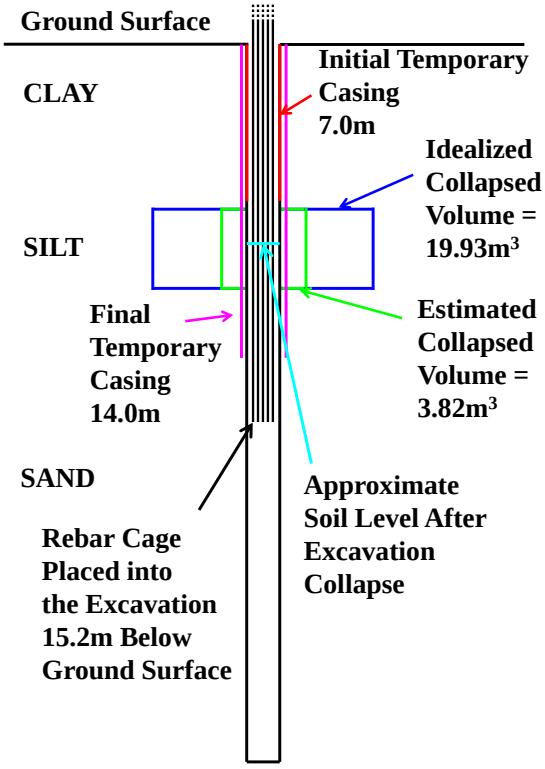

Figure 6.8. Schematic of the North 1.2m diameter DSF at the TATS (prior to and after the collapse).

6.6.3. After Collapse Axial Capacity-Depth and Movement-Resistance Predictions

The same software programs (FB-Deep and SHAFT) that were utilized to design the DSF, at the TATS, were also utilized to predict the amount of resistance, as a function of increased movement, of the DSF that was constructed within the redrilled excavation that had previously collapsed. Unlike the soil parameters that were input into the software programs for the initial predictions, the soil parameters that were input for the prediction of the DSF that was constructed within the previously collapsed excavation were modified to predict the effect of the collapse on the axial capacity and movement-resistance behavior. Assuming that the excavation collapse was the result of unbalanced fluid pressures, resulting in sidewall sloughing, the total unit weight within the silt layer was reduced to predict the capacity of the DSF that was

constructed within the collapsed excavation (Method 1). Because the collapsed excavation was not over reamed during redrilling but only over drilled (drilled to a deeper depth than originally designed but with the same diameter drill bit) it was assumed that the sidewalls below the silt layer were coated/lubricated by the silt that flowed into the bottom of the excavation (Method 2). Therefore, the silt properties (average unit weight and average undrained shear strength values of the silt from 6.1m to 9.1m) were utilized instead of the sand properties (below a depth of 9.1m) to resemble the decrease in the interface friction angle within the contaminated/smeared silt sidewall material, as compared with the interface friction angle within the native sand material. The final method (Method 3) was a combination of the stress reduction (Method 1) and strength reduction (Method 2) methods; albeit the strength was only reduced for the top 3m of the sand layer, for reasons discussed in the Results section.

The initial mean values of the soil properties and the soil properties associated with the three methods (corresponding to the three assumptions about how the soil behaved) are presented in Figure 6.9. Although the reduced total unit weight values that are shown in Figure 6.9 are presented as a 10 percent reduction (Method 1), a sensitivity analysis was also performed in which the total unit weight values were reduced by 10, 20, 30, or 40 percent to simulate the loss of horizontal stress at the location of the collapsed section of the DSF excavation.

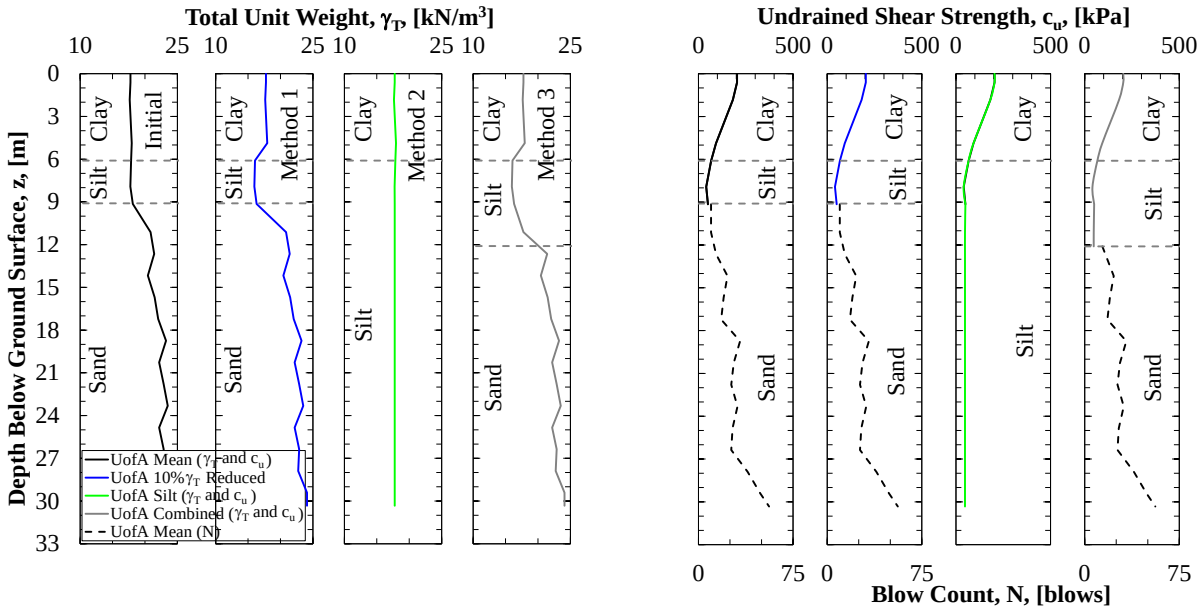

(a)

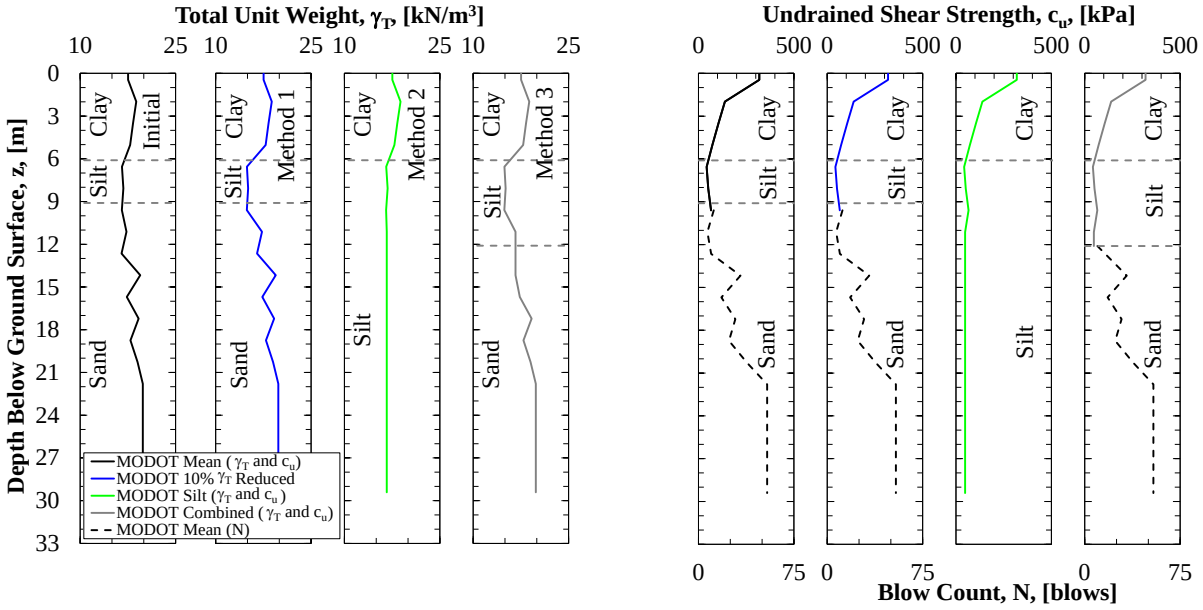

(b)

Figure 6.9. Modified soil properties (total unit weight and undrained shear strength) input into FB-Deep and SHAFT based on the a) UofA and b) MODOT geotechnical investigation techniques.

6.6.4. Full-Scale Testing

Concrete testing and sampling (unconfined compressive strength [f_c'] and modulus of elasticity [E], as determined using ASTM C39 [2013] and ASTM C469 [2013], respectively) was performed on 100 percent of the concrete trucks that provided concrete for the DSF. Crosshole sonic logging (CSL) testing was performed on the South 1.2m diameter DSF on January 9, 2014. Based on the CSL testing results, anomalies were present within the bottom 0.3m of the South 1.2m DSF. Therefore, it is likely that a small layer of sediment was trapped at the bottom of the South 1.2m DSF. However, the South 1.2m diameter DSF was considered sound and continuous based on the results obtained from the analysis of the CSL testing (GEI Consultants, Inc. 2014).

CSL testing was performed on the North 1.2m diameter DSF on January 10, 2014. Initially, frozen portions of the polymer slurry located within the North 1.2m DSF CSL pipes prevented CSL testing. However, the slurry was blown out using an air compressor, and then clean water was utilized within the CSL pipes to perform CSL testing to a depth of 19.2m. The complete length of the North 1.2m DSF was not tested because silt filled the CSL pipes below this depth in all but one of the CSL pipes. It was observed, at the time that the rebar cage was removed from the excavation following the excavation collapse, that all but one of the CSL pipes separated at the rubber coupling located at the BLC. Therefore, it is hypothesized that silt within the excavation filled the bottom portions of the CSL pipes when the rebar cage was removed. Although it was observed that the coupling had separated, no thought was given to the possibility that the bottom portions of the pipes were filled with silt. Therefore, this hypothesis was not developed until the time of CSL testing when the CSL probes could not pass below the level of the couplings in three of the four CSL pipes. Based on the CSL testing results, there are

possible segregation layers at depths of approximately 7.9m and 10.1m below the ground surface corresponding to the approximate depth of silt layer. However, it was concluded that the overall quality of the concrete was of good quality above the BLC (GEI Consultants, Inc. 2014).

Following completion of the CSL testing, full-scale BLC tests were performed in accordance with ASTM D1143 (2013) on the South 1.2m and North 1.2m diameter DSF on January 10 and 11, 2014, respectively. The required capacity of the BLC was not attainted for either of the DSF due to 1) problems with the air compressor at high pressures (South 1.2m) and 2) large downward movements (North 1.2m). Also, the strain gauges located immediately below the BLC were not located far enough away from the BLC (this strain gauge level was located less than the required one diameter away from the BLC); therefore, the measured strain values obtained from this level of gauges were considered unreliable. From the full-scale BLC tests, the upward and downward movements of the BLC, with respect to the applied load, and the strain gauge readings were recorded. The unit side resistance and end bearing resistance values, as well as other relevant movement-resistance data, as determined from the BLC tests, are discussed in the next section.

6.7. Results

The collapse of the sidewall of the North 1.2m diameter DSF, within the silt layer, was likely associated with rapid drawdown conditions. The water level after the time of collapse was approximately 3m below the bottom of the temporary casing (approximately 4m lower than at the time of sonic borehole testing). The combination of increasing the water level to perform the sonic borehole diameter test, the high permeability of the sand layer below the silt layer (especially the soil below a depth of 24.4m), and the low viscosity of the polymer slurry resulted

in the collapse of the silt layer (an idealized 19.9m^3 of soil moving within the excavation, from the top portion of the excavation to the bottom portion of the excavation).

As previously discussed, three assumptions were investigated to determine the effects of the collapsed excavation on the value of axial capacity and the movement-resistance response. Although two of the assumptions were investigated by modifying the parameters using a sensitivity analysis, a combination of the first two assumptions (reduction in lateral stress in the silt layer and a reduction of strength parameters for the zone located from the bottom of the silt layer to a depth of 3m below the silt layer) was verified by comparing the predicted and measured results. Specifically, the results obtained from: the initial prediction, the field measurements, and the prediction that was conducted after the collapse of the excavation are discussed and compared below.

6.7.1. Initial Predicted Responses

The initial predicted axial resistance-depth, axial resistance-movement, movement-unit side resistance, and movement-end bearing resistance responses are presented in Figure 6.10. Because the shafts were designed for a length of 26.2m, based on the results obtained from the FB-Deep program when utilizing the soil properties obtained from the UofA geotechnical investigation program (Figure 6.10a), the axial resistance-movement, movement-unit side resistance, and movement-end bearing resistance responses were all developed for a 1.2m diameter by 26.2m long DSF. Furthermore, because the values of axial capacity in the axial resistance-depth plot were obtained by assuming the amount of movement was 5%D (6.0cm), the 5%D line is presented in each of the corresponding movement related responses (axial resistance-movement, movement-unit side resistance, movement-end bearing resistance).

The predicted results that were obtained utilizing the data from the AHTD geotechnical investigation were significantly lower than the responses that were obtained using the MODOT or UofA geotechnical investigation data, regardless of which software program was utilized. Although the slopes of the axial resistance-depth curves were similar within the sand layer (Figure 6.10a), the higher values of undrained shear strength that were obtained from the UofA geotechnical investigation resulted in higher capacity predictions that corresponded to the increased axial resistance within the clay. The exception to the curves possessing similar slopes was for the curves obtained by using the MODOT geotechnical investigation techniques from a depth of 18.0m to 21.0m. The rapid increases in axial capacity, at these given depths, were associated with the refusal of the cone during the cone penetration test.

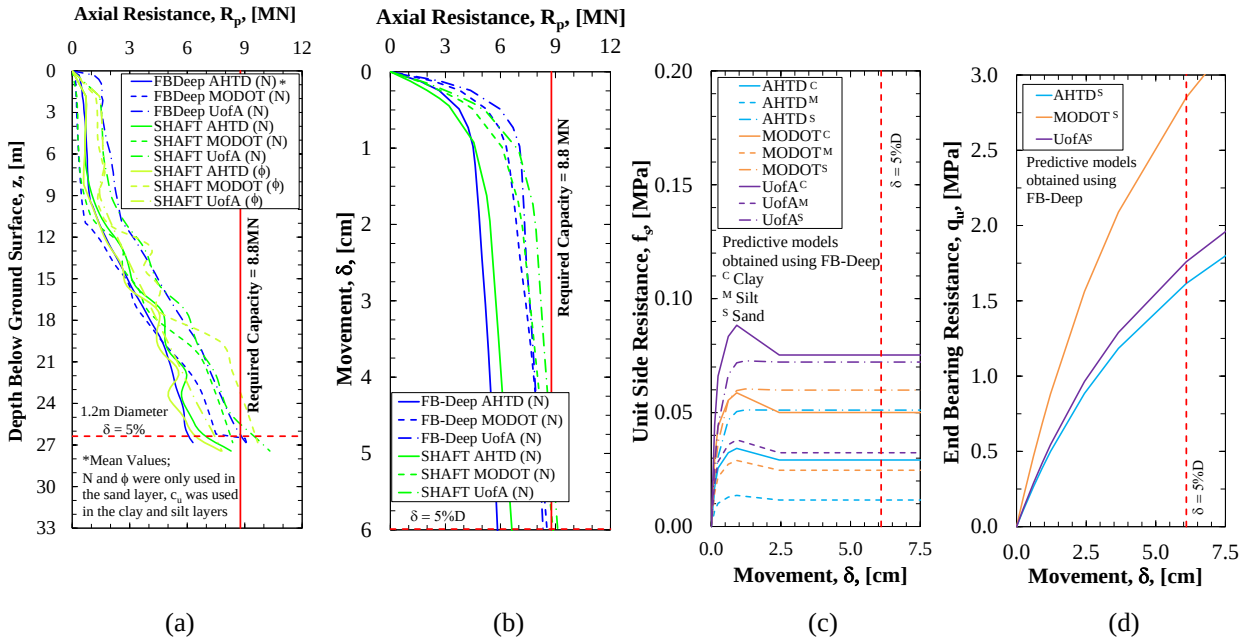

(a) (b) (c) (d)

Figure 6.10. Predicted a) resistance-depth curves, b) resistance-movement curves, c) movement-unit side resistance curves, and d) movement-end bearing resistance curves.

The lower capacity values that were predicted by using the data obtained from the AHTD geotechnical investigation methodology are more evident in Figure 6.10b, Figure 6.10c, and Figure 6.10d. Specifically, for a DSF that was tipped at 26.2m below the ground surface, the

predicted axial resistance-movement curves reach the vertical asymptote at lower values of axial resistance than the axial resistance-movement curves that were obtained by using the data from the other geotechnical investigations (UofA and MODOT). Furthermore, more movement was predicted, when using the AHTD geotechnical investigation data for the same value of axial resistance, which will result in larger diameter DSF being required if the AHTD geotechnical investigation methodology and a deformation limit state were utilized. Like with the axial resistance-movement curves, the unit side resistance (Figure 6.10c) and unit end bearing resistance (Figure 6.10d) curves predicted using the data obtained from the AHTD geotechnical investigation were lower than curves predicted using the other methods. The combined contribution of the unit side resistance and unit end bearing resistance, as predicted using the data obtained from the UofA and MODOT geotechnical investigation, appear to compensate (the predicted UofA curve is higher in unit side resistance but lower in unit end bearing resistance) because the same axial capacity values were predicted using both methods.

6.7.2. Measured Responses

The measured nominal load-movement (upward/downward), measured axial resistance-movement (equivalent top-down), measured movement-unit side resistance, and measured movement-end bearing resistance responses were determined from the data that were collected during the full-scale BLC tests (Figure 6.11). Although the South 1.2m diameter DSF and the North 1.2m diameter DSF were constructed 32.3m apart from each other, the measured nominal load-movement (upward/downward) and measured axial resistance-movement responses for the DSF constructed in the uncollapsed excavation and measured nominal load-movement (upward/downward) and measured axial resistance-movement responses for the DSF constructed in the collapsed excavation were significantly different. Specifically, at the maximum measured

nominal axial load (5.0MN), the amount of upward/downward movement that was observed for the South 1.2m diameter DSF was 1.1cm/2.8cm while the amount of upward/downward movement that was observed for the North 1.2m diameter DSF was 3.3cm/7.5cm. Furthermore, at the maximum equivalent top-down axial resistance (7.4MN) that was obtained for the South 1.2m diameter DSF, the amount of movement that was observed for the South 1.2m diameter DSF was 1.3cm (slightly higher than the 1.1cm from the nominal load due to elastic compression) while the amount of movement that was observed for the North 1.2m diameter DSF was 3.5cm.

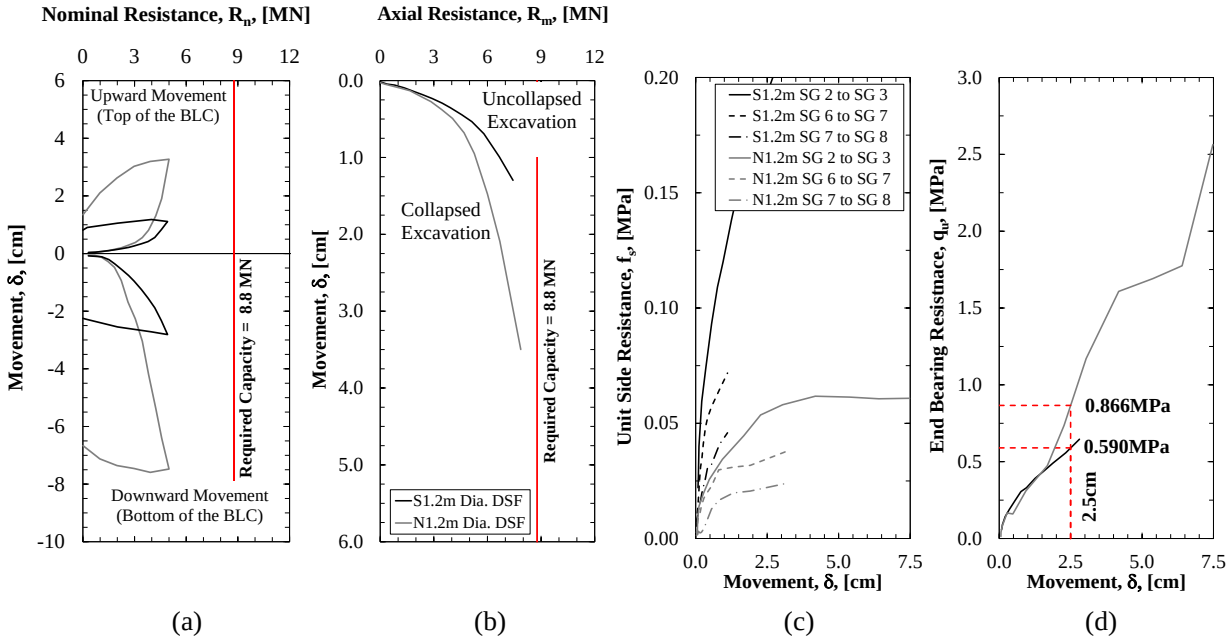

Figure 6.11. Measured a) upward/downward movements, b) equivalent top-down resistance-movement curves, c) movement-unit side resistance curves, and d) movement-end bearing resistance curves.

As observed in Figure 6.11b, the shapes of the measured equivalent top-down axial resistance-movement for the two shafts were similar until 0.25cm of movement and then began to deviate from one another; with the DSF constructed in a collapsed excavation requiring more movement to achieve the same amount of resistance. The similarity of the resistance values, at small movements, was likely due to the similarity in the end bearing resistance, for small

amounts of movement, because the unit side resistance values within the silt and sand layers that were obtained for the South 1.2m diameter DSF (Figure 6.11c) were larger than the unit side resistance values that were obtained for the North 1.2m diameter DSF (the DSF that was constructed within the redrilled excavation).

As tabulated in Table 6.5, the average values of unit side resistance within the clay layer was greater for the North 1.2m diameter DSF than it was for the South 1.2m diameter DSF (as associated with upward movements of 3.3cm and 1.1cm, respectively). However, at movements of 1.1cm (the maximum upward movement of the South 1.2m diameter DSF), the measured unit side resistance values for both of DSF within the clay layer were similar (Table 6.6). In contrast, the average unit side resistance values within the sand layer were 0.12MPa and 0.09MPa for the South and North 1.2m diameter DSF, respectively, for downward movements of 2.8cm and 7.5cm. The measured unit side resistance values were greater (at the same upward/downward displacement values of 1.1cm/2.8cm) for the South 1.2m diameter DSF than for the North 1.2m diameter DSF, except for the depths between 16.5m and 20.4m (directly above and below the BLC). Although the North 1.2m diameter DSF excavation collapsed and was redrilled, higher end bearing resistance values were measured for North 1.2m diameter DSF, at movements in excess of 1.5cm, than were measured for the South 1.2m DSF (uncollapsed excavation). Specifically, at 2.5cm of movement, the measured end bearing resistance for the North 1.2m diameter DSF was 0.9MPa while the measured end bearing resistance for the South 1.2m diameter DSF was 0.6MPa. The difference in end bearing resistance was attributed to 1) the North 1.2m diameter DSF possibly being tipped into a reported cemented sand layer because it was constructed 0.3m deeper than the South 1.2m diameter DSF, and 2) the unit side resistance for the North 1.2m diameter DSF being less than the unit side resistance for the South 1.2m

diameter DSF resulting in more of the load being transferred to the end of the North 1.2m diameter DSF.

Table 6.5. Average unit side resistance and end bearing resistance measured for the DSF at the TATS.

Soil Type	Average Unit Side Resistance, f_s, [MPa]		End Bearing Resistance, q_u, [MPa]	
	South 1.2m[1]	North 1.2m[2]	South 1.2m[1]	North 1.2m[2]
Desiccated Clay	0.016	0.030	N/A	
Clay	0.040	0.060		
Silt	0.046	0.024		
Sand	0.121	0.089	0.647	2.563

[1]Maximum Upward Movement = 1.1cm, Maximum Downward Movement = 2.8cm
[2]Maximum Upward Movement = 3.3cm, Maximum Downward Movement = 7.5cm

Table 6.6. Measured unit side resistance values along the length of the DSF at the TATS at maximum movements (upward and downward, respectively) observed for the South 1.2m DSF.

Approximate Depth Below Ground Surface [m]			Soil Type	Movement, δ [cm]	Measured Unit Side Resistance, f_s, [MPa]	
					South 1.2m	North 1.2m
0.0	-	2.4	Clay	1.1	0.016	0.028
2.4	-	4.9	Clay	1.1	0.032	0.035
4.9	-	7.3	Clay	1.1	0.049	0.043
7.3	-	9.8	Silt	1.1	0.046	0.019
9.8	-	12.2	Sand	1.1	0.072	0.030
12.2	-	14.0	Sand	1.1	0.104	0.073
14.0	-	16.5	Sand	1.1	0.173	0.054
16.5	-	18.9	Sand	1.1	0.056	0.242
19.5	-	20.4	Sand	2.8	0.142	0.118
20.4	-	22.9	Sand	2.8	0.204	0.057
22.9	-	26.2	Sand	2.8	0.110	0.041

The contributions of the unit side resistance and the end bearing resistance were better visualized in the load contribution schematic presented in Figure 6.12a. Specifically, for 1.1cm of upward movement at all depths, the nominal load obtained for the South 1.2m diameter DSF was higher than the nominal load obtained for the North 1.2m diameter DSF. Furthermore, for

2.8cm of downward movement, the nominal load obtained for the South 1.2m diameter DSF was higher than the nominal load obtained for the North 1.2m diameter DSF to a depth of 23.0m and then the nominal load obtained for the South 1.2m diameter DSF was lower than the nominal load obtained for the North 1.2m diameter DSF there below. As previously mentioned, the difference in the depth of the tip of each of the drilled shaft was the cause for the inversion in the end bearing capacity. This difference was further exacerbated because the first level of strain gauges was positioned at 22.9m below the ground surface for both shafts even though the tip of the North 1.2m diameter DSF was located 0.3m below the tip of the South 1.2m diameter DSF thereby resulting in higher values for the longer shaft. Likewise, because more creep was measured during the BLC test for the North 1.2m diameter DSF than during the BLC test for the South 1.2m diameter DSF, higher values of end bearing resistance were expected for the North 1.2m DSF (Figure 6.12b).

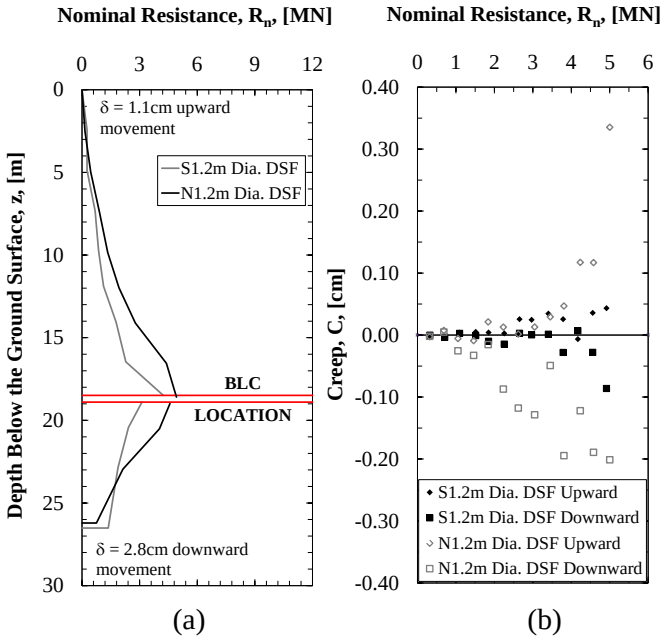

Figure 6.12. Measured a) load transferred as a function of depth and b) creep.

6.7.3. Predicted and Measured Comparisons

The predicted and measured axial resistance-movement, movement-unit side resistance, and movement-end bearing resistance responses were compared, for the South 1.2m DSF, to determine the effectiveness of the software programs at predicting the response of the DSF constructed in the uncollapsed excavation to loading. For the South 1.2m diameter DSF, the predictions obtained from both software programs (FB-Deep and SHAFT) matched the measured response (Figure 6.13a) when the soil properties that were obtained from the UofA or MODOT geotechnical investigations were utilized within the programs. Although the predicted axial resistance-movement response was also predicted using the soil properties that were obtained from the AHTD geotechnical investigation, as previously shown in Figure 6.13b, these responses were not included in Figure 6.13a because the use of these soil properties grossly underpredicted the measured capacity. From the results presented in Figure 6.13a, it appears that the SHAFT program better predicted the axial resistance-movement response and that the FB-deep program overpredicted the amount of resistance for small amounts of movement but underpredicted the resistance for large amounts of movement. As previously mentioned, the SHAFT program did not enable determination of the movement-unit side resistance and movement-end bearing resistance responses like the FB-Deep program did. Therefore, even though the prediction obtained from the SHAFT program better predicted the axial resistance-movement response, the measured movement-unit side resistance response (Figure 6.13b) and measured movement-end bearing resistance response (Figure 6.13c) were compared with the predictions generated from the FB-Deep program.

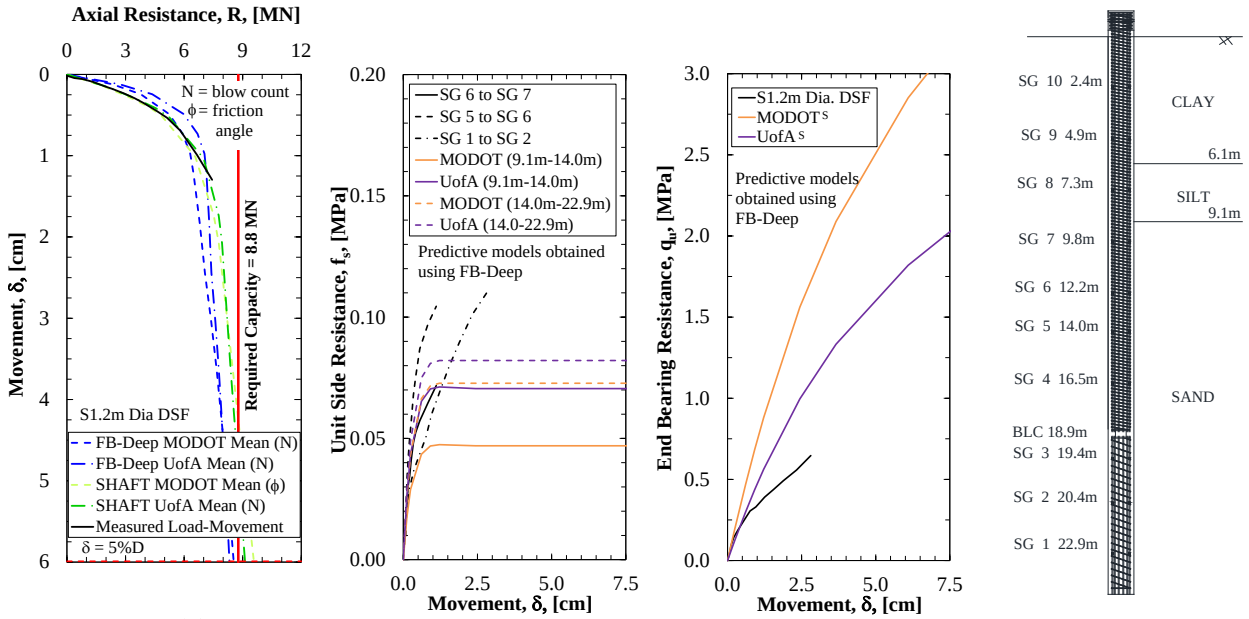

Figure 6.13. Predicted and measured a) resistance-movement curves, b) movement-unit side resistance curves, c) movement-end bearing resistance curves, and d) schematic for the South 1.2m diameter DSF.

Regardless of the 1) the depth of the strain gauges that were used for the readings (Figure 6.13d), 2) the type of soil stratum (Figure 6.13d), or 3) the utilized soil data (previously presented in Figure 6.6), the amount of unit side resistance (Figure 6.13c) was overpredicted within the clay layer and underpredicted within the silt and sand layers when using the FB-Deep deep program. Although the slopes of the elastic portion of the curves were similar, the predicted yield points in the silt and sand were much lower than the measured yield points (even though yield, followed by a plastic response, was not achieved in the measured silt and sand data). The predicted values of end bearing resistance, as obtained using the data from the UofA geotechnical investigation, were similar to the measured resistance values until a movement of 1.0cm. Then the measured values of end bearing resistance were less than the predicted values of end bearing resistance at movement values that were larger than 1.0cm.

As shown in Figure 6.13b, the predicted unit side resistance values within the clay (3.0m to 6.1m) and silt (6.1m to 9.1m) layers were better predicted using the data obtained from the MODOT geotechnical investigation, but the predicted unit side resistance values within the sand layer (9.1m to 15.2m) were better predicted using the data obtained from the UofA geotechnical investigation. Specifically, the predicted response using the MODOT geotechnical investigation data, as obtained for the clay (3.0m to 6.1m) and silt (6.1m to 9.1m), matched the measured response from strain gauge levels 8 to 9 (4.9m to 7.3m) and 7 to 8 (7.3m to 9.8m), respectively. Even though 1) the UofA predicted unit side resistance in the upper portion of the sand layer (9.1m to 15.2m) matched the measured unit side resistance in the upper portion of the sand layer between strain gauge levels 6 and 7 (9.8m to 12.2m), 2) the prediction that utilized the UofA data better matched the measured response for all of the other strain gauge levels that were in the sand layer, and 3) most of the axial resistance for the DSF resulted from side resistance in the sand layer, the prediction that utilized the MODOT data better matched the measured response than the prediction that utilized the AHTD data.

The importance of the contribution of the unit side resistance to the total amount of axial resistance was evident when considering that the unit side resistance values that were predicted using the soil properties obtained from the UofA geotechnical investigation were similar to, or bounded by, the measured values of unit side resistance until a movement of 1.0cm while the predicted end bearing resistance values were similar to the measured end bearing resistance until a movement of 1.0cm. The combination of unit side resistance and unit end bearing resistance resulted in an underprediction of axial resistance, at movements larger than 1.0cm, when using the UofA geotechnical investigation data even though the software program overpredicted the

measured end bearing resistance because the measured unit side resistance was significantly higher than the predicted unit side resistance, at movements larger than 1.0cm.

6.7.4. Post Collapse Response Predictions

As previously mentioned, although the expected resistance-movement responses were initially predicted to determine the appropriate length of the 1.2m diameter DSF, additional analyses, including sensitivity analyses, were required to determine the resistance-movement response of the DSF that was constructed in the redrilled excavation. As shown in Figure 6.14, a movement values less than 1.6cm, the axial resistance of the DSF that was constructed in the redrilled excavation was overpredicted by utilizing the mean values of the UofA and MODOT geotechnical investigation data within the FB-Deep program. In general, the measured axial resistance-movement curve had less curvature than the predicted axial resistance-movement curves.

For movement values up to 1.6cm, the input soil profile utilized to best match the measured and predicted axial resistance-movement responses was the combined soil profile (10 percent reduction of the total unit weight within the silt layer and modeling the top of the sand layer as additional silt instead of sand between 9.1m and 12.1m). For movement values larger than 1.6cm, the slope of the measured axial resistance-movement curve was not estimated by any of the predicted models. However, at movement values of 1.6cm and 2.9cm, the measured axial resistance was predicted by utilizing the mean values of the MODOT geotechnical investigation data and the UofA geotechnical investigation data, respectively, within the FB-Deep program. For movement values larger than 3.0cm, all of the predictions underpredicted the measured axial resistance.

The rationale for modeling the silt portion of the profile with a reduced unit weight, for Method 1, was to simulate the decrease in lateral stress within the silt layer that was caused by the collapse. The drop in the unit weight values had a negligible effect on the shape of the axial resistance-movement curve (Figure 6.14a). Likewise, the motivation for modeling the sand layer as a silt layer, for Method 2, was to simulate a coated/lubricated sidewall that may have resulted from the collapse of the DSF at the TATS. Because the values of the predicted axial resistance-movement response, as obtained by utilizing Method 2, were significantly less than the axial capacity values that were measured (Figure 6.14a), it does not appear that the silt coated the sidewall of the shaft for the complete depth of the shaft. However in this case, based on the unit side resistance results (Figure 6.14b), the silt may have coated the region between strain gauge levels 6 and 7 (12.2m to 14.0m) but does not appear to have coated the region between strain gauge levels 5 and 6 (14.0m to 12.2m).

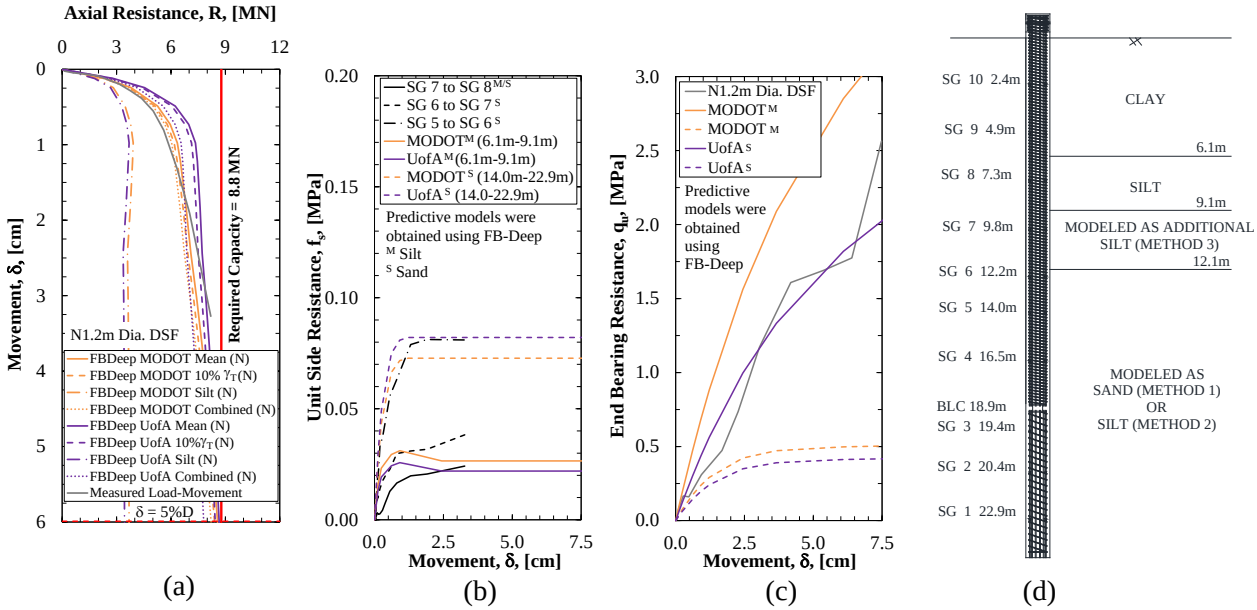

Figure 6.14. Predicted and measured a) resistance-movement curves, b) movement-unit side resistance curves, c) movement-end bearing resistance curves, and d) schematic for the North 1.2m diameter DSF.

Therefore, the reasoning for modeling the soil profile for the collapsed DSF at the TATS with an additional 3.0m thick silt layer (from 9.1m to 12.1m), below the existing silt layer, for Method 3, was twofold. First, based on the measured and predicted movement-unit side resistance responses, the unit side resistance between strain gauges 6 and 7 (9.8m to 12.2m) was best modeled using silt soil properties (Figure 6.14b). The depth of the additional silt layer was stopped at 12.1m because the measured unit side resistance response between strain gauge levels 5 and 6 (12.2m to 14.0m) was best modeled using the sand soil properties. Second, based on the measured and predicted movement-end bearing resistance responses, the measured end bearing resistance response (Figure 6.14c) was best modeled using the sand soil properties.

Like with the results obtained from the DSF that was constructed in the uncollapsed excavation, the contribution of the unit side resistance outweighed the contributions of the end bearing resistance in determining the total amount of axial resistance. Specifically, even though the end bearing resistance that was predicted using the sand parameters that were obtained from the MODOT geotechnical investigation were significantly higher than the measured end bearing resistance, the model that contained the MODOT parameters better matched the total axial resistance when compared to the results obtained from the model that contained the UofA parameters because the unit side resistance values that were obtained using the MODOT geotechnical investigation better matched the measured unit side resistance values (Figure 6.15). Based on the predicted and measured results that are presented in Figure 6.15, the contribution of unit side resistance to the predicted axial resistance-movement curve is more apparent than those presented in Figure 6.14b. Until a movement of 1.0cm, almost all of the measured responses were lower than the predicted responses that were obtained using the data from the UofA and MODOT geotechnical investigations. Although all of the predicted responses (clay, silt, and

sand) decrease or remain constant after 1.0cm of movement, the measured values of unit side resistance continued to increase after 1.0cm of movement (except for the measured curve associated with strain gauge levels 1 and 2). Therefore, because of the observed response of increasing measured values of unit side resistance at displacements in excess of 1.0cm, the axial capacity-movement curve could not be predicted, at large movement values, using currently available movement-unit side resistance curves (t-z curves) regardless of the method (aforementioned Methods 1, 2, 3) that was employed to model the response of a DSF that was constructed in a redrilled excavation.

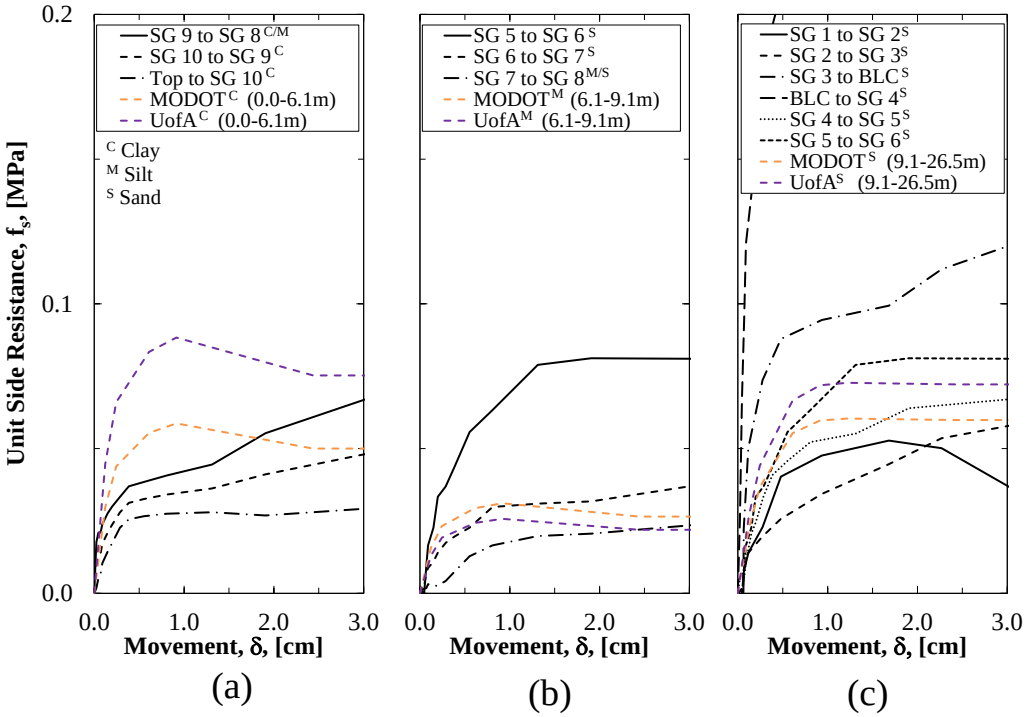

Figure 6.15. Predicted and measured movement-unit side resistance curves in a) clayey, b) silty, and c) sandy soils.

6.8. Recommendations

Although the excavation for the North 1.2m diameter DSF collapsed and was redrilled, it was successfully proven that drilling below the prescribed bottom depth (26.5m instead of 26.2m) was a reasonable method to reduce the negative effects of the collapse on the end bearing

resistance. Although not included as part of this investigation, the loss of side resistance may also be remedied by over-drilling (increased diameter) the entire length of the excavation to remove the collapsed material from within the excavation and to remove the collapsed/contaminated material along the wall of the excavation. If an excavation does collapse, a reduction in the total unit weight values is recommended when predicting the capacity to more accurately model the movement-resistance response for a DSF constructed within a previously collapsed excavation. Additional full-scale load tests on DSF constructed in redrilled excavations are recommended to determine the movement-unit side resistance response for a redrilled excavation and to verify the response of increasing values of unit side resistance as a function of increasing movement that was observed for the North 1.2m diameter DSF that was constructed in the redrilled excavation. Furthermore, if an excavation does collapse, strain gauges should be added to the rebar cage at 3.0m intervals prior to placement of the rebar cage into the redrilled excavation. The completed DSF should then be proof tested to a movement of at least 2.5cm or to the required axial capacity to determine if the movement-unit side resistance response is increasing as a function of increasing movement. Although guidance was provided for how to modify the input soil parameters to determine the axial capacity response of a DSF constructed in a redrilled excavation, based on the observations presented in this case history, the measured response obtained from a DSF test shaft constructed in a redrilled excavation should not be used to predict the response obtained for a production DSF constructed in a uncollapsed excavation. Likewise, the measured response obtained from a DSF test shaft constructed in an uncollapsed excavation should not be used to predict the response obtained for a production DSF constructed in a redrilled excavation. For future DSF excavation collapses, it is recommended

that the mechanism of failure (i.e. partial lubrication of the side wall for the collapsed DSF at the TATS) be considered for the capacity of the DSF).

6.9. Conclusions

The major effects of a collapsed excavation, as observed for the full-scale BLC testing on DSF at the TATS, included: larger upward and downward movements, greater movements for the equivalent top-down resistance-movement curve, reduced unit side resistance values, and possible higher end bearing resistance for the DSF that was constructed in the redrilled excavation. While the required capacity was not achieved for the North 1.2m diameter DSF (collapsed) or South 1.2m diameter DSF (uncollapsed), the amount of movement of the North 1.2m diameter DSF was approximately three times the amount of movement for the South 1.2m diameter DSF at similar axial loading conditions. Similarly, it was verified that any reduction in the end bearing resistance could be remedied by drilling to a depth below the original prescribed depth. Furthermore, without over reaming along the length of the collapsed excavation at the TATS, more load was transferred to end bearing for the DSF constructed in the redrilled excavation because of lower unit side resistance values within the redrilled excavation.

The resistance-movement curve for the South 1.2m diameter DSF, constructed in the uncollapsed excavation, was matched using the FB-Deep program with the soil properties obtained from the MODOT and UofA geotechnical investigation techniques, but was not matched using the FB-Deep program with the soil properties obtained from the AHTD geotechnical investigation technique. For the North 1.2m diameter DSF, constructed in the redrilled/collapsed excavation, the measured resistance-movement curve was modeled to a movement of 1.0cm by using 1) a 10 percent reduction in the total unit weight values and 2) a 3.0m layer of silt at the top of the sand layer, instead of sand, within the FB-Deep program with

the soil properties obtained from the MODOT and UofA geotechnical investigation techniques. For the collapsed DSF at the TATS, the reduction in the measured unit side resistance resulted from the reduced horizontal effective stress (less material in the silt layer) and a larger silt layer that was caused by the lubrication along a portion of the length of the shaft (collapsed silty soil coating the sandy soil). Although this case history is limited to only two shafts constructed in one soil deposit, the findings should be further investigated for other soil deposits to develop new movement-unit side resistance curves to be applied to predict the axial resistance-movement response for DSF constructed in collapsed/redrilled excavations.

6.10. Acknowledgements

The authors thank the Arkansas State Highway and Transportation Department, the Missouri Department of Transportation, ADSC – the International Association of Foundation Drilling, Razorback Concrete, McKinney Drilling Company, GEI Consultants, Inc., Foundation Technologies, Inc., Polymer Drilling Systems, Inc., and Loadtest, Inc., for financial and/or in-kind contributions. The authors would also thank the editors and the reviewers of the article for providing constructive comments that improved the quality of the manuscript.

6.11. References

American Association of State Highway and Transportation Officials (2007). LRFD Bridge Design Specifications, Fourth Ed., AASTHO, Washington, D.C., 1938 pgs.

American Society for Testing and Materials (2013). “Standard Test Method for Compressive Strength of Cylindrical Concrete Specimens.” Annual Book of ASTM Standards, Designation C39, Vol. 4.02, ASTM, West Conshohocken, PA.

American Society for Testing and Materials (2013). “Standard Test Method for Static Modulus of Elasticity and Poisson’s Ratio of Concrete in Compression.” Annual Book of ASTM Standards, Designation C469, Vol. 4.02, ASTM, West Conshohocken, PA.

American Society for Testing and Materials (2013). “Standard Test Methods for Deep Foundations Under Static Axial Compressive Load.” Annual Book of ASTM Standards, Designation D1143, Vol. 4.08, ASTM, West Conshohocken, PA.

Brown, D.A. (2002). “Effect of Construction on Axial Capacity of Drilled Foundations in Piedmont Soils.” Journal of Geotechnical and Geoenvironmental Engineering, Vol. 128, No. 12, pp. 967-973.

Brown, D.A. (2004). “Zen and the Art of Drilled Shaft Construction: The Pursuit of Quality.” Geo-Institute International Conference on Drilled Foundations, ASCE Geotechnical Special Publication No. 124, pp. 19-33.

Brown, D., Turner, J., and Castelli, R. (2010). “Drilled Shafts: Construction Procedures and LRFD Methods.” FHWA Publication No. NHI-10-016, Federal Highway Administration, Washington, D.C., 970 pgs.

Bustamante, M. and Gianeselli, L. (1982). “Pile Bearing Capacity Prediction by Means of Static Penetrometer CPT.” Proceedings of the 2nd European Symposium on Penetration Testing Vol. 2, pp. 493-500.

Dapp, S.D., Muchard, M., and Brown, D.A. (2006). “Experiences with Base Grouted Drilled Shafts in the Southeastern United States.” Proceedings of 10th International Conference on Deep Foundations, Amsterdam, Netherlands, 10 pgs.

FB-Deep (2012). Bridge Software Institute, Gainesville, Florida, Version 2.04.

GEI. Consultants, Inc. (2014). “Integrity Testing of Drilled Foundation Shafts Turrell, Arkansas.” Report for TRC-1204, March 2014, 21 pgs.

Meyerhof, G. (1976). “Bearing Capacity and Settlement of Pile Foundations.” Journal of Geotechnical Engineering, Vol. 102, No. 6T3, pp. 195-228.

Mullins, G. and Ashmawy, A.K. (2005). “Factors Affecting Anomaly Formation in Drilled Shafts – Final Report.” Florida Department of Transportation BC-353-19, 276 pgs.

O’Neill, M. and Reese, L. (1999). “Drilled shafts: Construction Procedures and Design Methods.” FHWA Publication No. IF-99-025, Federal Highway Administration, Washington, D.C., 537 pgs.

Quiros, G. and Reese, L. (1977). “Design Procedures for Axially Loaded Drilled Shafts” FHWA Publication No. TX78-1765F, Federal Highway Administration Final Report, Washington, D.C., 176 pgs.

Race, M.L., Bey, S.M., and Coffman, R.A. (2013). “Discussion of ‘Implementation of LRFD of Drilled Shafts in Louisiana’ by Xinbao Yu, Murad Y. Abu-Farsakh, Sungmin Yoon, Ching Tsai, and Zhongjie Zhang.” Journal of Infrastructure Systems, Vol. 19, No. 3, pp. 351-353.

Race, M.L. and Coffman, R.A. (2013). “Effect of Uncertainty in Site Characterization on the Prediction of Liquefaction Potential for Bridge Embankments in the Mississippi Embayment.” ASCE Geotechnical Special Publication No. 231, Proc. GeoCongress 2013: Stability and Performance of Slopes and Embankments III, San Diego, California, March, pp. 888-897.

Reese, L. C., O’Neill, M. W. (1988). ‘‘Drilled Shafts; Construction Procedures and Design Methods.’’ Rep. No. FHWA-HI-88-42, U.S. Dept. of Transp., Federal Highway Administration, Washington, D.C.

Robertson, P.K., Cabal, K.L. (2012). “Guide to Cone Penetration Testing for Geotechnical Engineering.” Gregg Drilling and Testing, Inc, 145 pgs.

Schmertmann, J. H. (1967). “Guidelines for Use in the Soils Investigation and Design of Foundations for Bridge Structures in the State of Florida.” Research Bulletin 121 (RB-121), Report Prepared for the FDOT by the University of Florida, Gainesville, Florida.

Schmertmann, J.H., Hayes, J.A., Molnit, T., and Osterberg, J.O. (1998). “O-Cell Testing Case Histories Demonstrate the Importance of Bored Pile (Drilled Shaft) Construction Technique.” Proceedings of Fourth International Conference on Case Histories in Geotechnical Engineering, St. Louis, Missouri, pp. 1103-1115.

SHAFT (2012). ENSOFT, INC. Austin, Texas, Version 2012.

Vanikar, S.N. (1986). Manual on Design and Construction of Driven Pile Foundations. U.S. Department of Transportation Federal Highway Administration. FHWA-DP-66-1 (Revision 1), 57 pgs.

CHAPTER 7: DSF at the MATS

7.1. Chapter Overview

Three DSF were constructed at the Monticello Arkansas Test Site (MATS) designated as the North 1.2m, Center 1.8m, and South 1.2m DSF. The site stratigraphy consisted of 18.3m of clay with a 3.0m interbedded layer of fine sand underlain by at least 12.2m of medium dense sand. Upon a depth of drilling of the 1.2m DSF of 21.9m, the slurry level within the DSF excavation dropped at a rate of approximately 3.2m/hour. Construction problems encountered at the MATS included equipment failure during the drilling of both the Center 1.8m and the South 1.2m DSF and poor concrete placement within the South 1.2m DSF. In particular, the poor concrete placement in the South 1.2m DSF caused excess downward movement and large differential movements below the bottom of the BLC. The results of the BLC testing of the three DSF at the MATS were analyzed to determine the impact of the construction methods and problems on the axial capacity of the DSF. To determine the construction impact, the top-down equivalent movement curves, the unit side resistance curves, and the unit end bearing curves were compared for all three of the DSF. Because many of the construction problems occurred due to the insistence of constructing a DSF over the course of multiple days, it was determined that a DSF constructed in a single day in cohesionless soil could save upwards of $2000 (USD) per shaft.

Additional information contained in this chapter includes the scaling ratio of a 1.2m to a 1.8m DSF in the interbedded layers of cohesive and cohesionless soil at the MATS, and comparisons between the unit side resistance and the unit end bearing resistance for the North 1.2m and the Center 1.8m diameter DSF. The average scaling factor for the unit side resistance in clay was 0.85 which is slightly higher than the recommended scaling factor in rock of 0.8. The

deflection of the DSF as a function of the design lateral loading was predicted using LPILE (2012) software and the data obtained from the AHTD, MODOT, and UofA geotechnical investigation methods.

The paper contained within this chapter is being submitted to the International Journal of Geoengineering Case Histories. The full reference for the paper is: Race, M.L. and Coffman, R.A. (2015). “Case History: Drilled Shaft Foundation Construction Problems.” International Journal of Geoengineering Case Histories, Submitted for Review, IJGCH-S86.

7.2. Additional Results that are not included in Race and Coffman (2015)

To predict the unit end bearing resistance from a measured unit end bearing resistance on a smaller DSF, the scaling effects of DSF have typically only been considered for rock. Although the ultimate unit end bearing resistance was not measured, the ratio of the measured unit end bearing resistance for the Center 1.8m DSF to the measured unit end bearing resistance for the South 1.2m DSF was 0.41 (Figure 7.1). The difference in the end bearing resistance ratio is significantly different than the value of 1.68 that was presented in Chapter 6 for the DSF constructed at the TATS. The end bearing material at the MATS was medium to medium dense sand as compared to the medium dense to dense sand at the TATS. Additionally, there was not an equipment failure in the North 1.2m DSF at the MATS, but the 1.8m clean-out bucket broke while constructing the Center 1.8m DSF at the MATS; therefore, the bottom of the Center 1.8m DSF excavation was not sufficiently clean. A comparison of the measured unit side resistance in clayey and sandy soil is presented in Figure 7.2. The numerical unit side resistance and the scaling factor ratio for the Center 1.8m and the South 1.2m DSF is presented in Table 7.1. The average scaling factor ratio for the unit side resistance in clay is 0.85 compared to the 0.8 that is recommended for rock (Figure 17-7 from Brown et al. 2010). The overall (clay and sand)

average scaling factor is 1.1 (excluding the scaling factor from depths of 18.9m to 21.9m, the average value is 0.84) compared with the 1.0 that was obtained for the TATS, as presented in Chapter 6.

Table 7.1. Measured unit side resistance comparison and the scaling factor for the North 1.2m and Center 1.8m DSF at the MATS.

Depth [m]	Soil Type	Unit Side Resistance, f_s, [MPa]		Scaling Ratio
		North 1.2m DSF	Center 1.8m DSF	
0.0 to 9.4	Clay	0.094	0.088	0.94
9.4 to 12.5	Sand	0.148	0.122	0.82
12.5 to 15.5[1]	Clay	0.050	0.036	0.72
15.5 to 18.9	Clay	0.085	0.076	0.89
18.9 to 21.9	Sand	0.093	0.203	2.18

[1]Maximum unit side resistance

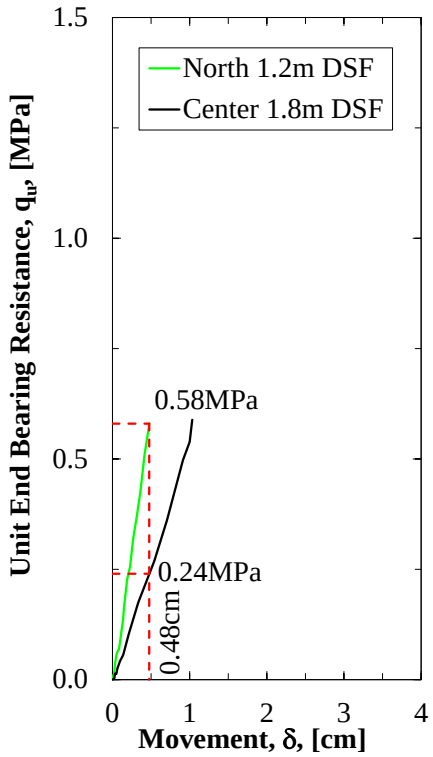

Figure 7.1. Comparison of the measured unit end bearing resistance for the North 1.2m and Center 1.8m DSF at the MATS.

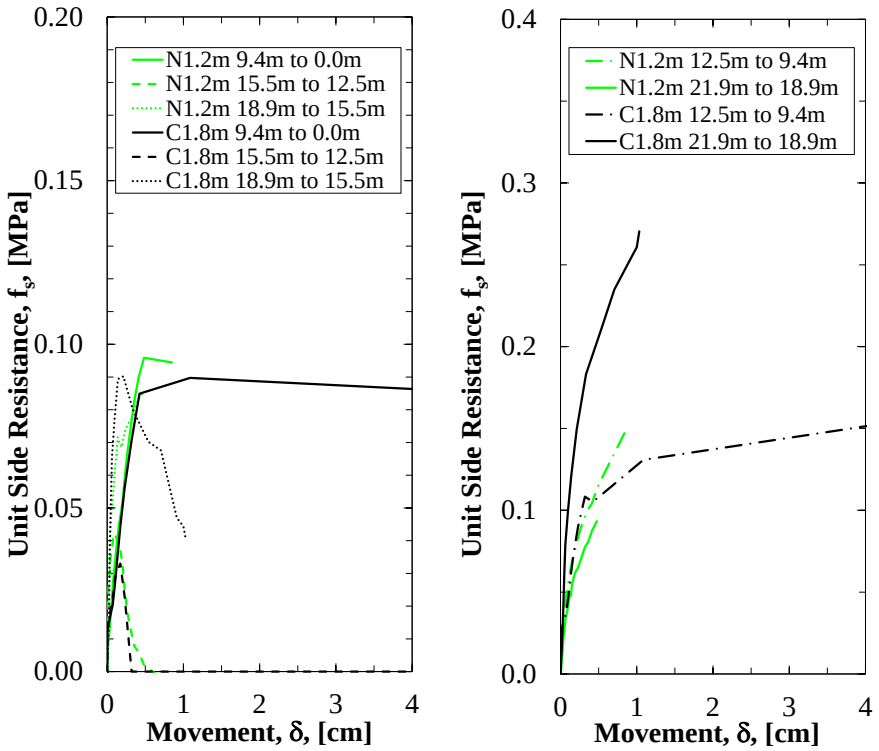

Figure 7.2. Comparison of the measured unit side resistance values for the North 1.2m and Center 1.8m DSF at the MATS in a) clayey soil and b) sandy soil.

Based on the as-built dimensions of the DSF at the MATS and the supplied loads (Table 7.2), the predicted top movements for the design lateral loading are 0.118cm, 0.053cm, and 0.111cm for the North 1.2m (presented in Figure 7.3), Center 1.8m, and South 1.2m DSF, respectively. The lateral deflection curves as a function of depth for all three of the soil sampling and testing methods are presented in Appendix C in Figure C.10.

Table 7.2. Design loads for lateral loading of DSF at the MATS.

Loading Type	Amount of Load		
	Axial	Longitudinal	Transverse
Force (MN)	3.980	0.103	0.013
Moment (MN*m)	N/A	1.125	0.083

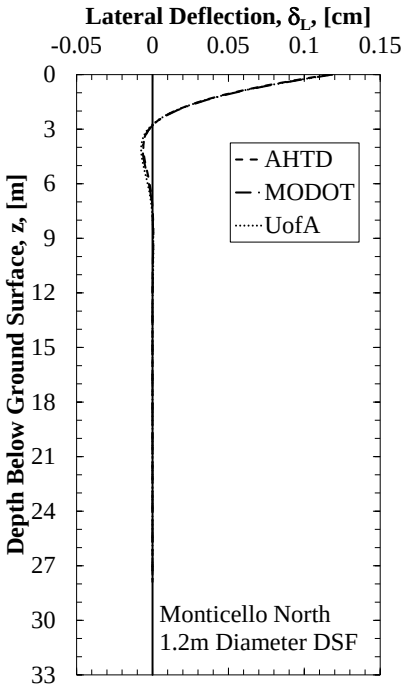

Figure 7.3. Lateral deflection of the North 1.2m diameter DSF at the MATS as predicted utilizing LPILE (2012) and the obtained geotechnical investigation data.

Case Study: Drilled Shaft Foundation Construction Problems

Morgan L. Race, SM.ASCE, EIT[1]
Richard A. Coffman, M.ASCE., PhD, PE, PLS[2]

7.3. Abstract

Various problems were encountered during the construction of three full-scale drilled shaft foundations (DSF) at the Monticello Arkansas Test Site (MATS). These construction problems included, but are not limited to: loss of slurry, broken equipment, and premature setup of the concrete. Comparisons between the results obtained from the bi-directional load cell (BLC) testing that was performed on each of the DSF aided in the determination of the effects of the construction problems on the axial capacity of the DSF. The measured unit end bearing resistance values were investigated to determine the effects of a field change in which a 1.2m diameter clean-out bucket was used instead of a 1.8m diameter DSF because the bottom plate of the 1.8m diameter cleanout bucket was lost downhole during construction. As a result of the premature setup of concrete within the South 1.2m diameter DSF, the bottom plate of the BLC moved more than predicted and the movement was differential and not uniform (diametrically opposed movements of 5.6cm and 10.8cm).

Soil data obtained by using the Arkansas State Highway and Transportation Department (AHTD) and University of Arkansas (UofA) geotechnical investigation methods, in conjunction with the FB-Deep software program, were used to accurately predict the unit side resistance responses for the three DSF at the MATS. Therefore, the use of these geotechnical investigation techniques and this software program are recommended for further use within the state of Arkansas. Due to the problems associated with maintaining an open DSF excavation overnight and the associated construction savings that may be obtained by constructing a DSF during a

single day (for cohesionless soils), it is also recommended that DSF be constructed (drilled and poured) in a single day.

Keywords: Drilled Shaft Foundations; Construction Problems; Full-Scale Load Testing

7.4. Introduction

As part of a state-specific (Arkansas) investigation to calibrate resistance factors for DSF, three DSF, designated as North 1.2m diameter, Center 1.8m diameter, and South 1.2m diameter, were constructed at the MATS by McKinney Drilling Company. The DSF were designed utilizing data collected from three different geotechnical investigation methods and two different geotechnical engineering software programs. The design lengths for the North 1.2m, Center 1.8m, and South 1.2m diameter DSF were 27.9m, 21.9m, and 27.9m, respectively. During the construction of the Center 1.8m diameter DSF and the South 1.2m diameter DSF, problems occurred with loss of slurry, equipment failure, premature setup of concrete, and possible sidewall collapse. To determine the effects of the construction problems, full-scale bi-directional cell (BLC) load testing and cross-hole sonic logging were performed on each DSF. Specifically, the resulting measurement values that were obtained from the full-scale load tests (e.g. upward and downward movement, unit side resistance, unit end bearing resistance, etc.) were utilized to determine the effects of the construction techniques/problems on the performance of each of the DSF.

7.5. Subsurface Conditions

The soil at the MATS consisted of interbedded layers of clay and sand to depths of at least 30.5m. The interbedded clay and sand layers and the corresponding soil properties are presented in a schematic (Figure 7.4). As previously mentioned, three methods were utilized to characterize the soil at the MATS. These methods included: 1) the Arkansas Highway and

Transportation Department (AHTD) method, 2) the Missouri Department of Transportation (MODOT) method, and 3) the University of Arkansas (UofA) method as further discussed in Race et al. (2015) and Race and Coffman (2015). The AHTD soil sampling and testing method consisted of performing the standard penetration test (SPT), according to ASTM D1586 (2011), using a standard split spoon sampler (30mm inner diameter) for all of the soils that were investigated. The MODOT method consisted of performing the cone penetration test (CPT), according to ASTM D3441 (2011), with a $10cm^2$ surface area cone until refusal, for all of the soils that were investigated. The UofA method consisted of performing unconsolidated undrained triaxial compression (UU) tests (ASTM D2850 [2011]) on samples from shelby tubes (ASTM D1587 [2011]) for the cohesive soils that were investigated and utilizing the SPT with a California split spoon sampler (60mm inner diameter) for the cohesionless soils that were investigated. The same geotechnical investigation techniques were performed at other sites within the state of Arkansas, as reported in Race et al. (2013), Race and Coffman (2013), Bey (2014), Race et al. (2015), and Race and Coffman (2015). To utilize the UofA data for the cohesionless soils, an empirical correlation value was determined to correlate the blow count values from a California split spoon sampler to a standard split spoon sampler. As described in Race and Coffman (2013), the empirical correlation value ($N_{30mm} = 0.55 \cdot N_{60mm}$) was determined from blow count data that were collected from the test site located in Turrell, Arkansas.

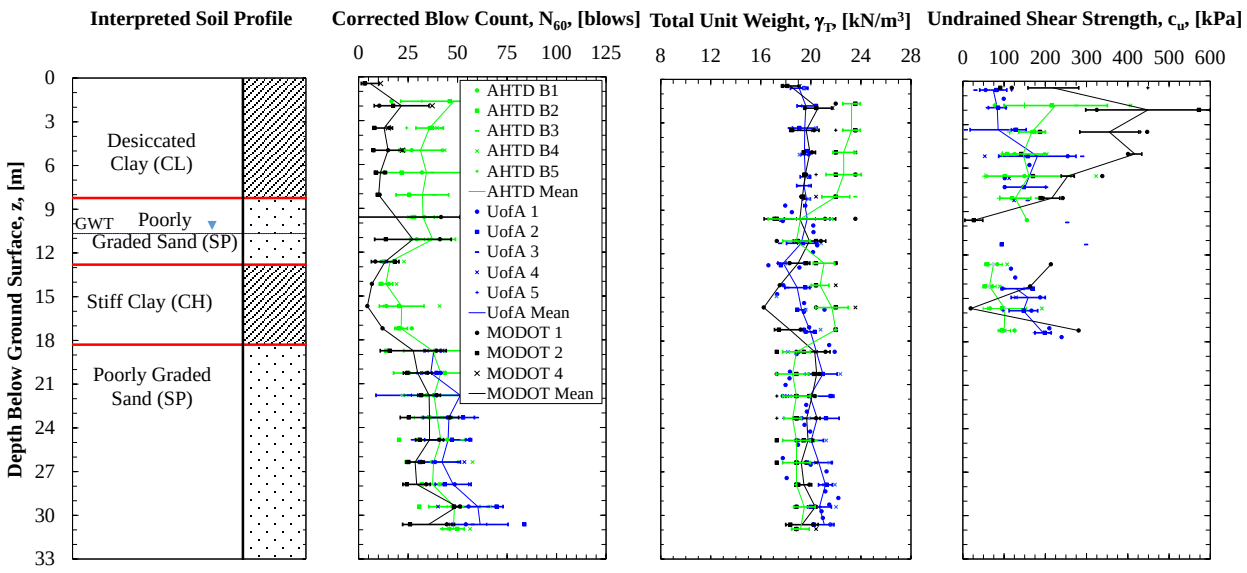

Figure 7.4. Soil properties determined at the MATS using the AHTD, MODOT, and UofA soil sampling methods (as modified from Race et al. 2015).

7.6. Drilled Shaft Foundation Construction

Three DSF were constructed by McKinney Drilling Company between September 23, 2014 and October 10, 2014. The site was located southeast of Monticello, Arkansas, at the intersection of the future Interstate 69 corridor and the Arkansas Midland Railway Company railroad tracks (33.595 Lat., -91.725 Long.). The combination of high plasticity top soil and several rain incidences led to a delay during the initial mobilization and a delay in the construction schedule (from August 18 to September 15 and October 2 to October 8), respectively.

On September 23, 2014, the drilling for the North 1.2m DSF (Table 7.3) was begun through a 5.5m long temporary casing with an outer diameter of 1.27m. On September 24, 2014, 1) the excavation was completed from a depth of 9.1m to a depth of 27.9m below the ground surface and 2) the rebar cage was instrumented with strain gages and a BLC. Upon reaching a depth of 27.9m there was a lack of polymer slurry due to the combination of 1) high permeability

cohesionless soils below a depth of 22.9m and 2) a limited amount of available water to add the polymer to make the polymer slurry (available water consisted of a half full, 75,708 liter water tank). Although more water was delivered to the site by the afternoon of the next day, the excavation remained open for an additional day (to a depth of 21.9m because the portion of the excavation from 21.9m to 27.9m was backfilled in an attempt to reduce the amount of outflow of the slurry). The backfill material was removed during the morning of September 25, 2014 and a Sonicaliper® was utilized to determine the profile of the excavated diameter prior to placement of the concrete into the excavation (Figure 7.5). The concrete was pumped to the bottom of the excavation through a 20.3cm inside diameter tremie. The average slump of the concrete was 20cm and the air content was consistently below 1.2 percent. The measured strength profile for the concrete, at the time of the BLC test, is presented in Figure 7.6 (unconfined compressive strength values near the required strength were measured for the concrete with slump values of 24.8cm).

Table 7.3. Geometric properties of the DSF constructed at the MATS.

DSF	Design Parameters		Constructed Parameters	
	Diameter [m]	Length [m]	Diameter [m]	Length [m]
North	1.2	27.9	1.33	27.9
Center	1.8	21.9	1.88	21.9
South	1.2	27.9	1.37[a]	28.0

[a]Assumed constructed diameter based on the outer diameter of the temporary casing

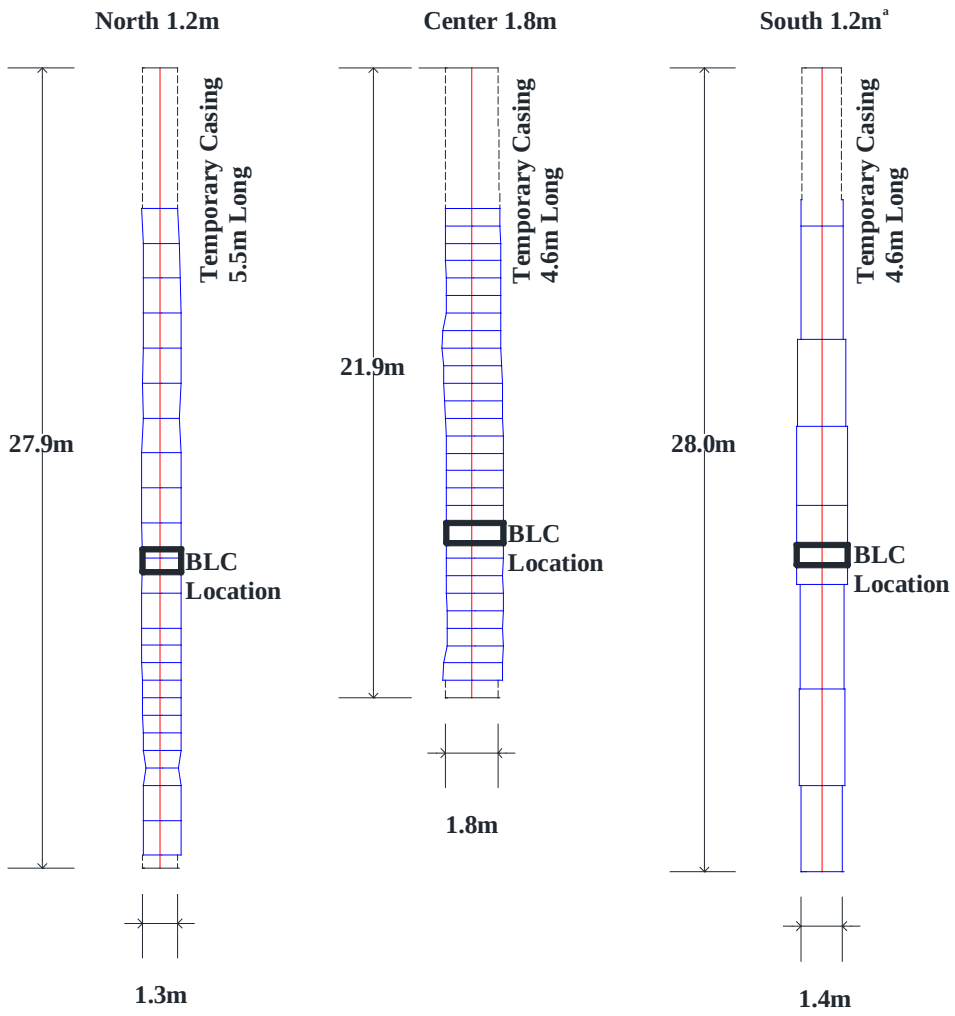

Figure 7.5. Excavation profile of the North 1.2m, Center 1.8m, and South 1.2m diameter DSF using the Sonicaliper® or concrete volume.

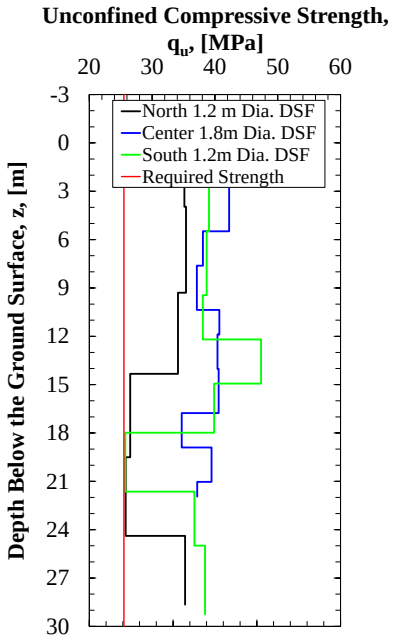

Figure 7.6. Concrete strength along the length of the various DSF at the MATS.

On September 29, 2014, the drilling for the Center 1.8m diameter DSF was started through a 4.6m long temporary casing with an outer diameter of 1.905m. The concrete was scheduled to be poured on the afternoon of September 30, 2014; however, the clean-out bucket sheared from the connection with the telescoping kelly bar, leaving the bucket at the bottom of the excavation (21.3m). After five hours, the bucket (minus the bottom closure plate) was retrieved using soil augers (61.0cm, 121.9cm, and 182.9cm diameters) and drilling commenced using the 121.9cm diameter clean-out bucket. Although the excavation was completed to the required depth on September 30, 2014, the only concrete supplier in the area was unable to deliver concrete until October 2, 2014 due to a prior scheduling conflict; however, the bottom plate of the bucket was retrieved during this delay. Two different Sonicaliper® profiles were measured, Pass 1 on October 1 and Pass 2 on October 2. There was negligible loss of slurry from the excavation while the excavation was open, to the final depth of 21.9m below the ground surface, which confirmed that the high permeability cohesionless soil layer was located below a

depth of 22.9m below the ground surface. As presented in Figure 7.7, there was a measured difference in the diameters of the two passes (larger measured diameter for Pass 2); however, the largest difference was only 3.4 percent (Table 7.4). On October 2, 2014, concrete was pumped to the bottom of the Center 1.8m diameter DSF excavation after the DSF excavation was cleaned out using a 121.9cm diameter clean-out bucket. The slump of the concrete ranged from 12.7cm to 19.7cm and the air content ranged from 0.8 to 1.7 percent. Similarly, the unconfined compressive strength profile (at the time of the BLC test) as a function of depth for the Center 1.8m diameter DSF was previously presented in Figure 7.6.

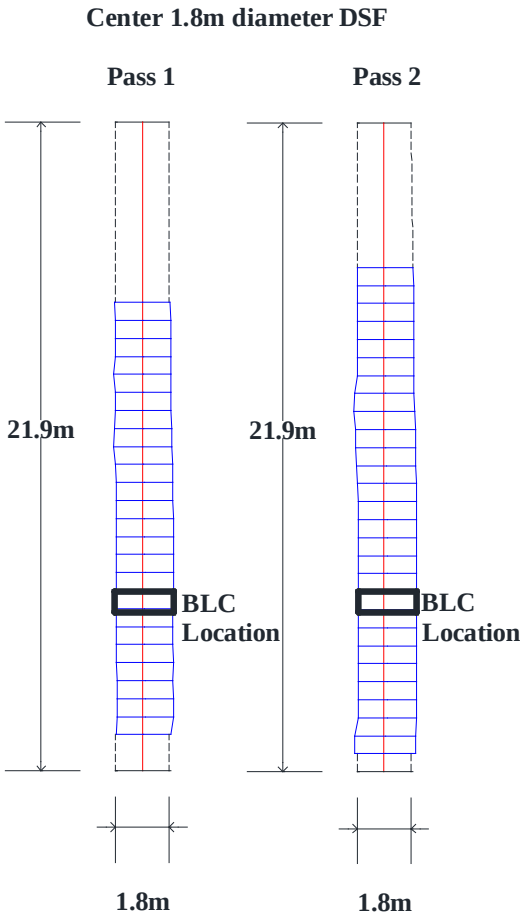

Figure 7.7. Excavation profile of the Center 1.8m diameter DSF for Pass 1 and Pass 2 of the Sonicaliper®.

Table 7.4. Diameter of the Center 1.8m DSF excavation as measured using the Sonicaliper®.

Depth Below Ground Surface (m)	Average Diameter (cm)		Percent Difference (%)
	Pass 1	Pass 2	
6.1 to 9.1	186.9	191.1	2.6
9.1 to 12.2	192.9	199.3	3.3
12.2 to 15.2	192.9	199.0	3.2
15.2 to 18.3	191.4	197.4	3.1
18.3 to 21.9	191.3	197.8	3.4

On October 1, 2014, the drilling for the South 1.2m diameter DSF was started in an attempt to efficiently drill and pour the final two DSF within three days. Because there was only one water tank (75,708 liters) and because the slurry that was within the Center 1.8m diameter DSF had to be recaptured into the tank, the amount of slurry required within the Center 1.8m (57,645 liters) and the South 1.2m DSF (18,063 liters) excavation was the limiting factor to the maximum depth of drilling for the South 1.2m DSF. The excavation for the South 1.2m diameter DSF was advanced to a depth of 17.9m below the ground surface on October 1, 2014 to ensure an adequate amount of slurry for an emergency loss of slurry in either of the open excavations. On October 2, 2014, at the time of completion of the Center 1.8m DSF, heavy rain forced personnel off of the site and prevented completion of the South 1.2m DSF. Prior to evacuation of the site, the South 1.2m DSF excavation (drilled to a depth of 25.9m) was subsequently backfilled to a depth of approximately 17.9m below the ground surface. The site remained impassable until October 8, 2014.

When drilling recommenced on October 8, 2014, the bottom of the drilling bucket was lost at a depth of approximately 19.8m within the excavation. An attempt was made to retrieve the bottom of the bucket using a 61.0cm soil auger. The 61.0cm soil auger was also utilized to advance the excavation to the design depth. The final depth of the excavation was 28.0m below the ground surface. At this time, the slurry level was approximately 9.8m below the ground

surface (located below the first 1.5m thick layer of cohesionless soil). The Sonicaliper® was used to determine the shape of the excavation prior to concrete placement; however, due to time constraints and lack of slurry within the excavation (specifically within the casing), the results obtained from the Sonicaliper® were meaningless because a calibration factor could not be obtained within a slurry filled casing. However, differences in the diameter of the excavation were calculated, using the amount of volume added to the excavation from each of the concrete trucks from depths of 28.0m to 9.45m below the ground surface (as presented previously in Figure 7.5). The excavation of the South 1.2m diameter DSF, presented previously in Figure 7.5, increased in diameter in the middle of the excavation (particularly for trucks 4 and 5) which may indicate a possible collapse due to a low slurry head (minimum of 3.0m).

Because no polymer was available after the weather interruption, water without any polymer was added to the excavation, due to the loss of polymer slurry into the formation surrounding the South 1.2m diameter DSF excavation during the weather delay. During the afternoon of October 10, 2014, concrete was pumped to the bottom of the excavation through a 20.3cm diameter tremie. The concrete began arriving at 15:00; however, the tremie was not ready for use until 16:00. Poor timing of the concrete trucks by the concrete plant resulted in the arrival of all four of the trucks that were utilized for the project to arrive within five minutes of the first truck (Table 7.5).

Table 7.5. Timing of the batching and placement for the concrete in the South 1.2m diameter DSF.

Batch Time	Placement Time	Difference in Time	Depth (m)	Slump After Water Added (cm)	Strength (MPa)
14:10	16:00	1:50	28.0 to 25.0	15.2	33.8
14:00	16:20	2:20	25.0 to 21.6	12.7	32.6
14:20	16:40	2:20	21.6 to 18.0	22.9	24.3
14:30	17:50	2:20	18.0 to 14.9	16.5	34.9
16:40	18:00	1:20	14.9 to 12.2	12.7	40.5
16:50	18:15	1:25	12.2 to 9.4	12.7	33.6
16:55	18:20	1:25	9.4 to 5.5	20.3	34.0
17:05	18:30	1:25	5.5 to 1.5	16.5	34.3
17:20	18:45	1:25	1.5 to 0.0	12.7	35.8

These problems associated with the poor timing were exacerbated by the initial slumps of the concrete being between 5.1cm and 10.2cm (well below the required 17.8cm slump). Although make-up water was added to each concrete truck (between 38 and 303 liters), to prevent the set and enable smoother flow of the wet concrete through the pump truck (attempted a slump of 15.2cm initially as previously presented in Table 7.5), some of the concrete prematurely setup while the concrete was within the concrete pump truck. Specifically, the concrete poured between depths of 18.0m to 19.8m was suspected to have setup before being placed into the excavation. While the bad concrete was removed from the pump truck, the tip of the tremie remained at a depth of 16.5m below the surface of the poured concrete. Like the strength profiles for the other DSF, the strength profile of the concrete that was used within the South 1.2m diameter DSF (not accounting for the lower compressive strength due to the premature setup of the concrete within the pump truck and within the DSF because the cylinders were obtained prior to adding the concrete to the pump truck) is presented in Figure 7.6. The unconfined compressive strength values were near the required strength for the concrete with slump values of 22.9cm.

7.7. Design Considerations

Construction methods directly affect the performance and properties of a DSF. This performance includes, but is not limited to, the load-movement response, the unit side resistance, and the end bearing resistance. The construction problems discussed in Table 7.6, including: open excavation/loss of slurry, concrete slump and strength, equipment failure, DSF diameter, and premature setup of concrete, will be presented and discussed in relation to the performance of the respective DSF that was observed during the full-scale load testing. The effects of some of the construction problems such as the loss of slurry and an open excavation are indiscernible due to the influence of the other construction problems. The performance measurements that will be discussed to determine the effects of the construction problems include the: upward and downward movement of the BLC, top-down load-settlement response, load transfer along the length of the DSF, unit side resistance, and unit end bearing resistance. Design considerations will also be presented and discussed with regard to the effects of the geotechnical investigation method on 1) the predicted the load-movement response and on 2) the unit side resistance for the respective DSF.

Table 7.6. Summary of the problems occurring during construction of the DSF at the MATS.

North 1.2m	Center 1.8m	South 1.2m
• Open excavation for 2 days • Significant loss of polymer slurry • High slump concrete	• Open excavation for 3.5 days • Clean-out bucket lost within the excavation but was eventually removed • Bottom of the excavation was cleaned using 1.2m diameter clean-out bucket instead of 1.8m diameter clean-out bucket due to the bucket damage for the 1.8m diameter bucket	• Open excavation for 8 days • Unknown amount of slurry loss within the excavation during this time • Bottom of the drilling bucket was lost in the excavation the bucket was removed but the plate remained in excavation • Possible collapse within the excavation • Premature setup of concrete during placement

7.7.1. Loss of Slurry

During the two hours that there was no slurry within the water tank to provide to the excavation, the slurry level within the excavation dropped 7.0m without ongoing drilling activities within the excavation, for the North 1.2m diameter DSF. The 7.0m drop in the level of the polymer slurry (POLY-BORE^{TM} IDP-620) corresponded to a cost of $170 USD for the dry polymer slurry. However, there appeared to be no excavation collapses within the soil of the North 1.2m diameter excavation overnight due to the loss of polymer slurry.

In the bottom of the South 1.2m diameter DSF excavation, there may have been a partial collapse, but it was not confirmed due to the excavation overdrilling that was associated with the loss of equipment and the unreliable Sonicaliper® data. As discussed in Race and Coffman (2015), a partial collapse of the excavation for a DSF may cause larger movement values (on the order of 2.5 to 3 times) at the required load. In this case, the measured top-down equivalent movement at the required axial capacity was 2.9cm for the South 1.2m diameter DSF as compared to 0.8cm for the North 1.2m diameter DSF. In the event of collapse within the excavation for a DSF, as associated with the loss of polymer slurry from within the excavation, 1) another DSF would have to be constructed, 2) the axial capacity would decrease, or 3) the DSF excavation would have to be overdrilled. The cost of loss of slurry within any size DSF excavation may range from the cost of the extra slurry to the cost of an additional DSF depending upon the extent of the damages on the DSF resistance that result from the loss of slurry into the formation. By considering the costs associated with extra dry polymer slurry and labor, the excess cost could be as high as of $2,000 USD per DSF (not including the estimated cost of $10,000 per day associated with the use of the drilling equipment).

7.7.2. Concrete Slump and Strength

As presented in Chang et al. (2008), the strength and consequently the modulus of elasticity of the concrete within a DSF can affect the load-movement response of the DSF. The amount of slump of the concrete, at the time of placement, and the unconfined compressive strength of the concrete, at the time of the BLC test, for the North 1.2m DSF were higher and lower, respectively, than the corresponding properties of the concrete for the South 1.2m diameter DSF (Table 7.7). The concrete unconfined compressive strength in the North 1.2m and South 1.2m diameter DSF at depths of approximately 18.0m to 24.0m was only slightly above the required strength of 24.1MPa. As presented in Figure 7.8, the amount of upward movement of the BLC for the North 1.2m DSF was greater than the amount of upward movement for the South 1.2m DSF at a nominal load value of 5.9MN (3.0cm compared to 1.2cm).

Table 7.7. Properties of the concrete within the DSF at the MATS.

DSF	Initial Slump (cm)			Strength (MPa)		
	Minimum	**Maximum**	**Average**	**Minimum**	**Maximum**	**Average**
North 1.2m	19.1	25.4	21.8	25.6	35.4	32.0
Center 1.8m	12.7	19.7	16.3	37.0	42.3	38.7
South 1.2m	7.6	22.9	15.6	24.3	40.5	33.7

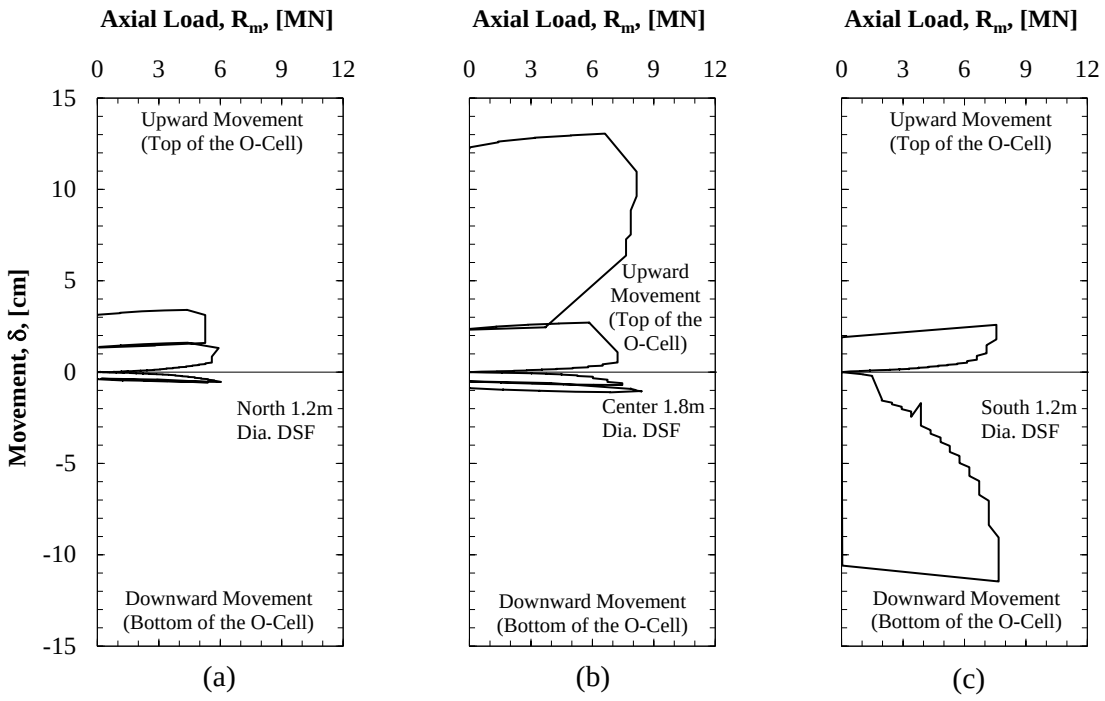

Figure 7.8. Upward and downward movements of the BLC for the a) North 1.2m, b) Center 1.8m, and c) South 1.2m diameter DSF at the MATS.

The more instantaneous failure of the upper portion of the North 1.2m diameter DSF (3.1cm of movement), as compared with the South 1.2m diameter DSF (0.4cm of movement), at a nominal load of 5.2MN, were partially attributed to the lower strength and higher slump values for the concrete in the North 1.2m diameter DSF (Figure 7.9). Specifically, the upward movement values of the BLC were directly related to the slump values, and the upward movement values were inversely related to the average concrete strength above the BLC. In this case, even when considering the low workability of the concrete in the South 1.2m diameter DSF, a higher average unconfined compressive strength of the concrete led to more resistance between the DSF and the soil and less measured upward movement of the BLC. Similarly, the amount of load transfer (7.6MN at a movement of 2.59cm) resisted by the DSF above the BLC

for the South 1.2m diameter DSF was significantly greater than the amount of load transfer (5.9MN at a movement of 3.4cm) resisted by the North 1.2m diameter DSF (Figure 7.10).

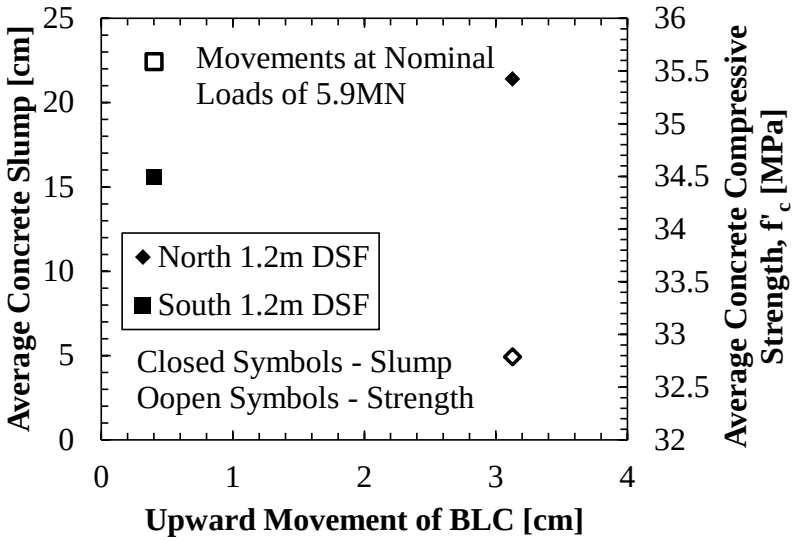

Figure 7.9. Measured upward movement values above the BLC as a function of the average concrete slump and the average concrete compressive strength.

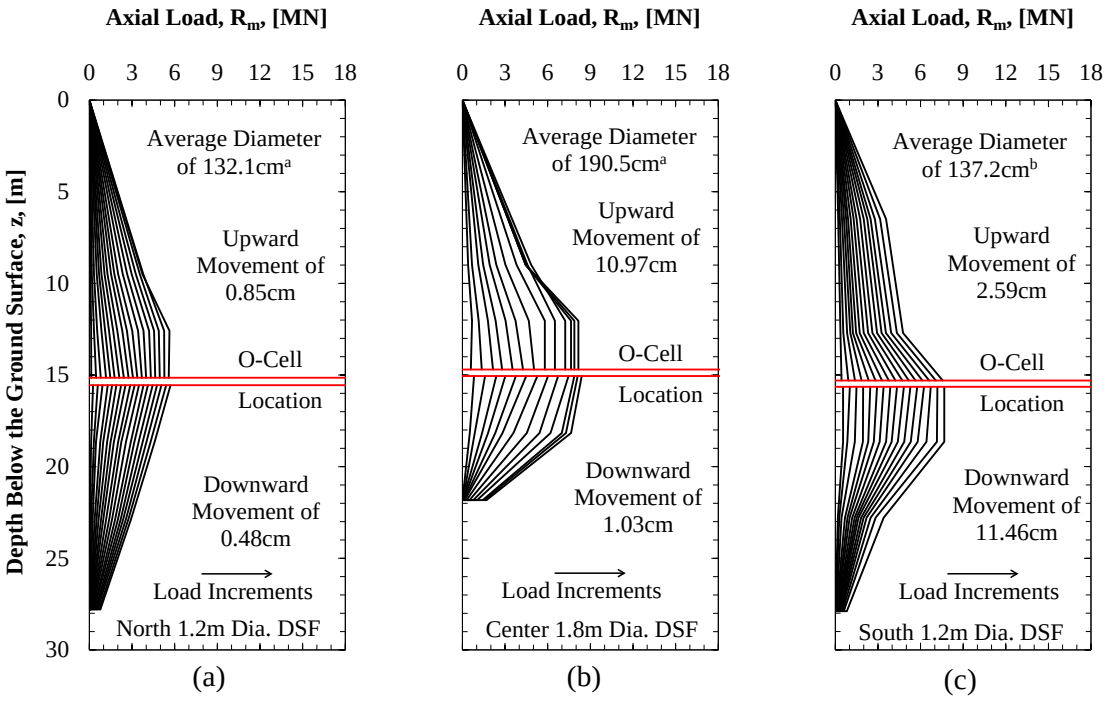

[a]Averaged from the Sonicaliper® Data.
[b]Approximated from the diameter of the temporary casing.

Figure 7.10. Load transfer along the length of the a) North 1.2m, b) Center 1.8m, and c) South 1.2m diameter DSF at the MATS.

7.7.3. Equipment Failure

Effects from equipment failure may include extraction of the clean-out bucket causing 1) damage to the side walls or 2) improper cleaning at the bottom of the excavation. To determine the difference of the amount of end bearing resistance between the Center 1.8m and North 1.2m diameter DSF, it was assumed that the cohesionless soil at the tip of the Center 1.8m diameter DSF and the cohesionless soil at the tip of the North 1.2m diameter DSF were the same. The average raw blow count values determined at depths of 21.9m and 27.9m for the Center 1.8m diameter DSF and the North 1.2m diameter DSF were 29 and 30, respectively, but the estimated amount of overburden pressure was 303.6kPa and 368.2kPa, respectively. The unit end bearing resistances were 0.58MPa and 0.24MPa at a downward movement of 0.5cm for the North 1.2m and Center 1.8m diameter DSF, respectively (Figure 7.11). The discrepancy in the unit end bearing values was either due to the inadequate clean-out method of the Center 1.8m diameter DSF, a scaling factor for unit end bearing resistance in cohesionless soil for different diameter DSF, a correction for the overburden pressure, or a combination of the three.

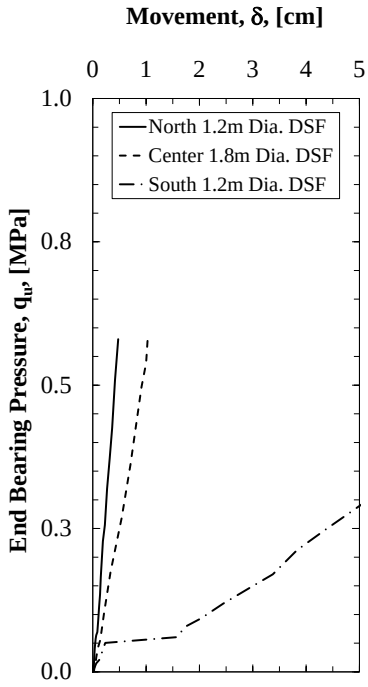

Figure 7.11. Unit end bearing resistance at the base of the DSF at the MATS.

The bottom plate of the soil drilling bucket was permanently lost at the bottom of the excavation while drilling of the South 1.2m diameter DSF. Unlike the loss of the bottom of the clean-out bucket at the bottom of the excavation for the Center 1.8m diameter DSF, the bottom of the bucket was not lost at the bottom of the excavation for the South 1.2m diameter DSF, but was lost at approximately 21.3m below the ground surface. When drilling to the design length using a soil auger, the bucket bottom was pushed to the bottom and side of the excavation. Because the bucket bottom was within the excavation while drilling, the drilling tools were utilized to inadvertently increase the diameter of the bottom portion of the excavation.

7.7.4. Diameter of DSF

As presented previously in Figure 7.8, at a nominal load of 5.9MN, the amounts of upward movement for the Center 1.8m and South 1.2m diameter DSF were less than the amount of upward movement for the North 1.2m diameter DSF. The depth to the top of the BLC for the

North 1.2m diameter DSF and the South 1.2m diameter DSF were within 0.3m of each other (with the top of the BLC for the South 1.2m diameter DSF being slightly higher). The diameter of the South 1.2m diameter DSF was at least 5.1cm greater than the diameter of the North 1.2m diameter DSF. Therefore, the greater nominal load measured for the South 1.2m diameter DSF (7.6MN) as compared to the North 1.2m diameter DSF (5.9MN), before excessive movement (greater than 3.0cm) of the top of the DSF, was attributed to the larger diameter of the South 1.2m diameter DSF.

The unit side resistance values, at a movement values of 0.8cm upward and 0.5cm downward (largest movement values for the North 1.2m diameter DSF), are presented in Table 7.8. Except for depths between 18.3m to 21.3m, the unit side resistance values that were measured for the North 1.2m diameter DSF were greater than the corresponding unit side resistance for the Center 1.2m diameter DSF (Figure 7.12). On average, the unit side resistance values for the North 1.2m diameter DSF are 17.3 percent greater than those for the Center 1.8m diameter DSF.

Table 7.8. Unit side resistance values for the North 1.2m and Center 1.8m DSF.

Approximate Depth of Measurement (m)	**Unit Side Resistance (kPa)**	
	North 1.2m DSF	**Center 1.8m DSF**
0.0 to 9.1[a]	94.5	88.0
9.1 to 12.2[a]	148.1	121.5
12.2 to 15.2[a]	40.7	33.0
15.2 to 18.3[b]	85.6	73.3
18.3 to 21.3[b]	93.3	202.8

[a]At 0.8cm of upward movement
[b]At 0.5cm of downward movement

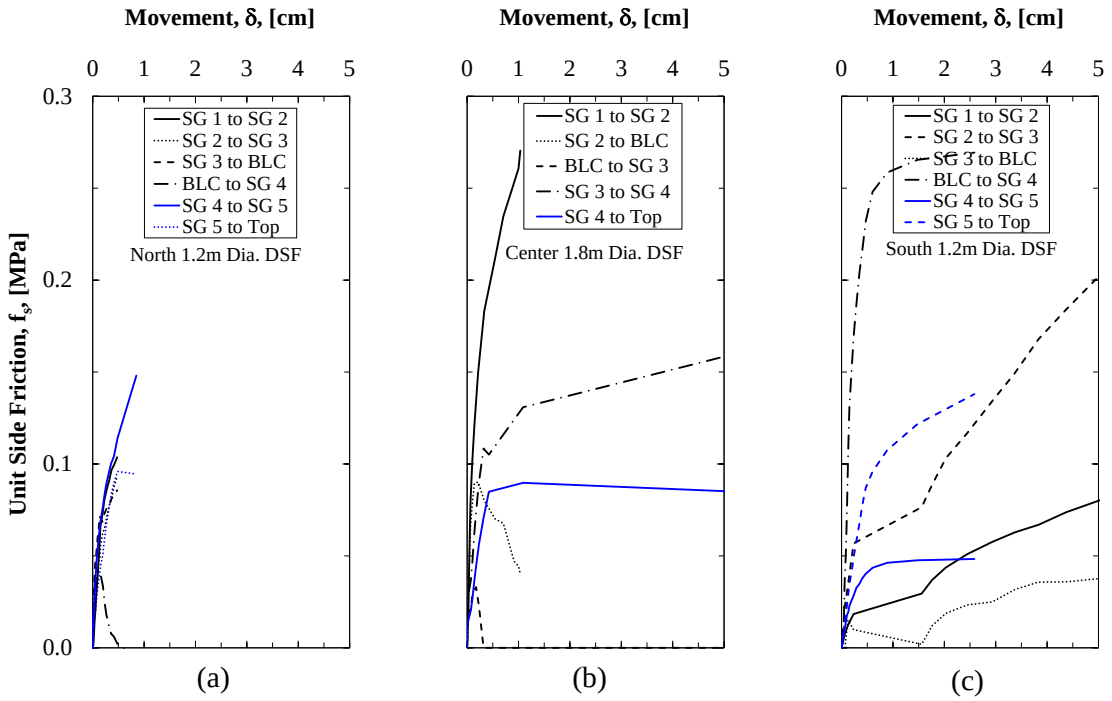

Figure 7.12. Unit side resistance along the length of the a) North 1.2m, b) Center 1.8m, and c) South 1.2m diameter DSF at the MATS.

7.7.5. Delayed Pour of Concrete

According to the cross-hole sonic logging test performed on the South 1.2m DSF, there was an anomaly in the concrete below the BLC at a depth of 17.1m, 17.7m, and 21.3m below the ground surface (GEI Consultants, Inc. 2014). Therefore, there was a weaker section of the DSF at a depth of approximately 17.1m below the BLC which caused the large downward movements and large differential movements across the bottom plate of the BLC. Due to this phenomenon, the amount of top-down equivalent movement required to achieve required loading was almost three times greater for the South 1.2m diameter DSF (2.9cm) than for the North 1.2m diameter DSF (0.8cm).

The unit side resistance values that were measured below the BLC were higher than the corresponding values that were measured for the North 1.2m diameter DSF; however, the diameter for the South 1.2m diameter DSF was not verified using the Sonicaliper®. The maximum unit side resistance values that were calculated, by using various diameter sizes (that were representative of the values that were computed from the concrete volumes), are presented in Table 7.9. Less side resistance was measured by the soil near the BLC as the diameter of the DSF was increased. The anomaly within the South 1.2m diameter DSF did not prevent the axial capacity of the DSF from being attained before a movement value of 6.1cm (5% of the diameter) for the strength limit state as presented in Figure 7.13. However, as shown in Figure 7.12, the required axial capacity was achieved for the North 1.2m diameter DSF and for the Center 1.8m diameter DSF prior to reach a movement value of 0.8cm, but the required axial capacity was not achieved for the South 1.2m diameter DSF prior to reaching a movement value of 1.3cm (the service limit state).

Table 7.9. Variation in unit side resistance values with regards to DSF diameter.

Depth (m)	Unit Side Resistance (kPa)			
Different Diameter Values (m)[a]	**1.37**	**1.52**	**1.68**	**1.83**
0.0 to 6.1[b]	147.2	161.4	175.7	190.1
6.1 to 12.5[b]	51.6	56.5	61.5	66.6
12.5 to 15.2[b]	182.6	65.3	23.6	0.0
15.2 to 18.6[c]	4.0	0.0	0.0	0.0
18.6 to 22.9[c]	210.3	146.5	90.2	39.5
22.9 to 27.7[c]	135.8	148.7	161.7	174.9

[a]Varying the diameter size in increments of 0.15m
[b]Value for an upward movement of 2.6cm
[c]Value for a downward movement of 11.5cm

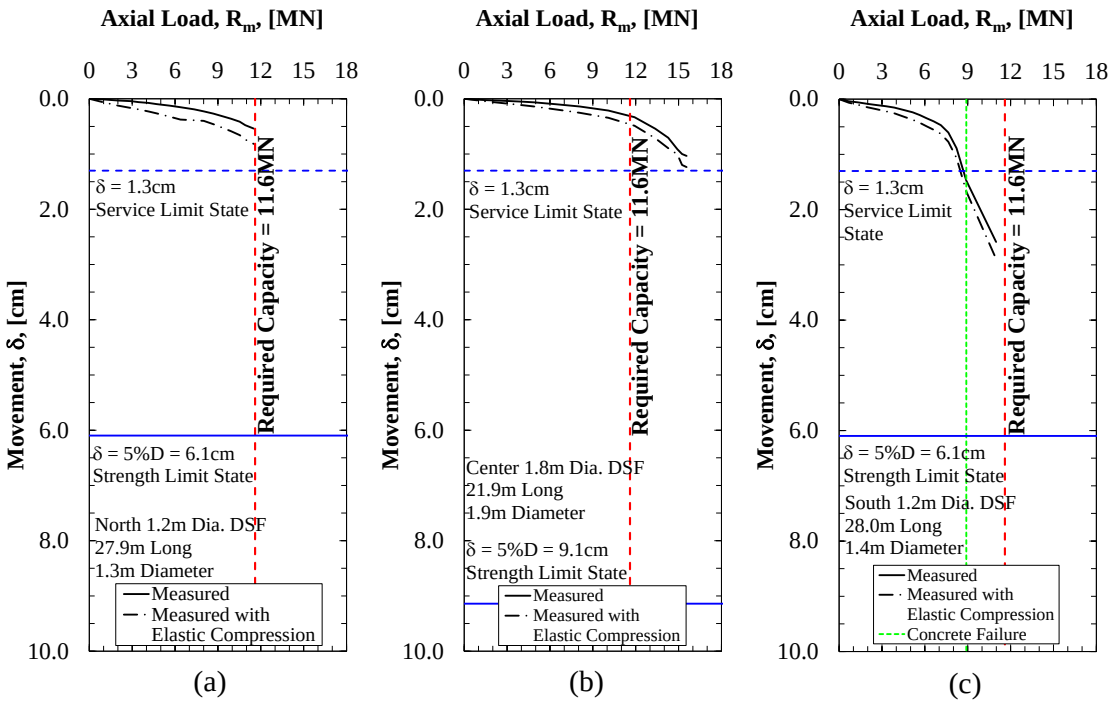

Figure 7.13. Equivalent top-down load-settlement response of the a) North 1.2m, b) Center 1.8m, and c) South 1.2m diameter DSF at the MATS.

Although it is not necessary to achieve the required capacity prior to a movement of 1.3cm (like was achieved for the North 1.2m and the Center 1.8m diameter DSF), it was determined that the reason the South 1.2m diameter DSF did not reach the required axial capacity prior to a movement value of 1.3cm was because of concrete crushing. Specifically, the

axial capacity of the South 1.2m diameter DSF at the initial concrete crushing was determined to be 8.9MN (77 percent of the required load). The measured downward movement values increased by 567 percent at load interval number four (from a movement value of 0.23cm to a value of 1.56cm). Specifically, the top-down equivalent crushing capacity was determined by adding the nominal load at the downward movement at the time of concrete crushing with the nominal load for the same amount of upward movement. After a movement of 1.5cm and a top load of 8.9MN, the excess movement during the BLC test of the South 1.2m DSF was a result of the concrete crushing.

The total side resistance values that were obtained for the DSF section located below the BLC (at approximate downward movements of 0.45cm) were much less for the South 1.2m diameter DSF (1.58MN) than for the North 1.2m diameter DSF (5.71MN). The predicted phenomenon of the resisted load along the length of the DSF without and with a void is presented in Figure 7.14. Because of the presence of the void, less load is resisted by the soil below the void (both side resistance and end bearing resistance) as presented in Figure 7.15a. However, the top of the South 1.2m DSF was not equally affected by the premature setup of the concrete. The measured unit side resistance values in the desiccated clay, above the BLC, were similar in magnitude for each DSF (Figure 7.15b). For upward movement values less than 0.8cm, the unit side resistance values for all three DSF at the MATS were approximately equal; however, the curves diverged thereafter.

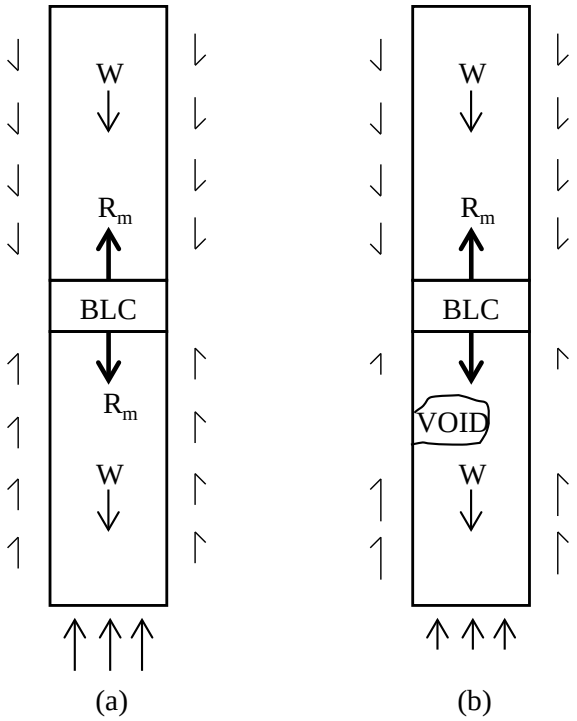

Figure 7.14. Schematic of a BLC test for the a) North 1.2m and b) South 1.2m diameter DSF at the MATS.

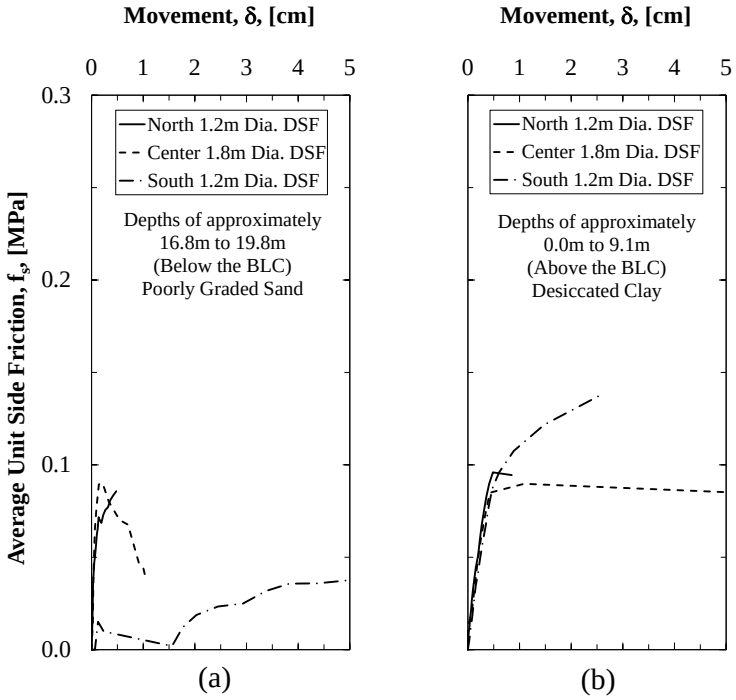

Figure 7.15. Comparison of the unit side resistance for the DSF at the MATS a) below the BLC and b) at the top of the DSF.

7.7.6. Predicted Load-Movement Response

As presented in Figure 7.16, the load-movement responses were predicted using the FB-Deep software program and the data obtained from the three geotechnical investigation methods. For the North 1.2m diameter DSF, the predicted responses that were obtained by utilizing the different soil sampling and testing methods slightly underpredicted the amount of movement when compared to the measured equivalent top-down load-movement response. Specifically, almost all of the predicted movement values for load values of less than 10MN were smaller than the measured movements. However, near the required capacity, the measured movement values were within 0.8 percent and 11.7 percent of the movement values that were predicted using the data obtained from the AHTD and UofA geotechnical investigation methods, respectively. The predicted load values, as obtained by using the MODOT method, were consistently greater than the measured data for the same amount of movement. However, for the Center 1.8m diameter DSF, the load-movement curve was best predicted by using the MODOT data. At the required capacity for the Center 1.8m diameter DSF, the measured movement values that were observed, and the values that were predicted using AHTD, MODOT, and UofA methods were 0.40cm, 1.05cm, 0.36cm, and 1.12cm, respectively.

Because the integrity of the South 1.2m diameter DSF was compromised, there were larger movements in the measured equivalent top-down load-movement response. Specifically, the measurement movement values, at the required capacity were 630.0, 307.4, and 210.6 percent larger than the predicted movement values that were obtained by utilizing the AHTD, MODOT, and UofA methods, respectively. Likewise, at the service limit state for the South 1.2m diameter DSF that was really 1.4m in diameter (1.27cm of movement), the measured axial capacity values were 50 to 70 percent greater than the predicted axial capacity values.

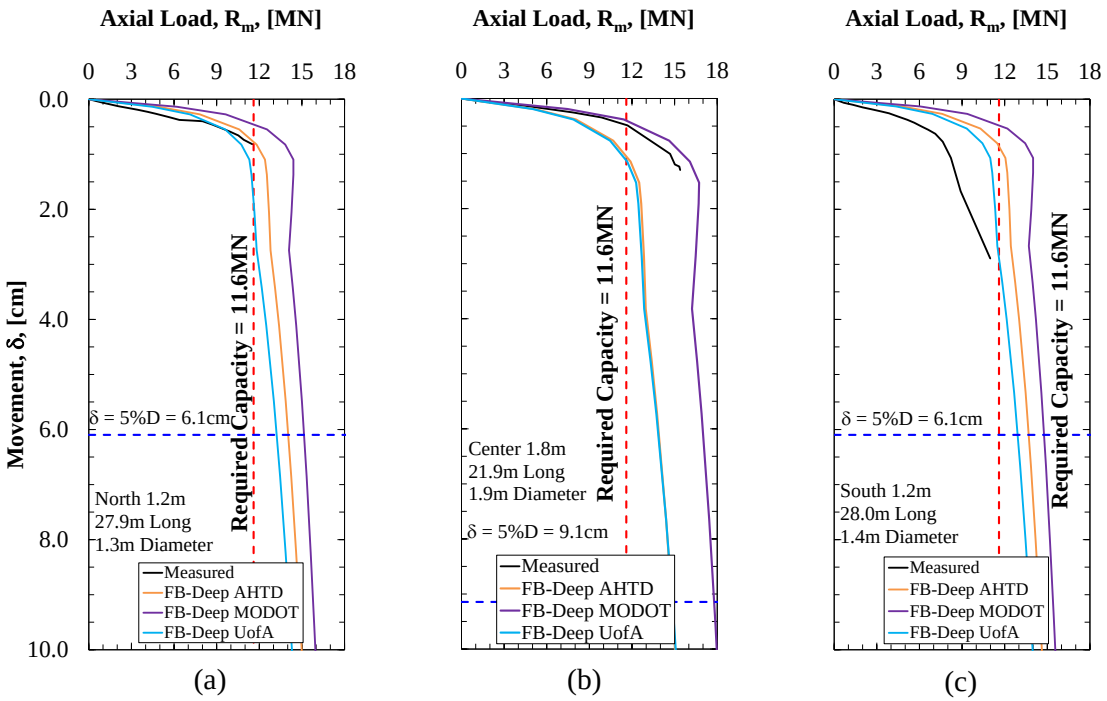

Figure 7.16. Predicted and measured load-movement response for the a) North 1.2m, b) Center 1.8m, and c) South 1.2m diameter DSF at the MATS.

7.7.7. Predicted Unit Side Resistance

The predicted unit side resistance values that were obtained by utilizing the FB-Deep program and the AHTD, MODOT, or UofA geotechnical investigation methods were compared to the measured unit side resistance values that were obtained from the BLC tests. As presented in Figure 7.17, the predictions of the unit side resistance values for cohesionless and cohesive soil for the North 1.2m diameter DSF best matched to the measured resistance values. However, there was not enough movement to determine the maximum unit side resistance of the cohesionless or cohesive soil for the North 1.2m diameter DSF; therefore, the closest estimate for the predicted unit side resistance cannot be determined from this test. From the maximum movement values that were observed during the test (0.5cm of upward movement and 0.8cm of downward movement), the unit side resistance values that were predicted by using the AHTD and UofA methods were the closest values to the measured unit side resistance values. From this

case study, the unit side resistance values for the soils at the MATS were not generalized at large movements due to the influence of the construction problems.

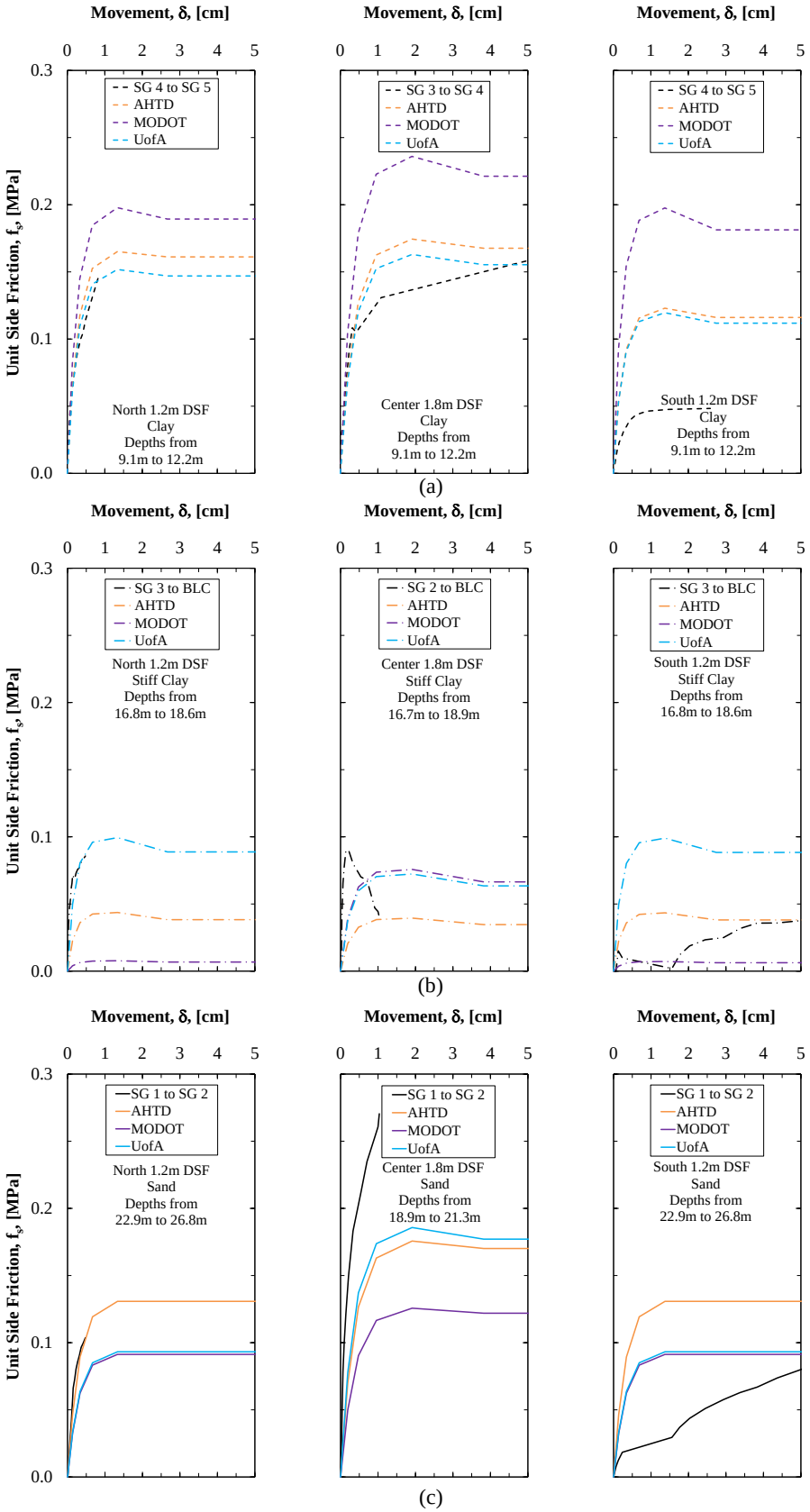

Figure 7.17. Predicted and measured unit side resistance values in a) sand, b) stiff clay, and c) clay for the North 1.2m, Center 1.8m, and South 1.2m (left to right) diameter DSF at the MATS.

For the Center 1.8m diameter DSF, within cohesionless soils, the measured unit side resistance values were higher than the predicted unit side resistance values for all movement values. Within the clay soil above the BLC for the Center 1.8m diameter DSF, the measured unit side resistance values did not level off after 2cm of movement, like the predicted unit side resistance values. As presented in Figure 7.17a, the measured unit side resistance values for cohesive soil that was located at the top of the DSF (above the BLC) were most closely predicted using the UofA method (at small movements), but were underpredicted at larger movement values when using the data obtained from all of the geotechnical investigation methods. The predicted values from the UofA data most closely represented the measured unit side resistance values in cohesionless soils. The predicted unit side resistance, as obtained using the data from the MODOT data, was not accurate in cohesionless soils because the MODOT method data only consisted of one single CPT record to a depth of 22.9m.

For the North 1.2m diameter DSF and the Center 1.8m diameter DSF, the unit side resistance response was most accurately modeled using the UofA method for cohesive soils (Figure 7.17a and b). In particular, for movement values less than 0.5cm, the measured unit side resistance values were predicted using the UofA method. For the unit side resistance values for the Center 1.8m diameter DSF, the unit side resistance values were lower than the predicted values for movement values that were greater than 0.5cm; however, in the clay located above the BLC, the unit side resistance linearly increased at larger movements instead of flattening out. The unit side resistance values that were predicted by using the AHTD and MODOT methods were higher than the measured values in desiccated clay (located above the BLC), but were lower in stiff clay (located near and below the BLC) at the MATS. The unit side resistance values that were measured near the BLC, in cohesive soil for the South 1.2m diameter DSF, were

lower than the predicted values (except within the stiff clay as obtained by using the data from the MODOT method).

As presented in Table 7.10, the percentage of load resisted by end bearing ranged from 1.9 to 10.8 percent for the measured data. The predicted amount of load that should have been resisted in end bearing, as obtained from the FB-Deep software program, ranged from 2.9 to 18.5 percent of the measured load at corresponding movement values. For the North 1.2m diameter DSF and for the Center 1.2m diameter DSF, the measured percentage resisted in end bearing was greater than the predicted percentage resisted in end bearing by using all of the geotechnical investigation data (AHTD, MODOT, UofA).

Table 7.10. Percentage of the measured and predicted load transferred to end bearing.

Test Shaft			Resistance Distribution (MN [%])	
			Side Shear	**End Bearing**
North 1.2m	Measured		10.21 [92.9]	0.78 [7.1][a]
	FB-Deep	AHTD	9.87 [95.9]	0.42 [4.1]
		MODOT	11.84 [97.1]	0.36 [2.9]
		UofA	8.86 [94.9]	0.47 [5.1]
Center 1.8m	Measured		13.93 [89.2]	1.69 [10.8][b]
	FB-Deep	AHTD	11.06 [92.9]	0.84 [7.1]
		MODOT	15.36 [95.6]	0.71 [4.4]
		UofA	10.76 [92.2]	0.91 [7.8]
South 1.2m	Measured		11.25 [98.4]	0.18 [1.6][c]
	FB-Deep	AHTD	11.03 [84.9]	1.96 [15.1]
		MODOT	12.60 [88.3]	1.66 [11.7]
		UofA	9.81 [81.5]	2.22 [18.5]

[a]Movement of 0.4%D
[b]Movement of 0.6%D
[c]Movement of 2.3%D

7.8. Recommendations Based on Case Study Observations

It is recommended that DSF that are constructed in cohesionless soil with high values of permeability be drilled and poured in one day or utilize bentonite slurry (rather than polymer slurry), if appropriate. By drilling and pouring in a single day, an open excavation may be

maintained and a significant loss of slurry may be prevented. Conversely, by requiring that the DSF is poured in a single day, there may be a rush to pour concrete that may lead to improper concrete truck scheduling and improper concrete placement. Although bentonite slurry was not used for this project, bentonite slurry may be utilized instead of polymer slurry when drilling in high permeability, cohesionless soils. However, it should be noted that the unit side resistance of the DSF will decrease and, therefore, the depth of the DSF will need to be increased to achieve the same required load. Therefore, additional DSF should be constructed using bentonite slurry technicques, at the MATS, and tested to determine the effects of the bentonite slurry.

Although the stress within the concrete with a reduced cross-section (i.e. poor placement) may not be so large as to fail the DSF at the required load, a larger top movement results from the reduced cross-section and there is a greater probability of failure of the foundation. It is recommended that the concrete have a slump of at least 12.7cm at the time of pouring to prevent weak pockets of concrete within a DSF that contains internal instrumentation. Similarly, it is recommended that the time between batching and placing the concrete within the DSF be limited to two hours unless a chemical retardant is added to the concrete during batching. It is recommended the water added to the concrete after batching be limited to 37.9 liters. These limits are recommended to avoid low strength concrete that would result from the on-site addition of water being used to delay the setup of the concrete. Specifically, these recommendations related to the concrete placement are recommended for use in a DSF to prevent major construction problems that may lead to failure of the foundation from excessive movement.

Other problems such as the loss of a clean-out bucket or the bottom of a soil drilling bucket should be minimized; however, as shown in this case history, the loss of a plate for a

cleanout bucket appeared to only slightly impact the total capacity of the DSF. For a DSF that is designed primarily rely upon end-bearing to reach the required capacity, it is recommended that the DSF should be load tested to at least the service limit state capacity (required capacity or 1.27cm of movement) because the unit end resistance when utilizing a smaller clean-out bucket was observed to decrease at the MATS. In lieu of a load test on an end-bearing DSF, it is recommended that the required capacity be decreased by 70 percent when improper equipment is utilized to construct a DSF.

For a DSF with minor construction problems, the load-movement curve was predicted using the FB-Deep software program. However, for a DSF with major construction problem(s) such as problems with the poor integrity concrete, it is recommended that the axial capacity value at the service limit be decreased by 70 percent. To predict the unit side resistance values at small movements, it is recommended that the FB-Deep software program be used in conjunction with the UofA method of acquiring samples from layered cohesive and cohesionless soils.

7.9. Conclusions

Although a DSF that is constructed to the exact design specifications without any construction problems is ideal in terms of time, cost, and reliability, this situation rarely occurs. If and/or when construction problems occur, it is necessary to address the related axial capacity issues to ensure that enough axial capacity available from the DSF. The construction problems that occurred while constructing the Center 1.8m diameter and the South 1.2m diameter DSF at the MATS included slurry loss, open excavation for excess time, high and low slump concrete, low strength concrete, equipment failure, varying DSF diameter size, and concrete placement delays. Effects of these construction problems included changes in the load distribution along the length of the respective DSF, higher measured than predicted values of movement, lower

measured than predicted values of unit side resistance, and lower measured than predicted values of unit end bearing resistance.

Based on the results obtained from the MATS, it is recommended that DSF be drilled and poured within a single day when the DSF is constructed within high permeability cohesionless soils that are present at a site. The cost savings associated with this requirement may be as high as $2000 per DSF for a 1.2m diameter DSF (including slurry and labor costs if any problems occur due to the loss of polymer slurry). Moreover, the placement of concrete within the South 1.2m DSF led to a reduced axial capacity at the service limit state, but the required capacity was still attained. The load-movement response and the unit side resistance response for DSF with major construction problems was not well predicted because the load-movement, the unit side shear-movement, and the unit end bearing-movement responses were less than the predicted responses that were obtained by using the FB-Deep software program with the geotechnical investigation data (AHTD, MODOT, or UofA).

7.10. Acknowledgements

The authors thank the Arkansas State Highway and Transportation Department, the Missouri Department of Transportation, ADSC – the International Association of Foundation Drilling, McKinney Drilling Company, GEI Consultants, Inc., Foundation Technologies, Inc., Halliburton, and Loadtest, Inc., for financial and/or in kind contributions.

7.11. References

American Society for Testing and Materials (2011) “Standard Practice for Thin-Walled Tube Sampling of Soils for Geotechnical Purposes.” Annual Book of ASTM Standards, Designation D1587, Vol. 4.08, ASTM, West Conshohocken, PA.

American Society for Testing and Materials (2012) “Standard Test Method for Mechanical Cone Penetration Tests of Soil.” Annual Book of ASTM Standards, Designation D3441, Vol. 4.08, ASTM, West Conshohocken, PA.

American Society for Testing and Materials (2011) “Standard Test Method for Standard Penetration Test (SPT) and Split-Barrel Sampling of Soils.” Annual Book of ASTM Standards, Designation D1586, Vol. 4.08, ASTM, West Conshohocken, PA.

American Society for Testing and Materials (2012) “Standard Test Method for Unconsolidated-Undrained Triaxial Compression Test on Cohesive Soils.” Annual Book of ASTM Standards, Designation D2850, Vol. 4.08, ASTM, West Conshohocken, PA.

Bey Sarah (2014) “Cost-benefit Analysis for Load Resistance Factor Design (LRFD) of Drilled Shafts in Arkansas.” M.S. Thesis, University of Arkansas, Fayetteville, Arkansas, pp. 410.

Chang N. and Nghiem H. (2008) “Drilled Shaft Axial Capacities Effects due to Anomalies.” Federal Highway Administration, FHWA-CEL/TD-08-008, pp. 148.

Race, M.L., Bey, S.M., Coffman, R.A. (2013). “‘Discussion of Implementation of LRFD of Drilled Shafts in Louisiana’ by Xinbao Yu, Murad Y. Abu-Farsakh, Sungmin Yoon, Ching Tsai, and Zhongjie Zhang.” Journal of Infrastructure Systems, Vol. 19, No. 3, pp. 351-353, doi:10.1061/(ASCE)IS.1943-555X.0000144.

Race, M.L. and Coffman, R.A. (2013). “Effect of Uncertainty in Site Characterization on the Prediction of Liquefaction Potential for Bridge Embankments in the Mississippi Embayment.” ASCE Geotechnical Special Publication No. 231, Proc. GeoCongress 2013: Stability and Performance of Slopes and Embankments III, San Diego, California, March, pp. 888-897.

Race M., Bey S., and Coffman R. (2015) “Statistical Analysis to Determine Appropriate Design Methodologies of Drilled Shaft Foundations.” Geotechnical and Geological Engineering Journal, DOI: 10.1007/s10706-015-9854-z.

Race, M. and Coffman, R. (2015). “Response of a Drilled Shaft Foundation Constructed in a Redrilled Shaft Excavation Following Collapse.” Deep Foundations Institute Journal, DOI:10.1179/1937525515Y.0000000003.

CHAPTER 8: Resistance Factor Calibration

8.1. Chapter Overview

In Load and Resistance Factor Design (LRFD) of drilled shaft foundations (DSF), a low national resistance factor was recommended due to the high variability of the national database (AASHTO 2007). One way to reduce the variability of the data, and to thereby increase the design resistance factor, is to calibrate resistance factor values from a localized database of full-scale tests on DSF. Localized calibration studies for DSF have occurred in states including Louisiana, Kansas, and Florida (Abu-Farsakh et al. 2010, Misra et al. 2007, McVay et al. 2002, respectively). In Arkansas, three DSF were constructed at three different test sites across the state. Because there was a small dataset for the design of DSF in Arkansas, the Bayesian updating method was utilized to determine "updated" distribution parameters based on the national database and a regional database from Louisiana/Mississippi.

The three geotechnical investigation methods were utilized at the three test sites and two different software programs were utilized to calculate the resistance factors for the state of Arkansas. Specifically, the geotechnical investigation methods, discussed in further detail in Chapter 4, were utilized within the software programs (FB-Deep and SHAFT) to determine the predicted amounts of resistance (total resistance, unit side resistance, and unit base resistance). Bias factor values for the resistance, corresponding to the ratio between the measured resistance and the predicted resistance, were calculated for each geotechnical investigation method and each software program. The bias factor values were then utilized as the "sample" dataset within the Bayesian updating method, in conjunction with the prior dataset, to determine the posterior parameter values. Finally, the Monte Carlo simulation method was utilized to determine the

resistance factor value for a reliability index of 3.0 (probability of failure of 0.001) from the posterior parameter values.

Resistance factor values were calculated for site-specific and geologic-specific design of DSF within the state of Arkansas By combining the Bayesian updating method and the Monte Carlo simulation method. Based on the results discussed in the enclosed paper, the resistance factor values calibrated for the state of Arkansas ranged from 0.57 to 0.97 in mixed soils depending upon the software program and the geotechnical investigation method that were used for the design of total resistance for DSF. The observed savings by employing the calculated site-specific resistance factor values was as high as $460,000 (approximately 29.7 percent of the estimated total foundation cost). Additional resistance factor values for site-specific and geologic-specific design of DSF within the state of Arkansas were calculated for total resistance, side resistance, and end bearing resistance (Appendix E).

Besides the resistance factor values calculated with the Bayesian updating method and the Monte Carlo simulation method, resistance factor values without using the Bayesian updating method, based on unit side resistance were calculated. It was recommended that for resistance factor calibration of unit side resistance of DSF, the method of load test (top-down, BLC, etc.) be considered when predicting the unit side resistance. Similarly, recommendations for the utilization of the Bayesian updating method in conjunction with the Monte Carlo simulation method included:

- employing the method for sites with low variability (site-specific calibration),
- obtaining at least ten different load tests on DSF from four different test sites (geologic-specific/state-wide calibration),

- collecting additional data from load tests on DSF constructed in moderately strong to strong limestone to develop calibrated resistance factor values, and
- applying resistance factor values along with "engineering judgment."

The paper enclosed within this chapter has been submitted to the Journal of Geotechnical and Geoenvironmental Engineering. The full reference for the paper is: Race, M.L., Bernhardt, M.L., and Coffman, R.A. (2015). "Utilization of a Bayesian Updating Method for Calibration of Resistance Factors." Journal of Geotechnical and Geoenvironmental Engineering, In Preparation.

8.2. Additional Information/Results

8.2.1. Literature Review/Background

Load factors (γ_{DL} and γ_{LL}) have been determined by Scott et al. (2003) utilizing the FOSM. The FOSM analysis was utilized by Scott et al. (2003) because the first two moments (mean and standard deviation) have been commonly utilized to characterize the transient load that had been modeled as a lognormal distribution. In Paikowsky (2004), the resistance factor values for DSF were determined using the FOSM and FORM methods (Figure 8.1). The resistance factor values that were determined by using the FORM method were 12.7 percent greater than the values that were obtained by using the FOSM method. The resistance factor values that were determined by using FOSM were calculated using Equation 8.1. Conversely, the Monte Carlo simulation method, an iterative process, has been used rather than the first-order methods, because the soil properties and the soil-shaft interaction behavior have been shown to be nonlinear (Hicher 1996, Guo 2013, Nanda and Patra 2014) and cannot be fully described by using the linear approximations that are contained within the FOSM and FORM methods (Nadim 2007).

$$\phi = \frac{\lambda_R \left(\gamma_{DL} \cdot \frac{Q_{DL}}{Q_{LL}} + \gamma_{LL}\right) \sqrt{\frac{1 + COV_{DL}^2 + COV_{LL}^2}{1 + COV_R^2}}}{\left(\lambda_{DL} \cdot \frac{Q_{DL}}{Q_{LL}} + \lambda_{LL}\right) \exp\left(\beta \sqrt{\ln[(1 + COV_R^2)(1 + COV_{DL}^2 + COV_{LL}^2)]}\right)}$$

(Yoon and O'Neill 1997)

Equation 8.1

The variables that are presented in Equation 8.1 include: the coefficient of variation of the dead load (COV_{DL}), the coefficient of variation of the live load (COV_{LL}), the coefficient of variation of the resistance (COV_R), and the reliability index (β).

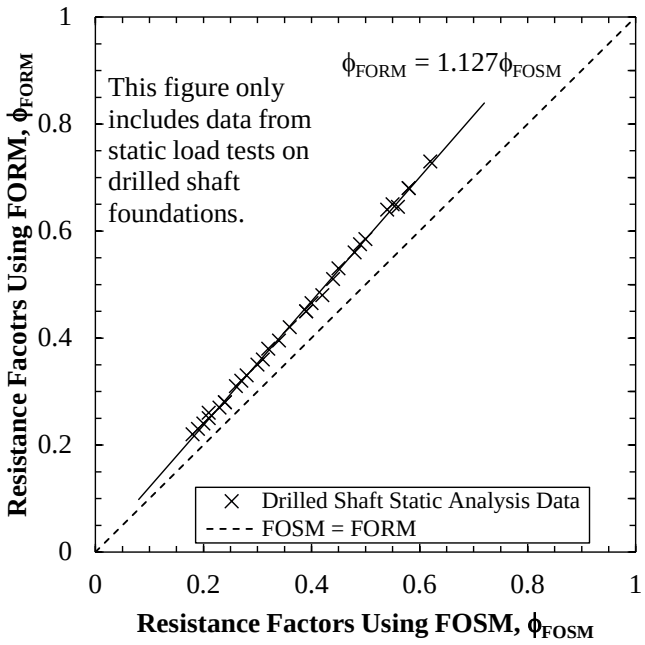

Figure 8.1. Comparison of resistance factor values, as obtained by using the first-order second-moment (FOSM) method and the first-order reliability method (FORM) [modified from Paikowsky 2004].

8.2.2. Sensitivity of Resistance Factor Values

It was observed that all of the obtained resistance factor values were dependent upon the value of the resistance bias factor; therefore, a sensitivity analysis was performed for a variety of mean (μ_R) values and coefficient of variation (COV_R) values of the bias factors of the resistance (Figure 8.2). In general, the higher values of the resistance factor increased as the mean value of

the resistance bias factor increased. From this observation, it was inferred that foundation failure was less likely as the μ_R increased because the measured resistance was greater than the predicted resistance of the DSF; therefore, a higher resistance factor value could be utilized. Similarly, as the μ_R increased, there was a greater difference within the calculated values of resistance factor when different COV_R values were utilized.

Because the uncertainty in the design and construction methods was increased, as characterized by the standard deviation value, the value for the resistance factor as associated with a reliability index of 3.0 was decreased. For instances where the mean value of the bias factor was increased and the standard deviation was constant, the value of the resistance factor was increased as a function of the σ_R (and not the COV_R value of the bias factor because the COV value varied). For example, in Figure 8.2a and e, for COV_R values, of the bias factor, of 0.3 and 0.2 (i.e. equivalent standard deviation values of the bias factor of 0.24), respectively, the resistance factor values shifted to the right due to the increased mean value of the bias factor. Similarly, the values of the resistance factor, as calculated for the COV_R values of 0.4 and 0.3 (Figure 8.2b and e) associated with the μ_R values of 1.2 and 1.3, respectively, were increased by the same interval as the mean value increased by the same interval for equivalent standard deviation values of the bias factor.

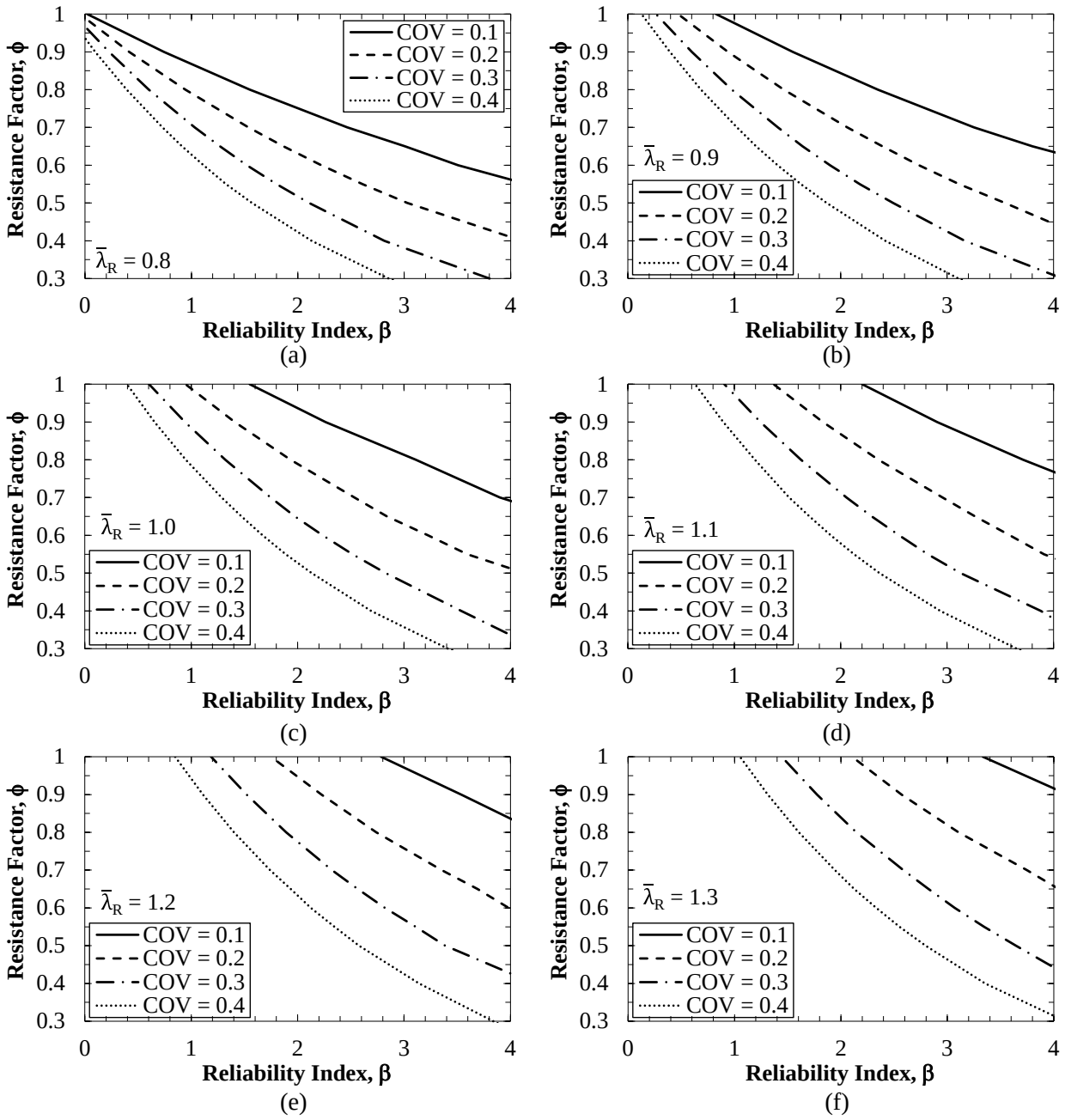

Figure 8.2. Sensitivity analysis of the resistance factors as a function of the reliability index, with respect to the resistance bias factors with a a) mean of 0.8, b) mean of 0.9, c) mean of 1.0, d) mean of 1.1, e) mean of 1.2, and f) mean of 1.3.

For mean values of the bias factor that were less than one, meaning that the measured resistance was less than the predicted resistance, the calculated resistance factors were above 0.58 for COV values less than 0.2. The standard deviation of the bias factors for low mean and

COV_R values of the bias factors was less than 0.15 which would likely only be achieved for a DSF that was constructed in 1) horizontally homogeneous soil stratigraphy with 2) very consistent construction methods. Conversely, for μ_R values that were greater than 1.2, COV values of 0.3 may be utilized to calculate an increased resistance factor (above 0.58). For a mean bias factor value of 1.0 (i.e. the measured resistance was approximately the same as the predicted resistance), the resistance factor value was increased only when the COV value was less than 0.2. Overall, a larger increase in the value of the resistance factor was caused by a lower value of COV_R (primarily due to a lower standard deviation value) than by a higher value of the mean.

There were some extreme cases where the resistance factor was calculated to be greater than 0.95 (some even greater than 1.0). Although these cases were unlikely (cases where the mean values of the bias factor were greater than 1.3 and the COV_R value of the bias factor was less than 0.2) , the use of engineering judgment is recommended for calculated resistance factors that are greater than 0.7 (the AASHTO recommended value for a site with three load tests). The geotechnical investigation methods, implemented software programs, and construction methods should be observed and considered for these cases (cases in which a resistance factor larger than 0.7 was used) to prevent excessively high resistance factors that may result in a possible foundation failure.

8.2.3. Possible Influence of Load Test Method

While the method of testing was not considered for this study, the method of testing (i.e. top-down, bi-directional, statnamic) should be considered in subsequent studies. There was a large variation in the measured (utilizing a bi-directional load cell) and predicted (utilizing FB-Deep and SHAFT) unit side resistance and unit end bearing resistance values in cohesive and cohesionless soils. When utilizing the bias factor values from the test sites, the COV value of the

unit side resistance was as high as 1.237 (the standard deviation value was 23.7 percent higher than the average value of the bias factor). On average for the geologic-specific resistance factors within the state of Arkansas, the COV value was 0.73 which was 97.3 and 15.9 percent higher than the COV value for the unit side resistance from the national database and the Louisiana/Mississippi database, respectively. It is recommended, particularly for the calibration of resistance factors for unit side resistance, that the method of load testing be considered because there was a large variation between the predicted load transfer determined when utilizing FB-Deep or SHAFT and the measured load transfer when utilizing a BLC (Figure 8.3). Even though the measured movement was less than the movement of the predicted load transfer values, the axial load of the constructed DSF was greater in many cases at the location of the BLC. The predicted load values, as a function of the depth of the DSF, were predicted assuming a top-down load test was performed; therefore, it is recommended to utilize a prediction method that simulates the method of load testing (i.e. load applied to the top of the DSF using Statnamic or a jack with reaction piles, load applied to the bottom of the DSF using BLC, or load applied in the middle of the DSF using BLC).

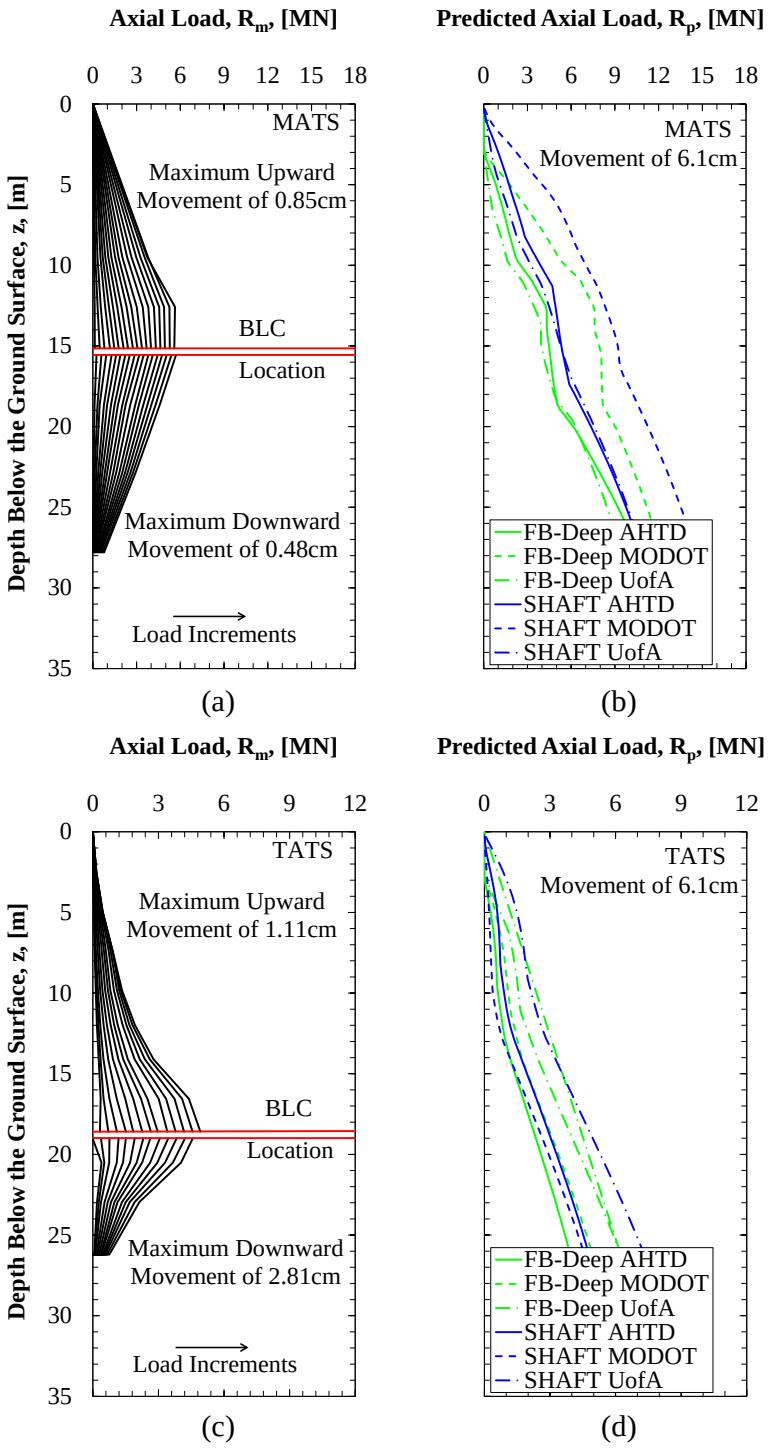

Figure 8.3. Load transfer along the DSF a) measured for the MATS, b) predicted for the MATS, c) measured for the TATS, and d) predicted for the TATS.

8.2.4. Additional Recommendations

Although the Bayesian updating method may be utilized in conjunction with a reliability method to calibrate resistance factors for DSF, the method should also be utilized in combination with engineering judgment. For example, if the calculated value for the site-specific resistance factor is greater than 0.7, then the site variability should be examined with regard to the: soil stratigraphy, geotechnical investigation methods, software program utilized, and construction methods. Finally, in extreme cases where the mean and variance values of the bias factor are high (mean values greater than 1.2) and low (variance values less than 0.6), respectively, and the calibrated resistance factor was greater than one, it is recommended that a resistance factor of 0.95 be utilized and that construction of the DSF be closely observed as previously mentioned.

8.2.5. Additional Resistance Factor Calibration for the State of Arkansas

The posterior distribution of the bias factors for the resistance for the UofA geotechnical investigation method, based on the bias factors for soil deposits within the state of Arkansas, is presented in Figure 8.4. The prior distribution parameters from Paikowsky (2004) were utilized to develop Figure 8.4a and b, and the prior distribution parameters from Abu-Farsakh et al. (2010) were utilized to develop Figure 8.4c and d. The standard deviation values for the bias factor of the sampled data (site-specific or geologic-specific data from Arkansas) were smaller than the standard deviation values for the bias factor of the respective prior distributions. Using the Bayesian updating method, smaller standard deviation values (and therefore smaller COV_R values) were calculated for the calibration studies than were obtained from the Paikowsky (2004) and Abu-Farsakh et al. (2010) databases. The mean values for the bias factor for the sampled data were dependent upon the geotechnical investigation methods/software programs, but as presented in Figure 8.4, the posterior mean values were not changed as significantly as the

change in the posterior standard deviation values (2.5 percent for μ_n as compared to 118.9 percent for σ_n in Figure 8.4a). As presented previously, a larger resistance factor was calculated due to the low variability in the resistance of the DSF because of the smaller the standard deviation of the sampled dataset for the bias factors.

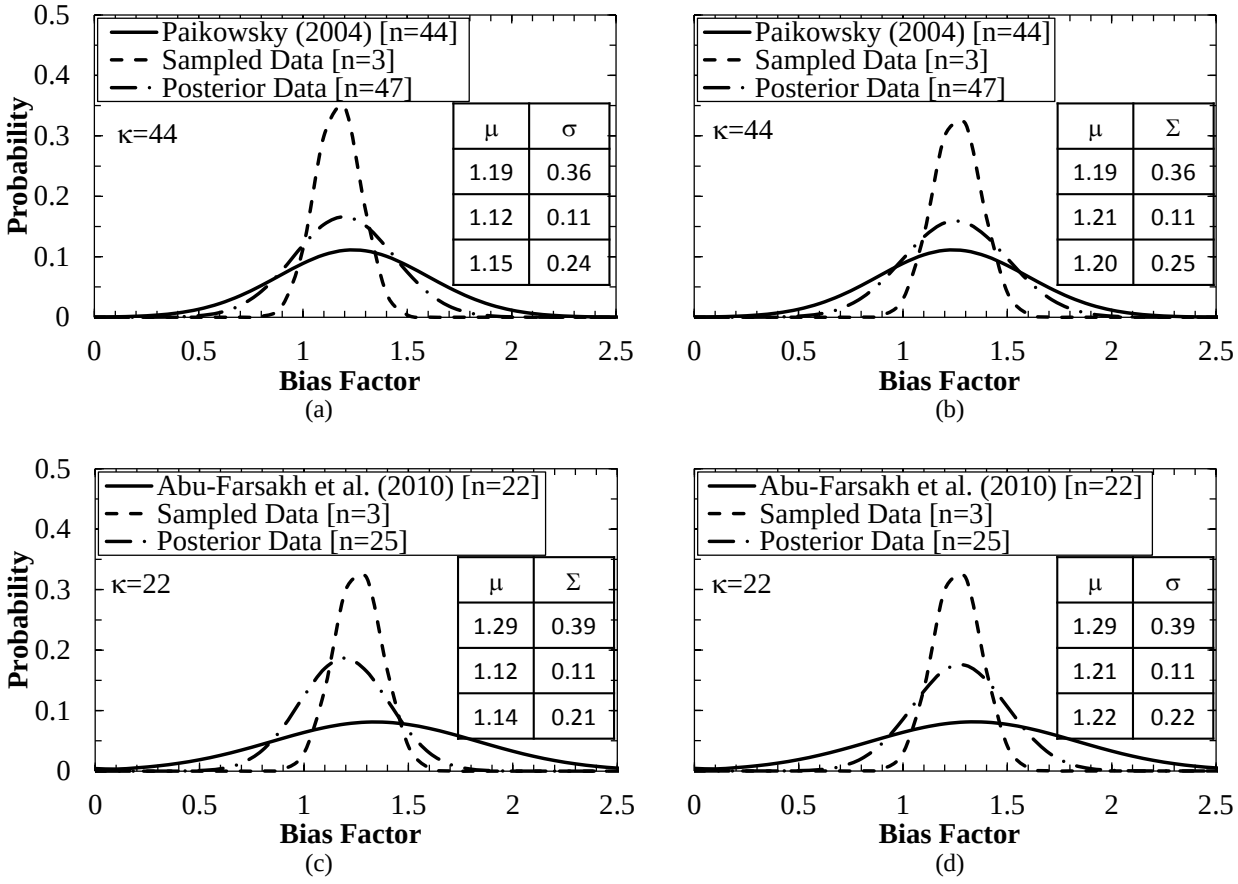

Figure 8.4. Bayesian updated distribution parameters based on the Paikowsky (2004) prior distribution for the a) SHAFT UofA and b) FB-Deep UofA sampled data at the MATS and on the Abu-Farsakh et al. (2010) prior distribution for the c) SHAFT UofA and d) FB-Deep UofA sampled data at the TATS.

Resistance factors were calibrated based on site-specific parameters and geologic-specific parameters. For the majority of the data, the Bayesian updating method was utilized to calibrate the resistance factors due to the minimal amounts of available full-scale test data available. Exceptions to this lack of data include the resistance factors for the unit side resistance values in

sand and clay which were calculated with and without using the Bayesian updating method before the reliability analysis. The tables for each step of the reliability analysis, including the original calculated distribution parameters, the calculated posterior distribution parameters as obtained from the Bayesian updating method, and the subsequent calculated resistance factors are presented in Appendix E. Moreover, the R software program computer code that was utilized for the normality testing and the Monte Carlo simulation is presented in Section E.7.

Resistance factor values for the design of DSF for unit side resistance with and without using the Bayesian updating method were calculated for sandy soils at the TATS and the MATS. The resistance factor values calculated within sandy soils were larger using the collected bias factors from the MATS and the TATS than the values when utilizing the Bayesian updating method. For the design in sandy soils at the MATS, the calculated average resistance factor values were 0.40 and 0.41 using SHAFT and FB-Deep, respectively. Similarly, for the design in sandy soils at the TATS, the calculated average resistance factor values were 0.40 and 0.48 using SHAFT and FB-Deep, respectively. These values were greater than the resistance factor values calculated using the Bayesian updating method by 0.5 percent (FB-Deep at MATS) to 40.1 percent (FB-Deep at TATS) when using Paikowsky (2004) as the prior distribution at the strength limit state.

In comparison, resistance factor values were calculated for the design of unit side resistance of DSF within clayey soils for the TATS and the MATS. The resistance factor values for the soil at the TATS calculated with the Bayesian updating method were lower than the values calculated without the Bayesian updating method. However, the resistance factor values calculated for the soil at the MATS using the Bayesian updating method were greater than the values without the Bayesian updating method. Particularly at the MATS where the clayey soil

comprised of two distinct layers (desiccated clay and very stiff, red clay), the variability of the bias factor values was high. Therefore, except at the MATS for the design of unit side resistance in clayey soils, the resistance factor values calculated using the Bayesian updating method was lower than the values calculated without using the Bayesian updating method. Moreover, the resistance factor values calculated for the design of DSF utilizing the unit side resistance were more conservative using the Bayesian updating method.

All of the resistance factors were calibrated based on the strength limit (movement of 5%D), a service limit of 1%D, and a service limit of 1.27cm. These three limit states were selected because of the precedence in the previous literature of the calibration of resistance factors for DSF (Paikowsky 2004, Abu-Farsakh et al. 2010). The predicted and measured total capacity/unit resistance for the DSF at the SSATS are presented in Tables E.1 to E.7. The predicted and measured total capacity/unit resistance for the DSF at the TATS are presented in Tables E.11 to E.23. For the DSF at the MATS, the predicted and measured capacity/unit resistance tables are presented in Tables E.24 to E.33.

Bias factors for the resistance, as obtained for the given software programs and the given geotechnical investigation data and as calculated as the ratio of the measured resistance to the predicted resistance, are presented in Tables E.34 to E.45. The sampled “distribution” parameters are based on the average and variation of the sampled data for the respective: site/soil type, software programs, and geotechnical investigation data. The resistance bias factors for the DSF at the SSATS are presented in Table E.34, Table E.35, and Table E.36 for the total capacity, unit side resistance, and unit end bearing resistance, respectively. The resistance bias factors for the DSF at the TATS are presented in Table E.37, Table E.38, and Table E.39 for the total capacity, unit side resistance, and unit end bearing resistance, respectively. The resistance bias factors for

the DSF at the MATS are presented in Table E.40, Table E.41, and Table E.42 for the total capacity, unit side resistance, and unit end bearing resistance, respectively. Combining the bias factors for the TATS and the MATS, the resistance bias factors calculated for the alluvial and deltaic deposits within the state of Arkansas for mixed soils (i.e. clay and sand) are presented in Tables E.43 to E.45. Due to the small amount of data, the distribution type could not be defined for the sampled data; therefore, the normal and lognormal distribution types were utilized based on previous calibration studies.

To perform the Bayesian updating method, it was assumed that the prior and sampled data was normally distributed. While it was determined from previous calibration studies that the lognormal distribution was closer to the resistance bias factor data for the national and Louisiana/Mississippi databases, the normal distribution was a reasonable assumption as discussed in Section 8.6.3. Similarly, the methodology behind the Bayesian analysis was further presented in Section 8.6.4. Therefore, the Monte Carlo simulation was performed on the parameters from the posterior distribution to calibrate the resistance factors. The R software program computer code that was utilized for the strength limit and the service limit analyses is presented in Section E.7.2 and E.7.3, respectively.

The posterior distribution parameter values for the DSF at the SSATS, based on the Paikowsky (2004) prior distribution, are presented in Tables E.46 and E.47. Posterior parameter values for the DSF at the SSATS, based on Yang et al. (2010) prior distribution, as presented in Tables E.54 and E.55. The posterior distribution parameter values for the DSF at the TATS, based on the Paikowsky (2004) prior distribution, are presented in Tables E.48 and E.49. The posterior distribution parameter values for the DSF at the TATS, based on the Abu-Farsakh et al. (2010) prior distribution, are presented in Tables E.56 to E.58. The posterior distribution

parameter values for the DSF at the MATS, based on the Paikowsky (2004) prior distribution, are presented in Tables E.50 and E.51. The posterior distribution parameter values for the DSF at the MATS, based on the Abu-Farsakh et al. (2010) prior distribution, are presented in Tables E.59 to E.61. The resulting posterior distribution parameter values for the DSF, for the state of Arkansas for geologic-specific alluvial and deltaic mixed soils, based on the Paikowsky (2004) prior distribution, are presented in Tables E.52 and E.53. The posterior distribution parameters for the DSF for the state of Arkansas for geologic-specific alluvial and deltaic mixed soils, based on the Abu-Farsakh et al. (2010) prior distribution are presented in Tables E.62 to E.64.

Resistance factor values were calculated for site-specific and geologic-specific calibration studies utilizing the Bayesian updating method and the Monte Carlo simulation method (Section E.6). The resistance factor values for the state of Arkansas were calculated from six BLC tests on DSF in mixed cohesive and cohesionless soils. It is recommended that the resistance factor values calculated for the state of Arkansas be utilized with engineering judgment because the small number of BLC tests (six total tests from two total test sites) may not encompass the soil-structure interaction of DSF constructed in Arkansas. It is recommended that additional information from a load test on DSF in the state of Arkansas (in mixed soil types) be added to a database that may be utilized to calculate geologic-specific resistance factor values.

For the SSATS, there were very few data points and very little movement was observed during the full-scale load test. It was not feasible to compare the measured resistance with the predicted resistance at a movement of 5%D; therefore, service limits of 0.1%D and of 0.1cm were utilized. Additionally, the Bayesian updating method was utilized for the information at the SSATS; however, previous calibration studies have been performed on soft to medium limestone or shale and not on moderately strong to strong limestone. The prior distribution parameter

values were different than the parameter values calculated from the three load tests on DSF at the SSATS because there were very small movements measured on the DSF at the SSATS. Although resistance factor values were determined (Tables E.66, E.70, and E.74), it is recommended that these resistance factor values not be utilized in the design of DSF in moderately strong to strong limestone because the values are too low, based on engineering judgement. Furthermore, the Bayesian updating method should not be utilized to calculate resistance factor values for DSF in moderately strong to strong limestone because there is not a database with enough comparable load tests to determine distribution parameter values.

It is recommended that a full-scale load test be performed to verify the capacity of a DSF constructed in moderately strong to strong limestone or a national database be created to assist with the design of DSF constructed in moderately strong to strong limestone. There were very few available full-scale load tests on medium strong to strong limestone, but three full-scale load tests were performed on DSF in moderately strong to strong limestone in St. Louis, Missouri (Axtell and Brown [2010]) and in Tennessee (Brown [2008]). The information from the measured total capacity was added to the database for DSF in medium strong to strong limestone as presented in Tables E.8 to E.10. Based on the compiled information on DSF in moderately strong to strong limestone, it is recommended that the service limit (less than 1%D or 1.27cm movement) be utilized in software programs because larger movements are unlikely at the design load.

8.2.6. Future Investigations

As recommended by committee members during the dissertation defense, particularly Drs. Bernhardt and Pohl, the use of a normal-gamma conjugate prior distribution and a flat/noninformative prior distribution, in addition to the normal prior distribution should have

been investigated within the Bayesian updating process. Therefore, these distributions (normal-gamma and flat/noninformative) were investigated because the sampled population for the Arkansas data was small. Specifically, although the variance was calculated for the data, the vaiance may have not been the true variance of the sampled population and therefore the normal distribution may not have been the correct distribution to utilize. At the time of submission of this dissertation, the framework has been developed, as discussed herein, to investigate the norma-gamma and flat/noninformative prior distributions. Three different methods for Bayesian updating (normal, normal-gamma, and flat/noninformative prior distributions) were performed to compare the calculated resistance factor values, calculated by using the various prior distributions within the Bayesian updating, for the site-specific and geologic-specific calibrations.

8.2.6.1. Normal-Gamma Conjugate Prior Distribution

According to Hoff (2009), for an unknown mean and variance, the conjugate prior population can be modeled using a normal-gamma distribution. For a sampled (likelihood function/distribution) dataset that is normally distributed, the resulting posterior population will also be normal-gamma distributed. Specifically, Hoff (2009) has shown that the posterior parameters can be calculated by using Equations 8.2 through 8.6.

$$\overline{\lambda_n} = \frac{\kappa_o \overline{\lambda_o} + n_s \overline{\lambda_s}}{\kappa_o + n_s} \quad \text{(modified from Hoff 2009)} \quad \text{Equation 8.2}$$

$$\kappa_n = \kappa_o + n_s \quad \text{(modified from Hoff 2009)} \quad \text{Equation 8.3}$$

$$\propto_n = \propto_o + \frac{n_s}{2} \quad \text{(modified from Hoff 2009)} \quad \text{Equation 8.4}$$

$$\beta_n = \beta_o + \frac{1}{2}\sum_{j=1}^{n_s}\left(\lambda_{s,j} - \overline{\lambda_s}\right)^2 + \frac{\kappa_o n_s \left(\overline{\lambda_s} - \overline{\lambda_o}\right)^2}{2(\kappa_o + n_s)} \quad \text{(modified from Hoff 2009)} \quad \text{Equation 8.5}$$

$$\sigma_n^2 = \frac{1}{\kappa_n}\left[\kappa_o\sigma_o^2 + (n_s - 1)\sigma_s^2 + \frac{\kappa_o n_s\left(\overline{\lambda_s} - \overline{\lambda_o}\right)^2}{2(\kappa_o + n_s)}\right]$$ (modified from Hoff 2009) Equation 8.6

The variables utilized in Equations 8.2 through 8.6 include: the posterior mean ($\overline{\lambda_n}$), the influence factor of the prior distribution (κ_p), the mean of the prior distribution ($\overline{\lambda_o}$), the number of sampled data (n_s), the mean of the sampled data ($\overline{\lambda_s}$), the influence factor of the posterior distribution (κ_o), the shape parameter for the posterior and the prior distributions (α_n and α_o, respectively), the rate parameter for the posterior and the prior distributions (β_n and β_o, respectively), the observation number (j), the sampled data ($\lambda_{s,i}$), the variance of the posterior distribution (σ_n^2), the prior variance ($\widetilde{\sigma}_o^2$), and the variance of the sampled data ($\widetilde{\sigma}_s^2$).

The framework utilized during implementation of Bayesian updating and Monte Carlo simulation techniques to determine posterior distribution parameters, using the normal-gamma prior distribution, is presented in Figure 8.5. Because the mean and variance of the data were treated as being unknown, the normal-gamma distribution was utilized to model the prior distribution (parameters of mean [μ_o], number of samples [κ_o], shape parameter [α_o], and rate parameter [β_o]) and the normal distribution was utilized to model the sampled data (likelihood function/distribution parameters of mean [μ_o] and variance [σ_o^2]). From Bayesian updating, the normal-gamma distribution may be used to model the posterior bias factor data.

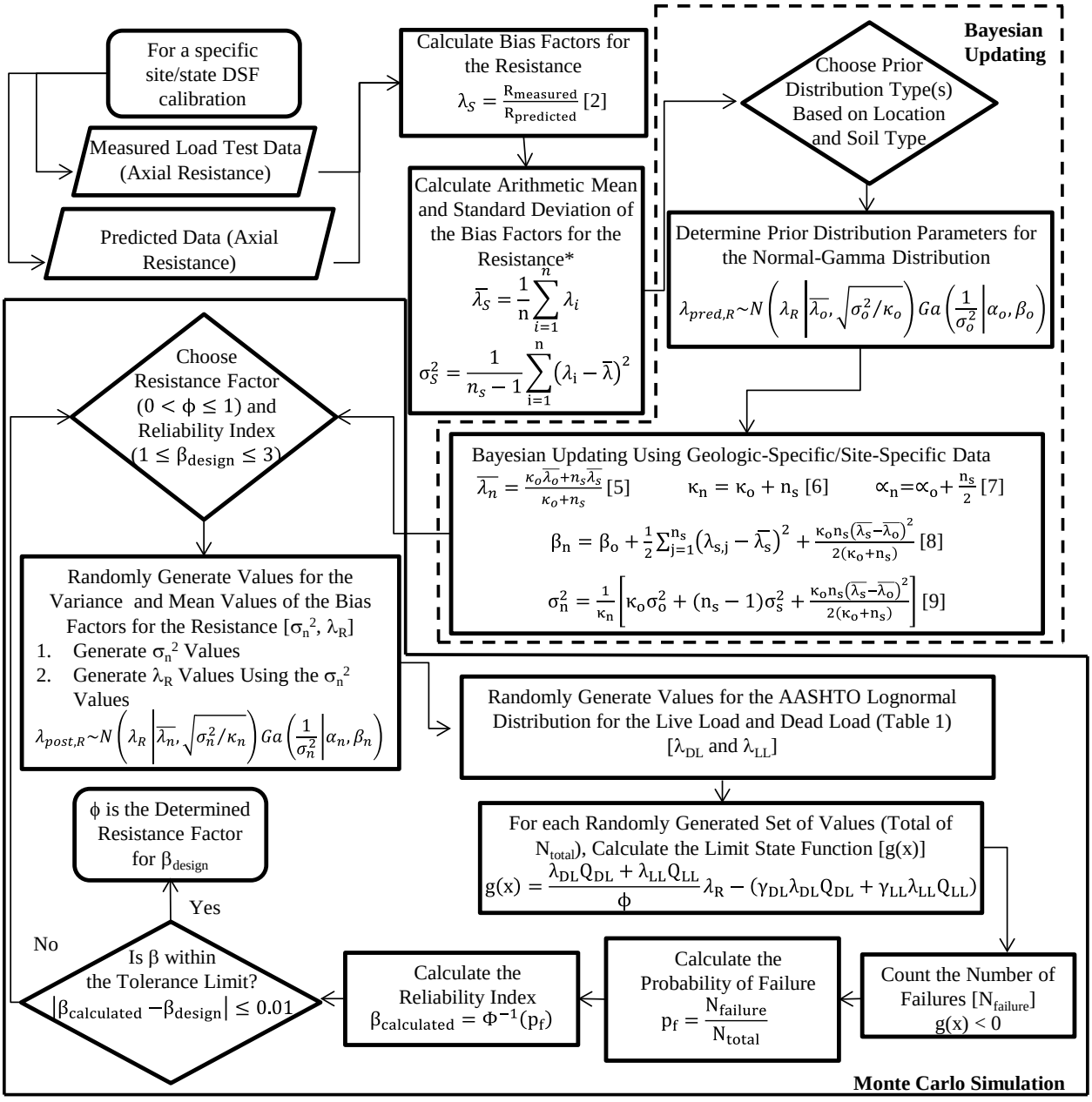

Figure 8.5. Framework for resistance factor caliberation using a normal-gamma prior distribution.

The Bayesian updated distribution parameters (μ_n, κ_n, α_n, β_n, and σ_n^2) were calculated for one geologic-specific (mixed soils) and two site-specific (MATS and TATS) calibrations. After the Bayesian updated distribution parameters were determined, the reliability analysis was performed by utilizing Monte Carlo simulation technique. Specifically, for each geotechnical

investigation method and each of the associated DSF design software programs, a resistance factor was determined for a reliability index (β) of 3.0. A summary of the generalized steps for Bayesian updating Iusing the normal-gamma prior distribution) in conjunction with Monte Carlo simulation, are outlined below.

1. Calculate the mean ($\overline{\lambda_s}$), variance (σ_s^2), and standard deviation (σ_s) of the sampled data.

2. Determine the parameters for the prior distribution for the normal-gamma distribution (μ_o, κ_o, α_o, β_o, and σ_o^2) from previous calibration database(s) chosen based on the soil type, the geotechnical investigation method, and the design software programs.

3. Calculate the Bayesian updated distribution parameters using Equations 8.2 through 8.6.

4. Choose an initial resistance factor value (ϕ) and a design reliability index value (β_{design}).

5. Generate random variables for the bias factor values for the resistance (n=500,000) based on 1) the gamma distribution (Ga) for the inverse of the variance then 2) the normal distribution (N) for the mean as presented in Equation 8.7.

$$\lambda_{post,R} \sim N\left(\lambda_R \left| \overline{\lambda_n}, \sqrt{\sigma_n^2/\kappa_n} \right.\right) Ga\left(\frac{1}{\sigma_n^2} \middle| \alpha_n, \beta_n\right) \quad \text{(modified from Hoff 2009)} \qquad \text{Equation 8.7}$$

6. Generate random variables based on the lognormal mean ($\lambda_{log,i}$) and lognormal variance ($\zeta_{log,i}^2$) bias factor values for the dead load and live load (n=500,000).

7. Calculate the limit state for each trial set (a g(x) function for each λ_{DLi}, λ_{LLi}, λ_{Ri} where i=1 to n).

8. Determine the number of foundation failures for the trail set (count[g(x) < 0]).

9. Determine the probability of failure as the ratio of the number of failures to the number of total foundations $\left(p_f = \frac{\text{count}[g(x)<0]}{n}\right)$.

10. Calculate the reliability index ($\beta_{calculated} = \Phi^{-1}[p_f]$).

11. Finally, if $|\beta_{\text{calculated}} - \beta_{\text{design}}| < \text{tolerance limit of } 0.01$, then ϕ is the calibrated resistance factor value, otherwise repeat steps 5-10 until the difference between the calculated and design values of the reliability index as less than the tolerance limit.

Following the above steps, recommended resistance factors for the geotechnical investigation methods and the software programs that were used for the design of DSF are presented in Table 8.1. Based on the three (for site-specific calibration) and six (for geologic-specific calibration) bias factor values, the resistance factor values were greater than the maximum recommended resistance factor value of 0.7. Furthermore, a 95 percent confidence interval of the resistance factor values was determined for each of the methodology alternatives for the design of DSF.

Table 8.1. Resistance factor values calculated using a normal-gamma conjugate prior distribution.

Site	Software Program	Geotechnical Investigation Method	Resistance Factor		
			ϕ	ϕ + 2.5%	ϕ – 2.5%
MATS	SHAFT	AHTD	0.721	0.753	0.720
		MODOT	0.716	0.748	0.715
		UofA	0.722	0.752	0.719
	FB-Deep	AHTD	0.720	0.753	0.720
		MODOT	0.718	0.751	0.718
		UofA	0.720	0.753	0.720
TATS	SHAFT	AHTD	0.730	0.765	0.729
		MODOT	0.725	0.758	0.724
		UofA	0.722	0.753	0.722
	FB-Deep	AHTD	0.732	0.769	0.731
		MODOT	0.725	0.758	0.724
		UofA	0.723	0.755	0.722
Arkansas	SHAFT	AHTD	0.726	0.760	0.725
		MODOT	0.718	0.748	0.717
		UofA	0.718	0.750	0.717
	FB-Deep	AHTD	0.729	0.763	0.728
		MODOT	0.718	0.751	0.717
		UofA	0.721	0.753	0.720

8.2.6.2. Flat/Noninformative Prior Distribution

A flat or noninformation prior distribution is used in cases where there is minimal impact of the prior distribution on the posterior distribution of the mean (Figure 8.6). In other words, the prior distribution is believed to be different than the sampled data (likelihood function/distribution) such that it is unreasonable to use the information from the prior distribution to describe the posterior distribution. Through a sensitivity analysis, a flat or noninformative prior distribution will be used in Bayesian updating to determine the influences of the prior distribution upon the posterior distribution. Furhtermore, resistance factor values will be determined for the site-specific and geologic-specific calibrations for each software program and geotechnical investigation method. Therefore, it is anticipated that the journal article that is presented in Sections 8.3 through 8.12 will be modified to include the new information prior to submission of the journal article but after submission of this dissertation.

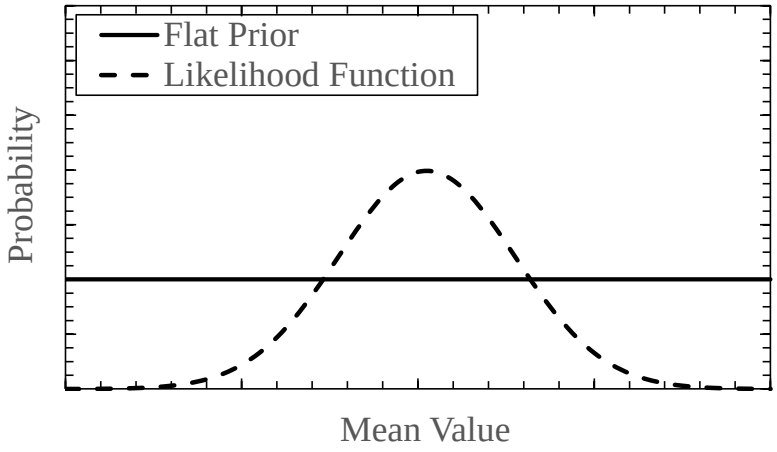

Figure 8.6. A flat prior distribution compared to a normally distributed likelihood function (sampled data).

In summary, the use of normal-gamma and flat/noninformative conjugate prior distribution models were recommended for small sample sets because the variance is considered unknown. The resistance factor values determined using a normal-gamma prior distribution were

lower than the values determined using a normal prior distribution. The normal-gamma distribution is utilized to account for the variation in the standard deviation values as well as the variation in the mean values of the bias factor of the resistance. However, for the site-specific and geologic-specific datasets presented, at least one DSF at each site failed (one from a collapsed excavation discussed in Chapter 6 and one from poor concrete placement discussed in Chapter 7). Furthermore, it may be possible to utilize a normal conjugate prior distribution for the site-specific and geologic-specific calibrations because the data includes a failed DSF at each site.

Utilization of a Bayesian Updating Method for Calibration of Resistance Factors

Morgan L. Race[1]
Michelle L. Bernhardt, PhD[2]
Richard A. Coffman, PhD, PE, PLS[3]

8.3. Abstract

The calibration of resistance factors, for the use in Load and Resistance Factor Design (LRFD) of deep foundations, is required to balance reliability and cost efficiency for geotechnical structures. Six full-scale load tests were performed on drilled shaft foundations (DSF) within interlayered sands and clays deposits located within the state of Arkansas. The Bayesian updating method, in conjunction with the Monte Carlo simulation method, was utilized to determine the localized resistance factors by using small sample sets (sample population between three and six).

Geologic-specific (alluvial and deltaic soil deposits in Arkansas) and site-specific (Turrell, AR, and Monticello, AR) resistance factors were calculated, for mixed layer soil deposits, based on the use of specific design software and/or geotechnical investigation methods. Observed cost savings, as obtained by using the site-specific resistance factors at the MATS, were up to $460,000 dollars (US) or 29.7 percent of the estimated total foundation cost. The Bayesian updating methodology and specific recommendations regarding the use and implementation of the Bayesian updating method to calibrate resistance factor values for DSF are discussed herein.

Keywords: Drilled Shaft Foundations; Statistics; Bayesian Analysis; Load and Resistance Factor Design

8.4. Introduction

The calibration of resistance factors has been of national and local concern for designers in the transportation related fields since the Load and Resistance Factor Design (LRFD) methodology was implemented for deep foundations by the American Association of State Highway and Transportation Officials (AASHTO 2001). The use of resistance factors was implemented, within the geotechnical engineering discipline, to account for multiple types of uncertainty including, but not limited to, the variability associated with the: site layout, geotechnical investigation method, implemented type of design software, and construction method. Numerous localized calibrations, as performed to determine resistance factors, have been completed across the United States to more efficiently design DSF. Traditional, reliability methods have been utilized to perform these calibrations. Specifically, the first order reliability method (FORM) and/or the Monte Carlo simulation method have been utilized; however, these methods require larger sample sizes than were available from the Arkansas dataset. Therefore, the Bayesian updating method was utilized to determine the localized resistance factors for site-specific databases with a small number of samples. Furthermore, in addition to obtaining resistance factors based on a given database, another benefit of the Bayesian updating method is that the method can also be utilized to "update" the value of the given resistance factor when additional full-scale load test data become available and are added to a given database.

8.5. Background/Literature Review

8.5.1. Load and Resistance Factor Design (LRFD)

For deep foundations, the LRFD methodology was implemented in the United States in 2001 (AASHTO 2001). As presented in Figure 8.7a, probability distributions of the load (Q), as determined by Nowak (1999), and the resistance (R), as determined from regional or national full-scale load test databases, have been utilized to account for variability in the design of DSF. As observed in Figure 8.7a, the variability within the load component (σ_Q) is typically less than the variability within the resistance component (σ_R). The specific items that may affect the variability of the load values include the: type of loading, magnitude of the load, and rate of occurrence; while, the specific variables that may affect the variability of the resistance values include the: soil strength, DSF dimensions (length and diameter), and DSF material strength (Nowak 1999). Historically, the limit state distribution, g(x) as presented in Figure 8.7b, was determined by subtracting the load values from the resistance values; the g(x) distribution has been commonly used to determine the probability of failure (p_f). The reliability index (β), as presented in Figure 8.7b, has been utilized to determine an appropriate value for the resistance factor that limits the probability of failure to 0.001 (1 failure in 1000 structures). In addition to the graphical presentation of the limit state distribution, the g(x) distribution has also been presented in numerical form (Equation 8.8) by subtracting the sum of the nominal load values (Q_n) from the nominal resistance values (R_n).

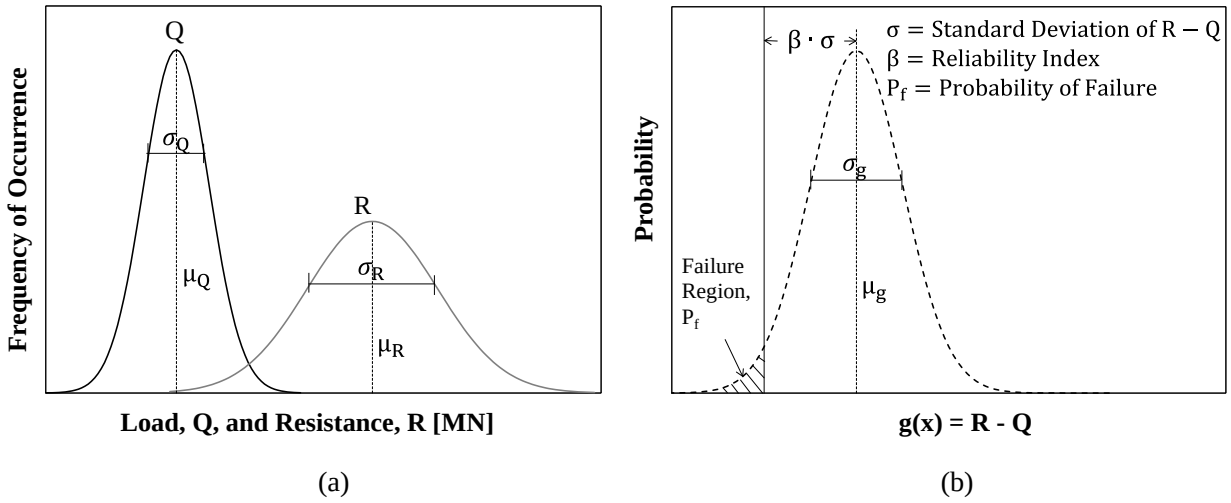

Figure 8.7. Load and resistance factor design using a) the individual forces and b) the failure region dependent upon the forces (modified from AASHTO 2007).

To calibrate the resistance factors for a specific site, the amount of uncertainty within the software programs and within the geotechnical investigation method have been accounted for by using a bias factor for the resistance (λ_R) that is determined using Equation 8.9 and was previously defined by Abu-Farsakh et al. (2010) as the ratio between the measured resistance value (R_m) and the predicted resistance value (R_p). As required by AASHTO (2001), the bias factors associated with various load types, load factors, and coefficient of variation (COV) values have been previously utilized to calibrate resistance factors (Table 8.). Allen et al. (2005), as presented in Equation 8.10, stated that the minimum amount of resistance (R_{min}) is equal to the sum of the products of the respective bias factor for a given load type (λ_i) and the load value for that load type (Q_i) divided by the resistance factor (ϕ). Subsequently, as presented in Equation 8.11, the limit state equation has also been rearranged to determine the resistance factor (ϕ) by incorporating the average bias factor for the dead load (λ_{DL}), for the live load (λ_{LL}), and for the resistance ($\overline{\lambda_R}$) and to also account for the required load factors that are associated with the dead load and live load (γ_{DL} and γ_{LL}).

$$0 \leq g(x) = R_n - \sum Q_n \qquad \text{(AASHTO 2007)} \qquad \text{Equation 8.8}$$

$$\lambda_R = \frac{R_m}{R_p} \qquad \text{(Abu-Farsakh et al. 2010)} \qquad \text{Equation 8.9}$$

$$R_{min} = \frac{\lambda_{DL} \cdot Q_{DL} + \lambda_{LL} \cdot Q_{LL}}{\phi} \qquad \text{(Allen et al. 2005)} \qquad \text{Equation 8.10}$$

$$g(x) = \frac{\lambda_{DL} \cdot Q_{DL} + \lambda_{LL} \cdot Q_{LL}}{\phi} \overline{\lambda_R} - (\gamma_{DL} \cdot \lambda_{DL} \cdot Q_{DL} + \gamma_{LL} \cdot \lambda_{LL} \cdot Q_{LL}) \qquad \text{(Allen et al. (2005)} \qquad \text{Equation 8.11}$$

Table 8.2. Loading factors as recommended from AASHTO (2007).

Load Type	Load Factor	Mean Bias Factor (λ_Q)	Standard Deviation (σ_Q)	COV $\left(\frac{\sigma_Q}{\lambda_Q}\right)$
Dead Load	1.25	1.08	0.14	0.13
Live Load	1.75	1.15	0.21	0.18

8.5.2. Previous Resistance Factor Calibration Studies

As previously mentioned, nationally obtained resistance factor values, for deep foundations, were utilized after LRFD was implemented by AASHTO in 2001. Specifically, based on a national database of full-scale tests on DSF, Paikowsky (2004) suggested certain resistance factor values. Following Paikowsky (2004), other researchers calibrated resistance factor values by utilizing load test results that were obtained from Florida, Kansas, Missouri, or Louisiana/Mississippi (Table 8.3). Economical savings were achieved, for DSF constructed in Florida limestone, by including full-scale load testing (bi-directional load cell tests or Statnamic tests) in combination with increased resistance factor values (ϕ). During the calibration of resistance factors in Missouri, the contributions from site characterization methods and the type of geologic features (i.e. clay or rock) were specifically investigated. According to Loehr et al. (2013), the coefficient of variation (COV) was dependent upon the soil type and the geotechnical

investigation method (standard penetration test [SPT] or cone penetration test [CPT]). Similarly, regardless of the COV, the resistance factor values were significantly increased by performing full-scale load tests, particularly in soil with low site variability (Table 8.4). However, unlike resistance factors for driven piles that may be as high as 0.90, the resistance factors for DSF have been limited to 0.70 (AASHTO 2007), even if multiple load tests were performed and higher resistance factor values were calculated.

Table 8.3. Summary of resistance factors.

State	Reference	Number of Tests	Stratigraphy Type	Probability of Failure	Resistance Factor
National	Paikowsy (2004)	44	Mixed Soil	0.001	0.58
Florida	McVay et al. (2002)	26	Limestone	0.001	0.59
Kansas	Roberts et al. (2011)	NR*	Shale	0.001	0.65
Louisiana/ Mississippi	Yu et al. (2012)	22 to 26	Mixed Soil	0.001	0.60
Missouri	Vu (2013)	25	Shale	0.001	0.65

*Not Reported

Table 8.4. Resistance factor values for deep foundations, as a function of the number of load tests and the site variability for a target reliability (β) of 3.0 (modified from AASHTO 2007).

Number of Load Tests Per Site	Resistance Factor, ϕ^{α} Site Variability		
	Low	Medium	High
1	0.80	0.70	0.55
2	0.90	0.75	0.65
3	0.90	0.85	0.75
≥ 4	0.90	0.90	0.80

[a]for DSF it is recommended that $\phi \leq 0.70$

8.5.3. Bayesian Updating Method

The Bayesian updating method has been utilized to determine the values of an updated mean and variance, for a sample set, in relation to prior distributions. According to Hoff (2009), for a prior population that is normally distributed and for a sampled dataset that is normally

distributed, the posterior population will also be normally distributed (Figure 8.8). Specifically, Hoff (2009) has shown that the posterior mean and posterior variance values can be calculated by using Equations 8.12 and 8.13.

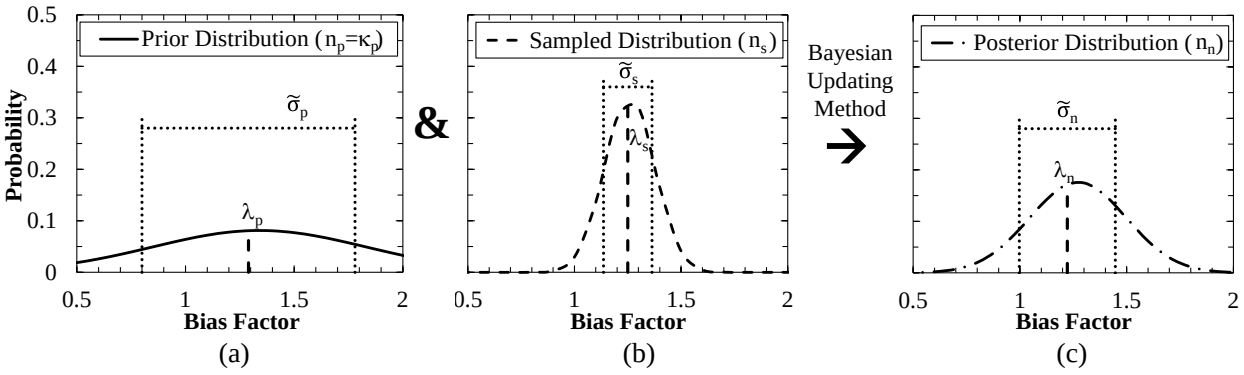

Figure 8.8. Example of the Bayesian updating method using a) a prior distribution, b) a sampled distribution, to obtain c) a posterior distribution.

$$\overline{\lambda_n} = \frac{\kappa_p \tilde{\sigma}_p^2}{\kappa_p \tilde{\sigma}_p^2 + n_s \tilde{\sigma}_s^2} \overline{\lambda_p} + \frac{n_s \tilde{\sigma}_s^2}{\kappa_p \tilde{\sigma}_p^2 + n_s \tilde{\sigma}_s^2} \overline{\lambda_s} \quad \text{(modified from Hoff 2009)} \qquad \text{Equation 8.12}$$

$$\sigma_n^2 = \frac{n_n}{\kappa_p \tilde{\sigma}_p^2 + n_s \tilde{\sigma}_s^2} \quad \text{(modified from Hoff 2009)} \qquad \text{Equation 8.13}$$

The variables in Equations 8.12 and 8.13 include: the posterior mean ($\overline{\lambda_n}$), the influence factor of the prior distribution (κ_p), the prior variance ($\tilde{\sigma}_p^2$), the number of sampled data (n_s), the variance of the sampled data ($\tilde{\sigma}_s^2$), the mean of the prior distribution ($\overline{\lambda_p}$), the mean of the sampled data ($\overline{\lambda_s}$), the variance of the posterior distribution (σ_n^2), and the total number of posterior data points ($n_n = \kappa_p + n_s$).

8.6. Methods and Materials

8.6.1. DSF Database in Arkansas

Two sites in eastern Arkansas were selected to perform full-scale load tests on three DSF per site (Figure 8.9a). The Monticello Arkansas Test Site (MATS), located in southeastern

Arkansas, consisted of mixed layers of cohesive and cohesionless soil types until a depth of at least 30.5m (Figure 8.9b). The Turrell Arkansas Test Site (TATS), located in northeastern Arkansas, consisted of 9.1m of cohesive soil underlain by at least 21.4m of cohesionless soil (Figure 8.9c). At each site, three geotechnical investigation methods were performed to characterize the soil properties and the associated variability with the soil properties. The geotechnical investigation methods, designated as Arkansas Highway and Transportation Department (AHTD), Missouri Department of Transportation (MODOT), and University of Arkansas (UofA) methods, consisted of traditional and/or advanced techniques. Specifically, the AHTD method consisted of performing standard penetration tests (SPT) in all types of soils using a standard split-spoon sampler. The MODOT method consisted of performing cone penetration tests (CPT) in all types of soils until cone tip refusal. The UofA method consisted of pushing shelby tube samples and performing unconsolidated undrained triaxial compression tests in cohesive soil and performing the SPT, with a California split-spoon sampler, in cohesionless soil. Further information about the geotechnical investigation methods has been previously discussed (Race et al. 2013, Race and Coffman 2013, Bey 2014, and Race et al. 2015).

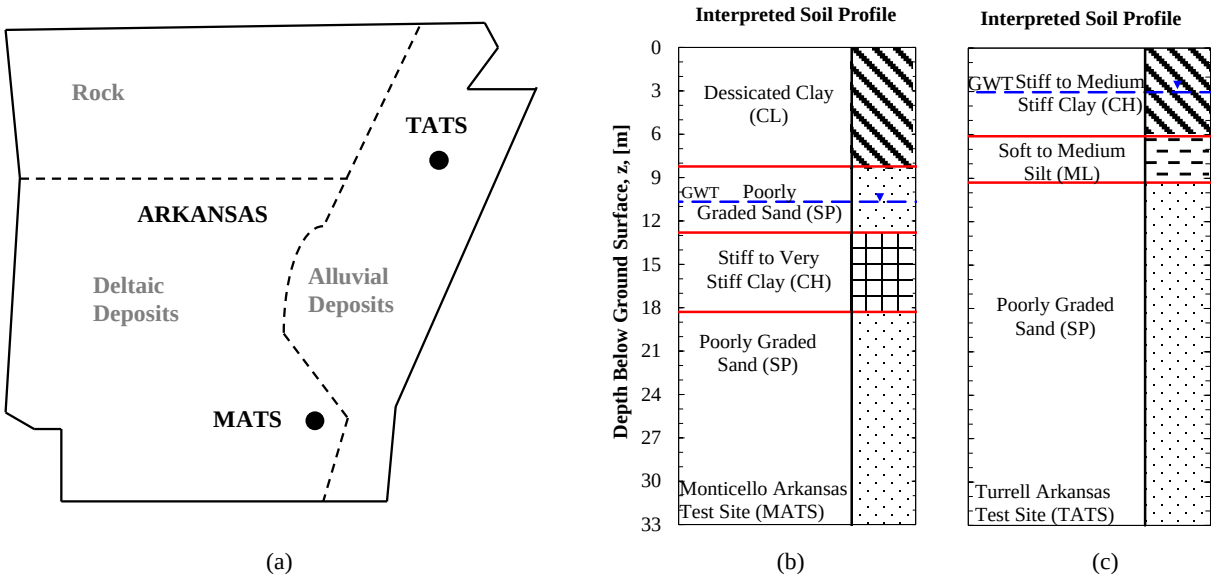

Figure 8.9. a) The location of the MATS and the TATS within the state of Arkansas and soil stratigraphy for the b) MATS and c) TATS (as modified from Race and Coffman 2013, Race et al. 2013, Bey 2014, Race et al. 2015, Race and Coffman 2015a, and Race and Coffman 2015b).

The design of the three DSF at the MATS and the TATS was based on the required axial capacity values that were supplied by the AHTD (7.9MN for the MATS and 9.9MN for the TATS). As described in detail in Bey (2014), the SHAFT (2012) and FB-Deep (2012) software programs were utilized to determine the design length, the predicted axial capacity, and the predicted load-settlement curves. The DSF were then constructed at the MATS and TATS; and the construction and testing of the DSF at the MATS and the TATS have been previously described in Bey (2014) and in Race and Coffman (2015a and 2015b).

As presented in Table 8.5, a load test database was created for the total resistance from the bi-directional load cell (BLC) test data that were collected in Arkansas (three data points from the MATS and three data points from the TATS). The predicted resistance of the DSF was calculated at movement values of five percent of the diameter (that corresponded to 6.1cm for a 1.2m diameter DSF and 9.1cm for a 1.8m diameter DSF). In a similar fashion to Abu-Farsakh et

al. (2010), the measured resistance was interpolated to a movement value of five percent of the diameter by using the equivalent top-down load-movement curve. Bias factor values (λ), calculated as the ratio of the measured resistance to the predicted resistance for a given DSF, were calculated using the data from each of the different geotechnical investigation methods and the different software programs. Furthermore, the mean (μ_λ) and variance (σ_λ^2) of the λ values were calculated by using the site-specific data (samples size of three for each site) and by using the geologic-specific data (sample size of six).

Table 8.5. Summary of DSF load test database for DSF constructed in Arkansas (strength limit state for total resistance).

Location	Dia. (m)	Length (m)	Software Program	Geotechnical Investigation Method	Measured Resistance [MN] +	Predicted Resistance [MN] *	Bias Factor
MATS	1.33	27.89	SHAFT	AHTD	13.7	13.3	1.03
				MODOT		16.2	0.85
				UofA		14.3	0.96
			FB-Deep	AHTD		13.9	0.99
				MODOT		14.9	0.92
				UofA		13.1	1.04
	1.89	21.95	SHAFT	AHTD	17.7	14.9	1.19
				MODOT		18.9	0.94
				UofA		15.7	1.13
			FB-Deep	AHTD		14.9	1.19
				MODOT		17.9	0.99
				UofA		15.0	1.19
	1.37	27.89	SHAFT	AHTD	13.6	13.7	1.00
				MODOT		16.4	0.83
				UofA		14.4	0.95
			FB-Deep	AHTD		14.3	0.96
				MODOT		15.3	0.89
				UofA		13.5	1.01
TATS	1.22	26.21	SHAFT	AHTD	11.0	6.9	1.60
				MODOT		8.1	1.35
				UofA		9.2	1.20
			FB-Deep	AHTD		5.9	1.87
				MODOT		8.6	1.28
				UofA		8.6	1.28
	1.83	18.89	SHAFT	AHTD	11.8	7.1	1.66
				MODOT		9.4	1.26
				UofA		9.2	1.27
			FB-Deep	AHTD		6.3	1.86
				MODOT		8.5	1.39
				UofA		8.9	1.32
	1.22	26.52	SHAFT	AHTD	8.7	7.3	1.21
				MODOT		8.6	1.02
				UofA		9.6	0.91
			FB-Deep	AHTD		5.9	1.48
				MODOT		8.6	1.02
				UofA		8.7	1.01

+Interpolated to 5%D Displacement
*Predicted at 5%D Displacement

8.6.2. Databases for Use in Bayesian Updating Method

The parameters of the sampled distribution from the λ values for the resistance term, including the: arithmetic mean ($\overline{\lambda_S} = \overline{\lambda_R}$ for the calibration), variance (σ_S^2), standard deviation (σ_S) and coefficient of variation (COV_S), were calculated for each site-specific and geologic-specific study. Prior distribution parameters from Paikowsky (2004) or Abu-Farsakh et al. (2010) were utilized for Bayesian updating procedure. The national database from Paikowksy (2004) included 44 DSF designed by using the design procedures discussed in Brown et al. (2010) and geotechnical investigation data that included blow count values from SPT, tip resistance, friction, and pore pressure ratio values from CPT, and undrained shear strength values from samples obtained using the shelby tube. The soil types in the national database included: cohesionless soils, cohesive soils, and mixed cohesionless and cohesive soils. Specifically, the national database, from Paikowsky (2004), was utilized as a prior distribution because the national data encompassed a variety of 1) soil types, 2) geotechnical investigation methods, and 3) design procedures from across the United States of America. The regional database that was obtained from Abu-Farsakh et al. (2010) was based on 22 DSF that were designed by utilizing the SHAFT program and then tested with a BLC. The soil, in which each DSF was constructed, consisted primarily of interbedded cohesionless and cohesive soils; the soil was sampled utilizing blow count values from SPT in cohesionless soils and undrained shear strength values in cohesive soils. The distribution parameters that were proposed in Abu-Farsakh et al. (2010) were utilized in this study because the soil types within the Abu-Farsakh et al. (2010) database were within close proximity to the Arkansas sites and were comparable deposits to the soil deposits at the test sites in Arkansas.

8.6.3. Distribution Determination

To utilize the Bayesian updating method, it was assumed that the national and regional data were normally distributed. However, previous studies (Barker et al. 1991, Withiam et al. 1998, McVay et al. 2002, Paikowsky 2004, Abu-Farsakh et al. 2010, Yu et al. 2012) have recommended that the lognormal distribution be utilized to model the bias factor data. But as presented in Figure 8.10, the empirical cumulative distribution frequency of the national and regional data could have been modeled using either the normal distribution or the lognormal distribution.

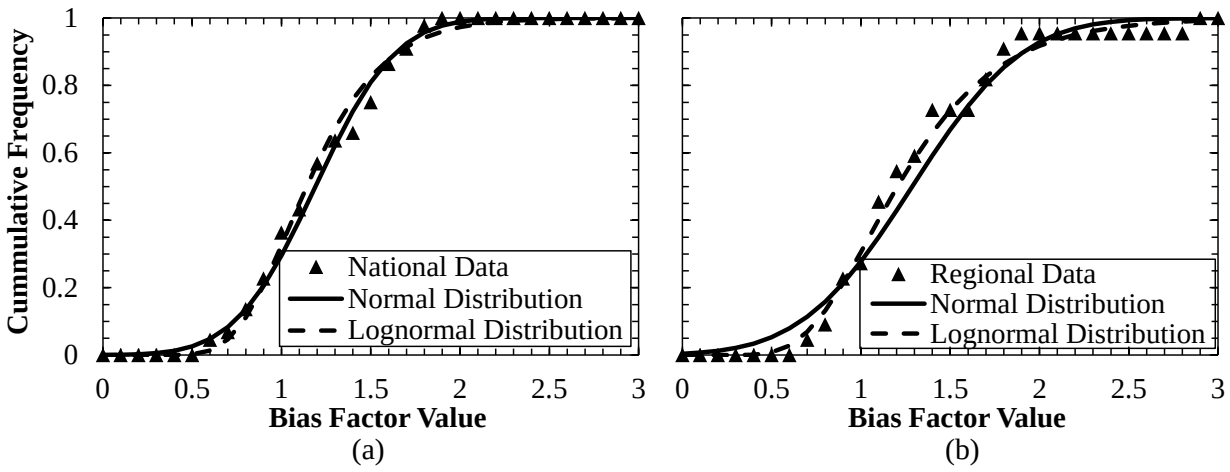

Figure 8.10. Comparison of the empirical cumulative distributions from the a) national dataset (Paikowsky 2004) and b) the regional dataset (Abu-Farsakh et al. 2010) to the normal and lognormal distributions.

To empirically confirm the assumption of normality, the Kolmogorov-Smirnov (KS) test, a nonparametric statistical test as described in Gibbons and Chakraborti (2003), was utilized to compare the empirical cumulative distribution frequency to the normal distribution and to the lognormal distribution. The resulting probability values for the national data were 0.63 and 0.45 for the normal distribution and for the lognormal distribution, respectively. The probability

values for the Louisiana/Mississippi data, as obtained by using the KS test, were 0.70 and 0.95 for the normal distribution and for the lognormal distribution, respectively. As shown in Figure 8.10 and as observed from the results of the KS test, it was verified that, with greater than 60 percent certainty, the normal distribution may be utilized to characterize the data that were used to obtain the national and regional bias factors. Although the normal distribution was utilized during the Bayesian updating, the posterior distribution parameters, as obtained from the Bayesian updating, were transformed to a lognormal distribution for the reliability analysis because the high probability (95 percent) that the regional data, which was believed to be similar to the sampled data, was lognormally distributed.

8.6.4. Validation Study of the Bayesian Updating Method

A validation study was performed using two prior calibration studies to validate the efficacy of utilizing the Bayesian updating method, in combination with the Monte Carlo simulation method, to calibrate localized resistance factors. For this study, the national load test database, as obtained from Paikowsky (2004), was utilized as the prior distribution and the regional database, as obtained from Abu-Farsakh et al. (2010), was utilized as the sampled distribution. The arithmetic values of the mean and coefficient of variation for the posterior distribution were determined, by using the Bayesian updating method, and are presented numerically in Table 8.6 and visually in Figure 8.11. Due to the higher mean and COV values from the Abu-Farsakh et al. (2010), the values of the mean and coefficient of variation (COV), for the Bayesian updated distribution, were larger than the corresponding values from Paikowsky (2004). The value of the resistance factor that was determined by using the Monte Carlo simulation method from the Bayesian updated lognormal posterior distribution parameters, was 0.50 for a reliability index of 3.0 (as compared to a reported value of 0.58 in Paikowsky 2004,

and a reported value of 0.52 in Abu-Farsakh et al. 2010). This method was considered valid because the calculated resistance factor was 3.8 percent less than the resistance factor recommended by Abu-Farsakh et al. (2010).

Table 8.6. Arithmetic distribution parameters for the values of the bias factor of the resistance values for the verification study.

Database	Source	Mean ($\bar{\lambda}_R$)	Coefficient of Variation (COV)	Standard Deviation (σ_R)	Resistance Factor (ϕ)
National	Paikowsky (2004)	1.19	0.30	0.36	0.58
Regional	Abu-Farsakh et al. (2010)	1.29	0.38	0.49	0.52
Geologic-Specific	Posterior Distribution	1.21	0.31	0.38	0.50

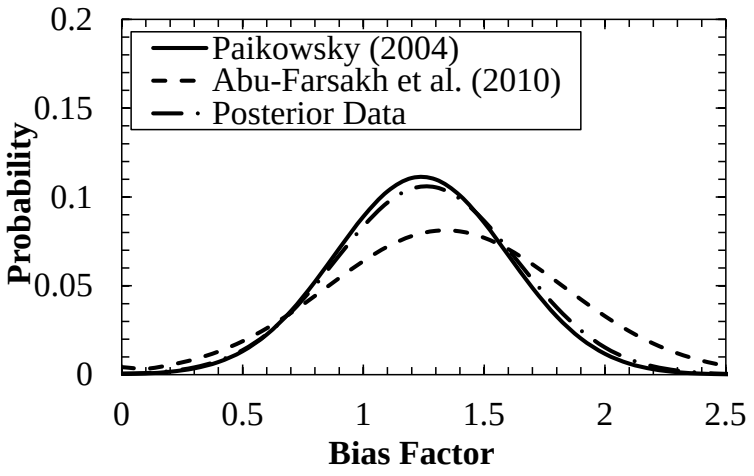

Figure 8.11. Bayesian updating method for the validation study.

The steps utilized during implementation of the Bayesian updating method and the Monte Carlo simulation method that were utilized to determine posterior distribution parameters are presented in Figure 8.12. By utilizing the previously presented Equations 8.12 and 8.13 and the sampled parameters presented in Table 8.7, the Bayesian updated distribution parameters (μ_n and σ_n^2) were calculated for two site-specific (MATS and TATS) and one geologic-specific (mixed soils) calibrations. After the Bayesian updated distribution parameters were determined, the

reliability analysis was performed by utilizing the Monte Carlo simulation method. Specifically, for each geotechnical investigation method and each of the associated DSF design software programs, a resistance factor was determined for a reliability index (β) of 3.0. A summary of the generalized steps for the Bayesian updating method in conjunction with the Monte Carlo simulation method, are outlined below.

1. Choose the prior distribution type in terms of $\overline{\lambda_p}$, σ_p, and n_p of the bias factors, as based on the soil type, the geotechnical investigation method, and the design software programs.

2. Choose the influence factor (κ_p) for the prior distribution ($\kappa_p \leq n_p$).

3. Calculate the Bayesian modified resistance distribution parameters using Equations 8.12 and 8.13.

4. Calculate lognormal parameters for the posterior distribution parameters using Equations 8.14 and 8.15.

$$\lambda_{\log,i} = \ln\left(\overline{\lambda_{n,ı}}\right) - 0.5\zeta^2_{\log,i}$$ (Haldar and Mahadevan 2000) Equation 8.14

$$\zeta^2_{\log,i} = \ln\left[1 + \left(\frac{\sigma_{n,i}}{\overline{\lambda_{n,ı}}}\right)^2\right]$$ (Haldar and Mahadevan 2000) Equation 8.15

Previously unintroduced variables that are utilized in Equations 8.14 and 8.15 include: the logarithmic mean of the bias factor for i ($\lambda_{\log,i}$), the type of load/resistance (i), and the logarithmic standard deviation of the bias factor for i ($\zeta_{\log,i}$).

5. Choose an initial resistance factor value (ϕ) and a design reliability index value (β_{design}).

6. Generate random variables ($n \geq 9900$ as in Abu-Farsakh et al. 2010) based on the lognormal mean and lognormal standard deviation bias factor values for the dead load, live load, and resistance (for this study n=50,000).

7. Utilize Equation 8.11 to calculate the limit state for each trial set (a g(x); for λ_{DLi}, λ_{LLi}, λ_{Ri} where i=1 to n).

8. Determine the number of foundation failures for the trail set (i.e. count[g(x) < 0]).

9. Determine the probability of failure as the ratio of the number of failures to the number of total foundations $\left(\text{i.e. } p_f = \frac{\text{count}[g(x)<0]}{n}\right)$.

10. Calculate the reliability index (i.e. $\beta_{calculated} = \Phi^{-1}[p_f]$).

11. Finally, if $|\beta_{\text{calculated}} - \beta_{\text{design}}| < \text{tolerance limit}$, then ϕ is the calibrated resistance factor value, otherwise repeat steps 5-10 until the difference is within the tolerance limit.

Table 8.7. Posterior distribution parameters (mean and standard deviation) calculated for the site-specific and Arkansas geologic-specific (a deltaic and alluvial soil deposit) calibration studies.

			Resistance Bias Factor Distribution Parameters		
Site	**Software Program**	**Geotechnical Investigation Method**	Mean (μ_R)	Standard Deviation (σ_R)	Coefficient of Variation (COV_R)
MATS	SHAFT	AHTD	1.07	0.10	0.10
		MODOT	0.87	0.06	0.07
		UofA	1.01	0.10	0.10
	FB-Deep	AHTD	1.04	0.13	0.12
		MODOT	0.93	0.05	0.06
		UofA	1.08	0.09	0.09
TATS	SHAFT	AHTD	1.49	0.25	0.17
		MODOT	1.21	0.17	0.14
		UofA	1.13	0.19	0.17
	FB-Deep	AHTD	1.74	0.23	0.13
		MODOT	1.23	0.19	0.16
		UofA	1.20	0.17	0.14
Arkansas Geologic-Specific (Mixed Soils)	SHAFT	AHTD	1.28	0.28	0.22
		MODOT	1.04	0.22	0.21
		UofA	1.07	0.15	0.14
	FB-Deep	AHTD	1.39	0.41	0.30
		MODOT	1.08	0.20	0.19
		UofA	1.14	0.14	0.12

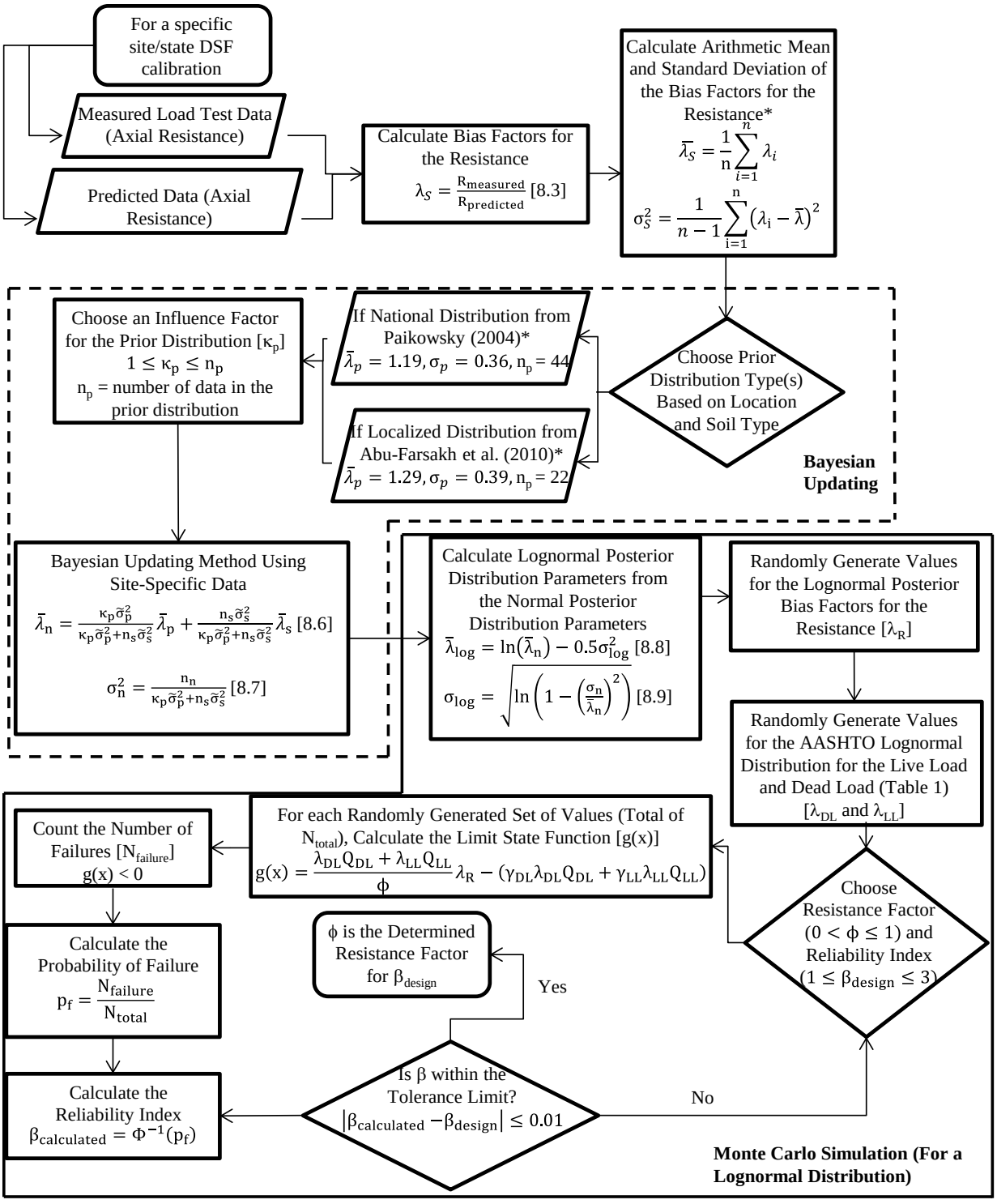

Figure 8.12. Flowchart of the Bayesian updating method utilized in conjunction with the Monte Carlo simulation method.

8.6.5. Potential Cost Savings

Potential cost savings for DSF designed and constructed at a given project site (24 DSF) were calculated based on the resistance factor values obtained from Paikowsky (2004), from Abu-Farsakh et al. (2010), and from the site-specific calibrated values. The lengths for 1.2m diameter DSF were calculated by using the various software programs in conjunction with the data obtained from the various geotechnical investigation methods, and the corresponding resistance factor value. For a 1.2m DSF, an average cost per linear foot of $500 was utilized (ITD 2014 and TXDOT 2015). The cost of the DSF project, when utilizing the recommended resistance factor values from Paikowsky (2004) and from Abu-Farsakh et al. (2010), only included the cost of the DSF and no load tests. However, to evaluate the use of the site-specific calibrated resistance factor values, the cost of the DSF project included the cost of the DSF and the cost of three full-scale load tests (approximately $75,000 US dollars, per test as reported in Brown 2008 and Bey 2014). The cost of the DSF project, as estimated by using the previous assumptions, was compared for the different designs to determine the possible cost savings when performing a site-specific calibration study.

8.7. Results

8.7.1. Localized Calibration

The results of the site-specific and geologic-specific (mixed soils) calibration of the resistance factors in Arkansas were presented in Table 8.8. Except for a few of the results obtained for the various geotechnical investigation/software program combinations, the resistance factor values were higher than the values that were recommended by Paikowsky (2004) and Abu-Farsakh et al. (2010). In general, the resistance factor values for the geologic-specific soil deposits (alluvial and deltaic) within the state of Arkansas were increased, except

when utilizing the Abu-Farsakh et al. (2010) prior distribution along with the SHAFT software program and the MODOT data or along with the FB-Deep software program and the AHTD data. When the UofA data were utilized, the resistance factor values were increased by utilizing either of the software progams and either of the prior distributions. Therefore, because the deltaic and alluvial soil deposit calibration was calculated from six full-scale load tests that were performed on DSF in the state of Arkansas, it was determined that a larger database of DSF should be utilized to increase the accuracy of the values of the determined resistance factor. Particularly, additional tests should be included because of the construction problems that occurred while constructing two of the DSF (one at the MATS and one at the TATS). As discussed in Race and Coffman (2015a, 2015b), these problems affected the axial resistance, at a movement of 5%D, that resulted in a lower value for the mean bias factor and higher value for the standard deviation of the bias factor.

Table 8.8. Resistance factors determined utilizing the Bayesian updating method for the MATS, the TATS, and the state of Arkansas.

Site	Software Program	Geotechnical Investigation Method	Resistance Factor Values Calculated Utilizing the Bayesian Updating Method*	
			Paikowsky (2004) Prior Distribution	Abu-Farsakh et al. (2010) Prior Distribution
MATS	SHAFT	AHTD	0.754	0.815
		MODOT	0.796	0.796
		UofA	0.885	0.940
	FB-Deep	AHTD	0.695	0.748
		MODOT	0.891	0.908
		UofA	0.861	0.930
TATS	SHAFT	AHTD	0.644	0.693
		MODOT	0.612	0.609
		UofA	0.595	0.572
	FB-Deep	AHTD	0.662	0.745
		MODOT	0.607	0.599
		UofA	0.620	0.630
Arkansas	SHAFT	AHTD	0.616	0.625
		MODOT	0.590	0.570
		UofA	0.705	0.750
	FB-Deep	AHTD	0.585	0.570
		MODOT	0.612	0.603
		UofA	0.740	0.802

*Reliability Index (β) of 3.0

The resistance factor values for Arkansas geologic-specific (deltaic and alluvial) are presented in Figure 8.13, as a function of reliability index. These resistance factor values were calculated based on the prior distributions from a) Paikowsky (2004) or b) Abu-Farsakh et al. (2010). In general, the value of the resistance factor as calculated by using the Abu-Farsakh et al. (2010) prior distribution was greater than the value of the resistance factor that was calculated by using the Paikowsky (2004) distribution. Although the value of the COV_R of the bias factor that was obtained from the Paikowsky (2004) distribution was less than the value of the COV_R of the bias factor that was obtained from the Abu-Farsakh et al. (2010) distribution, the mean value of the bias factor that was obtained from Paikowsky (2004) was smaller (1.19 from Paikowsky

2004 as opposed to 1.29 from AbuFarsakh et al. 2010) thereby leading to the higher resistance factor values from the Abu-Farsakh et al. (2010).

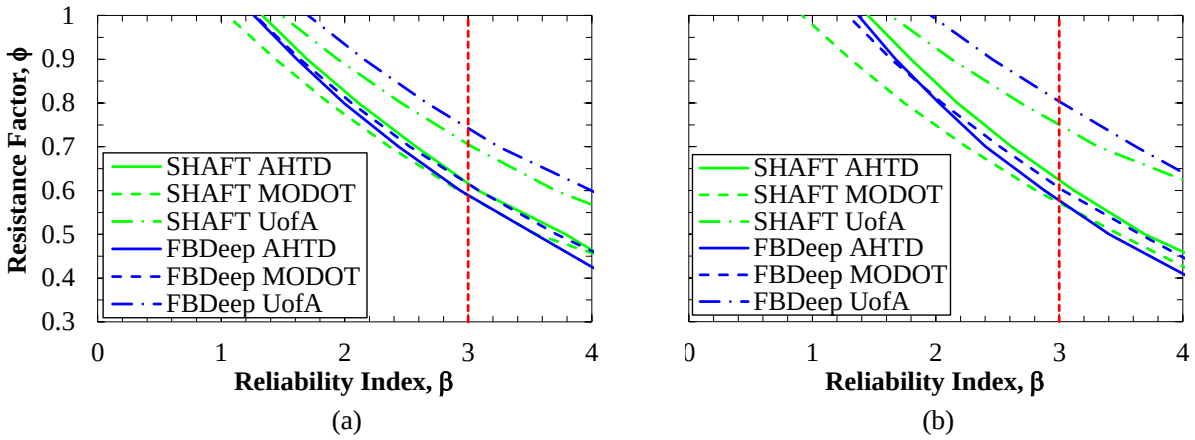

Figure 8.13. Resistance factor values for mixed soil sites within the state of Arkansas (n=6) as a function of reliability index, as obtained by using the Bayesian updating method with a prior distribution from a) Paikowsky (2004) and b) Abu-Farsakh et al. (2010).

The resistance factor values that were obtained by utilizing the SHAFT software program were typically less than the values that were obtained by utilizing the FB-Deep software program when the MODOT and UofA data were employed, but greater when the AHTD data was employed. Therefore, when designing a DSF, the geotechnical investigation method and the software program should be considered to reduce the uncertainty in the design of the DSF and, therefore, to obtain a higher resistance factor. For the AHTD and MODOT data, the difference in the resistance factor for different prior distributions was small (less than 0.02). The resistance factor values when using the UofA data were significantly greater (at least 0.12) than the recommended resistance factors. When using the prior distribution from Abu-Farsakh et al. (2010), the resistance factor values for the UofA method were at least 0.045 higher than the values obtained by using the prior distribution from Paikowsky (2004).

The resistance factor values that were calibrated for the combined deltaic and alluvial deposits within the state of Arkansas were generally lower than the resistance factor values that

were calibrated for each site. Even though the sites consisted of similar soil types (i.e. mixed soil), there was less uncertainty in the bias factors that were determined from the MATS than were determined from the TATS. Specifically, the variability of the bias factor was significantly reduced by performing a site-specific resistance factor calibration. Because the resistance factor values varied in regard to the test site, it was observed that the bias factors were affected by variables such as stratigraphy types and layers, construction crew, and construction methods. Like with the deltaic and alluvial soil deposit resistance factor calibration, the resistance factor values that were obtained for the site-specific resistance factor calibration, by utilizing the Abu-Farsakh et al. (2010) prior distribution were generally greater than the resistance factor values that were obtained by using the Paikowsky (2004) prior.

8.7.2. Cost Analysis

For all but one of the combined geotechnical investigation/software program/prior distribution methods (FB-Deep with AHTD data using the Paikowsky 2004 prior distribution), the site-specific resistance factors for the MATS were utilized to save money when compared to utilizing the AASHTO (2007) recommended resistance factors, as presented in Table 8.9. The largest cost savings of $463,800 US dollars (29.7 percent of the total) was obtained by utilizing the site-specific calibrated resistance factors for the MATS with SHAFT and the UofA data and the prior distribution from Abu-Farsakh et al. (2010) as presented in Table 8.10. Even though the measured total resistance of one of the DSF at the MATS was low due to poor concrete placement (as mentioned in Race and Coffman 2015b), the variance values of the bias factor were low and consequently the values of the resistance factor were high. Conversely, there was almost no cost savings when utilizing the calibrated resistance factor values for the TATS. Due to the large difference between the predicted and measured resistance for the DSF constructed

within a collapsed and redrilled excavation at the TATS (discussed in Race and Coffman 2015b), there was a large variation in the resistance bias factor and consequently low values for the resistance factors. At sites with three full-scale load tests and minimal problems associated with the measured resistance, site-specific resistance factor values may be utilized to significantly reduce project costs.

Table 8.9. Design lengths of a 1.2m diameter DSF by utilizing site-specific resistance factors (prior distribution from Paikowsky 2004) and the subsequent cost for a large project of 1.2m diameter DSF (24 total).

Site	Software Program	Geotechnical Investigation Method	Design Length (m)		Project Cost (USD)	
			Original	Calibrated	Original*	Calibrated+
MATS	SHAFT	AHTD	82	63	1,377,600	1,283,400
		MODOT	62	35	1,041,600	813,000
		UofA	82	55	1,377,600	1,149,000
	FB-Deep	AHTD	77	67	1,293,600	1,350,600
		MODOT	63	34	1,058,400	796,200
		UofA	77	60	1,293,600	1,233,000
TATS	SHAFT	AHTD	91	88	1,528,800	1,703,400
		MODOT	88	82	1,478,400	1,602,600
		UofA	82	81	1,377,600	1,585,800
	FB-Deep	AHTD	101	94	1,696,800	1,804,200
		MODOT	82	77	1,377,600	1,518,600
		UofA	83	78	1,394,400	1,535,400

*Cost included construction equipment, man hours, and materials

+Cost included construction equipment, man hours, materials, and three full-scale load tests

Table 8.10. Design lengths of a 1.2m diameter DSF by utilizing site-specific resistance factors (prior distribution from Abu-Farsakh et al. 2010) and the subsequent cost for a large project of 1.2m diameter DSF (24 total).

Site	Software Program	Geotechnical Investigation Method	Design Length (m)		Project Cost (USD)	
			Original	Calibrated	Original*	Calibrated+
MATS	SHAFT	AHTD	90	59	1,512,000	1,216,200
		MODOT	69	35	1,159,200	813,000
		UofA	93	52	1,562,400	1,098,600
	FB-Deep	AHTD	86	65	1,444,800	1,317,000
		MODOT	67	33	1,125,600	779,400
		UofA	89	57	1,495,200	1,182,600
TATS	SHAFT	AHTD	94	87	1,579,200	1,686,600
		MODOT	98	83	1,646,400	1,619,400
		UofA	86	83	1,444,800	1,619,400
	FB-Deep	AHTD	113	90	1,898,400	1,737,000
		MODOT	95	79	1,596,000	1,552,200
		UofA	90	76	1,512,000	1,501,800

*Cost included construction equipment, man hours, and materials

+Cost included construction equipment, man hours, materials, and three full-scale load tests

8.8. Recommendations

Recommendations from this research include: 1) the use of Bayesian updating method in conjunction with the Monte Carlo simulation method and 2) the implementation of resistance factors as developed from site-specific calibrations. The Bayesian updating method may be successfully utilized to calibrate the resistance factors of DSF for small datasets. In particular, a site-specific resistance factor calibration may be performed by utilizing the Bayesian updating method and the Monte Carlo simulation method. For future site-specific calibration studies that are within a previous localized calibration area (i.e. Florida, Louisiana/Mississippi, etc.), it is recommended that the corresponding regional specific data be utilized as the prior distribution data. Moreover, it is recommended that the same software program that was utilized for the regional specific database also be utilized. Specifically, it is recommended that a prior

distribution that contains data from similar soil types and within close proximity to the test site be used, if available; otherwise, the national database is an acceptable prior distribution.

In summary, software programs and geotechnical investigation methods should be considered when performing a site-specific resistance factor calibration for DSF. If the standard deviation of the resistance bias factors is high, then it is recommended that a different software program be used to reduce the amount of uncertainty associated with the software program. Similarly, if the mean of the bias factors is low (less than 0.9) or high (greater than 1.3), it is recommended that a different software program be used to more accurately predict the resistance provided by the DSF.

From this Arkansas specific (deltaic and alluvial soil deposit) resistance factor calibration study, it is recommended that data from more than six full-scale tests on DSF be utilized (particularly if the tests only come from two sites). While small quantities of tests may be utilized for site-specific resistance factor calibration, the calculated values for the resistance factor may be higher than the "true" resistance factor for the state. However, it is recommended to utilize the site-specific resistance factor values particularly at sites with low variability. The values for the resistance factors that were calculated for the state of Arkansas were higher than the resistance factors calculated for the TATS due to the poor dataset at the TATS. If the calculated values for the deltaic and alluvial soil deposit resistance factors were utilized for the TATS, the probability of failure increased from 0.001 to 0.0078 (almost 8 failures in 1000 foundations). It is, therefore, recommended that data for a more accurate deltaic and alluvial soil deposit resistance factor calibration for DSF be obtained from at least four different sites and from at least ten different load tests to account for the variance associated with different soil stratigraphy and different DSF construction contractors.

8.9. Conclusions

From this research, it was determined that the Bayesian updating method may be utilized in conjunction with the Monte Carlo simulation method to perform a site-specific calibration for resistance factors. From the verification study, in which two previous DSF databases were utilized, the calculated resistance factor that was obtained, by using the Bayesian updating method, was within 15 percent of either resistance factors that were obtained from the databases. For the test sites in Arkansas, identified as the MATS and TATS, the deltaic and alluvial soil deposit resistance factor values were increased from the recommended 0.52 and 0.58 up to 0.74 and 0.80 by using the FB-Deep software program and the UofA geotechnical investigation method based on the national and Louisiana/Mississippi prior distribution data, respectively. Cost savings associated with the site-specific calibration of resistance factor values for the MATS, by using the Bayesian updating method range from $127,800 (8.8 percent of the total) to $463,800 (29.7 percent of the total) when using FB-Deep AHTD method and SHAFT UofA method, respectively, in conjunction with the Louisiana/Mississippi database.

It is recommended that engineering judgment be utilized when performing site-specific calibration studies. For the Bayesian updating method, the prior distribution data should be from either the national database or a localized database that is within close geographical proximity to the test site and that contains the same or similar soil stratigraphy as the test site. Furthermore, for soil deposit calibration studies, the Bayesian updating method may be utilized for small sample sets (recommended for at least 10 full-scale tests and from at least four different sites) across a given state. However, it is recommended that at least a total of 10 full-scale tests acquired from at least four sites be utilized.

8.10. Acknowledgements

The authors thank all of the companies and individuals who made this project possible, including but not limited to: the Arkansas State Highway and Transportation Department, The International Association of Foundation Drilling, McKinney Drilling Company, Loadtest, Missouri Department of Transportation, Foundation Technologies, and GEI Consultants, Inc.

8.11. Notations

The following symbols are used in this paper:

COV = coefficient of variation;
COV_{DL} = coefficient of variation for the dead load;
COV_{LL} = coefficient of variation for the live load;
COV_R = coefficient of variation for the resistance;
DL = dead load;
g(x) = the limit state;
i = the type of load/resistance;
LL = live load;
n_n= the number representing the total number of posterior data points (κ_p+n_s);
n_s= the number of sampled data;
Q_i = the amount of load for the i^{th} load type;
Q_n = the sum of the nominal loads;
R = resistance;
R_m = the measured resistance value;
R_n = from the nominal resistance;
R_p = the predicted resistance value;
β_c = calculated reliability index value;
β_d = design reliability index value;
β_T = the target reliability index;
ϕ = the resistance factor;
γ_{DL} = load factor for the dead load;
γ_{LL} = load factor for the live load;
κ_p = the influence factor of the prior distribution;
λ_i = the respective bias factor for a given load type;
λ_{DL} = bias factor for the dead load;
λ_{LL} = bias factor for the live load;
$\lambda_{log,i}$ = the logarithmic bias factor for i;
$\overline{\lambda_n}$ = the posterior mean;
$\overline{\lambda_{n,i}}$ = the mean of the bias factor for i;
$\overline{\lambda_p}$ = the mean of the prior distribution;
λ_R = bias factor for the resistance;

$\overline{\lambda_R}$ = the mean of the bias factor for the resistance data;
$\overline{\lambda_s}$ = the mean of the sampled data;
$\zeta_{log,i}$ = the logarithmic standard deviation of the bias factor for i;
σ_n^2 = the variance of the posterior distribution;
$\tilde{\sigma}_p^2$ = the prior variance; and
$\tilde{\sigma}_s^2$ = the variance of the sampled data.

8.12. References

Abu-Farsakh, Y.M., Yu, X., Yoon, S., and Tsai, C. (2010). "Calibration of Resistance Factors Needed in the LRFD of Drilled Shafts." Rep. No. 470, Louisiana Transportation Research Center, Baton Rouge, LA.

Allen, T.M., Nowak, A.S., and Bathurst, R.J. (2005). "Calibration to Determine Load and Resistance Factors for Geotechnical and Structural Design." Transportation Research Board, Research Circular E-C079, Washington, D.C., 93 pgs.

AASHTO (American Association of State Highway and Transportation Officials). (2001). LRFD Bridge Design Specifications, American Association of State Highway and Transportation Officials, Washington, D.C.

AASHTO (American Association of State Highway and Transportation Officials). (2007). LRFD Bridge Design *Specifications*, 4th ed. American Association of State Highway and Transportation Officials, Washington, D.C., 1938 pgs.

Barker, R M, Duncan, J. M., Rojiani, K. B., Ooi, P. S. K., Tan, C. K. and Kim, S. G. (1991). Manuals for Design of Bridge Foundations, NCHRP Report 343, Transportation Research Board, Washington D.C.

Bey, Sarah (2014). "Cost-benefit Analyses for Load and Resistance Factor Design (LRFD) of Drilled Shafts in Arkansas." MS thesis, University of Arkansas. Ann Arbor: ProQuest/UMI, 410 pgs. (Publication No. 1554893).

Cheung, R., and Tang, W. (2000). "Bayesian Calibration of Slope Failure Probability." Geo-Denver 2000, Denver, Colorado, August, pp. 72-85.

Enright, M.P., and Frangopol, D.M. (1999). "Condition Prediction of Deteriorating Concrete Bridges Using Bayesian Updating." *J. Struct. Eng.*, DOI: 10.1061/(ASCE)0733-9445(1999)125:10(1118).

FB-Deep (2012). Bridge Software Institute, Gainesville, Florida, Version 2.04.

Gibbons, J.D. and Chakraborti, S. (2003). *Nonparametric Statistical Inference*. Marcel Dekker, Inc. New York.

Guo, Wei (2013). “Simple Model for Nonlinear Response of 52 Laterally Loaded Piles.” J. Geotech. Geoenviron. Eng., Vol. 139, No. 2, pp. 234-252.

Haldar, A., and Mahadevan, S. (2000). *Probability, Reliability, and Statistical Methods in Engineering Design*. Wiley, New York.

Hicher, Pierre-Yves (1996). “Elastic Properties of Soils.” J. Geotech. Engrg., Vol. 122, No. 8, pp. 641-648.

Hoff, Peter (2009). *A First Course in Bayesian Statistical Methods.* Springer, New York, 270 pgs.

IDT (2014). “Cost Estimate: Average Unit Prices for Standard Bid Items.” Idaho Transportation Department, pp. 8.

Jabo, Joseph (2014). “Reliability-Based Design and Acceptance Protocol for Driven Piles.” Ph.D. dissertation, University of Arkansas. Ann Arbor: ProQuest/UMI, 268 pgs. (Publication No. 3667200).

Loehr, J.E., Bowders, J.J., Rosenblad, B.L., Luna, R., Maerz, N., Stephenson, R.W., Likos, W.J., and Ge, L. (2013). “Implementation of LRFD Methods to Quantify Value of Site Characterization Activities.” Proc. Of the 18th Int. Conf. on Soil Mech. And Geotech. Eng., Paris, pp. 1831-1834.

McVay, M.C., Ellis, R.D., Birgisson, B., Consolazio, G., Putcha, S., and Lee, S.M. (2002). “Use of LRFD, Cost and Risk to Design a Drilled Shaft Load Test Program in Florida Limestone.” Transportation Research Record 1808, Transportation Research Board, Washington, DC, 19 pgs.

Nadim, Farrokh (2007). “Tools and Stratgeies for Dealing with Uncertainty in Geotechnics.” Probabilistic Methods in Geotechnical Engineering, Vol. 491, pp. 71-95.

Najjar, S.S., and Saad, M. (2011). “Bayesian Updating of Load Settlement Curves for Footings on Cohesionless Soil.” Geo-Risk 2011: Risk Assessment and Management, Atlanta, Georgia, June, pp. 263-270.

Nanda, S. and Patra, N.R. (2014). “Theoretical Load-Transfer Curves along Piles Considering Soil Nonlinearity.” J. Geotech. Geoenviron. Eng., Vol. 140, No. 1, pp. 91-101.

Nowak, Andrzej (1999). “Calibration of LRFD Bridge Design Code.” *Transport. Res. Bd.*, Publication NCHRP-368, 218 pgs.

Paikowsky, Samuel (2004). “Load and Resistance Factor Design (LRFD) for Deep Foundations.” NCHRP Report 507, National Cooperative Highway Research Program, Transportation Research Board of the National Academies, Washington, D.C. 126 pgs.

Park, J.H., Kim, D., and Chung, C.K. (2012). “Implementation of Bayesian Theory on LRFD of Axially Loaded Driven Piles.” *Comput. Geotech.*, Vol. 42, pp. 73-80.

Race, M.L., Bey, S.M., Coffman, R.A. (2013). "'Discussion of Implementation of LRFD of Drilled Shafts in Louisiana' by Xinbao Yu, Murad Y. Abu-Farsakh, Sungmin Yoon, Ching Tsai, and Zhongjie Zhang." *J. Infrastruct. Syst*., Vol. 19, No. 3, pp. 351-353, DOI: 10.1061/(ASCE)IS.1943-555X.0000144.

Race, M.L., Bey, S.M., and Coffman, R.A. (2015). "Statistical Analysis to Determine Appropriate Design Methodologies of Drilled Shaft Foundations." *Geotech. Geol. Eng.*, DOI: 10.1007/s10706-015-9854-z.

Race, M.L., and Coffman, R.A. (2013). "Effect of Uncertainty in Site Characterization on the Prediction of Liquefaction Potential for Bridge Embankments in the Mississippi Embayment." ASCE Geotechnical Special Publication No. 231, Proc. GeoCongress 2013: Stability and Performance of Slopes and Embankments III, San Diego, California, March, pp. 888-897.

Race, M., and Coffman, R. (2015a). "Response of a Drilled Shaft Foundation Constructed in a Redrilled Shaft Excavation Following Collapse." *DFI Journal*, DOI:10.1179/1937525515Y.0000000003.

Race, M., and Coffman, R. (2015b). "Case History: Construction Effects on Drilled Shaft Foundations." ISSMGE *IJGCH*, Submitted for Review, IJGCH-S86.

Roberts, L., Fick, D., and Misra, A. (2011). "Performance-Based Design of Drilled Shaft Bridge Foundations." *J. Bridge Eng.*, Vol. 16, No. 6, pp. 745-758.

Scott, B., Kim, B., and Salgado, R. (2003). "Assessment of Current Load Factors for Use in Geotechnical Load and Resistance Factor Design." *J. Geotech. Geoenviron. Eng.*, Vol. 129, No. 4, pp. 287-295.

SHAFT (2012). ENSOFT, INC. Austin, Texas, Version 2012.

Taflanidis, A.A., and Gidaris, I. (2013). "Health Monitoring and Bayesian Updating of Deteriorating Bridge Infrastructures." Structures Congress 2013, Pittsburgh, Pennsylvania, May, pp. 398-409.

TXDOT (2015). "Average Low Bid Unit Price – Construction – Statewide 3 Months Moving Average." Texas Department of Transportation, <http://ftp.dot.state.tx.us/pub/txdot-info/cmd/cserve/nov2014-jan2015.txt> (Feb. 11, 2015).

Vu, Thuy (2013). "Load and Resistance Factor Design of Drilled Shafts at the Service Limit State." PhD Dissertation, University of Missouri-Columbia. Ann Arbor: ProQuest/UMI, 405 pgs. (Publication No. 3577978).

Withiam, J.L., Voytko, E.P., Barker, R.M., Duncan, J.M., Kelly, B.C., Musser, S.C., and Elias, V. (1998). Load and Resistance Factor Design (LRFD) for Highway Bridge Substructures. Report FHWA HI-98-032. Federal Highway Administration, Washington, D.C.

Yoon, G.L., and O'Neill, M.W. (1997). "Resistance Factors for Single Piles from Experiments." *Transport. Res. Rec: J. Transport. Res. Bd*., Vol. 1569, No. 6, pp. 47-54.

Yu, X., Abu-Farsakh, M., Yoon, S., Tsai, C., and Zhang, Z. (2012). "Implementation of LRFD of Drilled Shafts in Louisiana." *J. Infrastruct. Syst.*, Vol. 18, No. 2, pp. 103-112.

CHAPTER 9: Conclusions and Recommendations

Results and recommendations from the previous chapters within this dissertation are subsequently presented herein. The sections in Chapter 9 include the introduction, the statistical analyses, the construction of DSF in moderately strong to strong limestone, the result of DSF constructed in a collapsed excavation, the effects of construction on the measured DSF resistance, and the calibration of resistance factor values using the Bayesian updating method. Similarly, the benefits of this research to the state of Arkansas and the geotechnical community at large are discussed as well as the main recommendations that were obtained from this research.

9.1. Introduction

The purpose of this research project was to calibrate resistance factors that will be used to design of DSF that will be constructed within the state of Arkansas. Because DSF are not commonly utilized in Arkansas, DSF were constructed and tested at three different sites across Arkansas to determine the feasibility and constructability of this deep foundation technique. At each site, three different geotechnical investigation methods were utilized to characterize the properties of the soil at the site and to assess the variability of these properties. Similarly, two software programs were utilized to determine the predicted axial capacity of the DSF. Once constructed, the DSF were tested using a BLC to determine the axial capacity and movement measurements that were associated with loading the DSF (i.e. total resistance, unit side resistance, and unit end bearing resistance). Finally, site-specific and geologic-specific resistance factors were calibrated for the design of DSF by utilizing the Bayesian updating method and the Monte Carlo simulation method.

The stratigraphy at the Siloam Springs Arkansas Test Site (SSATS) consisted of overburden soil underlain by moderately hard to hard limestone. The design length of DSF (1.2m and 1.8m diameter) at the SSATS was 7.9m with an embedment length in rock of 3.0m. The results of the BLC tests included the effects of shortened rock embedment length, predicted unit side resistance values, and design recommendations for moderately strong to strong limestone. The soil at the Turrell Arkansas Test Site (TATS) consisted of 9.1m of cohesive soil underlain by at least 21.3m of cohesionless soil. The design lengths at the TATS were 26.4m (for the 1.2m diameter DSF) and 18.9m (for the 1.8m diameter DSF). Due to the construction methods and environmental conditions at the TATS, there was a partial collapse within one of the 1.2m DSF. A comparison of the load test results from the two 1.2m diameter DSF (uncollapsed and collapsed) at the TATS was discussed in relation to the measured resistance and the predictive models. The soil stratigraphy at the Monticello Arkansas Test Site (MATS) consisted of 18.3m of cohesive soil with a 3.0m interbedded layer of cohesionless soil (depth of 9.2m to 12.2m) underlain by at least 12.2m of cohesionless soil. Numerous construction problems at the MATS included: the loss of slurry into the cohesionless soil deposit, equipment failure, and poor concrete placement. Based on the results obtained from the full-scale load tests, recommendations were presented to improve the construction methods of DSF in cohesionless soils.

To calibrate the resistance factors, the results from the full-scale load tests at the three test sites across Arkansas were utilized to determine bias factors (ratio of the measured resistance to the predicted resistance). Bias factors were calculated for each different geotechnical investigation methods (AHTD, MODOT, and UofA) along with each of the different software programs (FB-Deep and SHAFT). The Bayesian updating method was employed to combine the

sampled data with previous research data because the dataset in Arkansas was small (nine total tests, but only six tests within soil deposits). Finally, the Monte Carlo simulation was performed using the parameters that were obtained from the Bayesian updating method to determine the resistance factor values for the total resistance, unit side resistance, and unit end bearing resistance for a reliability index of 3.0 (probability of failure of 0.001).

9.2. Statistical Analysis of Soil Properties

The horizontal spatial variability of the soil properties, at the test sites within Arkansas, was determined by utilizing the values of the coefficient of variation (COV). The classification of the site variability and the distribution type of the soil property values was investigated for the soil at the MATS and the TATS. In general, the soil property data was not normally or log-normally distributed based on the statistical tests to 95 percent confidence; however, there were multiple soil layers within the cohesive and cohesionless soils that may have caused erroneous values from the statistical testing.

Statistical analyses were similarly utilized to determine the statistical difference between soil property values that were obtained from the different geotechnical investigation methods. The mean and variance soil property values were tested by using the T-test, Wilcoxon test, and F-test. Specifically, the soil property values that were tested included the: blow count, total unit weight, and undrained shear strength. No statistical difference was observed between the undrained shear strength, the total unit weight of clay, and the correlated blow count values that were determined from the UofA and MODOT geotechnical investigation methods; the variance values of the soil properties were not statistically different (95 percent confidence). The predicted axial capacities of DSF at the MATS and TATS, as well as the load-movement curves, were discussed in relation to the software program that was utilized and the geotechnical

investigation method that was utilized. There was an inverse relationship between the number of statistically similar soil properties and the percent difference in the load-movement values at failure. Finally, it was determined that the predicted axial capacity and load-movement response of the designed DSF were statistically dependent upon the geotechnical investigation methods (i.e. AHTD, MODOT, or UofA) and the software program that was utilized.

9.3. DSF in Moderately Strong to Strong Limestone

The constructed lengths of the DSF at the SSATS, designated as the West 1.2m, Center 1.8m, and East 1.2m diameter DSF, were 7.9m, 6.4m, and 7.0m, respectively. The field changes of the DSF lengths were problematic regarding the BLC test because there was not enough upward resistance within the shorter DSF to resist the base resistance. Problems occurring with the construction of the DSF at the SSATS included: 1) a lag time between drilling and concrete placement, 2) bad concrete placement below the BLC within the first DSF, and 3) missing telltales on the bottom plate of the BLC within the second and third DSF.

The unit side resistance in moderately strong to strong limestone of DSF may be predicted using procedures described in McVay and Niraula (2004), particularly for the weathered limestone at the SSATS. The unit side resistance in competent limestone could not be accurately predicted because the ultimate capacity was not determined from the BLC test of the West 1.2m DSF. Furthermore, the maximum unit end bearing resistance was not determined because the upward resistance within the Center 1.8m and East 1.2m DSF was not enough large enough to counterbalance the downward resistance that was required. Conversely, the concrete below the BLC was not competent in the West 1.2m DSF; therefore, the measured unit end bearing resistance was not an accurate representation of the downward movement of the BLC. Because the movement of DSF at the SSATS was very small, it was recommended that the

design of DSF in moderately hard to hard limestone be limited to a service limit of 0.2cm or 0.1%D. It was also recommended to add additional static weight to the top of the DSF and then reperform the BLC test to measure larger load and movement values for the DSF (particularly for the Center 1.8m and East 1.2m) at the SSATS.

9.4. Effects of a DSF with a Collapsed Excavation

Three DSF were constructed at the TATS with lengths of 26.2m, 18.9m, and 26.5m for the South 1.2m, Center 1.8m, and North 1.2m diameter DSF, respectively. The soil at the TATS consisted of 6.1m clay over 3.0m of liquefiable silt underlain by at least 21.3m of liquefiable medium dense to dense sand. The results of the BLC tests, including the upward and downward movement of the BLC, the load transfer along the DSF, the creep, the top-down equivalent load-movement response, the unit side resistance, and the unit end bearing resistance, were presented in Chapter 6.

Due to the difficult site conditions during construction, the excavation of the North 1.2m diameter DSF partially collapsed within the silt layer. Because of the proximity of the North 1.2m DSF to the South 1.2m DSF, a comparison of the DSF properties between a DSF with a collapsed excavation (North 1.2m DSF) and a DSF with an uncollapsed excavation (South 1.2m DSF) was performed. Primary effects of the collapsed excavation included: larger upward and downward movement values, larger top-down equivalent movement values, and reduced unit side resistance values. Even though the excavation collapsed, the required axial capacity was met and the effect of the collapse upon the unit end bearing resistance was remediated by drilling an additional 0.3m below the depth of the excavation following the collapse.

The FB-Deep program was utilized to predict the equivalent top-down load-movement response and the unit side resistance-movement response for the South 1.2m and for the North

1.2m DSF. The responses of the South 1.2m DSF (uncollapsed excavation) were most closely modeled by using the MODOT and UofA soil sampling and testing methods in conjunction with the FB-Deep software program. The post-collapse unit side resistance-movement response of the North 1.2m DSF (collapsed excavation), at the TATS, was best modeled by using 1) a 10 percent reduction in the total unit weight values within the silt layer and 2) an additional 3.0m layer of silt within the top of the sand layer. The justification of the modified model, for the North 1.2m DSF at the TATS, was a reduction in the horizontal effective stress due to less material being located within the silt layer and due to lubrication along the top portion of the DSF, within the sand layer, that was caused by the silty soil coating the DSF within the sandy soil (a function of redrilling with the same diameter). Further investigation into the effects of collapsed DSF, on axial capacity, should be performed to develop unit side resistance-movement responses for DSF constructed within a redrilled excavation.

The scaling effect of DSF was investigated with the comparison of the unit side resistance of the South 1.2m and the Center 1.8m. The scaling ratio (the ratio of the unit side resistance for the Center 1.8m DSF to the unit side resistance for the South 1.2m DSF) was calculated along the length of the DSF. The scaling ratio ranged from 0.60 to 1.50 with an average of 1.0. The scaling factor for the unit end bearing resistance of the Center 1.8m to the South 1.2m DSF was determined to be 1.68. It is recommended to perform additional full-scale load tests on various diameter sizes of DSF. Scaling factors for the unit side resistance and the unit end bearing resistance would enable the use of smaller diameter DSF to be constructed and tested during the geotechnical investigation phase to provide design parameters that will enable more accurate design of full-scale DSF.

9.5. Construction Effects on DSF Capacity

At the MATS, three DSF were constructed to depths of 27.9m, 21.9m, and 27.9m for the DSF designated as the North 1.2m, Center 1.8m, and South 1.2m diameter DSF, respectively. Problems that occurred during construction of the DSF at the MATS included: 1) slurry loss in to the cohesionless soil deposits, 2) extended periods of open excavation, 3) equipment failure, and 4) poor concrete placement. The results of three full-scale BLC tests performed on the DSF at the MATS were discussed in Chapter 7 with respect to the construction effects. In particular, the construction effects included higher measured movement values, lower measured unit side resistance values, and lower measured unit end bearing resistance values.

Problems associated with the concrete placement that occurred within the South 1.2m diameter DSF at the MATS were the cause of the large downward movement of the BLC; however, the required capacity of the DSF was still attained. The equivalent top-down response of the DSF with minor construction problems (i.e. loss of slurry) was modeled using FB-Deep; however, the measured response of the DSF, with major construction problems (i.e. poor concrete placement), was significantly lower than the predicted response.

Because of the problems that occurred while constructing the DSF at the MATS, it is recommended that DSF that are constructed (drilled and concrete poured) in high permeability, cohesionless soil be constructed in a single day. The cost savings associated with the loss of slurry may be upwards of $2000 per day plus the addition of the cost of equipment ($10,000 per day for a 33m tall crane and an AF220 drill). Recommendations regarding the placement of concrete within DSF that were discussed included: 1) a minimum slump of 12.7cm at the time of pouring into the DSF excavation, 2) a maximum time to placement of 2 hours (time starts once the concrete enters the drum truck and ends once the concrete enters the DSF excavation), and 3)

a maximum addition of 37.9 liters of makeup water to nine cubic meters of concrete, after the time of batching.

9.6. Resistance Factor Calibration

From the nine full-scale load tests that were performed across the state of Arkansas, site-specific and geologic-specific resistance factor values were calculated for the design of DSF. Due to the small number of tests, resistance factors were calculated by using the Bayesian updating in conjunction with the Monte Carlo simulation. Three different conjugate prior distributions (normal, normal-gamma, and flat/noninformative distributions) were used in the Bayesian updating to determine posterior distribution parameters. The validity of the Bayesian updating method was confirmed by comparing bias factors for eight DSF tests in Greenville, Washington county, Mississippi to a predictive posterior distribution calculated from the national loadtest database and the Louisiana/Mississippi loadtest database (minus the eight Greenville tests).

The calibrated total resistance factors ranged from 0.57 to 0.94. Based on subsequent cost analyses that were performed on the modified lengths that were determined by using the site-specific resistance factors, the cost savings associated with performing a site-specific resistance factor calibration were between $127,800 to $463,000 when using the FB-Deep/AHTD method and the SHAFT/UofA method at the MATS (when the Louisiana/Mississippi database as a prior distribution), respectively.

It is recommended that site-specific resistance factor calibration studies be performed at sites with low to medium spatial variability (COV $\leq$ 0.4). In many cases, the calculated resistance factor values were greater than the recommended maximum value of 0.7 (AASHTO 2007); therefore the use of resistance factors greater than 0.7 should be utilized with engineering

judgment and the construction methods should be closely monitored for consistency. Although the Bayesian updating method may be utilized in conjunction with the Monte Carlo simulation method (using the national database as a prior distribution) to calculate site-specific and geologic-specific resistance factor values, it is recommended that the prior data that is utilized to calculate distribution parameters be chosen with consideration to the soil/rock type, load test type, and quality of the test data.

In summary, geologic-specific calibrated resistance factors were calculated for DSF constructed in mixed soil (clay and sand) within Arkansas for the total resistance, unit side resistance, and unit end bearing resistance. The state-wide resistance factor values were determined from six full-scale load tests on DSF that were constructed in Arkansas. A summary of the resulting state-wide calibrated resistance factors for the Strength I limit state (5%D) are presented in Table 9.1. The resistance factor values for the total resistance were generally higher than the recommended national resistance factor values (0.58 for a site with low spatial variability). Conversely, the resistance factor values for the unit side and unit end bearing resistance were lower than the national values (but similar in magnitude to the recommended resistance factor values that were obtained from the Louisiana/Mississippi loadtest database).

Table 9.1. Summary of the alluvial and deltaic geologic-specific calibrated resistance factor values for the strength limit state for a reliability index (β) of 3.0.

Design Property	Soil Type	Design Method	Geotechnical Investigation Method	Resistance Factor (Efficiency, ϕ/λ) Prior Distribution Source	
				Paikowsky (2004)	Abu-Farsakh et al. (2010)
Total Resistance	Mixed (Clay and Sand)	SHAFT	AHTD	0.616 (0.576)	0.625 (0.584)
			MODOT	0.590 (0.676)	0.570 (0.653)
			UofA	0.705 (0.697)	0.750 (0.741)
		FB-Deep	AHTD	0.585 (0.560)	0.570 (0.546)
			MODOT	0.612 (0.656)	0.603 (0.646)
			UofA	0.740 (0.685)	**0.805 (0.745)**
Unit Side Resistance	Clay	SHAFT	AHTD	0.206 (0.146)	0.134 (0.095)
			MODOT	0.195 (0.106)	0.127 (0.069)
			UofA	**0.214 (0.248)**	0.140 (0.162)
		FB-Deep	AHTD	0.218 (0.109)	0.145 (0.072)
			MODOT	0.204 (0.128)	0.125 (0.079)
			UofA	0.210 (0.159)	0.132 (0.100)
	Sand	SHAFT	AHTD	0.380 (0.182)	0.364 (0.175)
			MODOT	0.361 (0.188)	0.337 (0.175)
			UofA	0.333 (0.212)	0.289 (0.184)
		FB-Deep	AHTD	0.280 (0.167)	0.233 (0.139)
			MODOT	0.305 (0.200)	0.254 (0.166)
			UofA	**0.294 (0.234)**	0.238 (0.189)
Unit End Bearing Resistance	Sand	SHAFT	AHTD	N/A	0.496 (0.118)
			MODOT		0.137 (0.036)
			UofA		0.250 (0.077)
		FB-Deep	AHTD		0.280 (0.448)
			MODOT		0.182 (0.360)
			UofA		**0.287 (0.472)**

It is theorized that the resistance factor values calculated for the unit side resistance and unit end bearing resistance was dependent upon the load test method (i.e. BLC versus top-down); however, a comparative study of resistance factor values from data collected using multiple load tests methods is needed to confirm this theory. Geologic-specific and site-specific resistance factor were similarly determined for Service limit states (1%D and 1.27cm) as presented in Appendix E. It is recommended, for a more comprehensive and accurate calibration of resistance factors in Arkansas, that at least six more full-scale tests from two or more sites be performed

(total of ten load tests from four different test sites). These tests should be performed, as test shafts, in conjunction with full-scale construction projects. Because the Bayesian method was used, the results of these new tests can be added to the newly developed database and new resistance factors can be calculated after adding each test to the database by following the framework that is presented herein.

Regaring the calibration of resistance factors for the design of DSF within the alluvial and deltaic deposits in the state of Arkansas, it is recommended to utilize the UofA geotechnical investigation methods to collect soil data. Similarly, the FB-Deep software program should be utilized to more accurately predict the load-movement response (top-down, unit side resistance, and unit end bearing resistance) of a DSF that is designed/constructed within the state of Arkansas. The most efficient (highest ϕ/λ) combination of design software program and geotechnical investigation method was the FB-Deep program using the UofA geotechnical data because the calculated resistance factor values were the highest for the total resistance. The most efficient combinations for the design of DSF using the unit side resistance and the unit end bearing resistance were the SHAFT or FB-Deep program using the UofA geotechnical investigation data and the FB-Deep software program using the UofA geotechnical investigation data, respectively. The design of DSF using the AHTD geotechnical investigation data is not recommended because the efficiency of the design is typically lower than when using the MODOT or UofA geotechnical investigation data (i.e. obtained undrained shear strength values from the AHTD data led to an underprediction of the DSF resistance).

9.7. Benefits to Geotechnical Engineering Community

The determination of the uncertainty within the design of DSF, as attributed to the effects of geotechnical investigation methods, the utilized design software program, and the construction

methods, may be utilized to enable a more efficient design in terms of reliability and cost. Besides the documentation of the construction effects and the recommendations from the nine full-scale DSF, the framework for determining the site-specific and geologic-specific calibration of the resistance factors for the design of DSF may be beneficial for the state of Arkansas and the geotechnical community at large. Specifically, the benefits from this research included.

- Establishment the amount of uncertainty due to the geotechnical investigation methods as determined by the quantity (and close physical proximity) of measured soil properties.
- Determation of the uncertainty in the results obtained from various software programs and the corresponding geotechnical investigation methods to more accurately predict the soil-structure interaction.
- Recommendations for the design limits in moderately hard to hard limestone (service limit to 0.1%D or 0.2cm of movement).
- Examination of the effects of a collapsed excavation of a DSF in relation to the axial capacities and movements that were from a BLC test.
- Verification of the effects of construction methods upon the soil-structure interaction in full-scale testing.
- Determination about the effects of diameter size on the unit side resistance values for DSF.
- Utilization of the Bayesian updating method and the Monte Carlo simulation to calibrate site-specific and geologic-specific resistance factors across Arkansas.

9.8. Recommended Future Work

Some of the findings presented in this document were based on individual site conditions and were not verified from other case histories. With consideration of the construction methods

and modified design parameters, it is recommended that further studies be conducted when the data becomes available. In particular, the soil-shaft interaction for a DSF within a redrilled excavation should be investigated to determine a modified design method that may be utilized instead of over-reaming the excavation. Similarly, the effects of poor concrete placement should be investigated to determine if the required capacity of a DSF may still be attained based on the data obtained from other full-scale load tests. It is recommended that the DSF properties be investigated in the event of an excavation collapse or if there is poor concrete placement within the construction of DSF, but the DSF may be utilized for axial loading with reduced capacities or larger acceptable movement limits.

At the SSATS, because there was not sufficient upward resistance to resist the end bearing resistance DSF, it is recommended that static load be applied to the top of the shaft in association with a BLC test. This would enable unit end bearing resistance in the moderately hard to hard limestone may be determined for larger movements. Due to the large resistance in moderately hard to hard limestone, few full-scale load test results were publically available; therefore, it is recommended that any full-scale DSF in moderately hard to hard limestone be added to a national database. Subsequently, resistance factors for DSF in moderately hard to hard limestone may be calibrated once a larger amount of data is available (at least 10 load tests). Resistance factors and design considerations of DSF in moderately hard to hard limestone should then be considered once a national or regional database is established.

While the Bayesian updating method was utilized for the determination of resistance factors for specific sites and for specific geologic conditions within the state of Arkansas, it is recommended that more full-scale load tests on DSF be performed to ensure an accurate estimation of the variation across the state of Arkansas. It is recommended that full-scale load

test data be collected from at least a total of four test sites with similar soil stratigraphy across a state to perform a state-wide resistance factor calibration utilizing the Bayesian updating method. Similarly, other site-specific calibration studies should be performed to validate the use of the Bayesian updating method across the United States. Finally, locally calibrated resistance factors for DSF may be more accurately determined using more full-scale load test data collected within or near the state of Arkansas, particularly with similar soil stratigraphy. Subsequently, it is recommended that axial load test data, in and around the state of Arkansas, be added to a state-wide database which can then be utilized to modify the localized resistance factors.

Regarding the design of DSF within the alluvial and deltaic deposits in the state of Arkansas, it is recommended to utilize the MODOT or UofA geotechnical investigation methods to collect soil data because of the MODOT method was rapid and accurate and the UofA method was accurate. Similarly, the FB-Deep software program should be utilized to more accurately predict the load-movement response (top-down, unit side resistance, and unit end bearing resistance) of a DSF designed/constructed within the state of Arkansas. The “best” combination of geotechnical investigation method and design software program was the UofA method using the FB-Deep program because the calculated resistance factor values were the highest for the total resistance. The “best” combinations (highest resistance factor values) for the design of DSF using the unit side resistance and the unit end bearing resistance were the UofA method using the SHAFT or FB-Deep software program and the AHTD method using the SHAFT software program, respectively.

It is recommended that every DSF be proof tested to ensure that the required axial capacity of the DSF can be met (for a specific contractor). Furthermore, the results from the proof tests on DSF could be added to the load test database to more accurately calibrate

resistance factors for the geologic-specific areas (alluvial or deltaic deposits and rock) within the state of Arkansas. Finally, the future utilization of DSF within the state of Arkansas is recommended because this foundation technology increases the reliability of the foundation system while reducing the cost.

9.9. Summary

The results obtained from this project included the: statistical analyses of geotechnical investigation methods and design software programs, design of DSF in moderately strong to strong limestone, influence of an excavation collapse on the resistance of a DSF, effects of the construction methods, and site-specific and geologic-specific resistance factor values. The construction methods/problems and consequent recommendations regarding the measured and predicted axial resistance were previously discussed for DSF constructed in a collapsed excavation or poor concrete placement. Recommendations on the geotechnical investigation methods and the design software programs were discussed. In particular, the FB-Deep software program should be utilized with the MODOT and UofA geotechnical investigation methods because this technique was most suitable for the design of DSF within alluvial and deltaic deposits in the state of Arkansas. From this research, resistance factor values were determined utilizing the Bayesian updating method in conjunction with the Monte Carlo simulation method. Lastly, resistance factor values were determined for the design of DSF of total resistance, unit side resistance, and unit end bearing resistance for the various geotechnical investigation methods utilized (AHTD, MODOT, and UofA), software programs utilized (FB-Deep and SHAFT), and Strength/Service limit states (5%D, 1%D, 0.1%D, 1.27cm, or 0.1cm).

9.10. References

AASHTO (American Association of State Highway and Transportation Officials). (2007). LRFD Bridge Design *Specifications*, 4th ed. American Association of State Highway and Transportation Officials, Washington, D.C., 1938 pgs.

McVay, M.C. and Niraula, L., 2004. Development of P-Y Curves for Large Diameter Piles/Drilled Shafts in Limestone for FBPIER. Florida Department of Transportation Report No. 4910-4504-878-12, 158 pgs.